

Organic Trace Analysis using High Resolution Mass Spectrometry for the Characterization of Ancient, Present and Simulated Atmospheric Systems

Dissertation

zur Erlangung des Grades
„Doktor der Naturwissenschaften“
im Promotionsfach Chemie

am Fachbereich Chemie, Pharmazie und Geowissenschaften
der Johannes Gutenberg-Universität Mainz

vorgelegt von

Christoph Zuth

geboren in Weilburg an der Lahn

Mainz, Juni 2018

Dekan:

1. Berichterstatter:

2. Berichterstatter:

Tag der mündlichen Prüfung: 27.06.2018

D77 Dissertation der Johannes Gutenberg-Universität Mainz

“Who would have guessed reading and writing would pay off!”

Homer Simpson

Zusammenfassung

Atmosphärische Aerosolpartikel haben einen großen Einfluss auf Luftqualität, Klima und die menschliche Gesundheit. Insbesondere die Bildung, Eigenschaften und Lebensdauer von Wolken, aber auch das menschliche Atmungs- und Herz-Kreislaufsystem werden durch atmosphärische Aerosole maßgeblich beeinflusst. Trotz umfangreicher Forschungen in den letzten Jahrzehnten bestehen noch große Unsicherheiten hinsichtlich des organischen Anteils solcher luftgetragenen Partikel, die meist zum Großteil der Partikelmasse beitragen. Diese organischen Aerosole (OA) bestehen aus einer hochkomplexen Mischung, die kontinuierlich atmosphärischen Umwandlungen unterliegt und deren Messung geeignete Instrumente erfordert, um die zugrundeliegenden Prozesse aufzuklären. Die Massenspektrometrie (MS) bietet eine hohe Empfindlichkeit und Selektivität gegenüber einzelnen Molekülen und eignet sich daher besonders gut für die chemische Analyse atmosphärischer Aerosolpartikel. Obwohl sich die Massenspektrometrie bereits als ein vielseitiges und leistungsfähiges Werkzeug auf dem Gebiet der Aerosolforschung erwiesen hat, erfordert die Identifizierung und Spurenanalyse einzelner organischer Moleküle weiterhin Verbesserungen aufgrund oft unzureichender Massenauflösung. Insbesondere ultrahochauflösende, massenspektrometrische Konzepte nach aktuellem Stand der Technik, wie die Orbitrap, als jüngste Entwicklung der Massenspektrometer, sind in diesem Forschungsgebiet noch wenig etabliert.

Ziel dieser Arbeit war es, analytische Methoden zur Analyse einzelner organischer Verbindungen in hochkomplexen atmosphärischen Matrices zu entwickeln und die ultrahochauflösende Massenspektrometrie als ein vielseitiges Werkzeug in der atmosphärischen Aerosolforschung zu etablieren. Insbesondere wurde die Ultrahochleistungs-Flüssigkeitschromatographie (*ultra-high-performance liquid chromatography*, UHPLC) in Kopplung mit Elektrospray-Ionisation und ultrahochauflösender Massenspektrometrie (*electrospray ionization ultra-high-resolution mass spectrometry*, ESI-UHRMS) zur Quantifizierung von Marker-Molekülen in Eisbohrkernen, sowie zur molekularen Charakterisierung von im Labor erzeugten Aerosolen eingesetzt. Darüber hinaus wurde die Technik der chemischen Ionisierung bei Atmosphärendruck in Verbindung mit Orbitrap-Massenspektrometrie (*atmospheric pressure chemical ionization Orbitrap mass spectrometry*, APCI-Orbitrap-MS) verwendet, um einzelne Moleküle mit positiver und negativer Ionisierung in Echtzeit in der Umgebungsluft zu bestimmen.

Der Schwerpunkt des ersten Teils dieser Arbeit lag auf der Entwicklung einer umfassenden spurenanalytischen Methode zur sensitiven Quantifizierung von neuen und besser geeigneten, schwerflüchtigen atmosphärischen Markern in Schnee- und Eisproben. Die analysierten Moleküle umfassten eine Reihe von atmosphärischen Marker-Molekülen bestehend aus Levoglucosan, Ligninstämmigen Waldbrandmarkern, Markern für sekundäres organisches Aerosol (SOA) aus Isopren, Monoterpenen und Sesquiterpenen sowie Fettsäuren. Zur Extraktion und Anreicherung der Verbindungen aus der geschmolzenen Probenmatrix wurde die Festphasenextraktion (*solid phase extraction*, SPE) mit Anionenaustauscher-Funktion verwendet. Eine Erhöhung der Signalintensitäten der Analyten im Ionisierungsprozess wurde durch Einleiten einer Ammoniaklösung in Methanol nach der Trennsäule erreicht. Im Fokus der Methodenentwicklung standen die Anpassung der Konzentrationen und Flussraten der Ammoniaklösung sowie die Optimierung der chromatographischen Trennung und die massenspektrometrische Detektion im Tandem MS Modus (MS²) unter Berücksichtigung der hohen Anzahl an unterschiedlichen Markerverbindungen.

In einer Machbarkeits-Studie wurde die optimierte Methode zur Analyse von Eisbohrkern-Proben aus dem Belukha-Gletscher im Altai-Gebirge eingesetzt. Mehrere organische Spurenanalyten wurden erstmals in einem Eisbohrkern des Belukha-Gletschers nachgewiesen und mit einer einzigen analytischen Methode im niedrigen ng/g-Bereich quantifiziert. Weiterhin zeigte eine Hauptkomponentenanalyse (*principal components analysis*, PCA), dass Biomasseverbrennung und biogenes SOA, Pflanzenwachse, sowie Sesquiterpen-Oxidationsprodukte und kurzkettige Fettsäuren die Hauptfaktoren sind, welche die Probenahmestätte beeinflussten.

Im zweiten Teil wurde die Kopplung aus UHPLC und UHRMS für eine umfassende molekulare Charakterisierung von Submikrometerpartikeln genutzt, welche in der CLOUD-Kammer (*Cosims Leaving Outdoor Droplets*, CLOUD) bei der Europäischen Organisation für Kernforschung (*European Organization for Nuclear Research*, CERN) in Genf generiert wurden. Im Rahmen der CLOUD 10-Kampagne wurde insbesondere die Partikelneubildung aus den flüchtigen organischen Substanzen (*volatile organic compounds*, VOCs) α -Pinen und Δ -3-Caren in Anwesenheit von SO₂ und NO_x untersucht. Die gesammelten Filterproben wurden mit Hilfe eines Wasser/Acetonitril-Gemischs mehrfach extrahiert und anschließend mit dem Ansatz eines *Non-Target-Screenings* analysiert. Neben einer Zuordnung der identifizierten Moleküle zu bestimmten Molekülklassen lag ein besonderer Fokus auf der Identifizierung von hochoxidierten multifunktionellen organischen Verbindungen (*highly oxidized molecules*, HOMs). Darüber hinaus wurden dimere Strukturen von Organonitraten und Nitrooxy-Organosulfaten durch MS²-Studien aufgedeckt. Es wurde zudem gezeigt, dass unterschiedliche Konzentrationen an SO₂ zu unterschiedlichen Anteilen an Mono- und Di-Organonitraten geführt haben, was auf einen SO₂-abhängigen Bildungsweg hinweist. Zusammenfassend wurde eine einzigartige Liste an identifizierten SOA-Verbindungen erhalten, einschließlich der exakten Molekülmasse und Retentionszeit nachgewiesener Isomere.

Schließlich wurde, inspiriert durch die Teilnahme an der CLOUD 10-Kampagne am CERN, der Bedarf nach hochauflösender Massenspektrometrie in Echtzeit festgestellt, was zu der Entwicklung und Charakterisierung der APCI-Orbitrap-MS für die Echtzeit-Messung von Aerosolpartikeln geführt hat. Die Optimierung und Charakterisierung der APCI-Orbitrap-MS erfolgte durch im Labor erzeugtes Modellaerosol und wies eine hohe Zeitauflösung, eine lineare Abhängigkeit für Partikel kleiner als 100 nm über drei Größenordnungen und Nachweisgrenzen im unteren ng/m³-Bereich auf.

In einer ersten Anwendbarkeitsstudie wurde die Zusammensetzung des Aerosols in der Umgebungsluft analysiert, indem Partikel der Größe PM_{2.5} (*Particulate Matter* < 2,5 μ m) in der Umgebungsluft außerhalb des Laborgebäudes in abwechselnden Ionisationsmodi beprobt wurden. Aufgrund des sanften Ionisierungsprozesses blieben die Molekülonen erhalten und die Signale der deprotonierten oder protonierten Moleküle stellten jeweils das Hauptsignal dar. Ein anschließendes *Non-Target-Screening* sowie der Nachweis und die Quantifizierung einzelner organischer Verbindungen in Aerosolen wurden unter atmosphärischen Bedingungen, ohne jegliche Anreicherung oder Filterprobenahme, durchgeführt. Insbesondere wurde die molekulare Zusammensetzung des organischen Aerosols in der Außenluft zu Tages- und Nachtzeit im negativen und positiven Ionisierungsmodus untersucht. Mit dem hier vorgestellten massenspektrometrischen System konnten weiterhin hochoxidierte Mono- und Di-Organonitrate und Nitrooxy-Organosulfate mit sehr hoher Zeitauflösung in der Partikelphase der Umgebungsluft nachgewiesen werden.

Zusammenfassend konnte gezeigt werden, dass die Orbitrap-Technik als ein vielseitiges Werkzeug eingesetzt werden kann, welche eine Reihe von Vorteilen für die Analyse von organischen Aerosolen sowohl im *offline*- als auch im *online*-Modus bietet, um die atmosphärische Zusammensetzung und Bildungsmechanismen von Aerosolen aufzuklären.

Abstract

Atmospheric aerosol particles are strongly affecting air quality, climate, and human health. Particularly, atmospheric aerosols can have major effects on the formation, properties and lifetime of clouds and significantly affect the human respiratory and cardiovascular system. Despite extensive research over the last decades, large uncertainties still remain regarding the organic fraction of such airborne particles, which is often accounting for the majority of the particulate mass. Such organic aerosols (OAs) consist of a highly complex mixture that is subject to continuous atmospheric transformations, the measurement of which requires suitable instrumentation to elucidate the underlying processes. Providing high sensitivity and selectivity towards single molecules, mass spectrometry (MS) is a well-suited technique for the chemical analysis of atmospheric aerosol particles. Although MS has been proven to be a versatile and powerful tool in the field of aerosol research, the identification and trace analysis of single organic molecules still demands improvements due to insufficient mass resolution. Particularly, state of the art ultra-high-resolution mass spectrometric techniques, such as the Orbitrap mass spectrometer, are not yet fully established in this field of research.

The aim of this work was to develop analytical methods for the analysis of single organic compounds in highly-complex atmospheric matrices and to establish ultra-high-resolution mass spectrometry (UHRMS) as a versatile tool in atmospheric aerosol research. In particular, ultra-high-performance liquid chromatography (UHPLC) coupled to electrospray ionization ultra-high-resolution mass spectrometry (ESI-UHRMS) was used for the quantification of tracer molecules in ice cores and molecular characterization of laboratory generated aerosols. Furthermore, an atmospheric pressure chemical ionization Orbitrap mass spectrometry (APCI-Orbitrap-MS) technique was applied for the real-time determination of single molecules in ambient air using negative and positive ionization mode.

The first part of this study is focused on the development of a single, comprehensive trace analytical method for the sensitive quantification of new and more appropriate low-volatile marker compounds in snow and ice samples. The analyzed molecules covered a broad range of atmospheric tracers, comprising levoglucosan, lignin-derived biomass burning markers, atmospheric secondary organic aerosol (SOA) markers originating from isoprene, monoterpenes, and sesquiterpenes as well as fatty acids. Solid phase extraction (SPE) using anion exchange functionalities was used for extraction and enrichment of the compounds from the molten sample matrix. A post-column injection of ammonia in methanol was employed to enhance signal intensities of the analytes during electrospray ionization. The focus of the method development was on the evaluation of concentrations and flowrates of the ammonia-solution as well as the optimization of chromatographic separation and mass spectrometric detection using the MS² mode whilst taking into account the high number of diverse marker compounds.

As a proof-of-principle, the optimized method was applied for the analysis of ice core samples from the Belukha glacier in the Altai mountain range. Several organic trace components were determined for the first time in an ice core from the Belukha glacier and quantified in the low ng/g-range within a single analytical method. Furthermore, a principal components analysis (PCA) revealed biomass burning and biogenic SOA, plant waxes, and sesquiterpene oxidation products and short chain fatty acid emissions to be the main parameters influencing the sampling site.

In the second part, UHPLC coupled to UHRMS was applied for the comprehensive molecular characterization of submicron-particles generated in the Cosmics Leaving Outdoor Droplets (CLOUD) laboratory chamber at the European Organization for Nuclear Research (CERN), Geneva. Filter samples were taken at the CLOUD 10 campaign focusing on new particle formation experiments of volatile organic compounds (VOCs) (i.e., α -pinene and Δ -3-carene) with sulfuric acid vapor and NO_x. The filters were multiply extracted by a water/acetonitrile-mixture and further analyzed using a non-target screening approach. Besides attributing the identified molecules to certain molecular classes, a special focus was on the identification of highly oxidized multifunctional organic compounds (HOMs). Furthermore, dimeric structures of organic di-nitrates and nitrooxy organosulfates were observed in MS²

studies. It was shown that, varying mixing-ratios of SO₂ led to a different distribution of organic mono-/di-nitrates, indicating an SO₂-dependant formation pathway. In conclusion, a unique compound-list of identified SOA molecules including the exact molecular mass and the retention time of detected isomers was obtained.

Finally, inspired by the participation in the CLOUD 10 campaign at CERN, the need for real-time ultra-high-resolution mass spectrometry was noticed and led to the development and characterization of APCI-Orbitrap-MS for the real-time measurement of atmospheric aerosol particles. Optimization and characterization of the APCI-Orbitrap-MS was performed by laboratory-generated model aerosol exhibiting a high time resolution, a linear response over three orders of magnitude for sub 100 nm particles and detection limits in the low ng/m³ range.

As a proof of principle, the ambient aerosol composition was analyzed by sampling PM_{2.5} particles from the outside of the laboratory building in alternating ionization mode. Due to the soft ionization procedure, molecular ions are preserved and the deprotonated or protonated ions represent the main signal. A subsequent non-target screening, as well as single organic compound detection and quantification in aerosols, was performed under ambient atmospheric conditions without preconcentration or filter sampling steps. Particularly, in the non-target screening, the molecular composition of ambient organic aerosol during night- and daytime was examined both in negative and positive ionization mode. With the presented mass spectrometric system it was possible to detect highly oxidized organic nitrates, organic di-nitrates and nitrooxy organosulfates with a high time resolution in the ambient particle phase.

In conclusion, it has been shown that the Orbitrap technique can be used as a versatile tool offering a number of advantages for the analysis of organic aerosols in offline as well as online mode, which will help to shed light on the atmospheric aerosol composition and formation mechanisms.

Table of Contents

Zusammenfassung	i
Abstract	iii
1 Introduction	5
1.1 Atmospheric Aerosols	5
1.2 Secondary Organic Aerosol.....	7
1.2.1 Formation Mechanisms	7
1.2.2 Gas-Particle Phase Reactions	10
1.3 Ice Cores as Climate Archives.....	11
1.3.1 Drilling Sites	11
1.3.2 Dating of Ice Cores	13
1.4 Sample Extraction and Aerosol Filtration	14
1.4.1 Solid Phase Extraction	14
1.4.2 Filter Sampling	15
1.5 Mass Spectrometry in the Field of Aerosol Research	16
1.5.1 Offline Mass Spectrometry Techniques	16
1.5.2 Online Mass Spectrometry Techniques.....	18
1.5.3 Orbitrap Mass Spectrometry	20
1.6 Thesis Objectives and Outline	21
2 Organic Trace Analysis in Ice Cores	23
2.1 Introduction	23
2.2 Experimental: Method Development.....	25
2.2.1 Chemicals and Materials	25
2.2.2 Solid Phase Extraction	26
2.2.3 Ultra-High-Performance Liquid Chromatography–Mass Spectrometry	27
2.2.4 Preparation of Standards	28
2.3 Experimental: Belukha Glacier Ice Core Sections	29
2.3.1 Principal Component Analysis.....	30
2.4 Results and Discussion: Method Development	31

2.4.1	Ultra-High-Performance Liquid Chromatography-Mass Spectrometry	31
2.4.2	Solid Phase Extraction	34
2.4.3	Method Validation.....	35
2.5	Results and Discussion: Belukha Glacier Ice Core Sections.....	38
2.5.1	Principal Component Analysis.....	44
2.5.2	Seasonal Variation of the Analytes during 1866-1869	47
2.6	Conclusions and Outlook.....	50
3	Molecular Composition of SOA Particles at Nucleation Experiments at CERN.....	53
3.1	Introduction	53
3.2	Experimental.....	55
3.2.1	The CLOUD Chamber	55
3.2.2	Filter Analysis Using UHPLC-(H)ESI-UHRMS	56
3.2.3	Data Processing of UHRMS Data.....	57
3.2.4	Experimental Design	59
3.3	Results and Discussion	60
3.3.1	Extraction Efficiencies of α -Pinene SOA Proxy Compounds.....	60
3.3.2	Molecular Composition of SOA Particles at CLOUD 10	61
3.4	Conclusions and Outlook.....	75
4	Ultra-High-Resolution Mass Spectrometry of Atmospheric Organic Aerosol Particles in Real-Time	77
4.1	Introduction	78
4.2	Experimental.....	80
4.2.1	Characterization of the APCI-Orbitrap-MS with Organic Model Aerosol	80
4.2.2	Ultra-High-Resolution Orbitrap Analysis of Atmospheric Aerosol Particles in Real-Time	81
4.3	Results and Discussion	82
4.3.1	Characterization of the APCI-Orbitrap-MS with Organic Model Aerosol	82
4.3.2	Ultra-High-Resolution Orbitrap Analysis of Atmospheric Aerosol Particles in Real-Time	84
4.4	Conclusions and Outlook.....	93
5	Conclusions and Outlook	95
6	References	97

7	Appendix.....	112
7.1	Supporting Information to Chapter 2.....	112
7.2	Supporting Information to Chapter 3.....	117
7.3	Supporting Information to Chapter 4.....	126
7.4	List of Related Publications and Presentations.....	148
7.5	Acknowledgments	151
7.6	Curriculum Vitae	153

1 Introduction

1.1 Atmospheric Aerosols

Atmospheric aerosols originate from biogenic and anthropogenic sources and are ubiquitously present in Earth's atmosphere. Although aerosols are defined as liquid or solid particles suspended in air, the common usage refers to the particulate phase only. In this study, we will follow this widespread practice, unless explicitly stated otherwise. Particularly, this aerosol particle phase is crucial to the Earth's climate (Seinfeld & Pandis, NJ : Wiley, 2006).

One of the key roles of aerosols are light scattering and absorption of solar radiation. They are discussed to have major effects on the formation and lifetime of clouds by acting as cloud condensation nuclei (CCN) (IPCC, 2013). Participation in multiphase processes and heterogeneous chemical reactions may also have an eminent effect on the abundance of atmospheric trace gases (George *et al.*, 2015; Pöschl, 2005). Moreover, atmospheric aerosol particles can have serious impact on human health by entering the respiratory and cardiovascular system causing inflammation and allergic reactions (Lelieveld *et al.*, 2015; Pöschl, 2005; Pöschl & Shiraiwa, 2015; Schulz *et al.*, 2005).

Concerning the chemical composition of submicron atmospheric aerosols, one can classify the components into inorganic ions, organics, and black carbon. Inorganic ions are major components of the aerosols and have been observed with relatively high concentrations at multiple locations around the world (Jimenez *et al.*, 2009). Quantification was either performed by sampling the aerosols subsequently followed by analysis using ion chromatography or by direct measurements using an aerosol mass spectrometer (AMS). The most commonly identified anions include sulfate (SO_4^{2-}), nitrate (NO_3^-), and chloride (Cl^-). Accordingly, a relatively high variety of cations have been identified in aerosols, though solely ammonia (NH_4^+) showed high concentrations (Jimenez *et al.*, 2009). Considering the high complexity, the speciation of organics in atmospheric aerosols is much less understood and an active field of research. About 20-50 % (up to 90 % in forested regions like the Amazon) of the aerosol mass is comprised of organic carbon (Kanakidou *et al.*, 2005).

According to their sources, atmospheric aerosols are characterized as primary aerosols when they are emitted in the air directly as particles (e.g., biogenic/anthropogenic combustion particles, plant-debris, dust, volcanic eruption, sea-salt, and pollen) or secondary aerosols when they are formed in the atmosphere by gas-to-particle conversion and oxidation of gaseous precursors (Hallquist *et al.*, 2009; Seinfeld & Pandis, NJ : Wiley, 2006). Atmospheric particles generally range in diameter in the size from a few nanometers for molecular clusters to tens of micrometers for common primary particles (e.g., dust). Airborne particles can further change their size and composition due to condensation and evaporation of volatile organic compounds (VOCs), coagulation with other particles, chemical reactions, or by activation in the presence of water supersaturation to become fog and cloud droplets (Seinfeld & Pandis, NJ : Wiley, 2006). The atmospheric lifetime of aerosol particles is strongly linked

to their size. One can distinguish between particles larger than 1 μm in diameter, referred to as the coarse mode. These particles are usually of primary origin and contribute largely to the aerosol mass concentration. Atmospheric lifetimes are short due to the fast gravitational settling. Aerosol particles smaller than 1 μm are defined as the fine mode which is further subdivided into the nucleation mode ($<0.01 \mu\text{m}$), Aitken mode (0.01-0.1 μm), and accumulation mode (0.1-1 μm). Nucleation mode and Aitken mode particles are typically secondary in nature and contribute largely to the total number of atmospheric particles. They are formed either by condensation of low volatility compounds onto thermodynamically stable clusters of, e.g., sulfuric acid, or by pure biogenic nucleation followed by a rapid growth to larger sizes (Kirkby *et al.*, 2016; Kulmala *et al.*, 2013). Particles in the size range of the accumulation mode show the longest atmospheric lifetime, commonly in the range of several days to weeks (Finlayson-Pitts & Pitts, 2000). The main removal process of particles smaller than 1 μm from the atmosphere is wet deposition.

The influence of aerosols on the Earth's climate can largely be attributed to the so-called direct and indirect effects. Aerosols directly affect the Earth's radiative balance by scattering or absorption of solar radiation. Absorbed radiation caused by black carbon particles, for example, contributes to the global warming of the atmosphere (IPCC, 2013). Sulfate particles can efficiently scatter incident radiation, thus causing a net cooling effect (Schwartz, 1996). In general, particles in the size range of the accumulation mode are likely to absorb and scatter solar radiation.

The indirect effects of aerosols are mainly linked to particles in the size range of 50-100 nm which are capable to act as CCN. As an example, increasing aerosol concentration levels can produce clouds with smaller droplets, less likely to precipitate. Thus, the clouds persist longer and scatter more radiation, leading to a cooling effect on the Earth's atmosphere (Seinfeld & Pandis, NJ : Wiley, 2006). Sulfate particles, for example, cause brighter clouds due to a larger number of smaller droplets with longer average lifetimes, described as cloud albedo effect (Boucher & Lohmann, 1995). By influencing the precipitation, atmospheric aerosols have also significant influence on the Earth's hydrological cycle (Ramanathan *et al.*, 2001).

Estimations on the radiative forcing of aerosols and other atmospheric compounds are shown in Figure 1.1. The aerosol particles contribute to the largest uncertainty in the estimation of global radiative forcing (IPCC, 2013). While the direct effects of aerosols and relatively long-lived greenhouse gases are attributed to a high level of confidence, the understanding of the influence of aerosol-cloud interactions on the radiative forcing is still low. Due to the relatively short atmospheric lifetimes and continuous chemical and physical conversions of aerosol particles in heterogeneous and multiphase reactions, this understanding remains a challenging task (Ravishankara, 1997). Overall, anthropogenic cloud adjustments due to aerosols are believed to cool the atmosphere (IPCC, 2013).

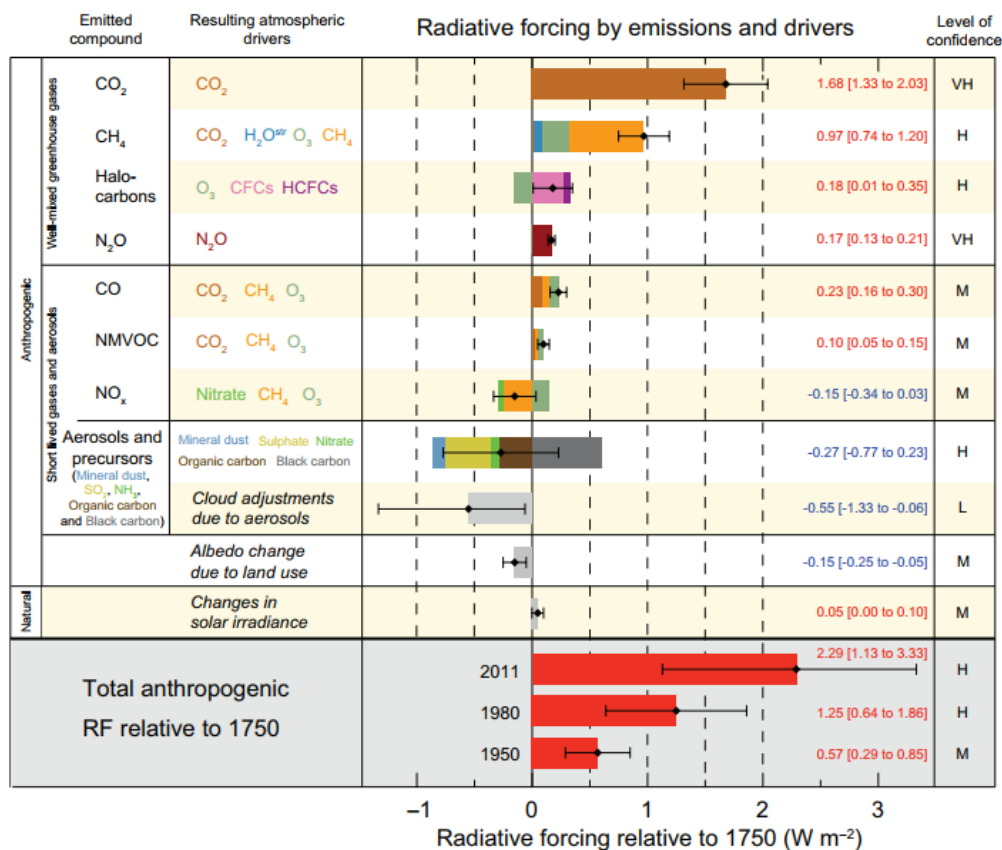


Figure 1.1 Radiative forcing estimates in 2011 relative to 1750 and aggregated uncertainties for the main drivers of climate change. The best estimates of the net radiative forcing are shown as black diamonds with corresponding uncertainty intervals. Abbreviations for the level of confidence of the radiative forcing by emissions and drivers are abbreviated as follows: VH-very high, H-high, M-medium, L-low (IPCC, 2013).

Additionally to the discussed climatic effects, several epidemiological studies link global atmospheric chemistry, including fine particulate matter and health impacts of ozone, with premature mortality (Lelieveld *et al.*, 2015; Pöschl & Shiraiwa, 2015; Schneidemesser *et al.*, 2015). It has been shown, that the health effects largely depend on the particle size as well as the chemical composition of the aerosol (Schulz *et al.*, 2005).

1.2 Secondary Organic Aerosol

1.2.1 Formation Mechanisms

The formation of secondary organic aerosol (SOA) commonly starts with the gas phase oxidation of VOCs. The produced condensable vapors form particulate matter via gas-to-particle transfer processes, such as nucleation or condensation on pre-existing particles.

The initiating step is caused by structure-dependent competing reactions of the VOCs with hydroxyl radicals (OH), O₃, nitrate radicals (NO₃) or via photolysis (Kroll & Seinfeld, 2008). The subsequent

oxidation of the VOCs leads to the generation of various organic products, containing oxygenated functional groups which significantly decrease the volatility and make the products more water soluble. Further reactions include ongoing oxidation mechanisms and the introduction of additional functional groups which lead to even higher solubility and lower volatility as well as fragmentation reactions of the carbon chains which form lower molecular weight (MW) oxygenates (Hallquist *et al.*, 2009). As a result, the atmosphere contains a highly complex mixture of structurally different oxygenated organic constituents possessing a wide range of properties. Figure 1.2 shows a simplified schematic of the initial oxidation process of VOCs in the gas phase.

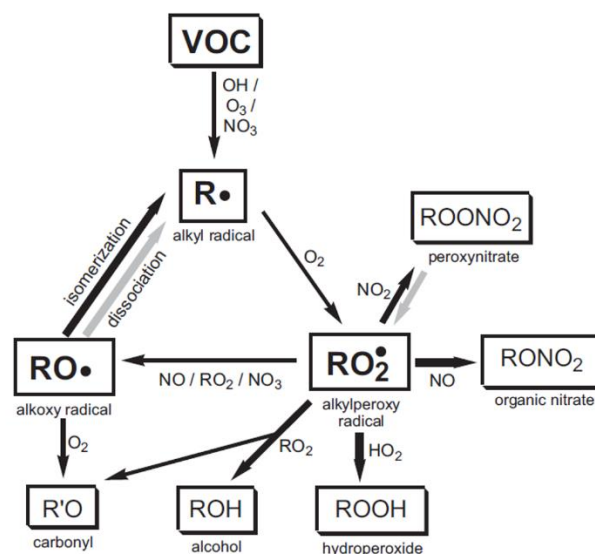


Figure 1.2 Simplified mechanism for the oxidation mechanism of a generic VOC. Thick black arrows denote reactions that can lead to a substantial decrease in volatility; gray arrows denote reactions that can lead to a substantial volatility increase (Kroll & Seinfeld, 2008).

Emitted VOCs react in an initial step with OH, NO₃, and O₃ and form an alkyl radical which further reacts with oxygen to an alkylperoxy radical (RO₂). Depending on the concentrations of RO₂, NO_x, and HO₂, the RO₂ radicals play a central role in the production of lower volatility products such as alcohols, hydroperoxides, organic nitrates or peroxynitrates. Furthermore, RO₂ can react with NO forming alkoxy radicals (RO) which can either isomerize or dissociate to alkyl radicals (R) or react with oxygen to carbonyls. An additional pathway to a class of highly oxygenated, high-molecular-mass oxidation products following ozonolysis and reaction with OH radicals, was suggested by Ehn *et al.* (Ehn *et al.*, 2012; Ehn *et al.*, 2014; Mentel *et al.*, 2015). Originally, these highly oxygenated compounds were referred to extremely low-volatility organic compounds (ELVOCs) because of their role in particle formation as extreme low-volatility condensable organic vapors (Bianchi *et al.*, 2016; Kirkby *et al.*, 2016). However, referring to the chemical structures and pathways, the notation as highly oxidized multifunctional molecules (HOMs) is more accurate and should thus be favored (Mentel *et al.*, 2015). After the initial oxidation steps, internal hydrogen abstraction by an RO₂ radical (H-shift) followed by an autoxidation process involving oxygen addition at the alkyl radical site leads to a higher oxidized

peroxy radical ($R_{ELVOC}O_2$). Subsequently, ongoing H-shifts and oxygen additions lead to gas-phase formation of HOMs, resulting in dimer-, monomer-, and, in the presence of NO, organic nitrate channels (Ehn *et al.*, 2014; Jokinen *et al.*, 2014). Figure 1.3 depicts a simplified schematic of ELVOC formation.

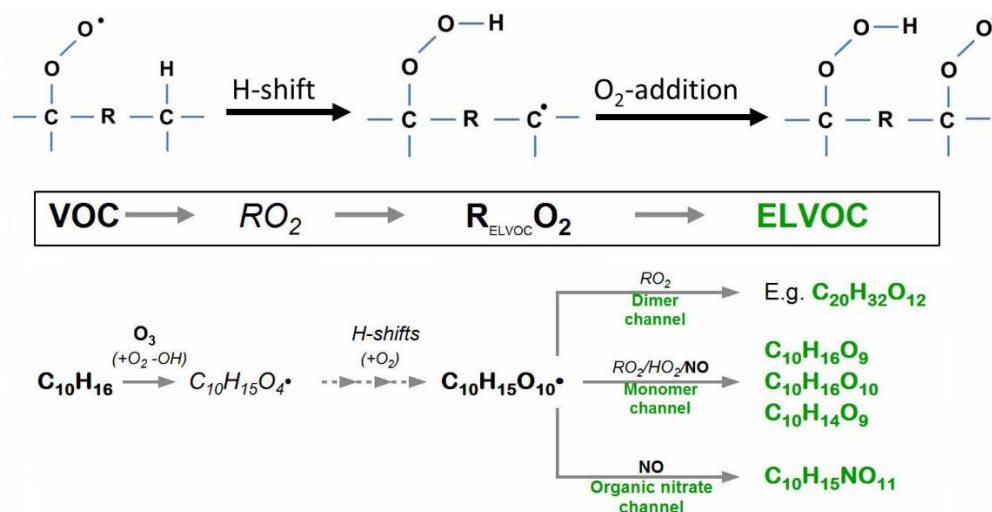


Figure 1.3 Schematic illustrations of ELVOC formation. The upper panel depicts the internal hydrogen abstraction by an RO_2 (H-shift), followed by oxygen addition at the alkyl radical site, forming a more oxidized peroxy radical. Depending on the structure of the RO_2 molecule, subsequent H-shifts and O_2 -additions can increase the oxygen content even further. The lower panel shows a specific example pathway from α -pinene ($C_{10}H_{16}$) ozonolysis resulting in dimer-, monomer-, and organic nitrate channels (adapted from Ehn *et al.*, 2014).

The most dominant precursors for SOA production on a global scale are biogenic VOCs, like isoprene (C_5H_8), monoterpenes ($C_{10}H_{16}$), and sesquiterpenes ($C_{15}H_{24}$) (Guenther *et al.*, 1995). Forested regions, such as the Amazon rainforest and the boreal forest, release large amounts of biogenic VOCs and thus contribute to the SOA fraction. A prominent example of the formation of SOA due to forest emissions is described as the “blue haze” effect. As a result of wavelength dependent Rayleigh scattering of light by SOA particles, a bluish form of haze occurs over forested regions in summer time and is responsible for the name of mountain regions around the world (Hoffmann *et al.*, 2007; Went, 1960). In contrast, anthropogenic emissions of VOCs are about a factor of 10 lower than global emissions of biogenic VOCs (e.g., alkanes and aromatics), but often play a key role on local or regional scales (Atkinson & Arey, 2003).

Organic condensation contributes to a large extent to the growth of atmospheric aerosol particles (Riipinen *et al.*, 2011; Tröstl *et al.*, 2016). For new particle formation, vapor molecules need to form a sufficient number of small molecular clusters of a few nanometers (< 2 nm) which needs to grow to larger sizes fast enough to avoid loss by coagulation (Donahue *et al.*, 2013; Kulmala *et al.*, 2013; Riipinen *et al.*, 2011). It was believed, that new particle formation is strongly associated with sulfuric acid vapors, as sulfuric acid is almost always present in the smallest molecular clusters (Donahue *et al.*, 2013). However, it was also shown that ultra-fine particles between 2 and 20 nm grow much faster than

condensation of sulfuric acid can explain, suggesting an additional influence from condensation of organic vapors (Donahue *et al.*, 2011). The detection and characterization of ELVOCs linked the role of condensed organics and sulfuric acid in initial nucleation processes in field and chamber experiments (Kirkby *et al.*, 2011; Kulmala *et al.*, 2013; Schobesberger *et al.*, 2013). Recently, it was shown, that new particle formation even occurs in the absence of sulfuric acid through both neutral and ion-induced nucleation of pure biogenic vapors (Kirkby *et al.*, 2016). Observational evidence at high altitudes demonstrated that new-particle formation occurs mainly through condensation of HOMs in addition to sulfuric acid-ammonia nucleation (Bianchi *et al.*, 2016).

1.2.2 Gas-Particle Phase Reactions

VOC oxidation products with higher vapor pressure are not necessarily only present in the gas phase but were also detected in the SOA particle phase. The partitioning process between the gas phase and the particle phase depends on the partitioning equilibrium and was described by Pankow (Pankow, 1994a, 1994b) and extended to SOA by Odum *et al.* (Odum *et al.*, 1996). The partitioning of the compounds between the phases is described by the equilibrium partitioning coefficient $K_{p,i}$ ($\text{m}^3 \mu\text{g}^{-1}$) or the saturation vapor concentration C_i^* ($\mu\text{g m}^{-3}$) (Donahue *et al.*, 2006):

$$\frac{C_i^p}{C_i^g} = K_{p,i} C_{OA} = \frac{C_{OA}}{C_i^*} \quad (1.1)$$

where C_i^g and C_i^p stands for mass concentrations of species i per unit volume of air ($\mu\text{g m}^{-3}$) in the gas phase and the particle phase, respectively, and C_{OA} is the mass concentration per unit volume of air ($\mu\text{g m}^{-3}$) of the total absorbing particle phase. Accordingly, a fraction of each semi-volatile compound will partition into the particle phase, although its gas phase concentration is below its saturation concentration, C_i^* . Furthermore, the exact mass fraction F_i of a semi-volatile compound in the particle phase can be obtained by equation 1.2 (Hallquist *et al.*, 2009):

$$F_i = \frac{C_i^p}{C_i^p + C_i^g} = \frac{C_{OA} * K_{p,i}}{1 + C_{OA} * K_{p,i}} = \frac{1}{1 + C_i^*/C_{OA}} \quad (1.2)$$

For instance, when the amount of absorbing material (C_{OA}) increases, molecules of greater volatility will increasingly partition into the particle phase. When $C_{OA} = C_i^*$, partitioning will result in a 50:50 distribution between particle and gas phase and when $C_{OA} \gg C_i^*$ the compound will be located almost completely in the particle phase (Hallquist *et al.*, 2009).

Parametrizations according to the volatility of organic compounds were recently developed to categorize certain molecule classes. Donahue *et al.* suggested a volatility basis set (VBS) where semi-volatile compounds are binned to predefined values for C_i^* , which are separated by one order of

magnitude (Donahue *et al.*, 2006). Li *et al.* developed parametrizations to predict the saturation mass concentration of organic compounds containing oxygen, nitrogen, and sulfur and mapped the compounds into molecular corridors to characterize the chemical nature (Li *et al.*, 2016).

Once the organic compounds migrated to the particle/condensed phase, they can undergo particle phase reactions (Kroll & Seinfeld, 2008). Generally, Kroll and co-workers (2008) categorized particle phase reactions, which include both heterogeneous and multiphase reactions, in non-oxidative or oxidative processes. Non-oxidative, or accretion reactions (Barsanti & Pankow, 2004), are described by the observation of oligomeric and high-molecular-weight species in SOA, respectively, in which the oxidation state of the total carbon remains unchanged. Reactions such as dimerization can play a crucial role in the formation of SOA due to a significant decrease in vapor pressure. Further reaction products including peroxyhemiacetals, aldol addition products, hemiacetals, ester, organosulfates, organic nitrates and criegee intermediate adducts may also affect the volatility of atmospheric organics. The particle phase organic compounds may also be oxidized by the most prominent atmospheric oxidants OH, O₃ and NO₃ radical. This process often referred to “aerosol aging”, affects the evolution of physical properties of aerosols in a broad and significant way (Rudich *et al.*, 2007).

Besides the above-mentioned aspects, crucial factors that are complicating the interpretation of partitioning and particle phase reactions are the dynamic chemical complexity and its temperature dependence (Hallquist *et al.*, 2009). In general, the reactions influencing the volatility of SOA are expected to be significant if they occur on timescales shorter than the lifetimes of tropospheric particles (4-7 days) (Kroll & Seinfeld, 2008).

1.3 Ice Cores as Climate Archives

The aim of studies on climatic and environmental archives is to obtain knowledge on the environmental conditions of the past, including atmospheric parameters. Such investigations are expected to help in understanding and modeling, e.g., present and future effects of climate change. Ice cores, which are a main focus of this study, are considered as such climate and environmental archives and are commonly drilled either from polar ice sheets or from glaciers of the high or mid-latitude mountain areas. In the following sections, information on the drilling sites and methods for the dating of ice cores are presented.

1.3.1 Drilling Sites

Polar ice cores provide information on global climate and environmental changes over periods of thousands of years. Ice core records were shown to indicate the pattern of glacial-interglacial cycles, the existence of abrupt climate changes and were used to reconstruct greenhouse gas concentrations (Giorio *et al.*, 2018). Their sampling is even more ambitious than for glacier ice cores. Long time scales are covered by deep ice cores from Polar Regions. Undisturbed records of parts of the last interglacial period

1. Introduction

are still very limited in their number (Jouzel, 2013). At the Vostok site in Antarctica, drilling started in the early 1970s (Petit *et al.*, 1999). The GRIP (Greenland Ice Core Project) project started in the early 1990s and more recently the EPICA (European Project for Ice Coring in Antarctica) project has involved the drilling of ice cores at Dome C and Dronning Maud Land (Maggi *et al.*, 2006). Until now, the obtained ice core from Dome C is the oldest continuous core ever retrieved, backdating 800 000 years. From 2007 to 2012, the NEEM (North Greenland Eemian Ice Drilling) project retrieved an ice core from the top of the ice sheet down to the bedrock. This ice core contains layers of ice reaching back 115 000 years, through the previous interglacial period, the Eemian (NEEM community members, 2013). In general, polar ice cores are typically drilled in remote areas of low snow accumulation. Consequently, the records of polar ice cores preserve global climate conditions and atmospheric parameters.

In contrast, ice cores originating from glaciers of the high or mid-latitude mountain areas provide more regionally influenced climate records because of their location close to natural or anthropogenic emission sources. In the framework of the Fifth Assessment of the Intergovernmental Panel on Climate Change (IPCC), the Randolph Glacier Inventory (RGI) was introduced to define mountain sites and to categorize glaciers around the world (Pfeffer *et al.*, 2014). Figure 1.4 shows the global distribution of ~198 000 defined glaciers. About one-fifth of the glaciers are located in Central Asia, whereas the Belukha glacier, which is part of this study, is attributed to the North Asia Region.

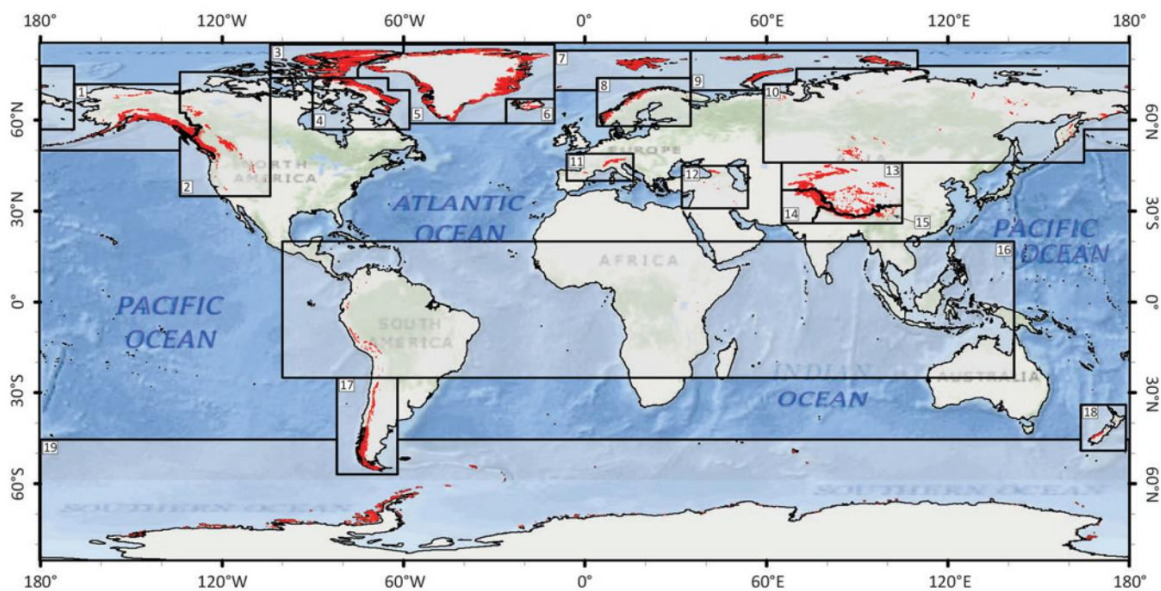


Figure 1.4 Global distribution of the defined RGI regions, with glaciers shown in red. Region numbers represent the 19 RGI regions. Cylindrical equidistant projection (Pfeffer *et al.*, 2014).

1.3.2 Dating of Ice Cores

For a relevant historic interpretation of the obtained data from glaciers and ice sheets, a precise chronological dating is indispensable. Especially for dating of older, deeper parts of an ice core, advanced methods are needed to overcome the strong annual layer thinning and non-linear age-depth relationship due to plastic deformation (Uglietti *et al.*, 2016). However, for a meaningful and accurate dating, complementary strategies are commonly needed in combination.

The most common approach is annual layer counting, which is dependent on seasonally fluctuating signals. A regular distribution of precipitation, a high snow accumulation, and minimal post-depositional snow erosion at the site are general requirements for accurate counting of snow-layers. Seasonally varying parameters are given by the stable isotope ratio of hydrogen or oxygen in the water ($\delta^2\text{H}$, $\delta^{18}\text{O}$), concentrations of trace components (e.g., ammonium, mineral-dust related trace elements or black carbon) and the presence of melt layers may vary with the season (Uglietti *et al.*, 2016). Easily identifiable events of an absolute date (“reference horizons”) are a useful tool in the context of reliable dating (Maggi *et al.*, 2006). Prominent examples of these “reference horizons” are depicted by dust storm events, sulfate emissions due to volcanic eruptions (e.g., Tambora 1815) or radioactive fallouts such as the 1963 tritium peak from thermonuclear atmospheric tests or ^{136}Cs emissions due to the 1986 Chernobyl nuclear disaster. The tritium peak actually is used as a world-wide marker as it was found also in Antarctic ice cores with a delay of 2-3 years after emission (Maggi *et al.*, 1998).

Another frequently applied dating method is the use of the decay of radioactive isotopes. The naturally occurring radioisotope ^{210}Pb , which is continuously formed in the troposphere from ^{222}Rn , is determined by a half-life of 22.3 years and accessible for dating in the order of 100 years. It is deposited on the Earth’s surface by wet and dry deposition.

The radiocarbon (^{14}C) analysis is dependent on sufficient organic matter such as plant, wood or insect fragments, which are unfortunately rarely found in ice core sections at the desired depth and resolution. An alternative way for ^{14}C dating is based on extracting the water-insoluble organic carbon (WISOC) fraction of carbonaceous aerosol (Uglietti *et al.*, 2016). Continuous improvements of this approach, which can be used for older and deeper parts of ice cores, reduced the sample amount to 300-800 g, extracting ~10 μg of WISOC for analysis.

1.4 Sample Extraction and Aerosol Filtration

1.4.1 Solid Phase Extraction

Solid Phase Extraction (SPE) is a targeted form of sample preparation for the extraction and enrichment of analytes dissolved in a liquid. Today, SPE is a commonly used sample preparation technique with an enormous variety of specification towards specific analytes. The main procedural steps are characterized in Figure 1.5.

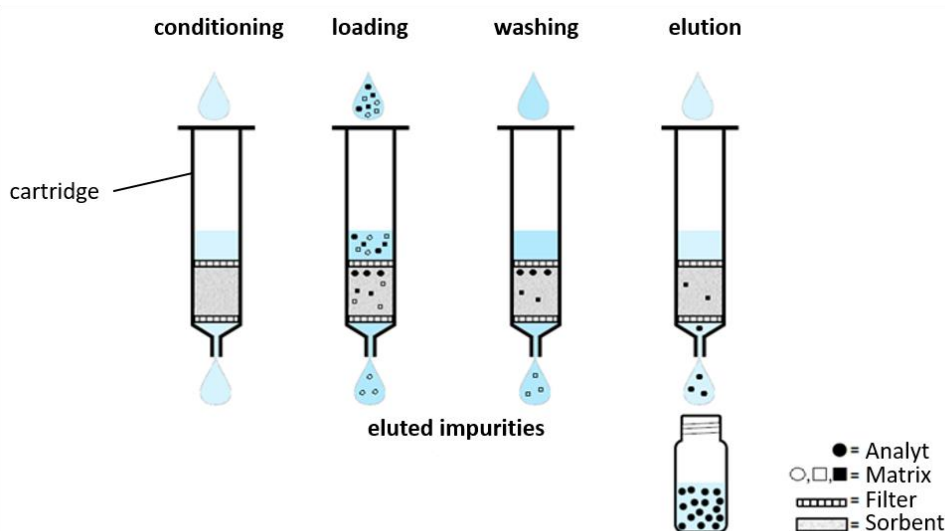


Figure 1.5 SPE procedure including the separate steps of conditioning, loading of the sample, washing, and elution of the analyte (modified from Thurman & Mills, 1998).

Typically, a polypropylene or glass cartridge contains the specific sorbent material which is placed between two filter frits. Prior to the application of the sample matrix, the sorbent material needs to be activated and possible contaminations have to be removed. This conditioning step is often composed of the addition of two or more solvents with different polarities. Subsequently, the pH of the sample is adjusted and the sample is loaded on the SPE cartridge by means of a reduced pressure or gravitational force only. The analyte of interest is retained through interactions with the functional groups of the sorbent, whereas other matrix compounds are eluted with the sample solution. Sufficient interaction between analyte and sorbent is crucial for SPE. Thus, the selection of sorbent material and flow rates largely affects the outcome of this technique. The elution of impurities can further be improved by an additional washing step with suitable solvents. Elution of the target analyte is performed by addition of a solvent with higher elution strength to weaken the linkage between sorbent and analyte.

Instead of enrichment of the analytes, SPE can also be used for a clean-up of samples and elimination of certain contaminations. In this case, the interaction between the sorbent and the contamination is high and the analyte is eluted during the loading and washing step.

The variety of specific sorbent materials and applications of SPE is immense, thus, comprehensive reviews and monographs can be found elsewhere (Hennion, 1999; Poole, 2003; Thurman & Mills, 1998). The most common sorbents are polymer based structures with different functional groups, strong/weak anion/cation exchange functionalities and silica-based materials modified with various chemical moieties like C_{18} or cyano groups (CN).

1.4.2 Filter Sampling

Filter sampling is one of the most common techniques to separate the particle phase from the gas phase due to its relative ease, flexibility, and low cost (Kulkarni *et al.*, 2011). Generally, filter holders and sampled filters do not require much space and are easy to transport and store. A typical setup including the essential components of a filter sampling system is presented in Figure 1.6.

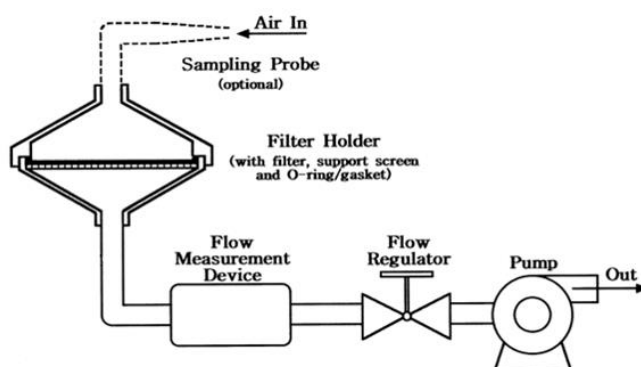


Figure 1.6 Schematic sketch of a filter sampling setup for aerosol measurement (Kulkarni *et al.*, 2011).

The setup is composed of an air inlet, a filter holder with an appropriate filter medium inside, a flow measurement device, a flow regulator, and a pump. Optionally, a pre-separator (e.g., impactor, cyclone) can be installed prior to the filter holder to exclude certain particle sizes from the airstream (e.g., PM_{10} , $PM_{2.5}$, PM_1). The accuracy of filter sampling and analysis is generally determined by two critical main steps. First, a convenient setup for filter sampling is mandatory to reduce sampling artifacts and increase the sampling efficiency. Second, the analytes on the sampled filters need to be extracted by suitable solvents and processed prior to analysis by the analytical apparatus. A reasonable compromise in terms of extraction efficiency, time and costs needs to be elucidated.

The main types of filters commonly used for aerosol measurement are fibrous filters, membrane filters, and capillary pore filters. However, a broad variety of filters, applications, and requirements exist. Thus, comprehensive reviews can be found elsewhere (Kulkarni *et al.*, 2011; Spurny, 1998).

1.5 Mass Spectrometry in the Field of Aerosol Research

The basic principle of mass spectrometry (MS) is the generation of ions from inorganic or organic compounds followed by their separation according to their mass-to-charge ratio (m/z). Quantitative, respectively qualitative information is given by detection of their m/z and the abundance (Gross, 2004).

In terms of the chemical analysis of atmospheric aerosol particles, MS provides high sensitivity with fast response times to chemically complex particles and is the most commonly applied technique (Farmer & Jimenez, 2010; Pratt & Prather, 2012b). In the context of aerosol research, we further distinguish between offline and online techniques. Generally, offline techniques provide much more detailed information on compound classes and individual compounds. Atmospheric particles are sampled (e.g., on filters) over several hours to days, undergo further sample preparation and are finally analyzed by MS techniques (Pratt & Prather, 2012a).

Online techniques provide high time resolution and the ability to examine the chemical composition and transformation of organic aerosols in real-time while eliminating potential artifacts due to long-term filter sampling (Pratt & Prather, 2012b).

A brief introduction of the applied methods and the differentiation of online and offline MS techniques is given in the following section. However, more detailed information of the current status of MS analysis in atmospheric chemistry can be found in recently published reviews (Laskin *et al.*, 2018; Nozière *et al.*, 2015; Pratt & Prather, 2012a, 2012b).

1.5.1 Offline Mass Spectrometry Techniques

Offline techniques commonly provide high selectivity and molecular speciation of aerosol components. Additionally, through the coupling of MS with pre-separation techniques more information within a single MS analysis can be obtained. Particles are mostly collected on quartz or polytetrafluoroethylene-coated filters. Another approach uses the technique of a Particle-into-Liquid Sampler (PILS), originally developed for the identification of inorganic ions present in aerosols, for the analysis of water-soluble organic aerosols (Bateman *et al.*, 2010; Weber *et al.*, 2001), whereas gases are sampled by suitable sorbents or in gas-tight containers. Afterwards, the samples are mostly processed by extraction or derivatization and analyzed in the laboratory. The most widely used separation methods in combination with MS are liquid chromatography (LC) and gas chromatography (GC) (Hallquist *et al.*, 2009).

LC-MS is nowadays a popular method for the analysis of medium polar to polar organic compounds in aerosol samples. The LC columns used in most of the studies contain reversed phase materials such as C18 or C8. However, a large variety of LC columns with differing functionalities in terms of polarity are commercially available. Particularly in combination with electrospray ionization (ESI), and in contrast to GC-MS, LC-MS is well suited to high-MW and polar molecules, without the need for derivatization prior to analysis (Hallquist *et al.*, 2009). For example, using LC-MS analyses it was shown

that sulfate, as well as nitrate groups, can be incorporated in SOA components (Iinuma *et al.*, 2007c; Surratt *et al.*, 2007; Surratt *et al.*, 2008). Detailed structural elucidation at a molecular level can further be performed by MSⁿ experiments using ion trap, quadrupole time-of-flight (QToF) or triple quadrupole MS. Moreover, unambiguous sum formulas can be obtained by the determination of the exact molecular mass of the analytes through ultra-high-resolution mass spectrometry (UHRMS), such as Fourier transform ion cyclotron resonance-MS or Orbitrap-MS. Furthermore, several of these instruments are nowadays capable of performing MS² analyses.

Besides the widespread use of the ESI technique, ionization for offline methods can also be ensured by atmospheric pressure chemical ionization (APCI) coupled to MS. In combination with high-performance liquid chromatography (HPLC), the soft ionization method is used for the determination of polar and ionic compounds, such as oxygenated polycyclic aromatic hydrocarbons (PAHs) in atmospheric aerosols (Cochran *et al.*, 2016; Lintelmann *et al.*, 2006).

Both, ESI and APCI are described as “soft” ionization techniques, as they are performed at atmospheric pressure and typically lead to the formation of ions with no or very little fragmentation of the analytes (Nozière *et al.*, 2015). Thus, the interpretation of highly complex MS data is facilitated.

Briefly, the ESI process is divided into three main steps: i) Formation of droplets at the needle tip connected to the HPLC outlet. ii) Decrease in droplet size due to evaporation of the solvent. iii) Formation of gaseous ions. A schematic sketch of the ESI process is illustrated in Figure 1.7.

The HPLC effluent flows through a small metal capillary to which a positive or negative electric field is applied between the tip of the metal capillary and a counter electrode at the inlet of the mass spectrometer. Ions with the desired polarity (i.e., positive or negative) are generated and transferred into the mass spectrometer by use of a vacuum interface. The electric field leads to a charge separation in the liquid and finally deformation of the meniscus into a so-called *Taylor cone* (Gross, 2004). As soon as a critical electric field strength is reached, the *Taylor cone* instantaneously forms a fine jet of liquid droplets. This jet further breaks up into a plume of smaller droplets which are pushed away from each other by Coulombic repulsion because of their charge.

The formation of gaseous ions is speculated by two different models: The *charge-residue model* (CRM) assumes an entire desolvation of an ion by loss of all solvent molecules from droplets that are sufficiently small to contain just one residual analyte molecule. A later theory of the *ion evaporation model* (IEM) describes the creation of desolvated ions in form of a direct evaporation from the surface of highly charged micro-droplets.

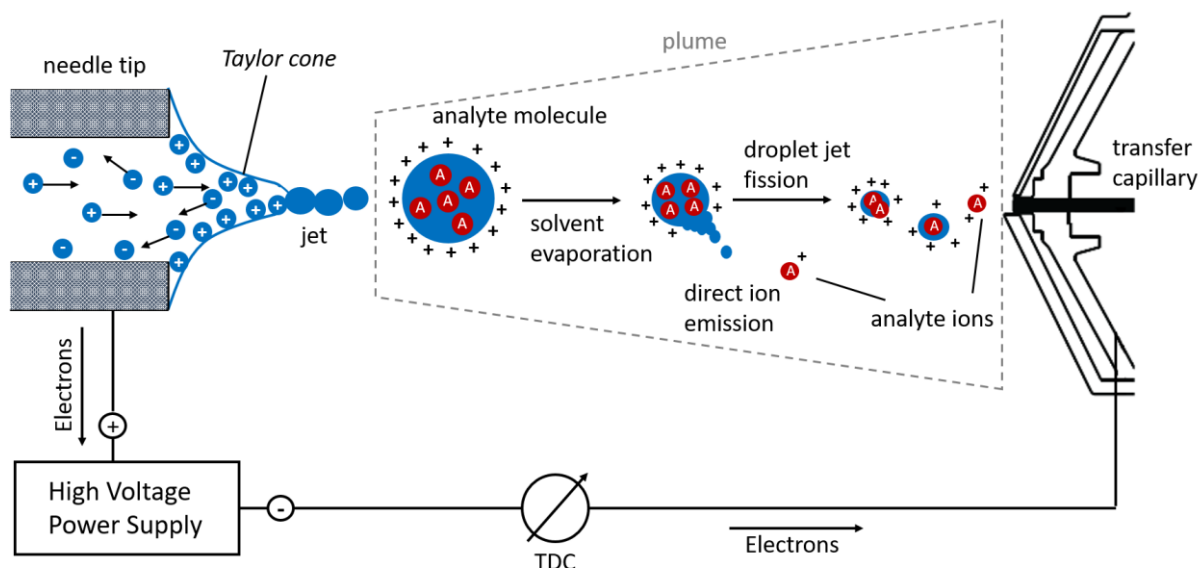


Figure 1.7 Schematic illustration of the ESI process. Highly charged droplets degenerate into smaller microdroplets. The formation of ions is illustrated by the IEM and the CRM model (adapted from Gross, 2004).

APCI was first described in 1975 as an LC-MS ionization method at atmospheric-pressure using ion-molecule reactions (Carroll *et al.*, 2002). A chemical ionization plasma is maintained by a corona discharge between a needle and a solvent spray chamber serving as counter electrode (Gross, 2004). The ions of the selected polarity are commonly transferred into the MS inlet by the same type of vacuum interface as employed in ESI.

1.5.2 Online Mass Spectrometry Techniques

Online MS techniques for the analysis of atmospheric aerosols can be subdivided into bulk aerosol MS and single-particle MS. Bulk measurements thermally vaporize thousands of particles and analyze the mean chemical composition, whereas single-particle MS techniques desorb particles separately using a pulsed laser ionization procedure (Pratt & Prather, 2012b).

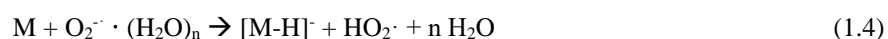
One of the main online instruments used for the characterization of submicron aerosol particles is the Aerodyne aerosol mass spectrometer (AMS) (Canagaratna *et al.*, 2007). Via a set of aerodynamic lenses, aerosol particles are drawn into a vacuum chamber and focused into a narrow particle beam. The compounds in the aerosol particle beam are thermally vaporized (~ 600 °C), ionized by electron ionization (EI) and analyzed by time-of-flight (ToF)-MS (Canagaratna *et al.*, 2007; DeCarlo *et al.*, 2006). The AMS is field-deployable and the 70 eV EI energy ensures quantitative ionization of all non-refractory compounds. Because of the rather limited mass resolution and the “hard” ionization technique, which induces a high degree of fragmentation of organic compounds, the identification and quantification of individual organic molecules is often impossible, thus, leading to lower level of chemical information about the organic fraction of atmospheric aerosol particles.

Accordingly, several instrumental techniques were recently developed to fill this gap and enhance the molecular characterization of organic aerosol components. Lopez-Hilfiker et al. developed a Filter Inlet for Gases and AEROsols (FIGAERO) coupled to a high-resolution time-of-flight chemical ionization mass spectrometer (HR-ToF-CIMS), which has been deployed to a variety of laboratory chambers and field sites (Lopez-Hilfiker *et al.*, 2014). As the name indicates, the FIGAERO allows measurement of both gas and particle molecular composition. While analyzing gases, particulate matter is collected on a Teflon[®] filter via a separate dedicated sampling port. A moveable tray simultaneously switches the sample flow entering the instrument between the two operating modes, i.e., the gas phase and collection mode and the filter analysis mode. The analysis of the collected particles is performed by a temperature-programmed thermal desorption using high purity N₂ as carrier gas. Additionally to the recorded mass spectra, a desorption thermogram of SOA can provide insights into molecular compositions and/or particle morphology (Lopez-Hilfiker *et al.*, 2014).

Intact molecular ions with little fragmentation of the favored organic compounds are also detected with “soft” ionization methods at atmospheric pressure, such as the Aerosol Flowing Atmospheric-Pressure Afterglow Mass Spectrometry (AeroFAPA-MS) (Brüggemann *et al.*, 2015; Brüggemann *et al.*, 2017). Other approaches modified the known ESI method, namely Extractive Electrospray Ionization (EESI), to allow direct characterization of organic compounds from a flow of aerosols (Gallimore *et al.*, 2017; Gallimore & Kalberer, 2013).

Previously, conventional atmospheric pressure chemical ionization mass spectrometry (APCI-MS) was also used for the online measurement of organic acids present in organic aerosols (Hoffmann *et al.*, 2002; Kückelmann *et al.*, 2000; Vogel *et al.*, 2013). The fundamental principles of the application in conjunction with HPLC or the ionization of aerosol particles are identical. The APCI ion source vaporizes an aerosol particle stream in a heated ceramic tube whereupon the evaporated molecules are ionized in the gas phase by a corona discharge between a needle and the transfer capillary of the MS. Depending on the polarity of the ion source, positive or negative ions are transferred into the vacuum system of the MS.

The basic chemical reactions leading to the ionization of the molecules in both ionization modes are shown in equation 1.3 and 1.4:



In negative ion mode, O₂⁻ ions in form of water clusters are produced at atmospheric pressure by the corona discharge. The O₂⁻ x H₂O-ions act as the chemical ionization reagent for the vaporized compounds. Analytes having a higher gas-phase acidity than O₂⁻ become ionized by proton transfer reactions forming the corresponding deprotonated ion [M-H]⁻ and HO₂.

In positive ion mode, sample ionization occurs in a series of reactions that start with the electron-initiated cation formation. Briefly, a combination of molecular collisions and charge transfer processes lead to the formation of a gas plasma. N_2^+ radicals are generated in the corona discharge region. Subsequent ion-molecule interactions with atmospheric water vapor eventually produce H_3O^+ ions which can undergo proton transfer reactions with analyte molecules, resulting in the protonated ion $[M+H]^+$ and H_2O .

1.5.3 Orbitrap Mass Spectrometry

Ultra-High-Resolution Mass Spectrometry (UHRMS) techniques, such as Fourier transform ion cyclotron resonance MS (FTICR-MS) or Orbitrap MS have successfully been introduced into the field of aerosol research in the past few years. As the main instrument applied in this study was an Orbitrap mass spectrometer a brief description will be given in the following.

The Orbitrap mass analyzer depicts a rather new type of mass spectrometers invented by Makarov and later commercialized by Thermo Fisher (Hu *et al.*, 2005; Makarov, 2000). The main characteristics of the Orbitrap are the high mass resolution (e.g., $R=140\,000$ @ m/z 200 for the Q Exactive version) and high mass accuracy (<2 ppm) which is comparable to FTICR-MS. Nonetheless, in contrast to FTICR-MS, the Orbitrap works without the need of a magnetic field which results in lower costs and lower space requirements. However, both instruments make use of an image current technique and subsequent Fourier transformation of the transient signal for detection of ions and generation of mass spectra. A schematic of a Hybrid-Orbitrap MS is shown in Figure 1.8.

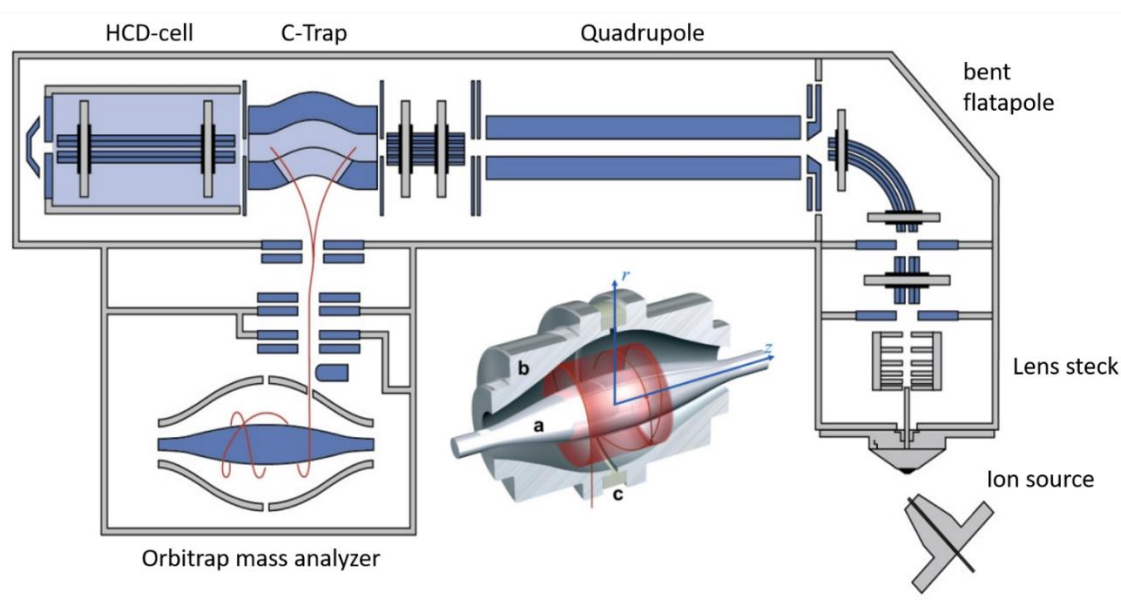


Figure 1.8 Schematic illustration of the Q Exactive Orbitrap MS (adapted from Thermo Fisher Scientific). The inset shows a cross-section of the Orbitrap mass analyzer consisting of a) a spindle-shaped central electrode, b) a barrel-shaped outer electrode, composed of two parts, and c) a ceramic ring for separation. Moving of ions along the z-axis is indicated by red orbits (Scigelova & Makarov, 2006).

The ions are generated by an ion source (i.e., commonly ESI or APCI) and transferred by a vacuum and electric fields to the inlet system. The ions are focused by a lens stack and further transmitted by a bent flatpole to a quadrupole for optional pre-selection of ions. Subsequently, the ions reach a curved linear trap for injection (C-Trap). In the C-trap, ions are focused by collisional cooling and transmitted either directly to the Orbitrap mass analyzer for detection or into the higher-energy collisional dissociation (HCD) cell for fragmentation. For MS² analysis, the fragmented product ions are again focused in the C-Trap and injected to the Orbitrap for detection.

The depicted cross-section of the Orbitrap shows, that it consists of a spindle-shaped electrode in the center and an outer barrel-shaped electrode, which is split in the middle by a ceramic ring. The ions are injected into the Orbitrap perpendicular to the z-axis and trapped in the space around the central electrode in an electrostatic field. The ions are forced to a rotational movement around the central electrode and an axial oscillation along the axis of the electrode caused by the electrostatic field gradient and the tangential injection. Due to the spindle-shaped central electrode, the movement of the ions is described to oscillate around the central electrode on complex orbits.

The axial harmonic oscillation ω_z is described by equation (1.5):

$$\omega_z = \sqrt{\left(\frac{z}{m}\right)k} \quad (1.5)$$

This harmonic oscillation frequency ω_z (in rad/s) is inversely proportional to the square root of the mass to charge ratio m/z of the ions, where k is the force constant of the electrical potential. Accordingly, the frequency ω_z is not dependent on the tangential velocity or the distribution of the oscillating ion, but correlates solely to the corresponding m/z ratio. All ions show the same amplitude but move with different frequencies depending on their m/z ratio. The frequency of the harmonic axial oscillation induces an image current which is detected by the two halves of the barrel-shaped coaxial outer electrode. The deconvolution of the image current by fast Fourier transformation finally results in an ultra-high-resolution mass spectrum (Gross, 2013).

1.6 Thesis Objectives and Outline

Complex matrices like ambient aerosols or ancient ice core records typically comprise thousands of different chemical compounds at low concentrations. Investigating the chemical composition of such samples is thus a challenging task, which demands analytical developments and adaptations of existing techniques. The analytical method needs to combine high sensitivity and the ability to detect a broad range of molecular masses to allow identification and quantification of the analytes of interest. In this respect, mass spectrometry (MS) was shown to be a promising choice for such endeavors, as it requires only an infinitesimal amount of material and the detection of the analytes can be performed either directly or after sample processing in the laboratory. Although MS has been proven to be a versatile and

powerful tool in the field of aerosol research, the identification and trace analysis of single organic molecules still demands improvements. In particular, state of the art ultra-high-resolution mass spectrometric techniques, such as the Orbitrap mass spectrometer, are not yet fully established in this field of research, offering promising approaches to enable new insights by providing more detailed information on the organic fraction of ambient aerosols, which were not accessible previously.

Concerning contrasting definitions of “high mass resolution” in the context of online mass spectrometric techniques, however, no instrumentation is capable to unambiguously identify the MS signals, especially at high m/z , without adjacent multiple “peak-fitting”.

The aim of this work was the development and application of an analytical method for trace analysis of single organic compounds in ice core records and aerosol particles, enabling the identification of single molecules as well as a comprehensive characterization of the organic fraction of atmospheric aerosols. Furthermore, a real-time analysis method for organic aerosol particles was supposed to be established, applying UHRMS and taking advantage of its unique features compared to common MS-based techniques.

The first two parts of this study focus on two applications of offline mass spectrometry techniques in conjunction with ultra-high-performance liquid chromatography (UHPLC). The development of an analytical method for the quantitative analysis of polar organic molecules in ice cores is presented. For purification and enrichment of the analytes, an SPE procedure using anion exchange functionalities was developed. Recovery rates and limits of detections (LODs) for single proxy compounds were determined. As a proof of principle, the developed method was applied for the analysis of an ice core from the Belukha glacier in the Altai Mountains. In the second part of the offline mass spectrometry techniques, filter samples from the Cosmics Leaving Outdoor Droplets (CLOUD) campaign at the European Organization for Nuclear Research (CERN) were qualitatively analyzed by a non-target approach. The experiments at CLOUD 10 were designed to mimic the natural conditions of the boreal forest site at Hyytiälä, Finland. Detailed data on the molecular characterization of highly controlled laboratory chamber experiments at atmospheric conditions allow novel insights into the organic composition of ambient submicron organic aerosol. The large amount of high-resolution data is presented in several visualization methods which aim to group and identify the organic molecules.

The third part of this study focusses on the development and application of UHRMS in combination with APCI for real-time analysis of SOA. The online APCI-Orbitrap-MS setup was characterized by measuring organic test aerosols containing common biogenic SOA marker compounds. Instrumental settings were optimized to obtain the lowest achievable detection limits, typically in the ng m^{-3} range. As a proof-of-principle, the composition of ambient aerosols was analyzed by sampling $\text{PM}_{2.5}$ particles from the outside of the laboratory building. Both, the quantification of single compounds in ambient aerosols and a comprehensive characterization by a non-target screening approach in negative and positive ionization mode were realized.

2 Organic Trace Analysis in Ice Cores

2.1 Introduction

Previously, most ice core studies focused on inorganic species, especially sulfate (Preunkert *et al.*, 2001; Schwikowski *et al.*, 1999), nitrate (Mayewski *et al.*, 1986; Preunkert *et al.*, 2003), ammonium and heavy metals (Barbante *et al.*, 2004; Gabrielli *et al.*, 2005). In contrast, organic compounds have been analyzed to a much smaller extent in ice cores (Giorio *et al.*, 2018; Legrand *et al.*, 2013). Concentrations of monocarboxylic acids, mainly formic acid and acetic acid, which also play a role in the acidity of precipitation, have been determined in ice cores from the Alps (Legrand *et al.*, 2003), Greenland (Legrand *et al.*, 1992; Legrand & Angelis, 1996) and Antarctica (Angelis *et al.*, 2012). These compounds have been attributed to emissions from vegetation emission, boreal forest fires or anthropogenic sources. Historic records of dicarboxylic acids (C₂-C₁₀), oxocarboxylic acids (C₂-C₉) and α -dicarbonyls (C₂-C₃) in an ice core from Greenland were reported by Kawamura *et al.* (Kawamura *et al.*, 2001). Long-chain carboxylic acids (C₁₄-C₂₂) were also detected in an ice core from Greenland (Kawamura *et al.*, 1996). As a marker for the oxidative capacity of the atmosphere, formaldehyde was analyzed in a firn core from Lys glacier (Largiuni, 2003) as well as in ice cores and snow from Greenland (Hutterli, 2003; Staffelbach *et al.*, 1991). Also, polycyclic aromatic hydrocarbons (PAHs) were determined in ice cores (Gabrieli *et al.*, 2010). Nevertheless, these organic species still represent only a very small fraction of the total organic material within ice cores. Thus, a wealth of information remains uncollected and a characterization of a larger fraction of the organic material present in ice and snow is highly desirable.

One of the most important sources of atmospheric aerosols are vegetation-derived organic aerosol components. In principle, pollen could be a major source of paleoclimatic proxy data for terrestrial environments. However, although some studies were conducted on polar ice cores (Bourgeois, 1986; Short & Holdsworth, 1985), pollen concentrations are typically very low in ice cores due to the large size of pollen (> 10 μm) and the resulting short atmospheric lifetime. For submicrometer aerosol, which possesses a much longer atmospheric lifetime and therefore larger transport distances, the largest contribution comes from biogenic SOA compounds. These compounds are formed from the oxidation of biogenic VOCs released in large quantities from terrestrial vegetation (Hallquist *et al.*, 2009). After the release of the precursor molecules (e.g., isoprene, monoterpenes, sesquiterpenes), the VOCs are rapidly oxidized and a fraction of the products undergoes gas-to-particle conversion (Hoffmann *et al.*, 1997). Since it is believed that SOA can also represent a significant source of new particles, especially in pristine remote regions, and – after their growth into the accumulation mode – can ultimately act as cloud condensation nuclei (CCN), pre-industrial and biogenic SOA is a key parameter that needs to be understood in order to quantify the anthropogenic climate forcing effect from aerosol pollution (Gordon *et al.*, 2016; Kirkby *et al.*, 2016). Only a few selected biogenic SOA markers have already been measured in ice cores (Müller-Tautges *et al.*, 2016) and arctic aerosol (Fu *et al.*, 2016). However,

additional individual biogenic SOA molecules do exist and have the potential to deliver more detailed information about the vegetation itself (sesquiterpene markers and multiple monoterpene markers) (Acosta Navarro *et al.*, 2014). Another source of vegetation-derived organic aerosol components is biomass burning (BB), which is suggested to be the most important parameter for the molecular composition of organic molecules present in ice (Müller-Tautges, 2014). The analysis of various biomass burning markers is essential. Ice cores and snow pit samples contain specific molecular markers and other pyrochemical evidence which provide much-needed information about the role of fire in the past climate and the possibility of current biomass burning affecting future global climate (Kehrwald *et al.*, 2012). Kehrwald *et al.* (2012) classified four chemical groups that can be used as proxies for fire-history reconstruction from ice cores: (I) monosaccharide anhydrides, (II) small carboxylic acids, (III) polycyclic aromatic hydrocarbons, and (IV) lignin burning products (Kehrwald *et al.*, 2010). Today, the most important tracer compound for biomass burning is levoglucosan (1,6-anhydro- β -D-glucopyranose), as it is only formed from cellulose at temperatures above 300 °C. Levoglucosan is generated from combustion of all types of cellulose-containing plant matter and is therefore not specific to a particular plant type or ecosystem (Simoneit *et al.*, 1999). Levoglucosan is injected into the atmosphere in convective smoke plumes, deposited on glacier surfaces through wet and dry deposition, and preserved in snow and ice (Gambaro *et al.*, 2008; Kehrwald *et al.*, 2012; Zennaro *et al.*, 2014). It has also been detected in several aerosol samples from urban, remote continental, marine as well as arctic sites (Kawamura *et al.*, 2012). Nonetheless, there is an intensive debate about the atmospheric reactivity of levoglucosan and its suitability as a quantitative tracer for aerosol source apportionment (Hoffmann *et al.*, 2010; Slade & Knopf, 2013). A recently proposed class of alternative biomass burning markers, correlating with levoglucosan, are methyl-nitrocatechols (Iinuma *et al.*, 2010). These SOA compounds originate from oxidations of VOCs emitted upon biomass burning and are supposed to influence the effect of aerosols on the Earth's albedo through absorption of light in the Ultraviolet-visible spectroscopy (UV/Vis) range (Kahnt *et al.*, 2013; Kitanovski *et al.*, 2012). Historic records of nitrocatechols are lacking and appropriate methods for the simultaneous detection of molecular tracers will contribute to a better understanding of (historic) biomass burning events.

Important quality criteria for suitable organic marker compounds are stability against chemical degradation and low volatility as a key parameter, determining their atmospheric lifetime. In fact, the atmospheric lifetime of many organic SOA markers, including biogenic SOA marker from isoprene, monoterpenes, and aromatics, are rather short (<1 day) (Nozière *et al.*, 2015). However, transport times of continental air masses carrying vegetation-derived marker compounds to the site of deposition are mostly in the range of several days to tens of days, in particular, in case of transport to Antarctica (Stohl & Sodemann, 2010).

As appropriate marker compounds for biogenic SOA are currently considered the low-volatile monoterpene marker 3-methyl-1,2,3-butanetricarboxylic acid (MBTCA), formed by OH radical initiated oxidation of *cis*-pinonic acid (Donahue *et al.*, 2012; Müller *et al.*, 2012; Szmigielski *et al.*,

2007), as well as several sesquiterpene oxidation products (van Eijck *et al.*, 2013). Besides isoprene and monoterpenes, sesquiterpenes play an important role in the formation of SOA due to the relatively low volatility of oxidation products and a high reactivity towards O₃ (Hallquist *et al.*, 2009). Various coniferous and deciduous plants are the main emitter of sesquiterpenes (Helmig *et al.*, 2007).

Furthermore, there exist also alternative organic biomass burning markers other than levoglucosan. Lignin, a major biopolymer in wooden tissue, derived mainly from the three aromatic alcohols p-coumaryl alcohol, coniferyl alcohol and sinapyl alcohol, whose proportions differ significantly among different plant classes (Simoneit, 2002). The proportions of the emitted combustion products are, therefore, also based on different types of biomass (Fine *et al.*, 2004).

Fatty acids are described to be more specific for source apportionment than C₁-C₁₀ mono- and dicarboxylic acids because of their lower volatility and decreased reactivity to oxidants in the atmosphere. They are not affected by direct photochemical reactions in the troposphere and their sources are limited to biological, but also anthropogenic activities (Fang *et al.*, 2002). Major sources of fatty acids are terrestrial plant waxes and marine organisms (Pokhrel *et al.*, 2015).

This chapter focusses on the development and application of a single, comprehensive trace analytical method for the sensitive quantification of new and more appropriate low-volatile marker compounds in snow and ice samples, originating from biogenic SOA or biomass burning events. Moreover, it is desired to compare these new markers simultaneously with already established compounds representative for vegetation, SOA, and biomass burning in a comprehensive analytical method.

2.2 Experimental: Method Development

2.2.1 Chemicals and Materials

Pimelic acid (96 %), 4-nitrocatechol (97 %), acetosyringone (97 %), *cis*-pinonic acid (98 %), salicylic acid (99 %), ketopinic acid (99 %), cinnamic acid (97 %), nonadecanoic acid (≥ 99.5 %), octacosanoic acid (≥ 98.5 %), tricosanoic acid (99 %), oleic acid (99 %), hexacosanoic acid (≥ 95 %), behenic acid (≥ 99 %), myristic acid (≥ 99.5 %), levoglucosan (99 %), lauric acid (> 99.5 %), BTCA (1,2,4-butanetricarboxylic acid, ≥ 88 %), terebic acid, heptadecanoic acid (≥ 98 %), formic acid (eluent additive for LC-MS) and ammonium hydroxide solution (p.a.) were purchased from Sigma-Aldrich (Steinheim, Germany). Vanillin (99 %) and p-hydroxybenzoic acid (99 %) were obtained from Acros Organics (Geel, Belgium). Vanillic acid (98 %) was purchased from Alfa Aesar (Heysham, UK). Pinic acid (3-Carboxy-2,2-dimethyl-cyclobutaneacetic acid) was synthesized according to a protocol by Moglioni *et al.* (Moglioni *et al.*, 2000). MBTCA (3-methyl-1,2,3-butanetricarboxylic acid) was synthesized following a protocol by Dette *et al.* (Dette *et al.*, 2014). β -nucaryophyllonic acid, β -caryophyllinic acid, and β -caryophyllonic acid were synthesized by A. van Eijck (van Eijck *et al.*, 2013).

Acetonitrile (Optima[®] LC-MS grade), Methanol (Optima[®] LC-MS grade) and water (Optima[®] LC-MS grade) were purchased from Fisher Scientific (Geel, Belgium). Formic acid ($\geq 98\%$) was purchased from Carl Roth (Karlsruhe, Germany). D-malic acid ($> 99.5\%$) was obtained from Merck. SPE cartridges (Oasis MAX 1cc, 10 mg, 30 μ m) were purchased from Waters (Milford, USA).

2.2.2 Solid Phase Extraction

Conditioning of the SPE cartridges was performed by successive equilibration with 2.5 mL methanol and 2.5 mL water followed by 4 mL ammonium hydroxide solution (5 %) for pH adjustment (i.e., pH 7 - 8). Similarly, the pH of the samples was adjusted to pH 7 - 8 by adding ammonium hydroxide solution (5 %). At the last equilibrium step, a volume of about 0.5 mL of the solution was left in the cartridges to prevent the sorbent from running dry before the sample flow was applied to the sorbent material. The samples (19 inner parts and 9 outer parts of the ice core, 12 - 43 mL) were applied to the cartridges using appropriate adapters and reservoirs. Throughout the loading and elution step of the sample, the flow rate was adjusted to less than 1 mL/min to ensure complete retention. Figure 2.1 shows the SPE extraction process during the loading of the SPE cartridges.



Figure 2.1 The picture shows the cartridges placed onto the upper part of the vacuum manifold during the loading process. The filled sample reservoirs are connected to the SPE cartridges via an adapter. The flow-through is collected in glass vials.

After loading the sample on the cartridge, a washing step was performed by adding 2.5 mL water followed by 2.5 mL ammonium hydroxide solution (5 %). The cartridges were emptied to dryness by a reduced pressure for about 30 s before elution. Elution was performed manually by gravitational force with 1 mL of formic acid in methanol (5 %). The eluate was reduced to a volume of $\sim 150\ \mu\text{L}$ at $40\ ^\circ\text{C}$ by means of a gentle nitrogen stream. The elution step was repeated two times. After the last extraction step, the residual eluate was evaporated to almost complete dryness and dissolved in $500\ \mu\text{L}$

water/acetonitrile (8/2). Subsequently, the solution was mixed by a vortex shaker and analyzed by Ultra-High-Performance Liquid Chromatography coupled to Ultra-High-Resolution Mass Spectrometry (UHPLC-UHRMS).

2.2.3 Ultra-High-Performance Liquid Chromatography–Mass Spectrometry

The chromatographic analysis was performed by an UltiMate 3000 UHPLC system (Dionex, Thermo Scientific, Germany) composed of a degasser, binary gradient pump, auto sampler, and temperature column compartment. The analytical column (Hypersil Gold, C18, 50x2.1 mm, 1.9 μm , Thermo Scientific) was tempered to 25 $^{\circ}\text{C}$ during analysis. Via a tee-union, post-column injection of 50 mM NH_4OH in methanol was performed by an isocratic solvent delivery system (S1021, Sykam, Germany) with a flow rate of 150 $\mu\text{L}/\text{min}$. The tee-union was installed prior to the divert valve to ensure a steady mixing ratio before switching the valve to the MS position. As eluents, ultrapure water with 2 % acetonitrile and 0.04 % formic acid (Eluent A) and methanol (Eluent D) were used in gradient mode with a flow rate of 350 $\mu\text{L}/\text{min}$. The optimized gradient was 1 % D at 0 min, 1 % D at 1.2 min, 30 % D at 3.3 min, 30 % D at 5 min, 95 % D at 7.5 min, 95 % D at 13.8 min, 1 % D at 14.1 min, and 1 % D at 14.3 min. The injection volume was 20 μL per run and every sample was measured in triplicate. High-resolution mass spectra were obtained by a Q ExactiveTM hybrid quadrupole Orbitrap mass spectrometer (Thermo Scientific, Germany). Ionization of the analytes was performed by a heated ESI source at 150 $^{\circ}\text{C}$ operated in the negative ionization mode. A schematic overview of the setup is shown in Figure 2.2. The settings of the heated ESI source were as follows: 40 psi sheath gas, 20 psi aux gas, 4.0 kV spray voltage, and 320 $^{\circ}\text{C}$ capillary temperature. The Full-MS mode was operated within a scan range of m/z 70-500 with a mass resolution setting of $R = 70\,000$ at m/z 200. The MS² mode was operated using individual inclusion lists with an isolation width of m/z 1 and a mass resolving power of $R = 17\,500$ at m/z 200. Data processing was performed using XCaliburTM 2.2 (Thermo Scientific, USA). The Q Exactive mass spectrometer was calibrated by a commercially available calibration mix (PierceTM Negative Ion Calibration Solution, Thermo Fisher). Additionally, the calibration range to lower masses was optimized prior to analysis using a 2 mM sodium acetate solution in water/acetonitrile (1/1).

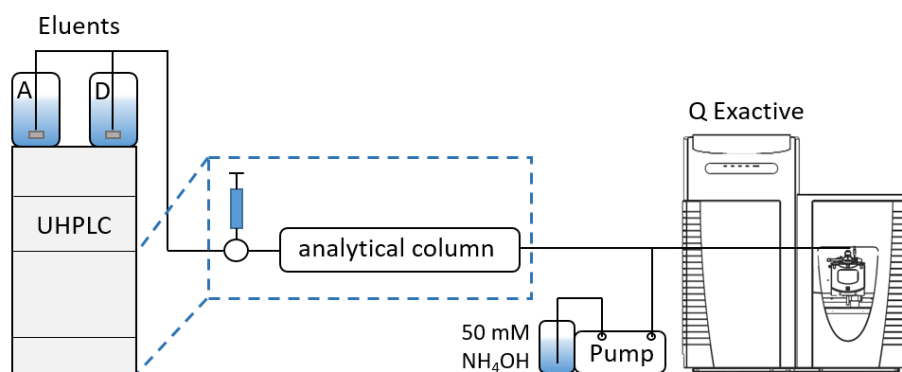


Figure 2.2 Schematic figure of the UHPLC system and post-column injection of 50 mM NH_4OH via an external pump.

2.2.4 Preparation of Standards

Stock solutions for quantification and method development of pimelic acid, *cis*-pinonic acid, 2-methyltetrols, levoglucosan, salicylic acid, terebic acid, BTCA, D-malic acid, oleic acid, heptacosanoic acid, keto-pinic acid, lauric acid, palmitic acid, hexacosanoic acid, heptadecanoic acid, nonadecanoic acid, myristic acid, behenic acid, octacosanoic acid, and tricosanoic acid were prepared in a concentration of 100 $\mu\text{g}/\text{mL}$ in acetonitrile. A solution containing 1 $\mu\text{g}/\text{mL}$ of each standard was prepared by diluting the stock solutions with acetonitrile. Packed in dry ice, the solution was sent to Mainz, Germany and stored at $-20\text{ }^\circ\text{C}$ until usage. Stock solutions of pinic acid, MBTCA, 4-hydroxybenzoic acid, vanillic acid, 4-nitrocatechol, vanillin, β -caryophyllonic acid, β -caryophyllinic acid, β -nocaryophyllonic acid, cinnamic acid, and acetosyringone were prepared in a concentration of $\sim 3\text{ mg}/\text{mL}$ and diluted with methanol to a solution containing 1 $\mu\text{g}/\text{mL}$ of each standard and stored at $-20\text{ }^\circ\text{C}$ until needed.

Calibration standards were prepared before usage by transferring distinct volumes of the standard solutions. Table 2.1 shows the calibration standards and the corresponding ions for detection and quantification.

Table 2.1 Analytes for quantification and method development.

precursor/class	analyte	elemental composition	m/z ([M-H] ⁻)	MS ² fragment for quantification (m/z)	neutral loss
biogenic	D-malic acid	$\text{C}_4\text{H}_6\text{O}_5$	133.0142	115.0036	$-\text{H}_2\text{O}$
anthropogenic	pimelic acid	$\text{C}_7\text{H}_{12}\text{O}_4$	159.0663	97.0658	$-\text{CH}_2\text{O}_3$
BB, cellulose	levoglucosan	$\text{C}_6\text{H}_{10}\text{O}_5$	161.0455		
BB, phenolic	salicylic acid	$\text{C}_7\text{H}_6\text{O}_3$	137.0244	93.0345	$-\text{CO}_2$
	4-hydroxybenzoic acid	$\text{C}_7\text{H}_6\text{O}_3$	137.0244	93.0345	$-\text{CO}_2$
	cinnamic acid	$\text{C}_9\text{H}_8\text{O}_2$	147.0451		
	4-nitrocatechol	$\text{C}_6\text{H}_5\text{N}_1\text{O}_4$	154.0145	124.0165	$-\text{NO}$
BB, methoxyphenolic	vanillin	$\text{C}_8\text{H}_8\text{O}_3$	151.0400	136.0165	$-\text{CH}_3$

2.3 Experimental: Belukha Glacier Ice Core Sections

	vanillic acid	C ₈ H ₈ O ₄	167.0349	152.0115	-CH ₃
	acetosyringone	C ₁₀ H ₁₂ O ₄	195.0662	180.0402	-CH ₃
isoprene	2-methyl-tetrols	C ₅ H ₁₂ O ₄	135.0663		
monoterpene	keto-pinonic acid	C ₁₀ H ₁₄ O ₃	181.0870		
	cis-pinonic acid	C ₁₀ H ₁₆ O ₃	183.1027	57.0345	-C ₇ H ₁₀ O ₂
	terebic acid	C ₇ H ₁₀ O ₄	157.0506	113.0608	-CO ₂
	pinic acid	C ₉ H ₁₄ O ₄	185.0819	141.0920	-CO ₂
	BTCA	C ₇ H ₁₀ O ₆	189.0405	127.0401	-CH ₂ O ₃
	MBTCA	C ₈ H ₁₂ O ₆	203.0561	185.0454	-H ₂ O
sesquiterpene	β-caryophyllonic acid	C ₁₅ H ₂₄ O ₃	251.1653	57.0345	-C ₁₂ H ₁₈ O ₂
	β-caryophyllinic acid	C ₁₄ H ₂₂ O ₄	253.1445	209.1546	-CO ₂
	β-nocaryophyllonic acid	C ₁₄ H ₂₂ O ₄	253.1445	57.0345	-C ₁₁ H ₁₆ O ₃
fatty acids	lauric acid	C ₁₂ H ₂₄ O ₂	199.1704		
	myristic acid	C ₁₄ H ₂₈ O ₂	227.2017		
	heptadecanoic acid	C ₁₇ H ₃₄ O ₂	269.2486		
	oleic acid	C ₁₈ H ₃₄ O ₂	281.2486		
	nonadecanoic acid	C ₁₉ H ₃₈ O ₂	297.2799		
	behenic acid	C ₂₂ H ₄₄ O ₂	339.3269		
	tricosanoic acid	C ₂₃ H ₄₆ O ₂	353.3425		
	hexacosanoic acid	C ₂₆ H ₅₂ O ₂	395.3895		
	heptacosanoic acid	C ₂₇ H ₅₄ O ₂	409.4051		
	octacosanoic acid	C ₂₈ H ₅₆ O ₂	423.4208		

2.3 Experimental: Belukha Glacier Ice Core Sections

As a proof of principle, we analyzed Ice core sections from the continental Siberian Altai (49°48′26″N, 86°34′43″E, 4062 m a.s.l.). The Altai mountain range is located on the boundary between Russia, Kazakhstan, China, and Mongolia exhibiting the highest degree of continentality in the world (Eichler *et al.*, 2009). It's location directly south of the Siberian forests represents unique information about biogenic emissions in the pre-industrial era. Precipitation in the Altai area mainly occurs in summer season. The accumulation record shows no long-term trend and an average accumulation of 0.5 m water equivalent per year (Henderson *et al.*, 2006). Vegetation in the Altai area is mainly dominated by boreal forest (Pines and Birch) and lowland feather-grass steppes (Eichler *et al.*, 2011). Figure 2.3 shows the location of the Belukha glacier and a section of the ice core prior to analysis.

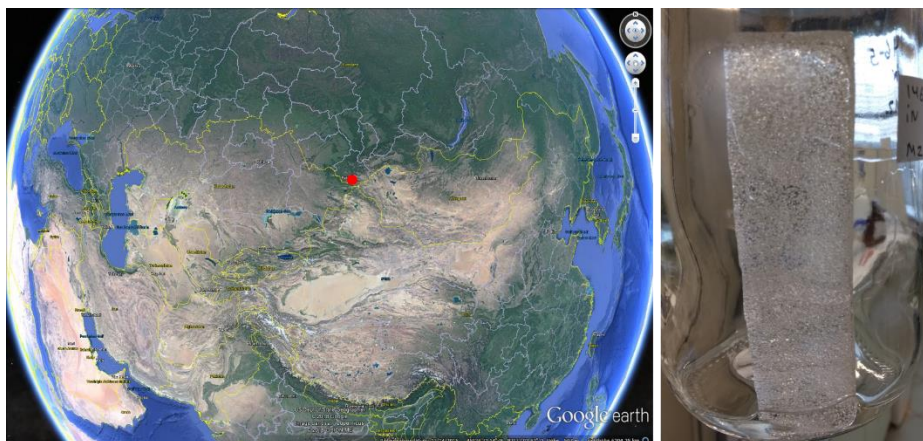


Figure 2.3 (left) Map showing the location of the Belukha glacier (red dot) in the Altai mountain range (Reference: Google Earth 7.1.5, 2015). (right) Section of a measured ice core before melting.

The ice core was drilled in 2001 by a team from the Paul Scherrer Institute (PSI), Villigen, Switzerland. An ice core with a length of 140 m and an inner diameter of 7.8 cm was recovered. Further information on the ice core drilling and dating can be found in the literature (Henderson *et al.*, 2006; Olivier, 2003). The ice core sections for our study date from 1866 – 1869 and 1826 – 1828. In a cold room at PSI in Villigen, Switzerland, 19 inner parts and 9 outer parts of the sections were cut out from the ice core using a band saw. 28 aliquots of the sections and three high-purity ice blank samples with a length of approximately 10 cm and volumes between 12 to 43 mL were stored separately in thoroughly cleaned glass jars. The cleaning process included a bake out of the glassware at 450 °C for more than 8 h. The sample-containing glass pots were closed tightly using PTFE-coated screw caps and sealed from the outside with Parafilm®. The sections were transported to Mainz and stored at -20 °C until analysis. The ice core sections were melted at room temperature prior to analysis.

2.3.1 Principal Component Analysis

A principal component analysis (PCA) was performed to group the analyzed compounds and to elucidate possible connections. The PCA was calculated by IBM® SPSS® Statistics 23 software and based on the dataset including the inside and outside sections of the ice core. Briefly, a PCA is used to convert and reduce a dataset of possibly correlated signals (variables) into a set of principal components (PCs) that are independent of each other and explain a certain proportion of the variance of the data. However, the main goals are to extract the most important information from a dataset, to compress and simplify the size of the dataset and to analyze the structure of the observations and variables (Abdi & Williams, 2010).

2.4 Results and Discussion: Method Development

2.4.1 Ultra-High-Performance Liquid Chromatography-Mass Spectrometry

A UHPLC-MS method for the chromatographic separation and quantification of organic species in ice cores was developed using standard analytes. Ionization parameters, heated ESI temperatures and flow rates of sheath- and auxiliary gases were optimized for maximum signal intensity and analytical stability in the negative ionization mode. For chromatographic separation, two commercially available UHPLC columns, a Hypersil Gold PFP (PFP, 50x2.1 mm, 1.9 μ m, Thermo Scientific) and a Hypersil Gold (C18, 50x2.1 mm, 1.9 μ m, Thermo Scientific), were tested for retention behavior. In general, the best results concerning separation and temporal distribution during the chromatographic run were obtained using the Hypersil Gold C18 column. Afterwards, method development was continued using binary mixtures of acetonitrile/water and methanol/water in gradient elution mode. Generally, the gradient systems exhibited only minor differences in peak shape and retention times (Rt). However, for very polar hydrophilic compounds like levoglucosan, D-malic acid, and 2-methyltetrols very short retention times, but better peak shapes were obtained with methanol/water gradients. Considering the high diversity of polarities of the analytes, a two-plateau gradient using methanol and water gave the best results, eventually. The optimized gradient is shown in detail in chapter 2.2.3.

Regarding the low concentrations of small organic acids, 2-methyltetrols, and levoglucosan in ice cores, the focus of method development was mainly to increase the instrumental sensitivity. Although a baseline separation of the analytes is generally preferred, potential drawbacks in separation and detection were accepted due to the measurement of the exact mass and MS² fragment, respectively.

2.4.1.1 Post-column Injection

In order to optimize sensitivity, an increase of the pH of the eluent system was tested. Instead of formic acid as eluent additive, eluents A and D were replaced by water and methanol (each with 40 μ L/L ammonium hydroxide added), respectively. As a result, a decrease in chromatographic separation was observed. Subsequently, the eluent system was replaced by eluents A and D and a post-column infusion of an ammonium hydroxide solution in methanol was tested. Based on a chromatographic separation method with an eluent flow of 500 μ L/min and a duration of 12 min, the post-column infusion approach was optimized on signal intensity of the analytes. A 50 mM solution of ammonia in methanol was injected post-column with different flow rates. Figure 2.4 shows a bar plot of selected compounds representative for the respective precursor class at different post-column flow rates. The signals are normalized to the flowrate showing the highest signal intensity. The chromatographic and post-column flow rates were adjusted to 500 μ L/min in total. The nebulization gas settings and temperature were kept at 40 psi (sheath gas), 20 psi (auxiliary gas) and 320 °C, respectively.

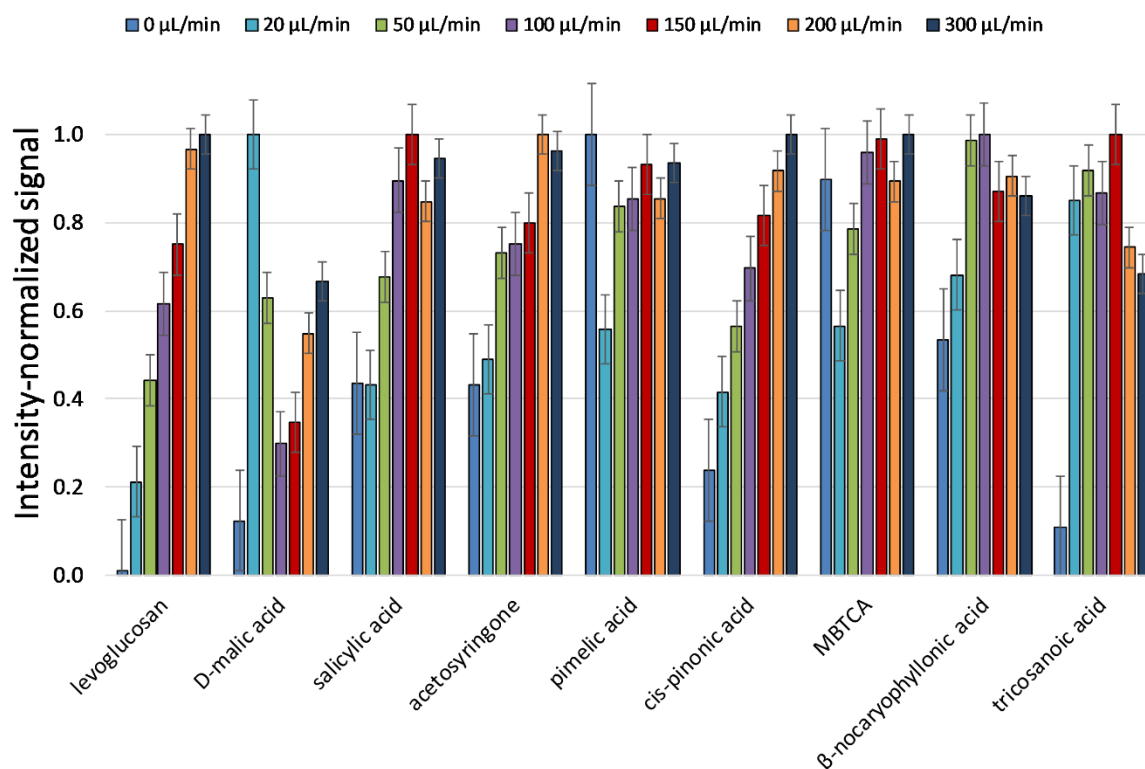


Figure 2.4 Normalized signal intensities of selected compounds at different post-column flow rates of a 50 mM solution of ammonia in methanol. The error bars denote the standard deviation of 1 σ .

As depicted in Figure 2.4, levoglucosan, as a representative molecule for alcoholic functions, showed enhanced signal intensity with increasing flow rates of the 50 mM ammonia solution. Eventually, the highest ionization efficiency in the negative mode was achieved at 300 $\mu\text{L}/\text{min}$ due to the basic medium. The higher pH supports a polarization of the hydroxyl-function and simplifies an ionization in negative mode. More acidic compounds like D-malic acid and MBTCA did not show a clear trend at different post-column flow rates. Due to the relatively low pK_a values of ~ 3.5 , both molecules are easily deprotonated to a high extent even at lower pH values. Thus, ammonia as a basic eluent additive does not significantly enhance the ionization efficiencies for these species. In contrast, acetosyringone, as an example of an aromatic molecule with relatively low acidity, showed enhanced ionization efficiencies at higher flow rates. However, higher flow rates of ammonia significantly increased signals for aliphatic carboxylic acids. Tricosanoic acid, as an example of a long-chain fatty acid, showed a high increase in signal intensity already for a post-column flow of 20 $\mu\text{L}/\text{min}$. Further increases in the flow rates showed no clear enhancement, but rather led to a decrease in signal intensities. Similarly for other compounds, ionization efficiencies increased with increasing flow rates of the ammonia solution. However, the highest signal was typically not observed at the highest flow rate. Moreover, optimum ionization conditions differed among the analytes. Nonetheless, we attempted to find a universal method regarding retention times and signal intensities for the entire range of compounds. Eventually, a post-column flow rate of 150 $\mu\text{L}/\text{min}$ showed the highest normalized signal intensity of 0.84 on average. Solely, for D-malic acid and 2-methyl-tetrols, the normalized signal

intensity was lower than 0.6 at this flow rate. Additionally, the retention times of all analytes were clearly shorter at the resulting chromatographic flow rate of 350 $\mu\text{L}/\text{min}$ than for higher post-column flows.

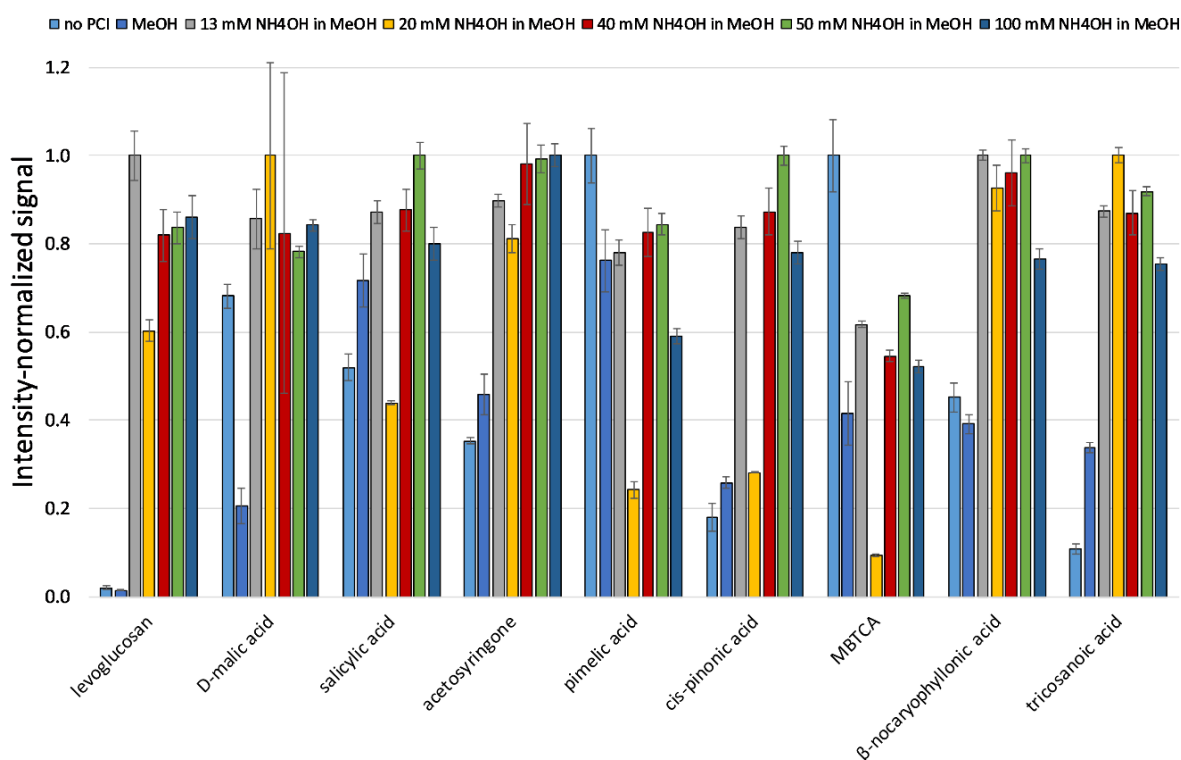


Figure 2.5 Normalized signal intensities of selected compounds at different concentrations of ammonia for post-column injection. The error bars result from analysis in triplicate.

As a final step, different concentrations of ammonia in methanol for post-column injection were tested. Concentrations of the ammonia solution (13 mM, 20 mM, 40 mM, 50 mM, and 100 mM) were analyzed at a flow rate of 150 $\mu\text{L}/\text{min}$. Additionally, a post-column injection of pure methanol and an experiment without post-column injection were performed with the optimized gradient. Figure 2.5 displays the normalized signal intensity for representative analytes. The 50 mM ammonia solution showed the highest sensitivity in negative ionization mode with an average value of 0.89 for all compounds. In general, post-column injection of each concentration enhanced the signal intensity, except for some more acidic compounds. Moreover, we found that an injection of pure methanol had no negative impact on the ionization efficiency. Solely, for the more acidic molecules, MBTCA, and D-malic acid a relatively large difference between no post-column injection and injection of methanol was observed. D-malic acid (0.51 min) and MBTCA (3.30 min) elute at aqueous, acidic eluent conditions which might have caused higher ionization efficiencies in this case. The more polar solvent may better stabilize already charged ions in solution. This observation may overcome the higher viscosity of water and resulting difficulties in efficient charge separation in the ESI process (Kostiainen & Kauppila, 2009). Furthermore, a phenomenon described as “wrong-way-round ionization” depicts a high sensitivity for

deprotonated molecules in acidic conditions contrary to expectation and agreement with ion evaporation theory (Zhou & Cook, 2000).

The negative impact of the post-column injection for these compounds is, therefore, not caused by the base itself, and the ionization efficiency increases with the addition of ammonia as observed for all other analytes (see D-malic acid). In the case of levoglucosan, as a representative species for small molecules with alcohol-functions, any concentration of ammonia enhanced the signal intensity dramatically. As previously reported in a method exclusively for the determination of levoglucosan (Gambaro *et al.*, 2008), a post-column injection of 13 mM ammonia in methanol using a flow rate of 5 $\mu\text{L}/\text{min}$ showed best results.

Aliphatic compounds with more than 9 carbon atoms and one carboxylic acid function showed comparable enhancements of signal intensities with the addition of ammonia (e.g., tricosanoic acid in Figure 2.5). Especially, fatty acids gained signal intensities already at 20 mM ammonia. The positive inductive effect of the alkyl-chain and the acidic conditions of the eluent at the time of injection (i.e., 99 % Eluent A), induce the fatty acids to remain mostly protonated. Fatty acids elute at retention times larger than 7.5 min when the eluent conditions have already changed to 95 % methanol. Due to this eluent composition and the basic post-column injection, the pH is increased and the weak acids become mostly deprotonated. Ionization efficiency in the negative mode is, therefore, enhanced. However, best signal intensities at high ammonia concentration (100 mM) were only observed for acetosyringone and 4-hydroxybenzoic acid which is probably due to ion suppression at higher concentration levels of ammonia.

2.4.2 Solid Phase Extraction

For the enrichment of the analytes and clean-up procedure, an SPE method was developed for which different SPE cartridges with an anion exchange function or hydrophilic-lipophilic balanced (HLB) copolymers were tested. Because the analyte mix contained many organic acids, anion exchange functions were assumed to be superior to HLB. Briefly, we checked various strong anion and weak anion exchange cartridges from three different suppliers with bed weights ranging from 10 mg to 130 mg and volumes of one to three mL. We found that mixed-mode anion exchange (MAX) cartridges (1cc, 10 mg, 30 μm , Waters, USA) showed best performance for further optimization. Sample preparation was developed on an Oasis® 2x4 Strategy for weak acids. The protocol included the following steps: conditioning with water, equilibration with methanol, washing with 5 % ammonia in water, and elution with 2 % formic acid in methanol. After concentration of the eluate with a gentle nitrogen stream at 40 °C, the concentrate was reconstituted in water. Optimization was focused on the elution step of the analytes. Therefore mixtures of 2 % formic acid in methanol, 5 % formic acid in methanol, formic acid/methanol (1/2), and acetic acid/methanol (1/2) were tested to elute the analytes from a 10 ppb loaded SPE-cartridge. The solutions of 5 % formic acid in methanol and formic acid/methanol (1/2) showed comparable recoveries higher than 60 % for most of the analytes. The 5 % formic acid solution

was favored over the 2 % formic acid solution for the more acidic analytes with two or more carboxylic acid functions. Acetic acid/methanol (1/2) showed mostly the best performance, but also weaknesses for several compounds. Therefore, we chose the solution of 5 % formic acid in methanol for elution. 2-methyl-tetrols showed minor and levoglucosan no signal with the tested elution mixtures. Without acidic functions in the structures, both molecules are not able to form ionic interactions with the SPE-cartridge. Due to this reason, the flow-through of the loading step was sampled and concentrated under a gentle nitrogen stream at 60 °C. A potential drawback of this procedure for the measurement of levoglucosan is caused by possible interferences with matrix constituents. Linear aliphatic carboxylic acids were also not detected in the SPE-eluate. Additionally to the ionic interaction with the SPE material, the fatty acids can form van-der-Waals forces between the long-chain carbon structure and the nonpolar parts of the SPE polymer. It was assumed, that the polar eluent methanol is not able to elute these structures from the SPE-cartridge, and thus, additional tests with nonpolar eluents (n-hexane and diethyl ether) were performed. Unfortunately, both eluents did not improve the detection. Due to the low hydrophilicity of the fatty acids, additional tests for the solvation of the concentrate were performed. We found that a mixture of 80 % water and 20 % acetonitrile enhanced the solubility of the fatty acids without decreasing the signal intensity of the polar analytes. Ultrasonic-assisted extraction (UAE) as an option to enhance the solubility of the fatty acids was tested briefly and showed promising results for the detection of fatty acids. Despite these first observations, the UAE was not included in the method, due to possible drawbacks and uncertainties in the stability of highly functionalized small organic compounds. Further optimization of the SPE method is discussed in chapter 2.6.

2.4.3 Method Validation

Linear regression analysis was applied to assess the linearity of the optimized method and to obtain calibration functions for all analytes of the standard mixture. External calibration was performed by spiking known concentrations of the analytes to water samples in quintuplicate. Quantification was performed by determination of the peak area either of the deprotonated ions of the analytes or the representative fragment ion in MS² mode (see Table 2.1). The resulting calibration parameters are presented in Table 2.2.

Table 2.2 Calibration data for quantification.

Compound	slope	intercept	R ²	lLOD (ng/mL)	LOD (pg/g Ice)
D-malic acid	2.1E+04	-3.8E+04	0.998	0.258 ^a	5.35 ^a
pimelic acid	1.1E+05	5.5E+05	0.992	0.803	16.20
levoglucosan	6.5E+03	7.8E+04	0.993	2.661	55.90
salicylic acid	2.4E+06	4.1E+05	1.000	0.017	0.36
4-hydroxybenzoic acid	3.4E+05	1.7E+05	0.999	0.272	5.52
cinnamic acid	4.5E+04	-4.5E+03	0.999	0.047	0.94
4-nitrocatechol	2.6E+05	-1.0E+05	0.996	0.023 ^a	0.47 ^a

2. Organic Trace Analysis in Ice Cores

vanillin	1.2E+05	1.7E+04	1.000	0.233	4.67
vanillic acid	1.2E+04	-1.4E+04	0.999	0.170 ^a	3.49 ^a
acetosyringone	1.2E+04	-6.0E+04	0.995	0.708 ^a	14.51 ^a
2-methyl-tetrols	3.3E+03	-5.6E+03	0.982	0.173 ^a	3.60 ^a
keto-pinonic acid	9.9E+03	6.0E+03	0.999	0.526	10.91
cis-pinonic acid	1.4E+04	-1.4E+04	1.000	0.591	12.61
terebic acid	4.4E+05	1.1E+06	0.998	0.037	0.76
pinic acid	1.5E+05	7.3E+04	0.999	0.074	1.41
BTCA	3.0E+03	-7.6E+03	0.996	0.626 ^a	12.66
MBTCA	8.3E+04	-8.9E+04	0.999	0.040 ^a	0.83 ^a
β -caryophyllonic acid	6.0E+05	5.1E+04	0.999	0.001 ^a	0.03 ^a
β -caryophyllinic acid	3.2E+05	3.4E+03	0.999	0.046	0.96
β -nocaryophyllonic acid	2.5E+05	1.2E+04	1.000	0.017	0.34
lauric acid	2.2E+05	5.1E+05	0.998	1.286	25.67
myristic acid	4.3E+05	2.1E+06	0.990	1.861	36.44
heptadecanoic acid	4.6E+05	-7.4E+04	0.995	0.502	10.37
oleic acid	9.2E+05	1.0E+06	1.000	1.414	27.88
nonadecanoic acid	1.5E+05	3.6E+04	0.998	0.365	7.46
behenic acid	2.8E+05	-3.6E+05	0.996	0.510	10.45
tricosanoic acid	1.5E+05	-1.9E+05	0.998	0.474	9.70
hexacosanoic acid	4.9E+04	-1.7E+05	0.995	3.731	77.66
heptacosanoic acid	3.3E+04	-1.0E+05	0.995	0.999	22.34
octacosanoic acid	6.1E+03	-4.2E+04	0.974	1.352	28.72

^a values determined using blank values from SPE-Blanks or averaged measurement blanks due to non-existing blank values.

Background subtraction was performed by correcting the results of the samples by subtracting the area of non-spiked high-purity ice samples. The correlation coefficient clearly shows a linearity of the calibration for all analytes. The instrumental limits of detection (ILOD) were determined by multiplying the standard deviations of the blank samples by three, divided by the slope of the linear regression function. The method limits of detection (LOD) are based on sample volumes between 12 and 42 mL. The values range from 0.03 pg/g ice for β -caryophyllonic acid to 77.66 pg/g for hexacosanoic acid. Overall, the LODs were in many cases better or comparable to previously reported LODs for HPLC-ESI-MS methods (Grieman *et al.*, 2015; Müller-Tautges *et al.*, 2016).

Detection of the MS²-fragment highly increased the validity of the analytes in snow and ice samples albeit the signal intensities of fragment ions were lower than signals of the deprotonated molecules in the *full-scan* mode. Background signals in the MS² mode were highly reduced or not existing.

Figure 2.6 shows the recovery rates of the analytes determined by spiking high-purity water samples with the analyte mixture in triplicate. Most of the analytes showed acceptable recovery rates larger than 60 %. Except for lauric acid and myristic acid, the recovery rates for the fatty acids are below 20 %. As discussed in chapter 2.4.2, the recovery rates of the fatty acids could be optimized from 0 to ~20 %, which remains, however, still non-satisfying.

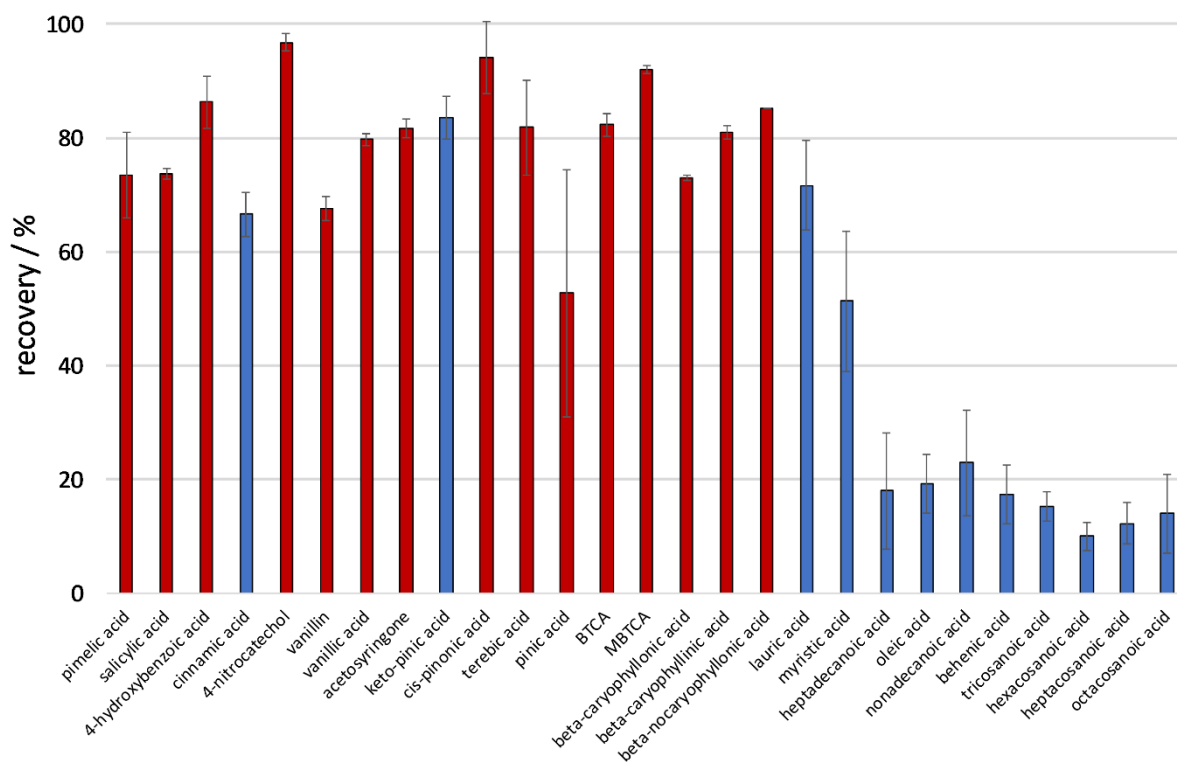


Figure 2.6 Recovery rates of the analytes. Signals measured using the deprotonated ion signal are shown in blue. Signals of MS² fragment ions are depicted in red.

The solvation of the long-chain fatty acids either in the last step of the SPE-method or in the preparation step of the aqueous spiked samples appears to be crucial. Especially, at the expected low concentrations of the analytes in ice and snow samples, high recovery rates are necessary to detect signals. Recovery rates for levoglucosan, 2-methyl tetrols, and D-malic acid could not be detected or were below 5 %. However, the procedure could be optimized for the signals of 30 analytes and the final results of the measured ice core samples were corrected with the corresponding recovery rates. Recovery rates for levoglucosan and 2-methyl tetrols were assumed to be 100 % in the flow-through of the SPE loading step, because of presumably missing ionic interaction and retention in the polymer cartridge.

The coefficient of variation as a parameter for the measurement precision caused by the UHPLC-ESI-MS system was determined by division of the standard deviation of the slopes of the analytes ($n = 5$) by the mean value of the slope. The coefficient of variation for all analytes was 13 % on average and 25 % for 4-nitrocatechol maximum.

2.5 Results and Discussion: Belukha Glacier Ice Core Sections

Twenty-eight samples (19 inner parts and 9 outer parts) of the Belukha glacier ice core were analyzed in a proof-of-principle analysis for the analytes shown in Table 2.1. The levels of the detected compounds ranged from below detection limit (BDL) to 1.3 $\mu\text{g/g}$ ice for levoglucosan. The average concentrations, as well as minimum and maximum values for all compounds, are presented in Table 2.3.

Table 2.3 Concentrations of the detected compounds in the Belukha glacier ice core (calendar years 1826 – 1828 and 1866 – 1869).

precursor/class	analyte	Concentration (ng/g ice)		
		average	minimum	maximum
biogenic	D-malic acid	1.635	0.198	5.865
anthropogenic	pimelic acid	2.233	BDL	9.818
BB, cellulose	levoglucosan	194.076	20.080	1327.412
BB, phenolic	salicylic acid	0.075	BDL	0.186
	4-hydroxybenzoic acid	0.326	0.064	1.973
	cinnamic acid	0.003	BDL	0.017
	4-nitrocatechol	0.012	BDL	0.131
BB, methoxyphenolic	vanillin	0.022	BDL	0.101
	vanillic acid	0.070	BDL	0.331
	acetosyringone	0.110	0.074	0.129
isoprene	2-methyl-tetrols	0.104	BDL	0.533
monoterpene	keto-pinic acid	1.673	0.086	6.866
	<i>cis</i> -pinonic acid	2.603	0.479	5.332
	terebic acid	1.906	0.376	4.995
	pinic acid	1.140	0.325	4.669
	BTCA	0.957	0.076	4.237
	MBTCA	0.838	0.192	2.628
	sesquiterpene	β -caryophyllonic acid	0.001	BDL
	β -caryophyllinic acid	0.036	0.004	0.103
	β -nocaryophyllonic acid	0.023	0.006	0.054
fatty acids	lauric acid	2.729	BDL	9.266
	myristic acid	1.905	BDL	8.562
	heptadecanoic acid	0.080	BDL	2.434
	oleic acid	BDL	BDL	3.313
	nonadecanoic acid	0.077	BDL	2.161
	behenic acid	1.005	0.170	7.770
	tricosanoic acid	0.752	0.019	8.080
	hexacosanoic acid	0.478	0.003	4.633
	heptacosanoic acid	0.997	0.101	8.780
	octacosanoic acid	12.361	BDL	92.903

The concentrations of levoglucosan ranged from 20 ng/g to 1327 ng/g ice with an average concentration of 194 ng/g ice. The maximum concentration was measured in an outer part of an ice core section from 1828. Interestingly, the maximum concentration of various compounds was measured in this section. However, the concentration of levoglucosan solely in this part was about five times higher than in the residual ice core sections. Besides this section, the second maximum value was measured at 290 ng/g ice. Levoglucosan, as one of the most prominent biomass burning markers, showed similar concentrations to ice cores previously measured with ESI-MS-techniques. For example, glacier ice core samples from the Tibetan area showed concentrations ranging from 10 to 718 ng/g (Muztagh Ata) and 10 to 93 ng/g (Tanggula) (Yao *et al.*, 2013). Likewise, You *et al.* determined levoglucosan concentrations in ice and snow samples from the Tibetan plateau of up to 1,14 ng/g (snow) and 7.56 ng/g (ice core) (You *et al.*, 2016) and of up to 1.93 ng/g at the Muztagh Ata glacier (You *et al.*, 2014). Ice core records from Antarctic regions showed lower concentrations from 4 to 30 pg/g (Gambaro *et al.*, 2008), whereas Greenland snow and ice core samples exhibited concentrations of up to 600 pg/g (Summit, Greenland) (Kehrwald *et al.*, 2012) and 1767 pg/g (NEEM, Greenland) (Zennaro *et al.*, 2014), respectively. Remarkably, these reported Arctic and Antarctic records are about 100 times lower than the concentrations measured in the Belukha glacier ice core sections. Besides 29 other molecular marker compounds, the optimized method is capable of detecting concentrations of levoglucosan as low as 58 pg/g ice, and therefore, seems promising for analyzing Arctic ice cores. Regarding the reported concentrations from Gambaro *et al.* (2008), the method can possibly be further optimized or specialized for the detection of levoglucosan in Antarctic ice cores.

4-hydroxybenzoic acid, as a phenolic BB marker derived from lignin combustion in conifer forest fires, ranged in the concentrations from 0.064 to 1.973 ng/g ice with an average value of 0.326 ng/g ice. Previously, 4-hydroxybenzoic acid was determined by HPLC-ESI-MS in an alpine glacier ice core (Müller-Tautges *et al.*, 2016), by IC-ESI-MS/MS in a Eurasian arctic ice core (Grieman *et al.*, 2017a) and in an ice core from the Ushkovsky ice cap by GC-MS (Kawamura *et al.*, 2012). Müller-Tautges *et al.* (2016) reported on concentrations from below detection limit (0.009 ng/g) to 0.15 ng/g ice with a mean value of 0.021 ng/g, whereas Kawamura *et al.* (2012) detected values from 0.005 ng/g up to 1.74 ng/g with an average value of 0.24 ng/g. Grieman *et al.* (2017a) reported concentrations from below detection limit (0.05 ng/g) to about 1 ng/g. In comparison to these studies, our results are well in accordance with the data reported by Kawamura *et al.* (2012) and Grieman *et al.* (2017a). The 4-hydroxybenzoic acid concentrations measured in the alpine ice core samples are about 15 times lower than in the Belukha glacier. Besides other variables, such as emission rates from the source, life time and transport, and deposition processes, a possible reason for this observation is the proximity of the Belukha glacier to the Siberian forests. Corroborating the assumption that forest fires are their main source, concentrations of levoglucosan and 4-hydroxybenzoic acid show a high correlation to each other ($r = 0.976$). Figure 2.7 shows the concentration records for the two species in the ice core section for the years 1826-1828 and 1866-1869. The concentrations of levoglucosan are about 595 times higher than

4-hydroxybenzoic acid. Emission rates of levoglucosan are reported to be quite abundant compared to other individual organic biomass burning markers, although they show a high variability (Mazzoleni *et al.*, 2007). Levoglucosan particle phase emission rates from fireplace combustion were determined in pine wood (1375 mg/kg), oak wood (706 mg/kg) and eucalyptus smoke emissions (Schauer *et al.*, 2001). Similar emission rates for levoglucosan were reported in another wood smoke study for pine (1380 mg/kg), oak (673 mg/kg), and eucalyptus (1490 mg/kg) (Nolte *et al.*, 2001). The emission rates of 4-hydroxybenzoic acid were described for pine wood (2.5 mg/kg), oak wood (1.2 mg/kg), and eucalyptus (2.4 mg/kg) (Nolte *et al.*, 2001). Calculating the factor of levoglucosan/4-hydroxybenzoic acid, the rates are 552 for pine wood, 560 for oak wood, and 621 for eucalyptus and therefore very similar to reported factors in our study. The detection and quantification of both BB-markers within the same method and subsequently the ratio of the compounds can reflect the composition of historic forests.

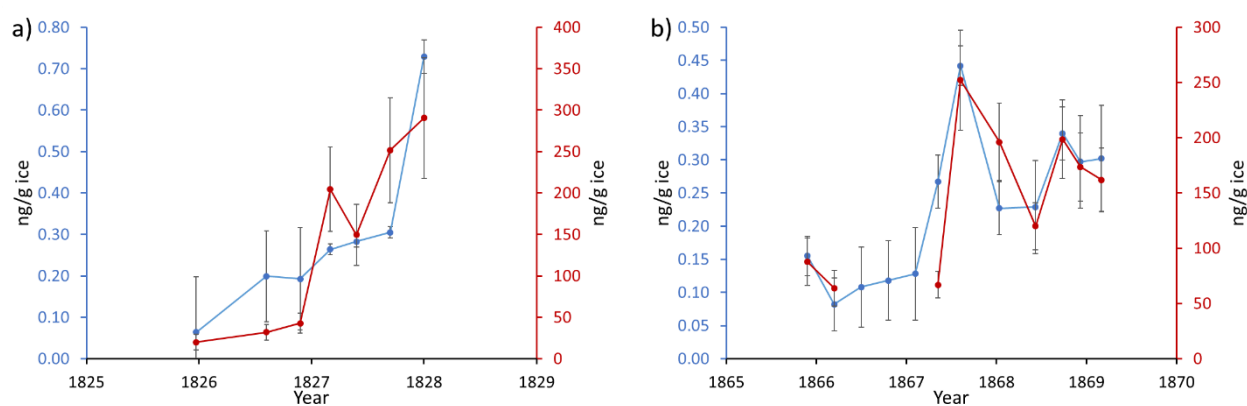


Figure 2.7 Historic record of 4-hydroxybenzoic acid (blue) and levoglucosan (red) between (a) 1826 to 1828 and (b) 1866 to 1869.

Concentrations of vanillic acid, as a representative BB-marker derived from lignin combustion, ranged from values below the detection limit (i.e., ≤ 0.004 ng/g) to 0.331 ng/g with an average value of 0.070 ng/g. These values are in the same range as previously reported for ice core samples from West-Central Greenland (McConnell *et al.*, 2007) and the Ushkovsky ice cap (Kawamura *et al.*, 2012). Vanillic acid concentrations with an overall mean of 0.226 ng/g were reported for the Akademii Nauk ice core, covering the time period of 200-300 (Grieman *et al.*, 2015). These values were approximately three times higher than in the present ice core sections. Müller-Tautges *et al.* (2016) found concentrations for an alpine ice core to be in the range of below the detection limit (i.e., ≤ 0.021 ng/g) to 0.36 ng/g with a mean value of 0.067 ng/g. This observation is well in agreement with the concentrations measured for the Belukha ice core sections in our study. A 2600-year proxy record from the Akademii Nauk ice core was found to show vanillic acid concentrations mainly between values below the detection limit (i.e., ≤ 0.01 ng/g) and 0.5 ng/g with single values up to 1 ng/g (Grieman *et al.*, 2017a). Vanillic acid levels were observed to elevate during 1780 to 1860 and to be mainly in the range between 0.01 ng/g and 0.3 ng/g. Comparable values were reported for the Belukha glacier section for this time periods in

this report. The average values of vanillic acid were four to five times lower than the reported values of 4-hydroxybenzoic acid. Müller-Tautges *et al.* (2016) reported values of vanillic acid three times higher than those of 4-hydroxybenzoic acid, whereas Kawamura *et al.* (2012) determined concentrations of vanillic acid 16 times lower than values of 4-hydroxybenzoic acid. Variations in the ratio of BB-markers may result from different atmospheric transport rates and vegetation sources. In general, the herein reported ratio of vanillic acid/4-hydroxybenzoic acid of 0.21 is comparable to the ratio for the Lomonosovfonna ice core (Grieman *et al.*, 2017b) and slightly lower than reported by combustion experiments with conifers that are characteristic for North America and European Boreal forests (Oros & Simoneit, 2001a). Reported emission rates for vanillic acid showed values of 8.5 mg/kg for pine wood smoke and 3.5 mg/kg for oak wood smoke (Nolte *et al.*, 2001). Emission rates of 4-hydroxybenzoic acid were assessed to 1.2 mg/kg for oak wood and 2.5 mg/kg for pine wood (Nolte *et al.*, 2001). Therefore the ratio of vanillic acid/4-hydroxybenzoic acid showed values of 3.4 (pine wood) and 2.9 (oak wood), which reflect the findings by Müller-Tautges (2016). However, a high variability of emissions of organic biomass burning markers, reflecting the composition of burned area is assumed.

Here, we quantified 4-nitrocatechol in an ice core section for the first time. The Chromatogram and the corresponding MS² spectrum are shown in the Supporting Information to chapter 2 in Figure 7.1. 4-nitrocatechol has been associated with biomass burning by filter analysis of atmospheric organic aerosol particles (Claeys *et al.*, 2012; Kahnt *et al.*, 2013; Kitanovski *et al.*, 2012) and combustion experiments (Iinuma *et al.*, 2007a). The concentrations of 4-nitrocatechol were in the range below the detection limit (i.e., ≤ 0.47 pg/g ice) and 0.131 ng/g with a mean concentration of 0.012 ng/g. For the analyzed ice core sections from the Belukha glacier, 4-nitrocatechol showed an overall correlation with the most prominent BB marker levoglucosan ($r = 0.834$). Historic records and ratios of these markers may contribute to the characterization of fire events before and after industrialization, as 4-nitrocatechol has also been suggested to be a marker for the photooxidation of benzene (Borrás & Tortajada-Genaro, 2012).

Ice core records of biogenic monoterpene and isoprene SOA tracers are scarcely described yet. In our study, concentrations of 2-methyltetrols (i.e., 2-methylthreitol and 2-methylerythritol) in the Belukha glacier sections ranged from below the detection limit, which is at 0.004 ng/g ice, to 0.533 ng/g with an average value of 0.104 ng/g. The representative isoprene SOA tracers were reported in an Alaskan ice core (Aurora Peak) with concentrations for 2-methylerythritol ranging from below detection limit (i.e., 0.001 ng/g ice) to 3.5 ng/g and a mean value of 0.692 ng/g and for 2-methylthreitol with concentrations from below detection limit (i.e., 0.001 ng/g) to 1.7 ng/g and an average value of 0.349 ng/g (Pokhrel *et al.*, 2016). Concentrations of 2-methyltetrols in the Ushkovsky ice core (Kamchatka Peninsula) ranged from 0.004 ng/g to 9.7 ng/g ice with average values of 0.587 ng/g (Fu *et al.*, 2016). Therefore, both studies showed on average five to six times higher concentration levels of 2-methyltetrols compared to our findings. However, during the early-to-middle 1800s, concentrations around 0.100 ng/g were determined, which is similar to the concentrations of the Belukha glacier for this time period.

Concentrations of monoterpene-derived oxidation products ranged from 0.076 ng/g for BTCA to 6.8 ng/g for keto-pinonic acid (see Table 2.3). Most abundant compounds were the first-generation oxidation products (i.e., *cis*-pinonic acid, terebic acid, and keto-pinonic acid), whereas MBTCA, a later-generation oxidation product, showed the lowest mean concentrations. On average, concentrations of *cis*-pinonic acid were 1.5 times the concentrations of keto-pinonic acid, about two times the concentrations of pinonic acid and three times the concentrations of MBTCA. The concentration ranges of pinonic acid and keto-pinonic acid were about seven, and 36 times higher, respectively, compared to those detected for an Alaskan ice core (Pokhrel *et al.*, 2016). However, the historical record of the Alaskan ice core also showed decreased concentrations during the mid-1800s. Mean concentrations of pinonic acid (0.147 ng/g), pinonic acid (0.059 ng/g) and MBTCA (0.004 ng/g) during the early-mid 1800s in the Ushkovsky ice core (Fu *et al.*, 2016) were about 10 to 200 times lower than in the Belukha ice core section. Differences result most likely from the location, transport and deposition processes. Historical records of atmospheric markers over several years/decades showed variations of more than 100 times. Therefore, the reported variations in this study are not unusual for timespans of only two to three years.

To our knowledge, we present the first data on β -caryophyllene-derived biogenic SOA markers detected and quantified in an ice core. The concentrations of β -nocaryophyllonic acid ranged from 0.006 ng/g to 0.054 ng/g with an average value of 0.023 ng/g ice. β -caryophyllinic acid was the most abundant tracer among the β -caryophyllene-derived SOA tracers with concentrations ranging from 0.004 ng/g ice to 0.103 ng/g and a mean value of 0.036 ng/g. Additionally, β -caryophyllonic acid showed concentrations from below the detection limit, which was at 0.03 pg/g ice, to 0.004 ng/g and an average concentration of 0.001 ng/g ice. Compared to isoprene- and monoterpene-derived SOA markers, oxidation products of sesquiterpenes are typically present in rather low concentrations, and thus, scarcely studied. Among β -caryophyllene-derived biogenic SOA tracers, β -caryophyllinic acid was sampled and analyzed the most (Ding *et al.*, 2011; Fu *et al.*, 2013; Shen *et al.*, 2015). Ambient air samples from Finland showed β -nocaryophyllonic acid to be the most abundant β -caryophyllene oxidation product (van Eijck *et al.*, 2013). Historical records of these SOA markers can show possible variations in the abundance and present information about former vegetation. It has been shown in this study, that β -nocaryophyllonic acid and β -caryophyllinic acid are a factor of 20 – 36 times more abundant than β -caryophyllonic acid. Figure 2.8 shows the trends of accumulated concentrations of β -caryophyllene-derived SOA tracers (i.e., β -nocaryophyllonic acid, β -caryophyllinic acid, and β -caryophyllonic acid) and α -pinene-derived SOA tracers (i.e., MBTCA, pinonic acid, *cis*-pinonic acid, keto-pinonic acid, and terebic acid) in the inner and outer part of the ice core sections. The concentrations of the β -caryophyllene-derived SOA tracers in the inner and outer part of the ice core sections are in the same range for the sections dating from 1826 – 1829. The concentrations of α -pinene-derived SOA tracers in the outer parts are roughly a factor of 2 – 3 higher than in the inner parts of the same ice core sections. Generally, an increasing trend in both concentrations is observed. Furthermore, a small decrease in both concentrations between 1827 and 1827.5 is shown in both parts of the ice core sections.

However, due to the small number of samples, a diversity between inner and outer parts cannot be concluded. Moreover, the generally higher concentrations of the analytes might result from contaminations on the outside of the ice cores.

In the ice core sections dating from 1866 – 1869, the concentrations of the β -caryophyllene-derived and α -pinene-derived SOA tracers are in comparable concentration ranges in both parts of the ice core sections. Generally, there is a decreasing trend from 1866 till 1869. Despite the small number of samples, the compounds are generally homogeneously mixed in the ice core sections.

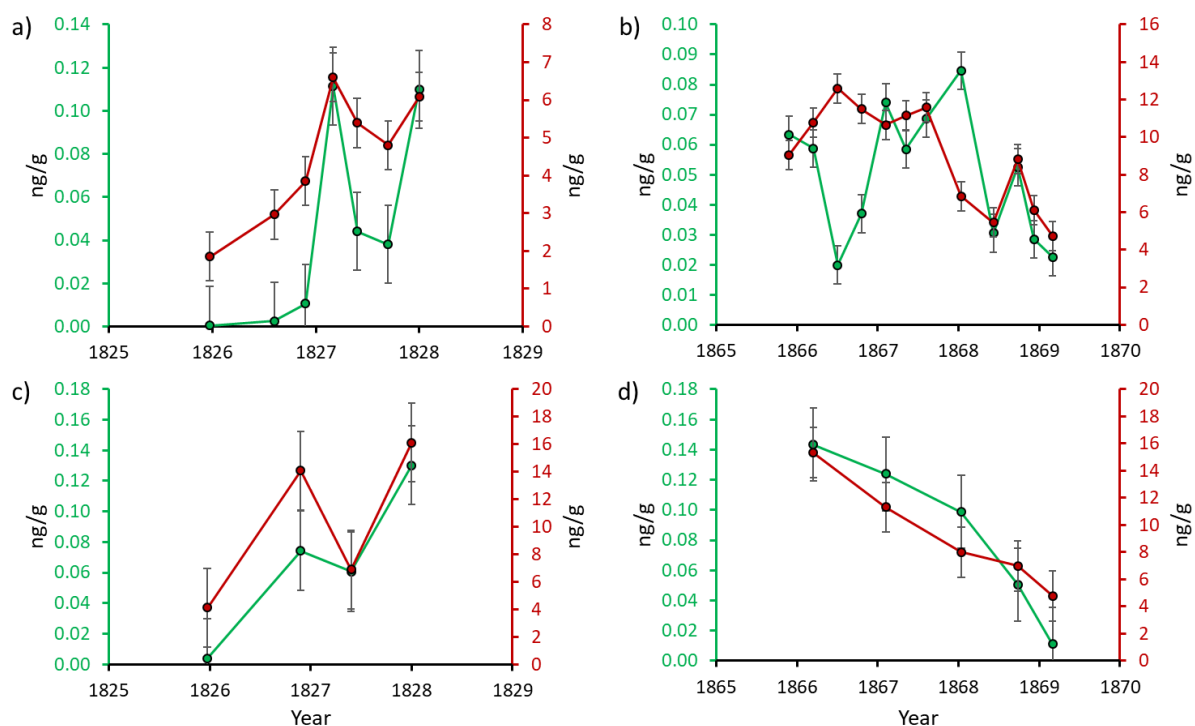


Figure 2.8 Trends in the accumulated concentrations of β -caryophyllene-derived SOA tracers (green) and α -pinene-derived SOA tracers (red) in the inside (a) and outside (c) part of the ice core section dating from 1826 – 1828 and inside (b) and outside (d) part of the ice core section dating from 1866 – 1869.

In total, there is a strong correlation between both SOA tracer classes. Correlation coefficients of the α -pinene related compounds and the β -caryophyllene-derived SOA tracers for the ice core section dating from 1826 – 1828 were $r = 0.909$ for the inner part and $r = 0.905$ for the outer part of the ice core. For the ice core sections dating from 1866 – 1869 the correlation coefficients were $r = 0.240$ for the inner part and $r = 0.923$ for the outside part, respectively. The positive correlations point towards similar sources and atmospheric transport histories for deposited SOA. The relatively low correlation in for the inner part of 1866 – 1869 is mainly caused by three differing values between the years 1866 – 1867. However, the trend of both concentrations after the year 1867 are comparable, indicating a high correlation. The correlation coefficient between 2-methyltetrols, as a representative species for isoprene-derived SOA products, and the sum of monoterpene SOA tracer is $r = 0.590$. In this case, the correlation is minor compared to α -pinene- and β -caryophyllene-derived SOA, but particular correlation is still

given. A possible reason for this observation may be originated in the emission sources of the differing VOCs. α -Pinene and β -caryophyllene are generally more attributed to “Needleleaf evergreen trees“, whereas isoprene is prevalently emitted by “Broadleaf Trees and Shrubs” (Guenther *et al.*, 1995; Guenther *et al.*, 2012). As the Siberian region is mostly dominated by “Needleleaf evergreen trees“, isoprene-related oxidation products may originate to a certain amount from other sources.

The optimized method enabled the detection of rather nonpolar organic molecules besides more or highly polar analytes. The detected fatty acids ranged from values below the corresponding detection limits up to 92 ng/g ice for octacosanoic acid (see Table 2.3). On average the concentrations of the quantified fatty acids were about 14 ng/g ice. Previous studies on historic records of fatty acids showed values from 1.9 ng/g to 105 ng/g and mean concentrations of 20 ng/g ice for a Greenland ice core (Kawamura *et al.*, 1996) and a concentration range from 0.8 ng/g to 20.3 ng/g for an Alaskan ice core (Pokhrel *et al.*, 2015).

Among the analyzed fatty acids, three classes were determined according to their correlation to each other. First, myristic acid and lauric acid showed a high correlation to each other ($r = 0.839$) and relatively low correlations to other fatty acids ($r < 0.5$). Oleic acid, as a representative for an unsaturated fatty acid, was denominated as a single class because it showed specific correlation but only a minor value compared to the other fatty acids ($r < 0.7$). Moreover, the concentration of oleic acid among the ice core sections was on average below the determined detection limit. This observation can be explained by the high continentality of the drilling area. Oleic acid as a major constituent of cell membranes in marine phytoplankton (Pokhrel *et al.*, 2015) is emitted by bubble bursting, and therefore, needs to be transported over long distances to reach the Altai mountain area. The higher molecular weight fatty acids (C₁₇-C₂₈) showed a correlation among each other with correlation coefficients higher than 0.85. Among the fatty acids, no significant differences between even and an odd number of carbon atoms were detected. On the basis of the few analyzed ice core sections, the most abundant source of fatty acids detected in the Belukha ice cores sections may originate from plant waxes emitted by terrestrial higher plants. For a more detailed source apportionment, backward trajectories and more samples representing longer timescales should be taken into account in future studies.

2.5.1 Principal Component Analysis

A principal component analysis (PCA) was performed to group the analyzed compounds and to elucidate possible connections.

The results of the PCA are presented in Table 2.4 and Table 2.5. 89.7 % of the variance was explained by six principal components with Eigenvalues higher than 1. The principal component with the highest percentage of explained variance (30.5 %) was PC1. The highest loadings contributing to PC1 (> 0.7) were signals from levoglucosan, 4-hydroxybenzoic acid, pinic acid, BTCA, MBTCA, 4-nitrocatechol, pimelic acid, 2-methyl tetrols, and D-malic acid. Evaluating the characteristics of the compounds, we attribute biomass burning SOA and biogenic SOA to the most influencing parameters

to the composition of organic aerosol at the Belukha glacier for this time periods. Hypotheses of enhanced emissions of α - and β -pinene at higher temperatures, e.g. during forest fires (Cheng *et al.*, 2011), support the detected relationship between biomass burning markers and biogenic, α -pinene-related SOA tracers.

Table 2.4 Principal components, Eigenvalues, and explained variance determined by principal component analysis.

Principal component	Rotation sums of Squared Loadings		
	Eigenvalue	explained variance / %	cumulative / %
PC1	9.138	30.461	30.461
PC2	8.021	26.736	57.197
PC3	4.529	15.098	72.295
PC4	2.114	7.047	79.342
PC5	1.637	5.458	84.800
PC6	1.487	4.957	89.756

The second principal component (PC2) accounts for 26.7 % of the variance and is mainly dominated by long chain fatty acids with loading above 0.9. Likewise, lauric acid, myristic acid, and oleic acid as representatives of short chain, and unsaturated fatty acids, respectively, show minor loadings on PC2. The link between these compounds indicate PC2 as a factor for fatty acids, most likely emitted from waxes of higher plants (Kawamura *et al.*, 1996).

PC3 shows high loadings of β -caryophyllinic acid, lauric acid, and *cis*-pinonic acid (> 0.8). Furthermore, all caryophyllene-related tracers and myristic acid contribute to PC3. A possible connection might exist in the biogenic origin of the analytes. Fine particle leaf abrasion from dead and green leaf composites might be a common source (Rogge *et al.*, 1993). Oros and Simoneit analyzed smoke particulate matter from deciduous trees that were burned under controlled smoldering and flaming conditions (Oros & Simoneit, 2001b). Emissions from the silver birch tree, highly distributed across northern Europe to central Siberia (www.euforgen.org/species/betula-pendula, European Forest Genetic Resources Programme), showed high emission factors of sesquiterpenoids, myristic acid as well as lauric acid which may explain a similar source. Thus, we generally assign PC3 to components that are representative of sesquiterpene oxidation products and short chain fatty acid emissions, explaining about 15 % of the variance. The fourth principal component (PC4) shows two positive loadings of cinnamic acid and β -caryophyllonic acid and two negative loadings of vanillin and vanillic acid. The highest impact is caused by a negative loading of vanillin (-0.8). Vanillin and vanillic acid are major constituents of pine wood smoke, whereas other coniferyl-type lignin pyrolysis products are not as high as expected in this type of wood smoke (Simoneit, 2002). The negative loading of both compounds might indicate other types of biomass burning emissions than from burning of pine trees. Accordingly, cinnamic acid is described as a compound generated from lignin pyrolysis or breakdown of polysaccharides (Urban *et al.*, 2016). Contrary to this consideration of PC4, vanillin and cinnamic acid are also speculated to be of anthropogenic origin (Keil *et al.*, 2011). However, it can be assumed that

2. Organic Trace Analysis in Ice Cores

the anthropogenic impact on total OA composition was only of minor importance at the time of deposition. PC5 shows a strongly negative loading of keto-pinic acid and a positive loading of cinnamic acid. Besides PC4, keto-pinic acid also loads on PC1 and PC4, which makes a clear assignment to a possible source even more ambitious. As keto-pinic acid is reported to be of biogenic origin and cinnamic acid is discussed to be of anthropogenic and biogenic origin, PC5 may be attributed to an anthropogenic factor. Nevertheless, because of the rural area and the age of the ice core, an anthropogenic impact is expected to be low.

Table 2.5 Rotated component matrix.

variable	Components					
	PC1	PC2	PC3	PC4	PC5	PC6
levoglucosan	0.946					
D-malic acid	0.797					
2-methyl-tetrols	0.834					
BTCA	0.887					
terebic acid	0.691					
MBTCA	0.875					
4-hydroxybenzoic acid	0.939					
vanillic acid	0.669			-0.483		
pimelic acid	0.849					
4-nitrocatechol	0.850					
vanillin				-0.837		
pinic acid	0.922					
acetosyringone						0.902
<i>cis</i> -pinonic acid			0.866			
salicylic acid		0.506	0.523			
keto-pinic acid					-0.846	
cinnamic acid	0.401			0.606	0.409	
β -nocaryophyllonic acid	0.697		0.609			
β -caryophyllinic acid			0.899			
β -caryophyllonic acid			0.596	0.573		
lauric acid		0.420	0.874			
myristic acid		0.554	0.676			
oleic acid		0.841				
heptadecanoic acid		0.901				
nonadecanoic acid		0.923				
behenic acid		0.953				
tricosanoic acid		0.989				
hexacosanoic acid		0.973				
heptacosanoic acid		0.924				
octacosanoic acid		0.950				

Factor loadings < |0.4| are not shown in terms of clarity.

PC6 accounts for 5 % of the variance and is only dominated by acetosyringone with a highly positive loading (0.9). Acetosyringone is mainly an indicator of lignin combustion of angiosperms (Simoneit, 2002). Therefore, PC6 is assumed to be representative for emissions from BB of Siberian grasslands.

2.5.2 Seasonal Variation of the Analytes during 1866-1869

Seasonal variations of the analytes in the ice core section dating from 1866 to 1869 are shown in Figure 2.9 and Figure 2.10. The main precipitation at the Altai region mainly occurred during April to the end of October (Henderson *et al.*, 2006). Most of the biomass burning marker regularly peak during these times of the year. This is in agreement with the assumption that emission rates are enhanced during summer, which is most likely due to higher temperatures and a higher probability of forest fires. Additionally, summertime circulation is mainly streaming southwards from the Kara Sea region (Henderson *et al.*, 2006) passing the Siberian Forests, which is possibly the dominant source of forest fires. However, some of the known lignin-derived biomass burning markers (i.e., vanillin, vanillic acid, acetosyringone) show the highest concentrations during winter times. A possible explanation for this observation could be long-range transport of analytes, eventually reaching the sample site in winter times. Hence, the climatology in winter times in the Altai region is dominated by a Siberian High causing a broad and persistent inversion layer (Henderson *et al.*, 2006), whereas long-range transport to the Belukha glacier is hindered. The inversion layer even reaches the higher land elevations at some times, prohibiting vertical transport. Another possible explanation for elevated concentrations of the BB marker compounds could be local forest fires of different kinds. In the context of the principal component analysis, factor PC4 (i.e., a negative loading of vanillin and vanillic acid) was attributed to be a non-pine wood factor. Analytes representing biogenic SOA, for example, MBTCA and pinic acid, show the highest concentrations at the end of summertime. This observation can easily be explained, because of higher emissions of VOCs (e.g., α -pinene) due to higher temperatures in summer and subsequent oxidation reactions in the atmosphere.

Interestingly, lauric acid and myristic acid exhibit distinct maxima during winter times. Contrary to this observation, all other fatty acids show high concentration peaks during summer. This is most likely also correlated to the southern wind directions crossing the Siberian forests.

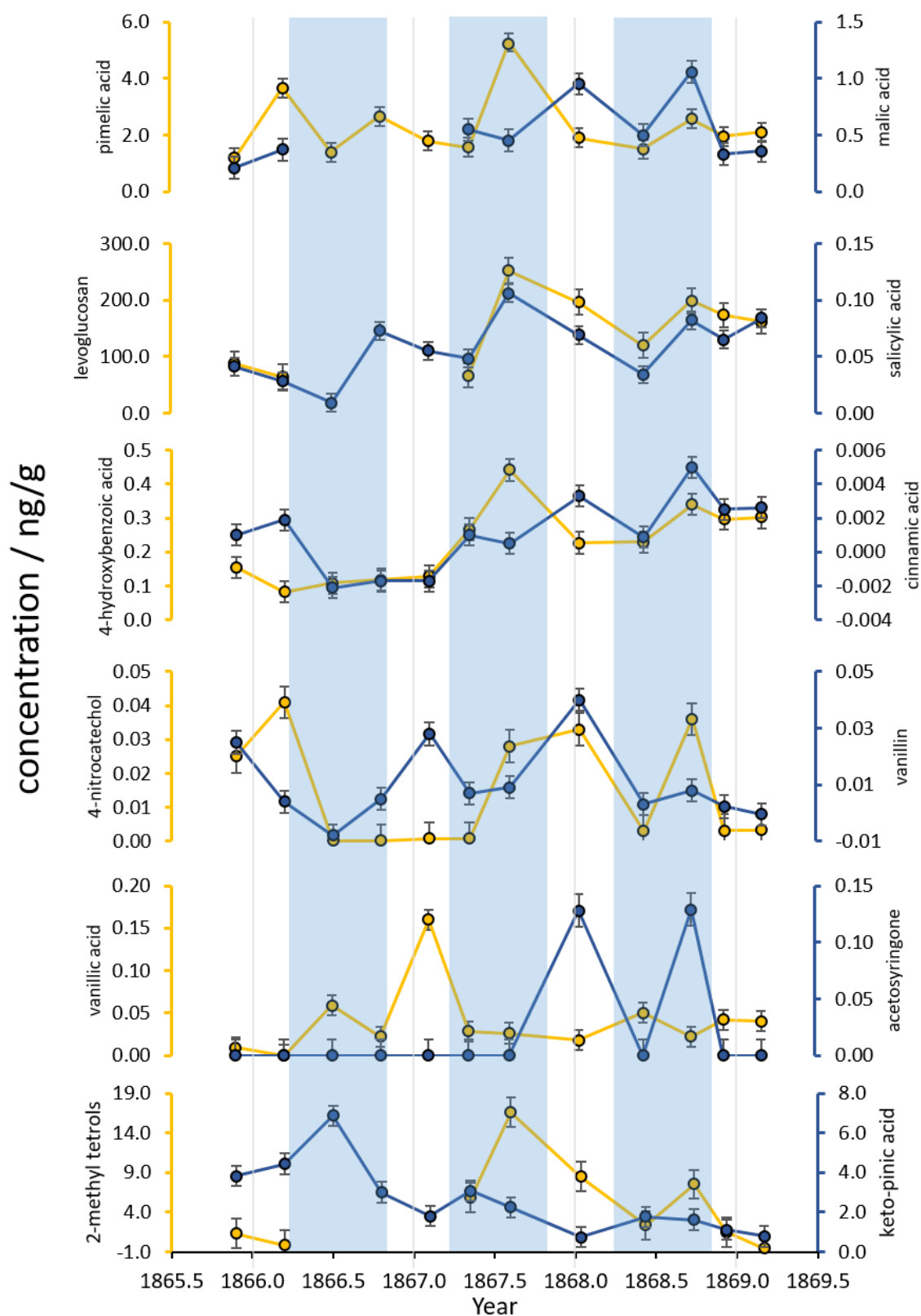


Figure 2.9 Seasonal variation of the analytes (Part 1) in the ice core section dating from 1866-1869. The main precipitation times (April to end of October) are highlighted in blue.

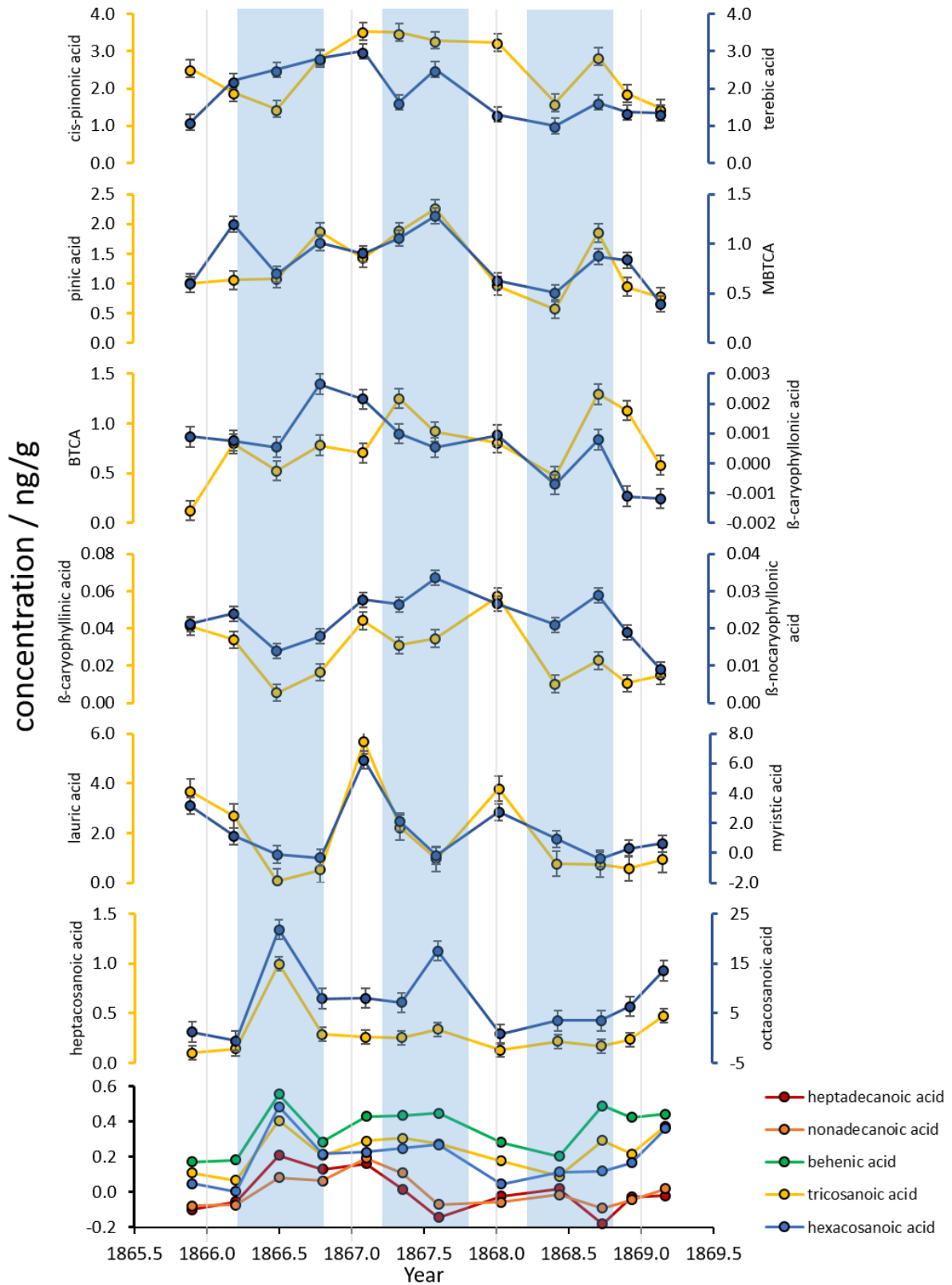


Figure 2.10 Seasonal variation of the analytes (Part 2) in the ice core section dating from 1866-1869. The main precipitation times (April to end of October) are highlighted in blue.

2.6 Conclusions and Outlook

A UHPLC-ESI-MS²-method for the simultaneous detection and quantification of small organic molecules in ice and snow samples was developed. The analyzed molecules covered a broad range of atmospheric tracers comprising levoglucosan, lignin-derived biomass burning markers, atmospheric SOA markers originating from isoprene, terpenes, and sesquiterpenes, as well as fatty acids.

For extraction and enrichment of the analytes, an SPE method using anion exchange functionalities was developed. Signal intensities of the analytes, especially levoglucosan, were highly enhanced by a post-column injection of a methanolic ammonia solution prior to ionization. Recovery rates were determined to be around 80 %. Unfortunately, the recovery rates for fatty acids with carbon numbers larger than 17 remained around 20 %, even after optimization. Most likely, the solvation process subsequently to SPE needs to be improved for the solubility of fatty acids. Besides the retention time and the exact mass determination by Orbitrap mass spectrometry, the identity of the analytes was ensured by additional MS² experiments. Limits of detection for the analytes ranged from 0.03 to 80 pg/g for sample volumes of 12-42 mL.

A proof-of-principle analysis of ice core sections from the Belukha glacier in the Altai mountain range demonstrated the performance of the developed method. The average concentrations of the detected analytes ranged from levels below the corresponding detection limit up to 194 ng/g.

For the first time, 4-nitrocatechol, keto-pinic acid, and sesquiterpene-derived tracers were detected and quantified in an ice core. Furthermore, several organic trace components were determined the first time in an ice core from the Belukha glacier in the Altai mountain range and quantified within a single analytical method. In general, concentrations of organic compounds reported in Alpine and Arctic ice cores were in comparable concentration ranges.

A PCA was performed and revealed six principal components accounting for ~90 % of the data variance in total. The principal components were attributed to i) biomass burning and biogenic SOA, ii) Plant waxes, iii) Sesquiterpene and short chain fatty acid emissions (*Betula pendula*), iv) non-pine wood biomass burning and anthropogenic emissions, v) anthropogenic emissions, and vi) BB emissions from Siberian grasslands. For most of the analytes, the concentration maxima were found in summertime, which coincides with the time of the main precipitation in the Altai mountain range. However, the methoxyphenolic lignin-derived BB marker and short chain fatty acids showed the highest concentrations in winter times. On the one hand, this may indicate a different source of emission. On the other hand, the observation was based on a proof of principle of a three year period and only a long-term analysis of an ice core could substantially support this hypothesis.

Further optimization of the quantification method should focus on the solvation of fatty acids and the detection of low molecular weight and very polar compounds, such as levoglucosan and D -malic acid. On the one hand, ultrasonic extraction showed potential to increase the recoveries for fatty acids. On the other hand, intense sonication could provoke decomposition of unstable molecules. Probably, a

more non-polar solvent mixture would optimize the absorption of the fatty acids. Both the retention time of levoglucosan and the ionic bonding during the SPE should be investigated in further studies. Due to the absence of carboxylic acid functions, levoglucosan is not retained by the anion exchange polymer and was only measured after concentration of the flow-through. Multi-layer cartridges with polymer-based ion exchange functions and a reversed phase layer should, therefore, be investigated in future studies. Another option to keep the detection of all kind of analytes in one method is a concentration of the sample matrix by a rotary evaporator instead of an SPE method. An option to extend the retention time of levoglucosan and other highly polar molecules would be a hydrophilic interaction liquid chromatography (HILIC) column. For this purpose, an LC method development is required to ensure appropriate retention times for the long chain fatty acids. Furthermore, it should also be taken into account that retention of the analytes at a higher fraction of methanol may further increase the ESI efficiency and signal intensity.

Concerning further studies of ice cores, it should be considered to extend the method to other adequate compound classes. A detection of anthropogenic markers like pesticides might be promising. Possibly, the method can also be adapted to other water-based matrices like fresh water. A detection of anthropogenic drug residues in freshwater might, thus, be an interesting future topic. Furthermore, a non-target screening could yield information on major chemical compound classes in historic ice core records. Especially, an anthropogenic influence in the years after the industrial revolution might be observable due to a higher amount of sulfur-, nitrogen- or halogen-containing compounds. Besides such studies, a non-target screening of an Antarctic ice core could give important data on the molecular composition of atmospheric chemical systems hundreds of thousands of years in the past.

3 Molecular Composition of SOA Particles at Nucleation Experiments at CERN

3.1 Introduction

Oxidation products of volatile organic compounds (VOCs) have an important influence on the formation of secondary organic aerosol (SOA) particles and cloud condensation nuclei (CCN), which affect global climate and human health (IPCC, 2013; Lelieveld *et al.*, 2015; Nozière *et al.*, 2015; Pöschl, 2005). According to the sources of the VOCs, SOA can be assigned mainly to two source categories, i.e., anthropogenic and biogenic SOA. Anthropogenic SOA may originate, for example, from industrial emissions and fuel combustion, whereas biogenic SOA originates from terrestrial and marine emissions, such as isoprene or monoterpenes (Hallquist *et al.*, 2009). It is presumed that biogenic SOA dominates the annual global SOA production by far (Hallquist *et al.*, 2009). It was shown that such biogenic OAs evolve by further oxidation reactions and aging processes making them a highly dynamic system (Donahue *et al.*, 2012; Jimenez *et al.*, 2009). Detailed knowledge of the SOA molecular composition is crucial for its characterization and elucidation of formation mechanisms and demands state-of-the-art analytical methods.

In general, the measurement techniques for the chemical composition and quantification of SOA are divided into three classes: indirect methods, online, and offline techniques (Hallquist *et al.*, 2009). Focusing on the direct methods (online and offline), typically the online techniques provide information on fast chemical processes and aerosol compositions in real-time. The Aerodyne aerosol mass spectrometer (AMS) for example is one of the most common online instruments that is used for the characterization of aerosol particles (Canagaratna *et al.*, 2007; DeCarlo *et al.*, 2006). Despite several unique advantages of the AMS compared to other online instruments, the mass resolution of the time of flight (ToF)-MS detector is rather limited ($R \sim 5000$) and the rather hard ionization technique (i.e., electron impact) induces a high degree of fragmentation of organic compounds, typically hindering an identification of individual organic molecules. Several instrumental techniques were recently developed to fill this gap and to facilitate molecular characterization of organic aerosol components. Particularly, the Filter Inlet for Gases and AEROSols (FIGAERO) coupled to a high-resolution time-of-flight chemical-ionization mass spectrometer (HR-ToF-CIMS) has been deployed to a variety of laboratory chambers as well as field sites (Lopez-Hilfiker *et al.*, 2014). Recent developments of inlet systems for submicron particles comprise the Chemical Analysis of Aerosol Online (CHARON) (Eichler *et al.*, 2015) and the Droplet Assisted Inlet Ionization (DAII) (Horan *et al.*, 2017). Other techniques with softer ionization methods mentioned in this context are the Flowing Atmospheric Pressure Afterglow Mass Spectrometry (AeroFAPA-MS) (Brüggemann *et al.*, 2015) or atmospheric pressure chemical ionization (APCI-MS) (Vogel *et al.*, 2013). Nonetheless, these mass spectrometric techniques alone are not capable

of an unambiguous identification of individual organic molecules, mainly due to a limited mass resolution.

Typically, “offline” techniques like ion-chromatography and gas or liquid chromatography coupled to MS, provide more detailed information on compound classes and individual compounds (Hoffmann *et al.*, 2011). Besides detection of m/z ratios and corresponding signal intensities, chromatographic offline techniques provide retention times as an additional dimension to characterize organic components of SOA particles. Moreover, such separation techniques can often easily be coupled to high-resolution mass spectrometers. Accurate high-resolution MS was developed over the last 40 years (Marshall & Chen, 2015). In this respect, Fourier transform ion cyclotron resonance MS (FTICR-MS) and Orbitrap MS can provide exact molecular formulas of individual organic molecules in aerosol particles without the need of analytical standards (Nizkorodov *et al.*, 2011). Generally, FTICR-MS provides the highest mass resolution and mass accuracy (Schmitt-Kopplin *et al.*, 2010), whereas the Orbitrap technique is the first commercially profitable ultra-high-resolution mass spectrometer.

Electrospray ionization (ESI) has been used as a universal soft ionization technique in numerous studies on the chemical characterization of organic aerosols generated in chamber experiments (Kourtchev *et al.*, 2015; Nizkorodov *et al.*, 2011; Romonosky *et al.*, 2017). The combination of ESI and Orbitrap MS via direct infusion is highly likely to be prone to changes in the ionization efficiency of the analytes due to the highly complex matrix (Nozière *et al.*, 2015). Ion suppression and clustering during ionization may be responsible for critical discrimination against certain molecular classes, leading to a commonly observed drawback that a majority of studies are limited to qualitative comparisons between different samples (Laskin *et al.*, 2018). One possibility to overcome this shortcoming is the combination of ESI-MS and ultra-high-performance liquid chromatography (UHPLC), which not only reduces ion suppression and clustering during ionization but also offers the retention time (R_t) as a third dimension besides signal intensity and exact molecular mass of the analytes. Furthermore, special chromatographic columns allow the separation of isomers at various polarities (Vogel *et al.*, 2016b; Wang *et al.*, 2017).

In this study, filter samples were taken at the Cosmics Leaving Outdoor Droplets (CLOUD) chamber at the European Organization for Nuclear Research (CERN), Geneva, during the CLOUD 10 campaign and analyzed using UHPLC Orbitrap MS. The MS data was processed by a non-target screening approach to identify significant signals. The experiments were focused on pure biogenic nucleation events with oxidation products of α -pinene, Δ -3-carene, and isoprene as well as mixed runs with sulfuric acid vapor, NO_x , and ammonia. Identified molecules were assigned to compound classes containing only carbon, hydrogen, and oxygen (CHO), nitrogen-containing organics (CHON), sulfur-containing organics (CHOS), and organic compounds containing nitrogen and sulfur (CHONS). A special focus of the studies was on a recently described class of oxidation products called highly oxidized multifunctional organic compounds (HOMs) (Ehn *et al.*, 2014; Mentel *et al.*, 2015). Primarily formed by the oxidation of biogenic VOCs (Jokinen *et al.*, 2015), these compounds are characterized by high O/C ratios and low vapor pressures, presumably making them major contributors to atmospheric aerosol

formation (Ehn *et al.*, 2014; Riccobono *et al.*, 2014; Riipinen *et al.*, 2012). In addition to several state-of-the-art online mass spectrometers which were running during the experiments, offline UHPLC-ESI-Orbitrap-MS was applied for exact molecular formula identification of the signals from collected filter samples. The soft ionization technique (i.e. ESI) commonly results in the formation of ions with very little or no fragmentation, facilitating the interpretation of mass spectra. Furthermore, Orbitrap MS offers the advantage to perform MS²-experiments for structural elucidation.

3.2 Experimental

3.2.1 The CLOUD Chamber

The CLOUD chamber is regularly operated since 2009 for various experimental aims. The facility at CERN is described in detail elsewhere (Duplissy *et al.*, 2016; Kirkby *et al.*, 2011) and only a brief description will be given here. In Figure 3.1, panel a) shows a technical schematic of the CLOUD chamber whereas the panels b) and c) show photographs of the chamber and filter sampling during CLOUD 10 campaign. The CLOUD experiment chamber is a 26 m³ stainless steel chamber designed to achieve highest standards of cleanliness and temperature stability. An insulated thermal housing provides stable experimental temperatures within 0.1 K in a range from 207 K to 310 K (Dias *et al.*, 2017). To ensure the highest standards of cleanliness, the electro-polished inner surface of the CLOUD chamber is cleaned before each campaign with ultrapure water and subsequently heated to 373 K. After the heat-out process, it is flushed at a high flow rate with humidified synthetic air containing several ppmv of ozone (Kirkby *et al.*, 2016). The chamber is furthermore constantly operated at + 5 mbar against ambient pressure in order to exclude contamination from the outside experimental hall. The CLOUD chamber is continuously exposed to natural galactic cosmic rays (GCR). A high-voltage field cage presented by two electrodes (top and bottom of the chamber) can be switched on to reduce the ion-pair concentration significantly by applying voltages of ± 30 kV (Duplissy *et al.*, 2016). This mode is referred to as neutral conditions (N). Furthermore, ion concentrations can be increased by the pion beam from the CERN Proton Synchrotron (3.5 GeV/c). During the experiments, the chamber is filled with either humidified or dry ultrapure synthetic air. All trace gases passed into the chamber were also on the highest levels of cleanliness with contamination levels of condensable vapors in the sub-pptv range (Kirkby *et al.*, 2016). UV light in a range of 250-450 nm is produced by Hg-Xe lamps and introduced via 239 optical fiber vacuum feedthroughs installed on the top of the chamber. Additionally, a Kr-F excimer laser ($\lambda = 248$ nm) can be used to increase the production of OH via O₃ photolysis.

The chamber is surrounded by state-of-the-art instruments to analyze and control the performed experiments including several mass spectrometers and instrumentation to measure the particle concentration and number size distribution in different size ranges.

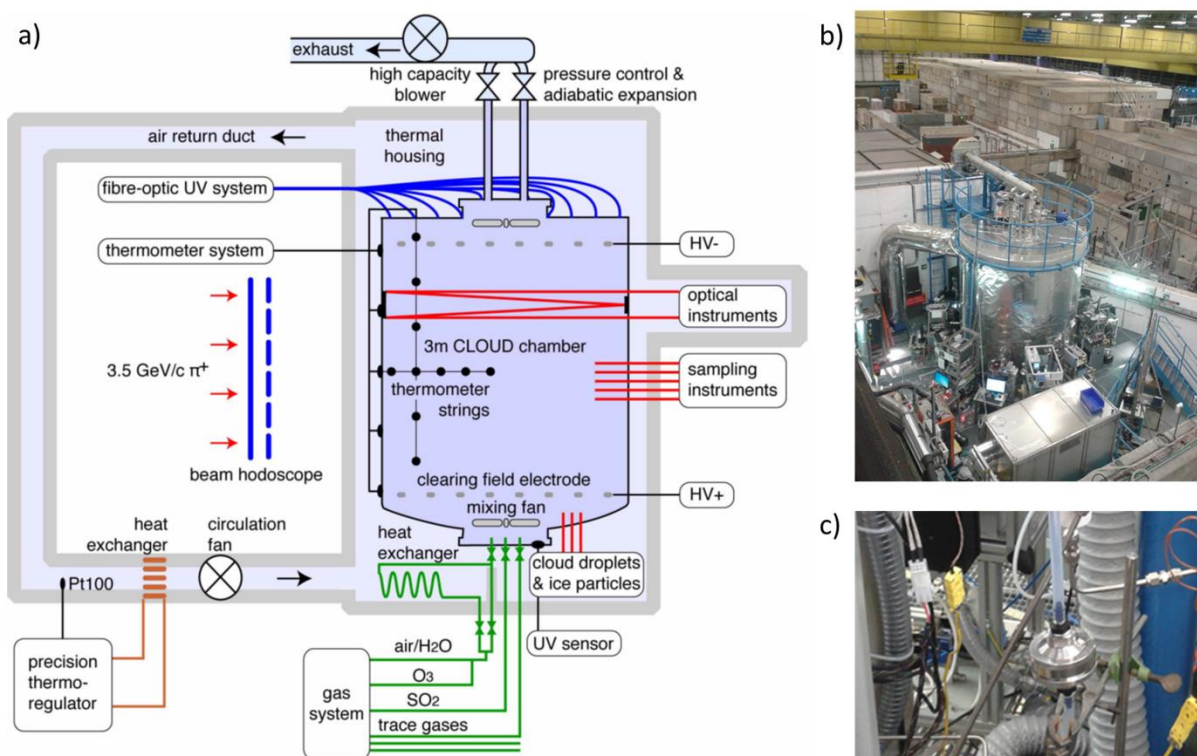


Figure 3.1 a) Schematic diagram of the CLOUD chamber at CERN Proton Synchrotron (Almeida *et al.*, 2013). b) Photograph of the CLOUD chamber during CLOUD 10 campaign. The photograph shows about 2/3 of the chamber volume surrounded by various sampling instruments. c) Photograph of the filter sampling device installed at the CLOUD chamber.

3.2.2 Filter Analysis Using UHPLC-(H)ESI-UHRMS

The data were obtained during the CLOUD 10 campaign between September and December 2015. SOA particles were sampled by passing an air flow of 10 L/min through PTFE-coated quartz fiber film filters (47 mm, Pallflex T60A20, Pall Life Science, USA) for distinct sampling times throughout the campaign (see Figure 3.1c). Sampled filters were transferred to previously pre-cleaned and baked-out (450 °C for minimum 8 h) amber glass bottles. Subsequently, the filters were stored at -18 °C until analysis. Blank filters were taken by placing a filter into the filter holder for different times, sampling the clean synthetic air inside the chamber. Additionally, two filters were taken directly out of the reservoir, stored in separate amber glasses and treated the same way as filter samples until analysis.

Extraction was performed by cutting the filter sample into pieces and adding 1.5 mL of a methanol/water solution (9/1). Subsequently, the sample was shaken for 30 min. The extract was filtered through a syringe filter (Micropur, PTFE, 3 mm, 0.2 µm) and transferred into a separate glass vial. The extraction step was repeated two times using 1 mL of the methanol/water solution. The combined extracts were concentrated by a gentle stream of nitrogen at 40 °C to almost dryness. The remaining extract was dissolved in 200 µL of a water/acetonitrile solution (9/1), shaken for 30 s using a vortex shaker and subsequently measured by UHPLC-MS.

The chromatographic analysis was performed by an UltiMate 3000 UHPLC system (Dionex, Thermo Scientific, Germany) composed of degasser, binary gradient pump, auto sampler, and temperature column compartment. The analytical column (Hypersil Gold, C18, 150x2.1 mm, 1.9 μm , Thermo Scientific) was kept at 25 $^{\circ}\text{C}$ during analysis. As eluents, solutions of ultrapure water (Optima[®] LC-MS, Fisher Scientific, USA) with 2 % acetonitrile (Optima[®] LC-MS, Fisher Scientific, USA) and 0.04 % formic acid (eluent additive for LC-MS) (Eluent A) and a solution of acetonitrile with 2 % of ultrapure water (Eluent B) were used in gradient mode with a flow rate of 500 $\mu\text{L}/\text{min}$. The optimized gradient was 1 % B at 0 min, 1 % B at 1.5 min, 20 % at 3.5 min, 20 % B at 6 min, 30 % B at 7.5 min, 50 % B at 8.5 min, 99 % B at 9 min, 99 % B at 11.5 min, and 1 % B at 11.55 min. The injection volume was 20 μL per run and every sample was measured in triplicate in both negative and positive ionization mode. High-resolution mass spectra were obtained by a Q Exactive[™] hybrid quadrupole Orbitrap mass spectrometer (Thermo Scientific, Germany). Ionization of the analytes was performed by a heated ESI source at 120 $^{\circ}\text{C}$. The settings of the heated ESI source were as follows: 60 psi sheath gas, 20 psi aux gas, 3.5 kV spray voltage, and 320 $^{\circ}\text{C}$ capillary temperature. The Full-MS mode was operated within a scan range of m/z 80 – 800 with a mass resolution setting of $R = 70\,000$ at m/z 200. The Q Exactive mass spectrometer was calibrated by commercially available calibration solutions (Pierce[™] Negative Ion Calibration Solution, Pierce[™] Positive Ion Calibration Solution, Thermo Fisher). Additionally, 4-hydroxybutanoic acid was added to the Negative Ion Calibration Solution for calibration and used as a lock mass to optimize the mass accuracy for smaller masses than 250 Da. Complementary MS² experiments were conducted using individual inclusion lists with an isolation width of m/z 1 and a mass resolving power of $R = 17\,500$ at m/z 200.

3.2.3 Data Processing of UHRMS Data

Data were processed by XCalibur[™] 2.2 (Thermo Scientific, USA) and further analyzed by Sieve[™] 2.2 (Thermo Scientific, USA) to perform a non-target screening approach. The software subtracts the background chromatograms and detects signals above a given threshold value (i.e., $1 \cdot 10^6$ a.u.) in the two-dimensional space of retention time (i.e., 0 – 11.5 min) vs. m/z (i.e., 80 – 800). Signals that vary significantly from the blank chromatogram will be assigned as a compound. Signals of corresponding isotopes and ion-clusters appearing at the same retention time and the exact mass difference will be assigned to the molecular ion compound. Molecular formulas for the identified signals were calculated using a mass tolerance of ± 2 ppm and the following constraints: $\#^{12}\text{C}$ (0 – 45), $\#^1\text{H}$ (0 – 60), $\#^{16}\text{O}$ (0 – 20), $\#^{14}\text{N}$ (0 – 4), and $\#^{32}\text{S}$ (0 – 2). Neutral formulas with chemically impossible compositions, non-integer or negative double bond equivalents (DBE) and unreasonable O/C and H/C element ratios were discarded.

Discussion and interpretation of UHRMS data was facilitated by several illustration methods. Such data plots support chemical grouping and identification of signal patterns, which help elucidating

relationships and underlying atmospheric chemical processes. A brief description of these methods will be given in the following.

The van Krevelen diagram is a plot of the H/C ratio versus the O/C ratio of each formula detected in a sample and can be applied to visualize possible reaction pathways, e.g., methylations/demethylations, hydrogenations/dehydrogenations, hydration/condensation, and oxidation/reduction (Kim *et al.*, 2003). Furthermore, due to van Krevelen diagrams one can also distinguish potential sources of organic aerosols by the corresponding position in the diagram (Wozniak *et al.*, 2008).

Double Bond Equivalent (DBE) reflect a value for the number of double bonds and rings in a molecule and is, therefore, an index for the hydrogen deficiency. The DBE is calculated for formulas according to the general type $C_cH_hN_nO_o$ using equation 3.1:

$$DBE = 1 + c - 0.5h + 0.5n \quad (3.1)$$

However, it should be noted that the DBE of molecules containing heteroatoms with multiple valences (e.g., Sulfur) should be considered with caution (Nozière *et al.*, 2015). Moreover, the sulfur-oxygen double bonds of the sulfate groups are not taken into account.

The average carbon oxidation state (\overline{OS}_C) was suggested by Kroll *et al.* as a valuable metric for the degree of oxidation of organic species in the atmosphere (Kroll *et al.*, 2011). Furthermore, it was shown that the \overline{OS}_C is linked to aerosol volatility, and thus, a useful metric to classify SOA (Nozière *et al.*, 2015). The \overline{OS}_C value is calculated for each molecular formula using the following equation 3.2:

$$\overline{OS}_C = - \sum_i OS_i \frac{n_i}{n_C} \quad (3.2)$$

In this equation, OS_i is the oxidation state associated with element i and n_i/n_C is the molar ratio of element i to carbon within the molecule.

Another useful tool to elucidate molecular (homologous) series and compound classes in complex data sets is given by the Kendrick Mass (KM) analysis (Hughey *et al.*, 2001). Originally, the KM of a base unit (e.g., CH_2 group) is calculated by renormalizing the exact IUPAC mass (14.01565 Da) of CH_2 to 14.00000. The KM and the Kendrick Mass Defect (KMD) can be calculated according to the equation (3.3) and (3.4):

$$KM_{CH_2} = \text{Observed Mass} * \left(\frac{14.00000}{14.01565} \right) \quad (3.3)$$

$$KMD_{CH_2} = \text{Nominal Mass} - KM_{CH_2} \quad (3.4)$$

Observed mass is the exact mass of a compound measured by UHRMS. According to this renormalization, compounds that differ only by the number of the base unit have exactly the same KMD and can be identified and grouped into homologous series.

3.2.4 Experimental Design

Prior to the analysis of filter samples of the CLOUD 10 campaign, measurements were performed to assess extraction efficiencies and ensure linearity of the filter extraction procedure. Therefore, filter samples were spiked with defined amounts of established SOA proxy compounds (i.e., MBTCA and pinic acid) and extracted using the filter method described in chapter 3.2.2. Quantification was conducted using external calibration of standard solutions. Accordingly, the linearity of the correlation between sampling time versus signal intensity was investigated. For this reason, α -pinene oxidation was performed in a smog chamber in a laboratory setup in Mainz, Germany. SOA was produced by injection of 300 ppb α -pinene and 1 ppm ozone in a 100 L smog chamber. The particle number size distribution between 10 and 100 nm was determined by a Scanning Mobility Particle Sizer (SMPS+C, Grimm Aerosol Technik, Ainring, Germany). As soon as the particle mass concentration reached a constant level, the SOA particles were sampled by passing an air flow of 2 L/min through PTFE-coated quartz fiber film filters (70 mm, Pallflex T60A20, Pall Life Science, USA) for distinct sampling times. A blank filter was placed on the filter holder for 30 min, without passing an air stream. Subsequent filter analysis was performed according to the method introduced in chapter 3.2.2.

The experiments at CLOUD 10 were designed to simulate atmospheric daytime conditions comparable to the conditions observed at the Hyytiälä SMEAR II station in the boreal forest region in Finland (Hari, P. & Kulmala, M., 2005). The main settings of the experiments are summarized in Table 3.1. The temperature was regulated to 5 °C with a relative humidity (RH) of ~40 %. Sunlight was imitated by the UV-light system to provide a broad range of UV light close to atmospheric levels. A Kr-F excimer laser (3 W, $\lambda = 248$ nm) was additionally used to produce OH radicals via O₃ photolysis and two UV LEDs (2 × 16.5 W, $\lambda = 370$ -390 nm) were used to photolyze NO₂ to NO. Ozone was injected at a constant rate throughout the experiments, maintaining a volume mixing ratio of ~40 ppbv. The monoterpenes (α -pinene/ Δ -3-carene in an initial mixing ratio of 2:1) were injected at neutral conditions with steady-state concentrations of 1300 pptv. Initial SO₂ concentrations ranged from 0 to 3.3 ppbv. After the generated particles grew beyond the nucleation mode, NO was injected into the chamber from 0 to 5 ppbv in three steps.

Table 3.1 Summary of experimental conditions for Hyytiälä simulation experiments at CLOUD 10.

	Experiment #			
	1749	1750	1751	1752
VOC (ppt)	1300	1300	1300	1300
O ₃ (ppb)	40	40	40	40
NO _x		0 - 5 ppb in 3 steps		
SO ₂ (ppb)	3.3	1.8	1.1	0

3.3 Results and Discussion

3.3.1 Extraction Efficiencies of α -Pinene SOA Proxy Compounds

The filter extraction method was evaluated for extraction efficiencies of two common α -pinene SOA proxy compounds, i.e., 3-methyl-1,2,3-butanetricarboxylic acid (MBTCA) and pinic acid. PTFE-coated quartz fiber film filters were cut into pieces and spiked with 500 ng/mL standard solution in high purity water. Extraction efficiencies were determined in triplicate. The filters were extracted according to the method described in chapter 3.2.2. The obtained calibration curve is depicted in Figure 3.2 and follows a linear relationship.

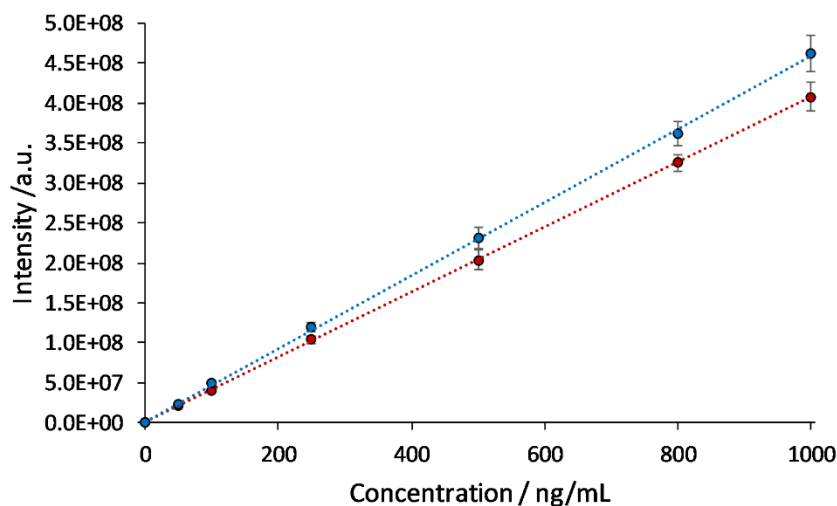


Figure 3.2 Calibration of MBTCA (red) and pinic acid (blue) for the determination of extraction efficiencies. Both measurement series exhibit a linear correlation (R^2 (MBTCA) = 1.000; R^2 (pinic acid) = 1.000).

Extraction efficiencies of 95.6 ± 2.1 % and 95.3 ± 3.0 % were determined by external calibration for MBTCA and pinic acid, respectively. Therefore, a quantitative extraction of α -pinene SOA components can be assumed for the applied filter extraction method.

For the investigation of the correlation between sampling time and signal intensity for SOA components, five PTFE-coated quartz fiber film filters were sampled with SOA particles for 1, 2, 4, 6, and 10 hours, respectively. In addition, a blank sample was analyzed in the same way, to account for

background values. The aerosol mass concentration during sampling was at $2 \mu\text{g}/\text{m}^3$. Accordingly, the sampled aerosol mass varied between $0.19 \mu\text{g}$ and $2.45 \mu\text{g}$ per filter.

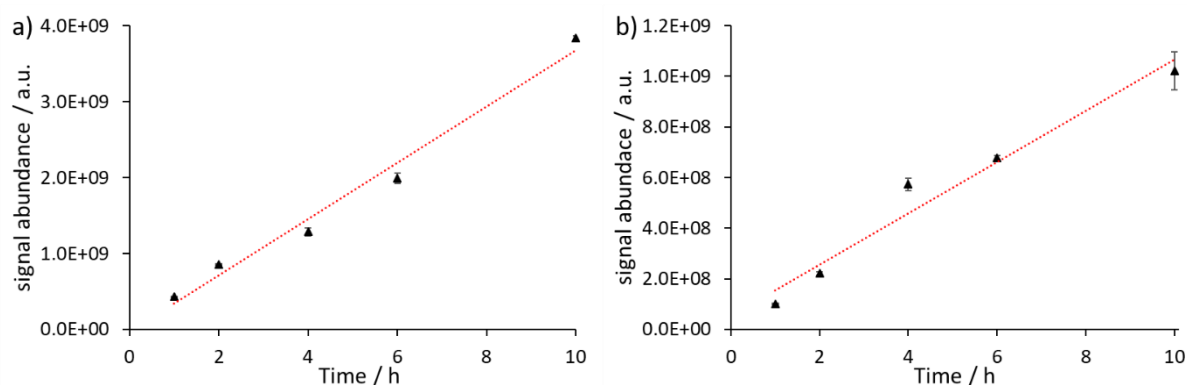


Figure 3.3 Signal abundance vs. sampling time for sampled SOA particle compounds. a) pinic acid (m/z 185.0819 ([M-H]⁻); $R^2 = 0.98$), b) pinonic acid (m/z 183.1026 ([M-H]⁻); $R^2 = 0.96$).

Figure 3.3 depicts the signal abundance versus the sampling time for the α -pinene-derived oxidation products pinic acid and pinonic acid, which are common constituents of biogenic SOA. Correlation coefficients of $R^2 = 0.98$ and $R^2 = 0.96$ were determined for pinic acid and pinonic acid, respectively, demonstrating a linear correlation between sampled SOA mass and signal intensity.

3.3.2 Molecular Composition of SOA Particles at CLOUD 10

The particle size distribution, particle number concentration (N_t), and the particle mass concentration of the Hyytiälä simulation experiments at CLOUD 10 are shown in Figure 3.4. The particles were measured by a combination of a Scanning Mobility Particle Sizer (SMPS) and a nano-SMPS (see Tröstl *et al.*, 2016 for detailed information). Drawbacks due to a defect charger in the SMPS system caused a noise and offset at 60 nm. These problems were fixed at the end of experiment 1751. The generated particles grew to a maximum particle diameter of ~ 100 nm in each experiment. Nucleation of the VOC precursors started under neutral conditions (i.e., 1st nucleation event in experiment 1749). Once the concentration of regularly observed molecules (e.g. HOMs) reached a steady state, the high voltage field was turned off to reach galactic cosmic ray conditions, resulting in a second ion-induced nucleation event (Kirkby *et al.*, 2016). After the particles grew beyond the size of nucleation mode, NO was injected stepwise into the chamber. Between the nucleation events three, four, and five of experiment 1749, the clearing field was activated for about 15 min to quench the previous nucleation event. However, the sub-micrometer particles were collected on one filter per experiment and the analysis of the molecular composition of different nucleation events is not possible with this offline technique. Filter exchange was performed directly before the start of the next experiments to avoid cross-contamination of particles from previous experiments.

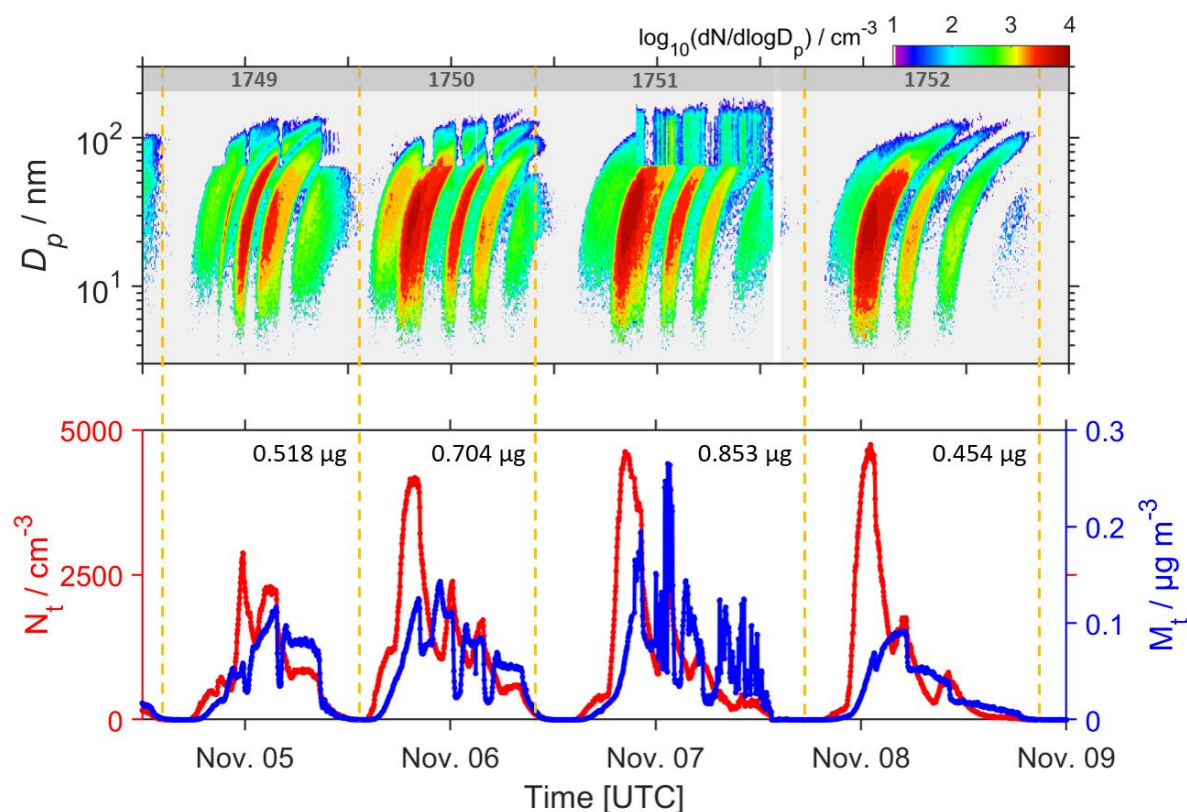


Figure 3.4 Temporal variation of particle number size distribution (upper panel), total particle number, and total particle mass (lower panel) during Hyytiälä simulation runs at CLOUD 10. The submicron aerosol particle size distribution was measured by a combination of an SMPS and a nano-SMPS. The dashed lines indicate filter changes between experiments 1749, 1750, 1751, and 1752. The sampled mass per filter ranged from 0.454 μg to 0.853 μg .

In all experiments, the maximum particle number concentration was about 5000 particles per cm^3 and the maximum particle mass concentration was at $\sim 0.25 \mu\text{g}/\text{m}^3$. The aerosol mass concentration was calculated according to the aerosol number concentration with an estimated effective aerosol density of $1.2 \text{ g}/\text{cm}^3$ (Hallquist *et al.*, 2009). The SO_2 mixing ratios were 3.3 ppb, 1.8 ppb, 1.1 ppb for experiment 1749, 1750, and 1751, respectively. At experiment 1752, no SO_2 injection was performed. Accordingly, the sampled aerosol mass on the filters was calculated 0.518 μg , 0.704 μg , 0.853 μg , and 0.454 μg for experiment 1749, 1750, 1751, and 1752, respectively.

The filter samples were subsequently processed in the laboratory and a non-target screening approach was applied to the obtained dataset. The compounds detected in negative ionization mode were divided into four subclasses: compounds containing only carbon, hydrogen, and oxygen (CHO); nitrogen-containing organics (CHON); sulfur-containing organics (CHOS); and organic compounds containing nitrogen and sulfur (CHONS). All these compounds classes are likely to exhibit acidic functionalities, which allow the detection in the negative mode (i.e., as $[\text{M}-\text{H}]^-$ species). For the four experiments, we assigned 217 – 357 signals of the corresponding LC-MS dataset to molecular formulas, including various numbers of isomers for each formula. Table 3.2 shows detailed information for each experiment including the molecular weight (MW), the mean DBE, O/C and H/C ratios, as well as the

average retention time of each sub-class. The data shows values averaged over the signal intensity of each signal. Furthermore, the signal intensity was normalized by the sampled aerosol mass on each filter.

Table 3.2 Summary of the non-target screening approach of the LC-MS analysis of the Hyttiälä simulation experiments detected in the negative ionization mode. The number of detected molecules (#) and averages for DBEs, H/C ratios, O/C ratios, \overline{OS}_C , and retention times (Rt (min)) is given for each subclass (i.e., CHO, CHON, CHOS, CHONS).

CHO							CHON					
experiment	#	DBE	H/C	O/C	\overline{OS}_C	Rt	#	DBE	H/C	O/C	\overline{OS}_C	Rt
1749	116	3.37	1.55	0.43	-0.69	6.18	28	3.95	1.60	0.71	-0.95	5.55
1750	140	3.25	1.55	0.45	-0.65	6.00	24	3.80	1.64	0.81	-0.94	5.66
1751	170	3.30	1.56	0.44	-0.67	6.41	30	3.94	1.63	0.88	-0.81	5.36
1752	177	3.12	1.57	0.44	-0.69	5.97	21	4.60	1.54	0.73	-0.85	5.75

CHOS							CHONS					
experiment	#	DBE	H/C	O/C	\overline{OS}_C	Rt	#	DBE	H/C	O/C	\overline{OS}_C	Rt
1749	141	1.89	1.84	0.58	-1.28	6.55	10	3.01	1.70	0.71	-1.38	7.74
1750	157	1.91	1.83	0.58	-1.27	6.53	8	3.00	1.70	0.71	-1.38	7.87
1751	150	1.86	1.85	0.58	-1.28	6.58	7	3.00	1.70	0.71	-1.39	8.32
1752	16	3.70	1.66	0.51	-1.17	7.43	2	3.00	1.70	0.70	-1.40	8.90

The majority of compounds were assigned to formulas containing CHO and CHOS. Figure 3.5 illustrates the summed relative intensity of each subclass normalized to the sampled aerosol mass. CHO- and CHOS-containing compounds showed the highest signal intensities, whereas CHON-containing compounds showed nearly no difference for the different SO₂ mixing ratios. Interestingly, at different experimental SO₂ concentrations, roughly the same number (~150) of CHOS compounds was detected. However, the summed signal intensity of these compounds decreased with decreasing SO₂ concentrations. Accordingly, the number of CHO compounds, as well as the percentage of the summed signal intensities increased with decreasing SO₂ concentration. It should be noted that the sulfur-containing compounds in experiment 1752 are likely a result of contaminations during the sampling process or remaining atmospheric H₂SO₄ in the chamber. The experiments with varying SO₂ injection only showed minor differences in the displayed characteristics in Table 3.2 among each other contrary to experiment 1752 without SO₂ injection.

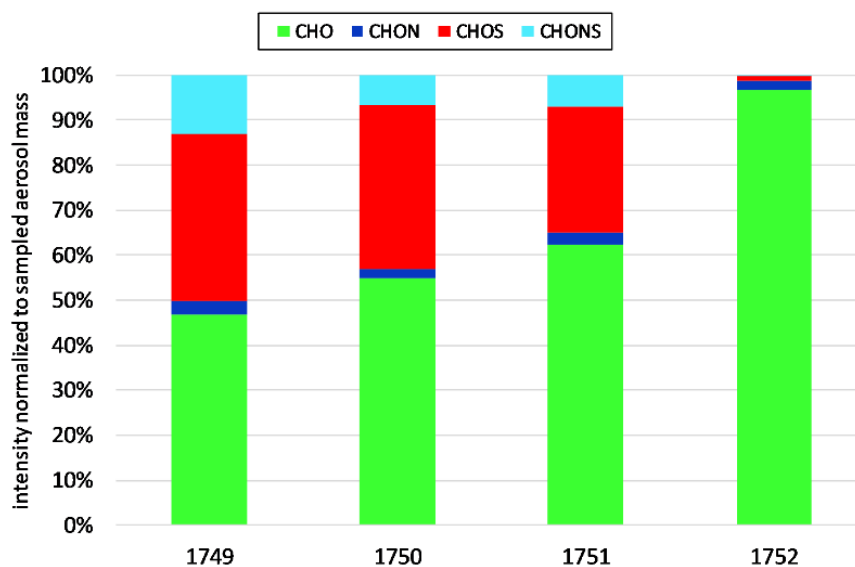


Figure 3.5 Normalized signal intensities of the assigned subclasses CHO (green), CHON (blue), CHOS (red), and CHONS (cyan). The experiment numbers 1749, 1750, 1751, and 1752 correspond to the SO₂ mixing ratios of 3.3 ppb, 1.8 ppb, 1.1 ppb, and 0 ppb, respectively.

A plot of the retention time versus the exact mass of each compound is shown in Figure 3.6 for each experiment. This two-dimensional space exhibits distinct areas for the different polarities of the compounds. The marker areas reflect the relative signal intensity of the single molecules. For each of the experiments, three areas can be distinguished: an area of small and highly polar compounds ($m/z < 200$, $Rt < 2$ min), an area of most likely monomer CHO-containing SOA compounds ($130 < m/z < 240$, $4 \text{ min} < Rt < 8 \text{ min}$) and corresponding sulfate functionalities ($210 < m/z < 300$, $4 \text{ min} < Rt < 6 \text{ min}$), and an area of dimer CHO-containing SOA compounds and sulfated molecules ($230 < m/z < 410$, $8.5 \text{ min} < Rt < 11 \text{ min}$). It is nicely shown, that the number of CHOS-containing compounds was not reduced with decreasing SO₂ mixing ratio from experiment 1749 to experiment 1751. In contrast, a decreasing signal intensity, exhibited by the marker size of the compounds, is clearly detected. In the experiment without SO₂ injection (i.e., 1752), almost no CHOS compounds were detected, whereas the relative intensity of the CHO-containing compounds increased remarkably in the monomer as well as dimer range. Especially in the monomer region, an association between CHO- and corresponding CHOS-containing compounds can be observed. Most of the sulfated compounds show a mass difference equivalent to H₂SO₄ and a decreased Rt due to a higher polarity.

The class of CHONS compounds almost exclusively consisted of isomers of the α -pinene related nitrooxy organosulfate C₁₀H₁₇NO₇S (Surratt *et al.*, 2007; Surratt *et al.*, 2008) and C₁₀H₁₇O₁₀NS (Iinuma *et al.*, 2007b; Surratt *et al.*, 2008). The signal intensities of the five isomers of C₁₀H₁₇NO₇S also decreased with decreasing SO₂ mixing ratio and were no longer detected in experiment 1752 without SO₂ injection.

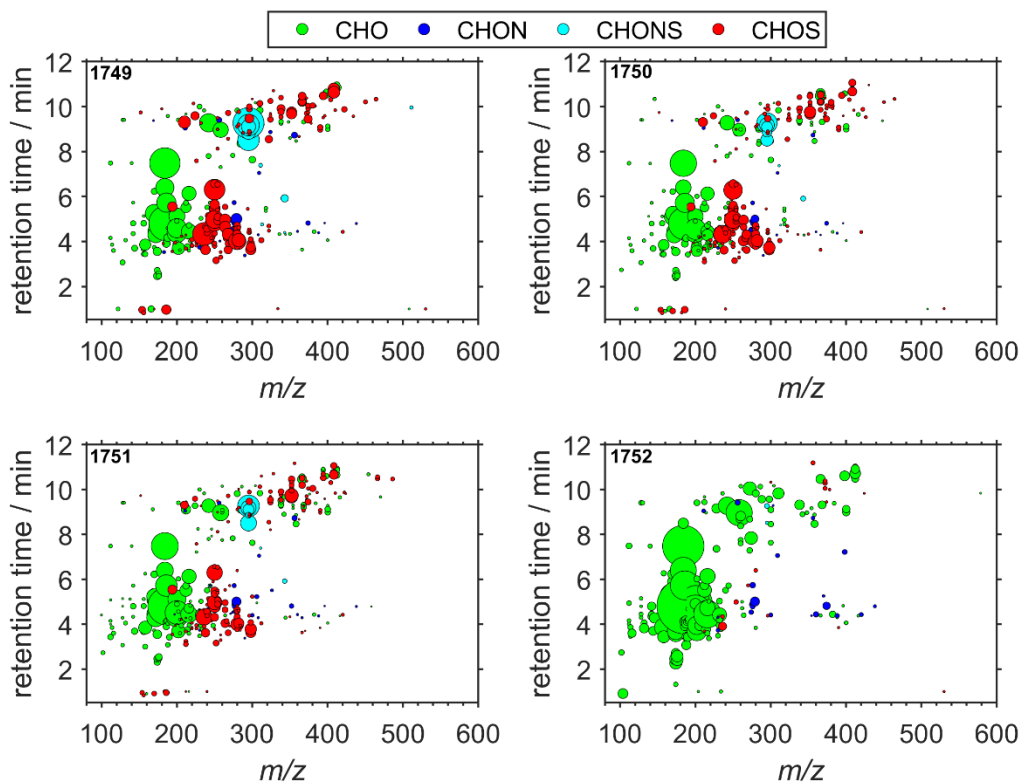


Figure 3.6 Retention time (Rt) versus mass to charge ratio (m/z) for detected compounds in the Hyttiälä simulations. The marker areas reflect the relative ion intensity of the signals.

Interestingly, CHON compounds did not show high compound numbers and high signal abundances, respectively. During CLOUD 10, many organic nitrates were detected by a FIGAERO-MS in real-time. Most likely due to an assumed short particle-phase lifetime of 2 – 4 h (Lee *et al.*, 2016), detection of most of the organic nitrates was not accessible by filter analysis using UHPLC-UHRMS. The most intensive CHON compounds were $C_{10}H_{17}NO_8$ and $C_9H_{12}N_2O_8$. The different compound classes are further discussed separately.

3.3.2.1 CHO compounds

The majority of ions detected in the Hyttiälä simulation filter extracts were assigned to molecular formulas containing CHO atoms. In total 75 – 101 formulas of CHO molecules were determined in the negative mode in a mass range from 102 – 454 Da. These formulas are distributed over 116 – 177 different isomers. 55 of the CHO formulas were detected in all filter extract, independent from the SO_2 concentrations, whereas 22 compounds were exclusively detected in experiment 1752. The highest abundances were centered around 180-200 Da, defined as monomer region (Ehn *et al.*, 2014). By analysis of the retention time and the exact mass, the most intense signal was identified as pinic acid (see Figure 7.2 in the Supporting Information to chapter 3).

In the van Krevelen plot presented in Figure 3.7a, O/C and H/C ratios of the detected compounds were mostly between 0.3 – 0.8 and 1.3 – 1.8, respectively. Moreover, the distribution of the compounds is in reasonable agreement with laboratory investigations of SOA analyzed by direct infusion UHRMS

(Tu *et al.*, 2016; Wozniak *et al.*, 2008). However, we detected much less marker compounds for α -/ β -pinene SOA compared to direct infusion UHRMS studies (Kourtchev *et al.*, 2015). A possible reason might be the approach of using chromatographic separation prior to ionization to reduce cluster formation. Moreover, the chromatographic separation is advantageous compared to direct infusion MS, because of the detection of molecular isomers with different R_t . In Figure 3.7a, we introduced a new classification of the van Krevelen diagram according to the \overline{OS}_C defined by equation 3.2. Two lines representing the $\overline{OS}_C = -0.67$ and $\overline{OS}_C = 0$, respectively, classify the van Krevelen diagram into specific regions of interest. Region I mainly shows oxidized molecules with oxidation states lower than the respective value of pinic acid, as a proxy for semi-volatile oxidized organic compounds (Kroll *et al.*, 2011). Region II includes molecules with \overline{OS}_C values between pinic acid and MBTCA, which serves as a proxy for highly oxygenated molecules. Molecules with similar or higher \overline{OS}_C are located in area III. This region is mostly composed of isomers of $C_{17-18}H_{17-19}O_{11}$ compounds, which possibly represent HOM-dimers (dimer fragments) that are assumed to be involved in new particle formation (Bianchi *et al.*, 2016; Kirkby *et al.*, 2016; Riccobono *et al.*, 2014).

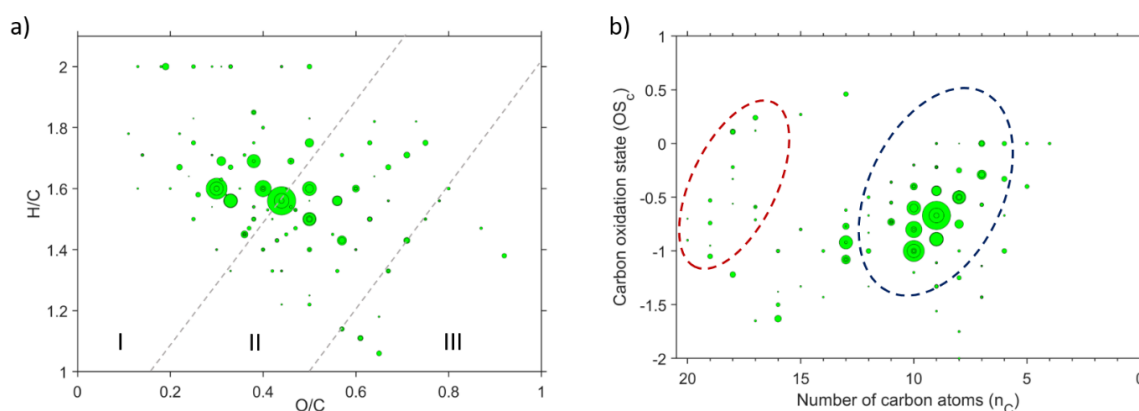


Figure 3.7 a) Van Krevelen plot for CHO compounds detected in the neg. ionization mode. The lines drawn in this plot define three areas according to \overline{OS}_C values. (I) $\overline{OS}_C < -0.67$, (II) $-0.67 \leq \overline{OS}_C < 0$, (III) $0 \leq \overline{OS}_C$. b) Carbon oxidation state plot for CHO compounds detected in the negative ionization mode. The ovals represent area characteristic for the HOMs dimer (red) and monomer mode (blue).

The \overline{OS}_C -plot of CHO compounds is presented in Figure 3.7b. The detected compounds showed values between 5 and up to 20 carbon atoms with \overline{OS}_C values ranging from -1.7 to 0.5, thus we assigned this region to show the signals of biogenic nucleation particles from α -pinene/ Δ -3-carene oxidation according to the precisely defined experimental conditions. Furthermore, we assigned certain areas in this region to monomer and dimer oxidation products, commonly both referred to as HOMs (Ehn *et al.*, 2014; Mentel *et al.*, 2015). In contrast to previous studies (Kourtchev *et al.*, 2015; Kroll *et al.*, 2011), we note that molecules with an \overline{OS}_C value between -0.5 and -1.5 do not necessarily originate from biomass burning organic aerosol. Furthermore, the defined space of semi-volatile and/or low volatility

oxidized organic aerosol components should be extended to \overline{OS}_C -1.5. However, a smooth transition needs to be considered in terms of classification into different compound classes or sources.

Table 3.3 shows the CHO compounds denoted as dimeric HOMs detected in the CLOUD 10 filter samples. Besides some compounds previously identified in the gas and particulate phase, several molecular formulas are identified here for the first time. Furthermore, the chromatographic analysis clearly demonstrates the existence of isomeric compounds for different CHO molecules. The dimers denoted as HOMs in this study possess 17 – 20 carbon atoms and 7 – 14 oxygen atoms.

Table 3.3 Elemental formulas, m/z values, elemental ratios, \overline{OS}_C values, and corresponding Rt of the isomers of CHO containing highly oxidized molecules (HOMs) detected by UHPLC(-)ESI-UHRMS during CLOUD 10.

elemental composition	measured m/z ([M-H] ⁻)	H/C	O/C	\overline{OS}_C	Rt (min)
C ₁₇ H ₂₆ O ₇	341.1603	1.53	0.41	-0.71	8.90; 9.67
C ₁₇ H ₂₆ O ₈ ^(a)	357.1553	1.53	0.47	-0.59	8.47; 8.88
C ₁₇ H ₁₈ O ₁₁	397.0779	1.06	0.65	0.24	10.61
C ₁₇ H ₂₀ O ₁₁	399.0930	1.18	0.65	0.12	4.06
C ₁₇ H ₂₆ O ₁₄ ^{(b), (c)}	453.1254	1.53	0.82	0.12	10.68
C ₁₈ H ₂₈ O ₇ ^(d)	355.1761	1.56	0.39	-0.78	9.64
C ₁₈ H ₂₂ O ₈	365.1238	1.22	0.44	-0.33	4.39
C ₁₈ H ₂₂ O ₉	381.1189	1.22	0.50	-0.22	4.44
C ₁₈ H ₂₈ O ₉ ^(e)	387.1659	1.56	0.50	-0.56	4.30
C ₁₈ H ₂₀ O ₁₁	411.0937	1.11	0.61	0.11	10.57-11.02
C ₁₉ H ₂₈ O ₇ ^(a)	367.1759	1.47	0.37	-0.74	9.21; 9.29; 9.32
C ₁₉ H ₃₄ O ₇	373.2230	1.79	0.37	-1.05	9.53
C ₁₉ H ₂₈ O ₉ ^(d)	399.1657	1.47	0.47	-0.53	8.99; 9.13
C ₂₀ H ₃₂ O ₇	383.2073	1.60	0.35	-0.90	9.39
C ₂₀ H ₃₂ O ₉	415.1972	1.60	0.45	-0.70	4.38

References: (a) (Yasmeen *et al.*, 2010), (b) (Ehn *et al.*, 2012), (c) (Krechmer *et al.*, 2016), (d) (Zhang *et al.*, 2015), (e) (Kristensen *et al.*, 2014).

According to previous studies on volatility, the detected compounds are not only highly oxygenated but can also be assumed to exhibit low to extremely low volatilities (Donahue *et al.*, 2014; Li *et al.*, 2016) making them feasible to act as nucleating clusters. The number and percentage of HOMs per experiment were as follows: 1749 (12, 3.78 %), 1750 (10, 2.25 %), 1751 (21, 4.54 %), and 1752 (18, 3.31 %). The percentage of dominant C₁₇₋₂₀H₁₈₋₃₄O₇₋₁₄ dimers observed in the particle phase ranged from 2 – 5 % of the summed signal and is comparable to other chamber and flow tube experiments (Tu *et al.*, 2016). A comprehensive list of all detected formulas and corresponding isomers during Hyytiälä simulations at CLOUD 10 is given in the Supporting Information in chapter 7.2.

3.3.2.2 CHON compounds

The percentage of CHON compounds of the sum of all signals and the total number of CHON compounds in the filter samples varied between 2 – 3 % and 20 – 30 compounds, respectively. The detected formulas covered a mass range from m/z 168 to 437 with average values around 290 Da. The CHON compounds were subdivided into organic mono-nitrates (i.e., CHON₁) and di-nitrates (i.e., CHON₂). Interestingly, the relative fraction of the CHON₁ and CHON₂ subclasses changed with varying SO₂ concentrations, whereas the overall percentage of the summed signal remained at the same level around 2 % (see Figure 3.8).

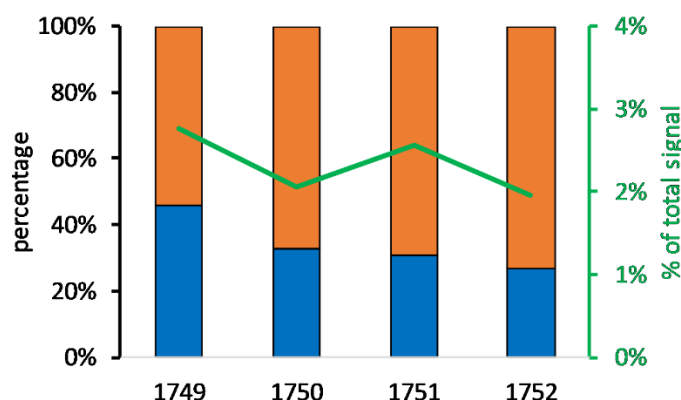


Figure 3.8 Distribution of organic mono-nitrates (blue) and di-nitrates (orange) for Hyttiälä simulation experiments at CLOUD 10. The percentage of compounds referred to organic mono-nitrates is reduced with decreasing SO₂ concentration. The percentage of the total signal (green) of CHON compounds remained at the same level. The experiment numbers 1749, 1750, 1751, and 1752 correspond to the SO₂ concentrations of 3.3 ppb, 1.8 ppb, 1.1 ppb, and 0 ppb, respectively.

The ratio of organic mono-nitrates to di-nitrates decreased from 46 % at 3.3 ppb to 27 % without SO₂ addition. Thus, we hypothesize that higher SO₂ concentrations could lead to particulate reactions forming CHOS compounds from organic mono-nitrates. Moreover, the SO₂ dependency of the organic nitrate formation may also indicate different particulate formation pathways for the dimer and the monomer channel.

One of the most prominent signals was attributed to the ion formula C₁₀H₁₆O₈N⁻ ([M-H]⁻) which was previously already detected in the particulate phase of ambient SOA (Lee *et al.*, 2016). Figure 3.9 shows the extracted ion chromatogram (EIC) of the proposed organic mono-nitrate. Additionally to the main signal at Rt = 5.03 min, three isomers at 3.88 min, 4.29 min, and 4.60 min were detected. The MS² spectrum of the parent ion at m/z 278.0878 shows an intense peak at m/z 61.9877 corresponding to NO₃⁻, which represents the collision-induced loss of an O-NO₂⁻ group. Due to the fragmentation, no additional fragments representing a possible oxidized α -pinene related structure were detected.

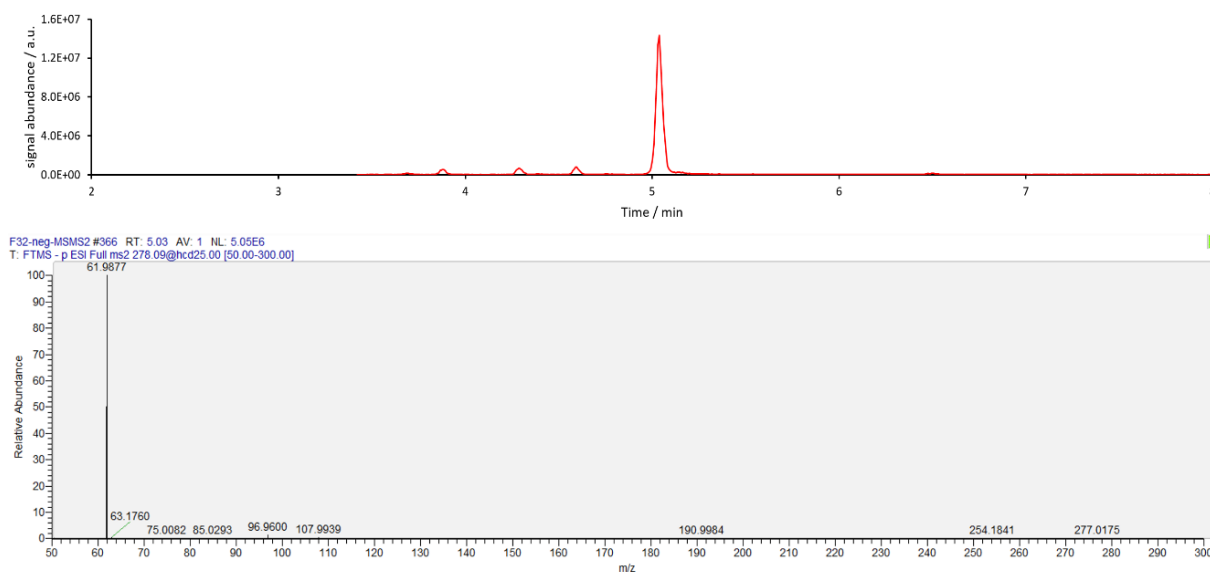


Figure 3.9 Extracted ion chromatogram (EIC) of m/z 278.0878 ($[M-H]^-$). The chromatogram shows the main signal at $R_t = 5.03$ min and less intense signals at 3.88 min, 4.29 min, and 4.60 min (upper panel). The MS^2 spectrum of the parent ion $C_{10}H_{16}O_8N^-$ ($[M-H]^-$) at m/z 278.0878 shows an intensive NO_3^- peak at m/z 61.9877 (lower panel).

The presence of dimeric organic nitrates was supported by MS^2 -studies. For example, Figure 3.10 shows an extracted ion chromatogram (EIC) and Figure 3.11 an MS^2 spectrum of the proposed dimeric organic nitrate $C_{19}H_{29}O_7N$ (m/z 382.1871 ($[M-H]^-$)).

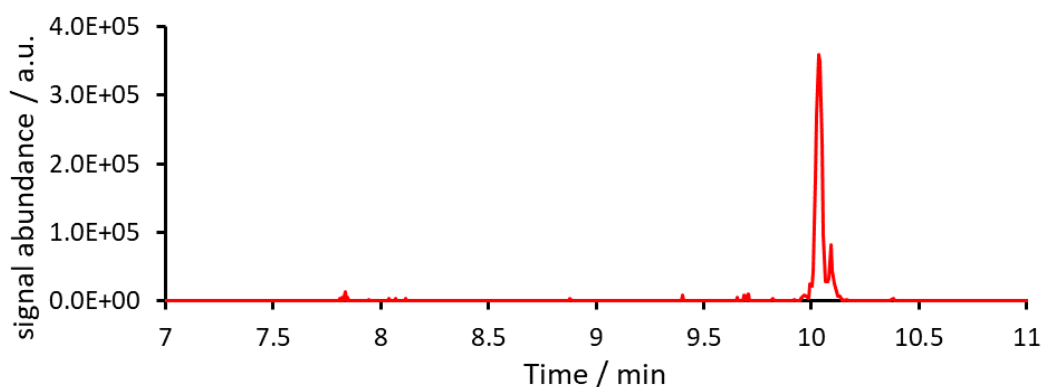


Figure 3.10 Extracted ion chromatogram (EIC) of m/z 382.1871 ($[M-H]^-$). $R_t = 10.04$ min.

Solely, one major ion signal of $C_{19}H_{28}O_7N^-$ ($[M-H]^-$) at a retention time of 10.04 min was detected. The rather high R_t is in good agreement with the suggested high number of 19 carbon atoms and a relatively low polarity.

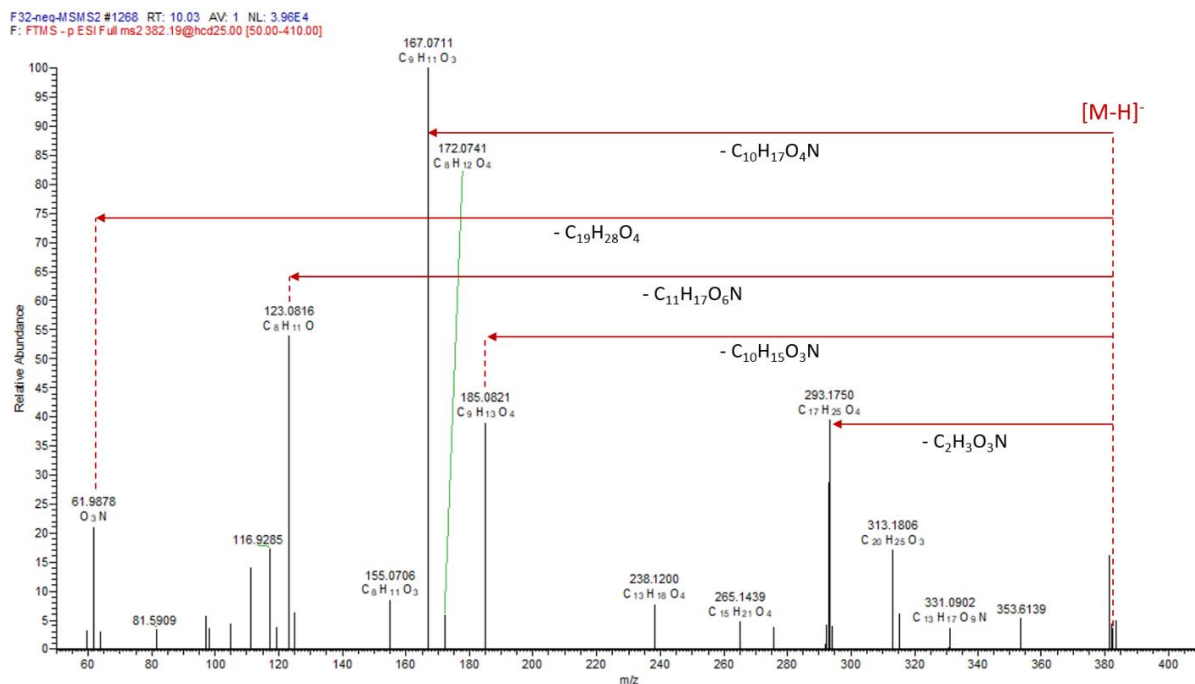


Figure 3.11 Negative mode MS² spectrum of the parent ion C₁₉H₂₈O₇N⁻ ([M-H]⁻) at m/z 382.1871. The fragmentation pattern indicates the presence of an organic nitrate: m/z 293.1750 = [M-C₂H₃O₃N]⁻, m/z 185.0821 = [M-C₁₀H₁₅O₃N]⁻, m/z 167.0711 = [M-C₁₀H₁₇O₄N]⁻, m/z 123.0816 = [M-C₁₁H₁₇O₆N]⁻, m/z 61.9878 = [M-C₁₉H₂₈O₄]⁻.

In Figure 3.11, a characteristic fragmentation pattern and an intense NO₃⁻ signal at m/z 61.9878 suggests the presence of an organic nitrate. Furthermore, the MS² spectrum indicates a dimeric structure composed of known first generation oxidation products at m/z 185.0821 ([M-H]⁻), which might represent the prominent SOA C₉-compound pinic acid (C₉H₁₄O₄), and a C₁₀-compound possessing an O-NO₂ group (C₁₀H₁₅O₃N). The most intense fragmentation signal is caused by the CHO-containing ion C₉H₁₁O₃⁻ (m/z 167.0711 ([M-H]⁻)), which indicates a hydrolysis product of pinic acid. The second most intense signal at m/z 123.0816 (C₈H₁₁O⁻) corresponds to C₉H₁₁O₃⁻ by the loss of CO₂, which is a prominent fragment of organic acid functions. A comprehensive list of all detected nitrogen-containing compounds is given in the Supporting Information to chapter 3.

3.3.2.3 CHOS and CHONS compounds

Generally, organosulfates and nitroxy organosulfates are expected to originate from mixed biogenic/anthropogenic emissions of VOCs, SO₂, and NO_x in the presence of acidic sulfate particles (Nguyen *et al.*, 2014; Nozière *et al.*, 2015; Surratt *et al.*, 2008). Depending on the SO₂ concentration, 141 - 157 CHOS compounds and 7 – 10 CHONS compounds were detected in the experiments 1749 – 1751. Hence, sulfur-containing compounds accounted for 28 – 37 % of the total number of signals. Even without addition of SO₂, i.e. at a remaining background SO₂ mixing ratio of about 0.5 ppb, 16 CHOS and 2 CHONS were still observed in experiment 1752. Similar to the CHO and CHON compounds, these compounds need to exhibit a certain gas-phase acidity to be detectable as deprotonated ions in the negative ionization mode. For this reason, the detected CHOS and CHONS compounds were assigned

to organosulfates and nitrooxy organosulfates possessing a deprotonable sulfate ester structure (R-OSO₃H).

Several sulfur-containing compounds were already detected in previous field and laboratory studies (Surratt *et al.*, 2008), however, a clear assignment to VOC precursors was often not possible. So far, the compounds C₃H₆O₅S (*m/z* 152.9863, [M-H]⁻), C₂H₄O₆S (*m/z* 154.9655, [M-H]⁻), and C₃H₆O₆S (*m/z* 168.9811, [M-H]⁻) detected here, were proposed to be isoprene-derived organosulfates (Surratt *et al.*, 2008). Due to the detection of these signals during the CLOUD 10 campaign with solely α -pinene and Δ -3-carene as VOC precursors, we suggest these organosulfates to be also derived from oxidation products of the respective VOCs. In agreement, previous studies already gave hypotheses on the formation of short-chain carbonyl compounds (C₁-C₄) due to decomposition reactions of HOMs (Mutzel *et al.*, 2015), which possibly contribute to the occurrence of organosulfates with carbon numbers of less than five. Small carbonyl compounds may either react with present HSO₄⁻ to form organosulfates or these low MW organosulfates are a decomposition product of dimeric highly oxidized organosulfates.

The detected organosulfates in the experiments 1749 – 1751 were grouped according to the number of carbon atoms per molecule into a monomeric range (C₇-C₁₀) and a dimeric range (C₁₇-C₂₀). Accordingly, 32 - 34 different CHOS formulas of the monomer range, were distributed among 76 – 80 isomers. In the dimeric range, 16 – 19 CHOS formulas, representing 20 – 40 isomers, were detected.

Organosulfates were found to be produced via reactive uptake of α -pinene oxide in the presence of acidified sulfate aerosol (Duporté *et al.*, 2016). Highly oxidized organosulfates (HOOS) are generally hypothesized to originate from follow-up reactions of gas-phase HOMs with particulate sulfate and might contribute to particle formation (Mutzel *et al.*, 2015). However, it is also assumed that the stabilized Criegee Intermediates (sCI), produced from ozonolysis, further reacted with gas-phase SO₂, building organosulfates (Ye *et al.*, 2018). Depending on the relative humidity (RH), heterogeneous uptake of SO₂ onto organic aerosol was found to be a dominant sink of SO₂, likely owing to reactions between SO₂ and organic peroxides (Ye *et al.*, 2018).

In order to investigate the HOOS, we extended the definition of HOOS (O/C > 1) and further included molecules with an O/C ratio higher than 0.85 to the class of HOOS. Table 3.4 lists the elemental composition of the HOOS and the Rt of the detected isomers. Interestingly, solely one HOOS (i.e., C₇H₁₂O₇S) was detected in earlier laboratory or ambient field studies (Brüggemann *et al.*, 2017; Mutzel *et al.*, 2015). This finding further supports the thesis of organosulfate formation by reaction of sCI with SO₂, as a pathway for organosulfates in the gas-phase without sulfate seed particles. Lower concentrations of the VOC precursors and a higher relative humidity (RH) compared to Mutzel *et al.* (2015) may have also changed the molecular distribution of HOOS. Another option is a contribution of Δ -3-carene as second VOC precursor, which may be involved in the formation process. A comprehensive list of all CHOS and CHONS containing compounds is given in the Supporting Information to chapter 3.

3. Molecular Composition of SOA Particles at Nucleation Experiments at CERN

Table 3.4 Highly oxidized organosulfates (HOOS) detected in experiments 1749 – 1751. A complete overview of all detected organosulfates is given in the Supporting Information.

elemental composition	measured m/z ([M-H] ⁻)	O/C	Δm (ppm)	Rt (min)
C ₇ H ₁₄ O ₆ S	225.0437	0.86	-0.23	3.81; 3.95; 7.58
C ₇ H ₁₂ O ₇ S ^{(a),(b)}	239.0231	1.00	-0.45	1.00
C ₈ H ₆ O ₇ S	244.9759	0.88	-0.84	4.13
C ₈ H ₁₈ O ₇ S	257.0699	0.88	-0.49	3.29; 3.52
C ₈ H ₁₄ O ₈ S	269.0336	1.00	2.04	3.92; 5.72
C ₈ H ₁₆ O ₉ S	287.0443	1.13	0.08	8.84
C ₉ H ₈ O ₈ S	274.9867	0.89	-0.19	4.60
C ₉ H ₁₆ O ₈ S	283.0492	0.89	-0.43	3.74; 3.94
C ₉ H ₁₆ O ₉ S	299.0447	1.00	1.70	5.23
C ₁₀ H ₁₆ O ₉ S	311.0441	0.90	-0.31	4.04
C ₁₀ H ₆ O ₁₁ S	332.9558	1.10	0.95	1.01

References: (a) (Mutzel *et al.*, 2015), (b) (Brüggemann *et al.*, 2017).

There were several nitrooxy organosulfates detected in this study. Four out of the five compounds were already described in earlier studies by filter sampling of aerosols (Nguyen *et al.*, 2014; Surratt *et al.*, 2008) and two out of five compounds by direct infusion via ESI-MS of rainwater samples (Altieri *et al.*, 2009). Regarding possible precursor VOCs, Nguyen *et al.* (2014) described C₁₀H₁₇O₈NS, C₉H₁₅O₉NS, and C₁₀H₁₇O₁₀NS to originate from limonene and α -terpinene, respectively. However, up to now a clear attribution to possible VOC precursors remained challenging. Nguyen *et al.* (2014) described C₁₀H₁₇O₈NS, C₉H₁₅O₉NS, and C₁₀H₁₇O₁₀NS to originate from limonene and α -terpinene, respectively. Our study clearly shows that such compounds are produced by a VOC mixture of α -pinene and Δ -3-carene (2:1). Table 3.5 lists the CHONS formulas and their detected isomers due to the chromatographic separation.

Table 3.5 Elemental formulas, measured m/z values, O/C ratios, mass deviation, and corresponding retention times of the isomers of CHONS containing molecules detected by UHPLC(-)ESI-UHRMS in experiments 1749 – 1751.

elemental composition	measured m/z ([M-H] ⁻)	O/C	Δm (ppm)	Rt (min)
C ₁₀ H ₁₇ O ₇ NS ^{(a),(b),(c)}	294.0651	0.70	-0.236	8.52; 8.86; 9.11; 9.18; 9.27
C ₁₀ H ₁₇ O ₈ NS ^{(a),(b)}	310.0602	0.80	-0.060	7.39
C ₉ H ₁₅ O ₉ NS ^{(a),(b)}	312.0394	1.00	-0.075	4.76
C ₁₀ H ₁₇ O ₁₀ NS ^{(a),(b),(c)}	342.0497	1.00	-0.360	4.40; 5.91
C ₂₀ H ₃₃ O ₁₂ NS	510.1646	0.60	-0.489	9.96

References: (a) (Surratt *et al.*, 2008), (b) (Nguyen *et al.*, 2014), (c) (Altieri *et al.*, 2009).

Interestingly, we detected a C_{20} nitrooxy organosulfate at SO_2 mixing ratios of 3.3 ppb which might be attributed to a dimeric CHONS compound. The corresponding R_t of 9.96 min is in accordance with other retention times of detected dimeric oxidation products. Furthermore, the MS^2 spectra (see Figure 7.3 in the Supporting Information to chapter 3) showed the characteristic fragmentation patterns of NO_3^- , SO_3^- , and HSO_4^- . To the best of our knowledge, this is the first report of a dimeric nitrooxy organosulfate formed by laboratory experiments.

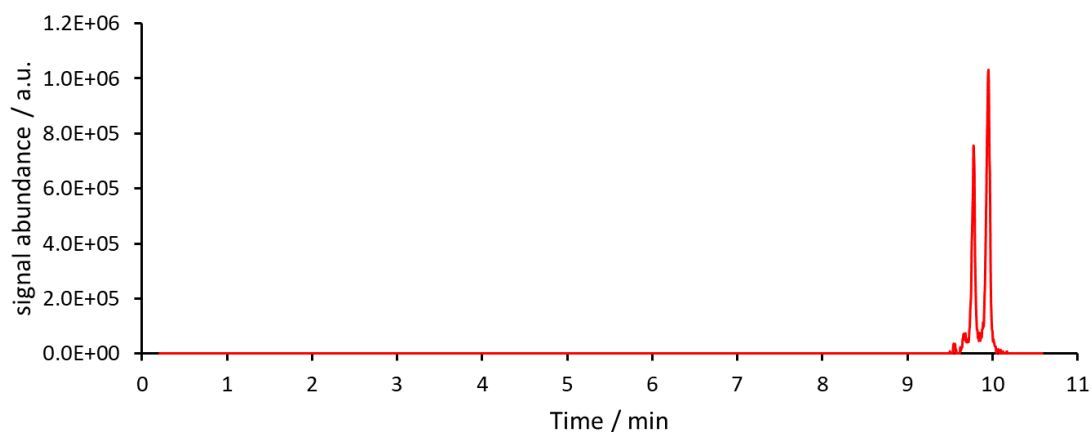


Figure 3.12 Extracted ion chromatogram (EIC) of m/z 510.1646 ($[M-H]^-$, $R_t = 9.96$ min). The signal at $R_t = 9.79$ shows most likely an isomer of $C_{20}H_{32}O_{12}NS^-$ ($[M-H]^-$). The isomer was not detected by the non-target screening, due to the selected intensity threshold and blank correction.

Figure 3.12 illustrates the EIC of m/z 510.1646 ($[M-H]^-$) proposed as the molecular compound $C_{20}H_{33}O_{12}NS$. A more intense signal for the isomer at $R_t = 9.96$ min and a less intense signal for a second isomer at $R_t = 9.79$ min. Most likely, due to the threshold and background correction settings of the non-target screening, the less intense isomer was not detected and assigned as a compound. However, we note that non-target screening approaches typically give solely a qualitative overview of the sample composition, whereas detailed information on single molecules need to be obtained via targeted analysis.

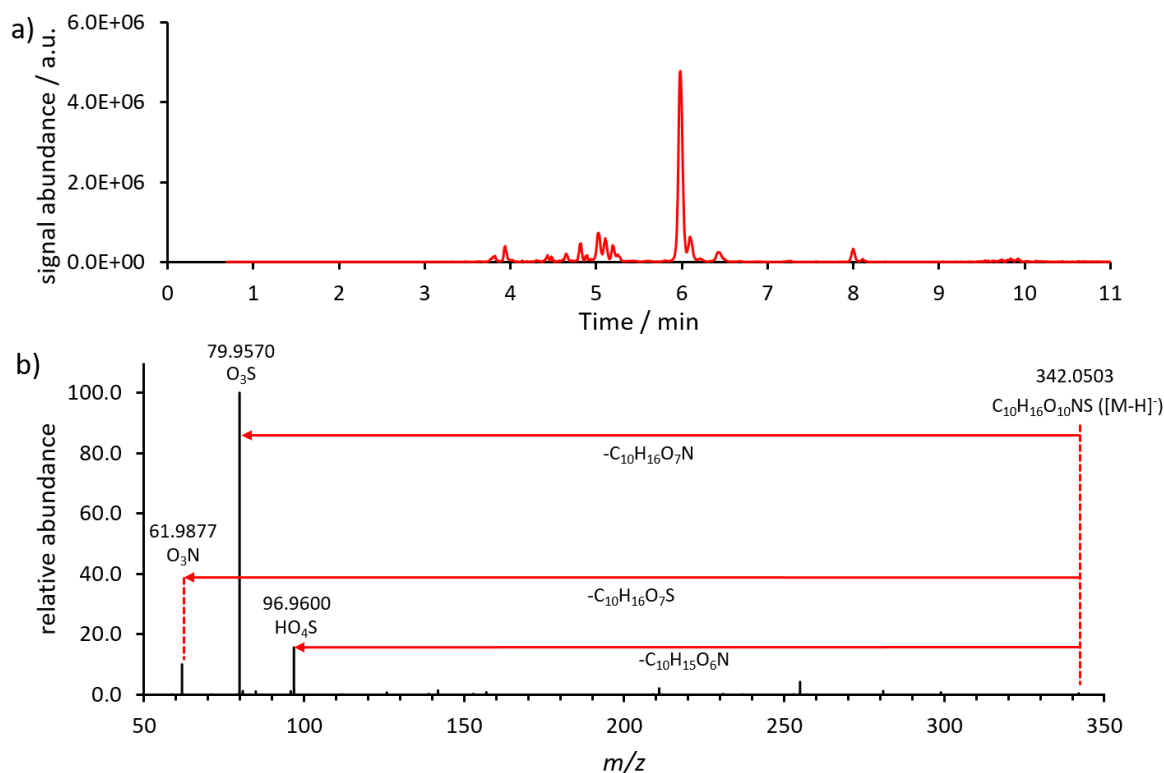


Figure 3.13 a) Extracted ion chromatogram (EIC) of m/z 342.0497 ($[M-H]^-$, $R_t = 5.98$ min). b) Negative mode MS^2 spectrum of the parent ion $C_{10}H_{16}O_{10}NS^-$ at m/z 342.0503 ($[M-H]^-$). The fragmentation pattern indicates the presence of a nitroxy organosulfate: m/z 96.9600 = (HSO_4^- ; $[M-C_{10}H_{15}O_6N]^-$), m/z 79.9570 = (SO_3^- ; $[M-C_{10}H_{16}O_7N]^-$), m/z 61.9877 = (NO_3^- ; $[M-C_{10}H_{16}O_7S]^-$).

Regarding monomeric nitroxy organosulfates, the signal for $C_{10}H_{17}O_{10}NS$ at m/z 342.0503 ($[M-H]^-$) was checked for characteristic fragmentation patterns by MS^2 studies. Figure 3.13 shows the chromatogram and the corresponding MS^2 . The chromatogram exhibits a single intense peak at $R_t = 5.98$ min which was further investigated by higher-energy collision-induced fragmentation (i.e., normalized collision energy of 30 %). As depicted in panel b) of Figure 3.13, the fragmentation pattern shows a relatively less intense signal for the deprotonated molecular ion ($[M-H]^-$). The organosulfate-function was identified by the characteristic fragment of the hydrogen sulfate anion HSO_4^- and the sulfur trioxide anion SO_3^- . In addition, the loss of NO_3^- denoted an organic nitrate-function. Moreover, the neutral losses of $C_{10}H_{16}O_7S$, $C_{10}H_{16}O_7N$, and $C_{10}H_{15}O_6N$, respectively, support the fragmentation pattern. A comprehensive list of all detected organosulfates and nitroxy organosulfates from α -pinene/ Δ -3-carene oxidation reaction is given in the Supporting Information to chapter 3.

3.4 Conclusions and Outlook

A filter sampling method for the analysis of SOA components during the CLOUD 10 experiment was developed and characterized. Extraction efficiencies for MBTCA and pinic acid were determined to be >95 %. Because of the structural relationship of CHO-containing SOA compounds, the extraction method was evaluated as suitable for the extraction of α -pinene/ Δ -3-carene oxidation products.

The molecular composition of sub-100 nm particles sampled during the CLOUD 10 campaign at CERN was investigated using UHPLC coupled to ESI-UHRMS. Unique and comprehensive lists of the molecular composition at biogenic nucleation experiments of α -pinene and Δ -3-carene VOC precursors in a perfectly clean CLOUD chamber were obtained. In total, 216 – 357 molecular formulas were assigned to negative ionization mode signals from in filter extracts, which were sampled during biogenic nucleation experiments with varying SO₂ concentration. Due to the negative ionization mode, we attribute the detected compounds to acidic compound classes such as nitrooxy- or organosulfates. The detected compounds were further subdivided into subclasses containing carbon, hydrogen, and oxygen (CHO), nitrogen-containing (CHON), sulfur-containing (CHOS), and nitrogen- and sulfur-containing (CHONS) subclasses. Generally, the total number of CHO signals dominated the mass spectra of all filter extracts, however, the CHOS subclass showed high percentages of around 30 % of the total summed signal intensities for the experiments with SO₂ mixing ratios of 1.1 – 3.3 ppb.

An optimized \overline{OS}_c -dependent classification of van Krevelen diagrams shows distinct areas of SOA products composed of CHO. Several already previously described HOM formulas were confirmed by this study. However, many CHO-containing HOMs and corresponding isomers were detected for the first time.

Furthermore, the UHPLC-UHRMS analysis of the filter extracts exhibited varying distributions for CHON mono- and di-nitrates possibly indicating different SO₂-dependent formation pathways. The structure of organic mono-nitrates was confirmed by MS² studies and the characteristic signal of NO₃⁻. Moreover, the dimeric structure of an organic di-nitrate (C₁₉H₂₈O₇N ([M-H]⁻)) was indicated by an MS² study showing characteristic fragmentation patterns.

CHOS-containing compounds, referred to as organosulfates, accounted for the second largest subclass in terms of total numbers and signal intensities. Within this subclass, several of the 11 detected formulas of highly oxidized organosulfates were formed in the gas-phase without sulfate seed aerosol and detected for the first time in the particle phase.

Nitrooxy organosulfates showed the lowest number of formulas compared to the other subclasses. Besides the most prominent and often described nitrooxy organosulfate (C₁₀H₁₇O₇NS), the formula of a C₂₀ nitrooxy organosulfate was detected for the first time. The chromatogram of C₂₀H₃₂O₁₂NS⁻ showed two isomeric compounds. As a representative compound for CHONS-containing compounds the MS² spectrum showed clearly a characteristic fragmentation pattern.

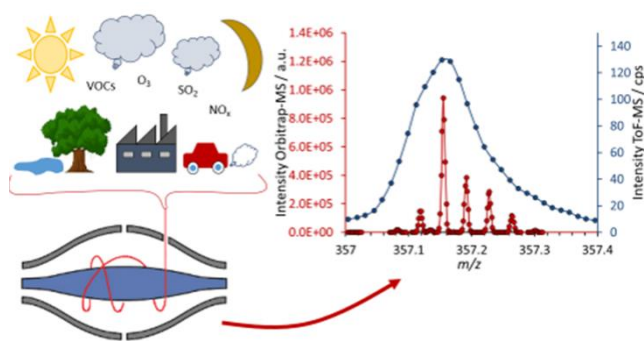
Future UHPLC-UHRMS method development might concentrate on the detection of C₁₇-C₂₀ HOMs as they eluted mostly at the very end of the HPLC method. Possible isomers of this compound class might be co-eluting due to the high amount of acetonitrile at the end of the method. However, organic synthesis of proposed C₁₇-C₂₀ HOMs demanded as laboratory standards need to be carried out prior to method development. Due to the high amount of CHOS compounds, further structural elucidation might contribute to a better understanding of the formation of organosulfates. UHRMS techniques like the herein used Orbitrap MS detect and confirm the formulas in particulate phase. These information and peak lists of the detected formulas should be examined in future chamber experiments using appropriate online mass spectrometric techniques. However, further developments of ambient ionization methods in combination with online (high resolution) mass spectrometry are needed to partly circumvent the filter sampling step and to benefit from high time resolution.

4 Ultra-High-Resolution Mass Spectrometry of Atmospheric Organic Aerosol Particles in Real-Time

This chapter is a reprint of the article:

Christoph Zuth, Alexander L. Vogel, Sara Ockenfeld, Regina Huesmann, Thorsten Hoffmann

Ultra-High-Resolution Mass Spectrometry of Atmospheric Aerosol Particles in Real-Time: Atmospheric Pressure Chemical Ionization Orbitrap Mass Spectrometry (APCI-Orbitrap-MS) of Atmospheric Organic Aerosol



Under Review in *Analytical Chemistry*

Abstract

The accurate and precise mass spectrometric measurement of organic compounds in atmospheric aerosol particles is a challenging task that requires analytical developments and adaptations of existing techniques for the atmospheric application. Here we describe the development and characterization of an atmospheric pressure chemical ionization Orbitrap™ mass spectrometer (APCI-Orbitrap-MS) for the measurement of organic aerosol in real-time. APCI is a well-known ionization technique, featuring minimal fragmentation and matrix dependencies, and allows rapid alternation between the positive and negative ionization mode. As a proof of principle, we report ambient organic aerosol composition in real-time, with alternating ionization, high mass resolution ($R = 140\,000$) and accuracy (< 2 ppm). The instrument was calibrated in the negative ion mode using 3-methyl-1,2,3-butanetricarboxylic acid (MBTCA) model aerosol. We obtain a detection limit of 1.3 ng/m^3 . Based on the performed calibration using MBTCA particles, the ambient concentration of MBTCA in the particle phase measured in an urban area in Mainz, Germany ranged between values from 10 and 80 ng/m^3 . For the first time, we apply a non-target screening approach on real-time data, showing molecular variability between ambient day- and nighttime aerosol composition. The detected compounds were grouped in the night- and daytime and analyzed by Ultra-High-Resolution MS (UHRMS) visualization methods. Among several prevalent biogenic secondary organic aerosol (BSOA) markers, 24 organic mono-nitrates and one organic di-nitrate were detected. We further estimate that, on average, organic nitrates contribute to 5 % and 14 % of the measured particulate organic aerosol at day and night, respectively.

4.1 Introduction

Atmospheric aerosol particles can affect climate by direct interaction with solar radiation or indirectly through their ability to serve as cloud condensation nuclei (CCN) (IPCC, 2013). Furthermore, there is increasing evidence that particulate matter (PM) is harmful to human health since especially fine particles can enter the respiratory and cardiovascular system (Lelieveld *et al.*, 2015; Pope & Dockery, 2006; Schulz *et al.*, 2005; Wilson & Suh, 1997). Volatile organic compounds (VOCs), whether of biogenic or anthropogenic origin, are well-established precursors for the formation of ultra-fine secondary organic aerosol (SOA). Particularly for source apportionment, the identification of sources and elucidation of formation and atmospheric aging mechanisms requires a detailed knowledge of the molecular composition of SOA (Nozière *et al.*, 2015). Organic aerosols are a highly complex mixture that undergoes continuous atmospheric transformations for which suitable instrumentation is needed to elucidate processes that alter chemical composition and properties in fast time intervals (Lee *et al.*, 2016). Providing high sensitivity and selectivity towards single molecules, mass spectrometry (MS) is the most commonly applied technique for the chemical analysis of atmospheric particles (Laskin *et al.*, 2018).

In general, the measurement techniques for the chemical composition and quantification of SOA are divided into three classes: indirect methods, offline and online techniques (Hallquist *et al.*, 2009). Within the direct methods (offline and online), typically the offline techniques provide much more detailed information on compound classes and individual compounds. In this case, the atmospheric particles are sampled on filters or impactors before they undergo further sample preparation. Finally, they are analyzed in the laboratory by common separation techniques such as ion chromatography and gas or liquid chromatography coupled to MS (Hoffmann *et al.*, 2011). Besides the determination of the m/z ratio for the identification and the corresponding signal intensity for quantification, chromatographic offline techniques deliver the retention time as another dimension to characterize the organic composition of aerosol particles. A relatively new technique to analyze organic aerosol particles is offered by the Orbitrap mass analyzer (Brüggemann *et al.*, 2017; Romonosky *et al.*, 2017; Tu *et al.*, 2016; Vogel *et al.*, 2016a; Wang *et al.*, 2017). Under certain conditions, Ultra-High-Resolution Mass Spectrometry (UHRMS) allows the unambiguous determination of the elemental formula for each ion signal, due to the high mass resolving power and high mass accuracy (Hu *et al.*, 2005).

Online mass spectrometry techniques avoid potential sampling artifacts associated with offline analytical methods, such as analyte evaporation and chemical reactions during long sample collection and analysis time periods (Pratt & Prather, 2012b). However, the major advantages of online mass spectrometry are the ability to examine the chemical composition and transformation of organic aerosols in real-time.

The Aerodyne aerosol mass spectrometer (AMS) is one of the main online instruments that is used for the characterization of aerosol particles (Canagaratna *et al.*, 2007). Via a set of aerodynamic lenses, aerosol particles are drawn into a vacuum chamber and focused into a narrow particle beam. The compounds in the aerosol particle beam are thermally vaporized, ionized by electron ionization (EI) and analyzed by time-of-flight (ToF)-MS (Canagaratna *et al.*, 2007; DeCarlo *et al.*, 2006). The AMS is field-deployable and the 70 eV EI energy ensures quantitative ionization of all non-refractory compounds. As a consequence of the limited mass resolution and the “hard” ionization technique, which induces a high degree of fragmentation of organic compounds, the identification and quantification of individual organic molecules are often impossible, thus leading to a lower level of chemical information about the organic fraction of atmospheric aerosol particles.

Accordingly, several instrumental techniques were recently developed to fill this gap and enhance the molecular characterization of organic aerosol components. Lopez-Hilfiker *et al.* developed a Filter Inlet for Gases and AEROsols (FIGAERO) coupled to a high-resolution time-of-flight chemical-ionization mass spectrometer (HR-ToF-CIMS) which has been deployed to a variety of laboratory chambers as well as field sites (Lopez-Hilfiker *et al.*, 2014). Intact molecular ions with little fragmentation of the favored organic compounds are detected with “softer” ionization methods at atmospheric pressure, such as Aerosol Flowing Atmospheric-Pressure Afterglow Mass Spectrometry (AeroFAPA-MS) (Brüggemann *et al.*, 2015) or atmospheric pressure chemical ionization (APCI-MS)

(Vogel *et al.*, 2013). Extractive Electrospray Ionization (EESI-MS) coupled to an LTQ Orbitrap Velos was used for characterization of organic aerosol in chamber experiments (Gallimore *et al.*, 2017). So far, the coupling of APCI and a Q Exactive Orbitrap MS has not been applied to ambient aerosol measurements.

The presented APCI-Orbitrap-MS-technique combines a “soft” ionization technique that permits the detection of deprotonated and protonated ions with little fragmentation, high mass resolution ($R = 140\,000$ at m/z 200) and accuracy (< 2 ppm) of a Q Exactive Orbitrap mass analyzer (Thermo Fisher Scientific, Germany) and the advantages of online measurement techniques. Real-time analysis of organic compounds in aerosol particles was performed with an adapted, commercially available APCI source producing protonated and deprotonated ions, respectively. The APCI-Orbitrap-MS-technique was used in several setups to test the performance of this coupling.

4.2 Experimental

The high-resolution analysis of atmospheric organic particles in real time was performed with a Q Exactive Orbitrap mass spectrometer (Thermo Scientific, Bremen, Germany). Ionization of the compounds was conducted using a modified Atmospheric Pressure Chemical Ionization (APCI) ion source. The APCI ion source vaporizes an aerosol particle stream in a heated ceramic tube whereupon the evaporated molecules are ionized in the gas phase by a corona discharge between a needle and the transfer capillary of the MS. The general technique was described in previous publications (Hoffmann *et al.*, 1998; Kückelmann *et al.*, 2000).

The Q Exactive Orbitrap mass spectrometer was externally mass calibrated using a 2 mM sodium acetate solution that provides a series of negative and positive adduct ions in the desired mass range. Mass spectra were obtained in a mass range of m/z 80 – 550 applying a mass resolving power of 140 000 at m/z 200 and a scan rate of 0.2 scans/s. The APCI vaporizer temperature was set to 350 °C, the discharge current was 2.50 μ A and the capillary temperature was adjusted to 250 °C.

4.2.1 Characterization of the APCI-Orbitrap-MS with Organic Model Aerosol

The qualitative and quantitative performance of the APCI-Orbitrap-MS was characterized using 3-methyl-1,2,3-butanetricarboxylic acid (MBTCA). MBTCA was synthesized according to Dette *et al.* (Dette *et al.*, 2014). For the generation of test aerosol particles and calibration, a 1 mM solution of MBTCA in methanol (Fisher Scientific, Optima LCMS grade) was nebulized by synthetic air. The solvent was removed after nebulization by an activated charcoal denuder. The polydisperse aerosol particles were then size-selected by a differential mobility analyzer (DMA) (model L-DMA 55-900, Grimm Aerosol Technik, Ainring, Germany) and counted by a condensation particle counter (CPC) (model CPC 5416, Grimm Aerosol Technik, Ainring, Germany). During the calibration experiments,

the aerosol flow was adjusted to 1.2 L/min with an external sheath air flow of 12 L/min. A scheme for the instrumental setup for the calibration procedure is shown in Figure 4.1.

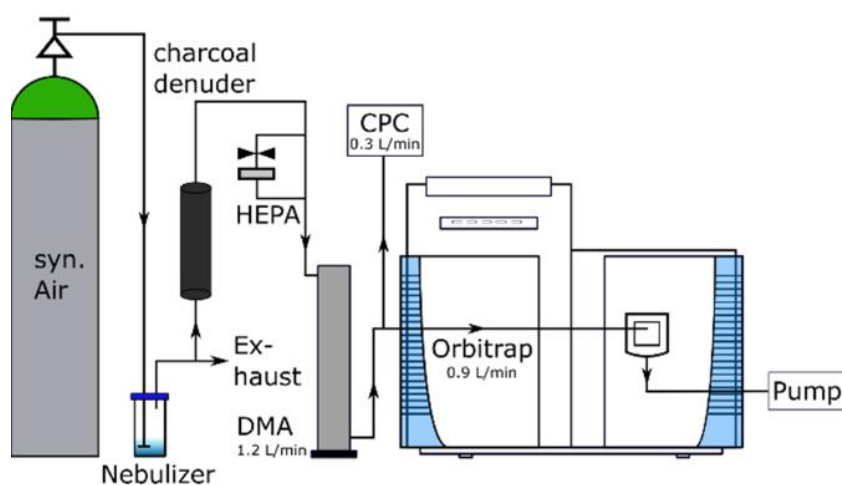


Figure 4.1 Schematic experimental setup used for size selection and APCI-Orbitrap-MS characterization of generated MBTCA aerosol particles.

4.2.2 Ultra-High-Resolution Orbitrap Analysis of Atmospheric Aerosol Particles in Real-Time

As a proof of principle, the ambient aerosol composition was analyzed by sampling $PM_{2.5}$ particles from a height of 4 m above ground level outside the MS laboratory. The Q Exactive mass spectrometer was sampling with a flow rate of 3 SLPM through conductive PTFE tubing (PTFE EX, Bohlender GmbH, Grünsfeld, Germany). Before entering the APCI ion source, the aerosol stream passed a charcoal denuder in order to remove gaseous species from the aerosol sample. The particle number-size distribution between 10 and 1100 nm was determined by a Scanning Mobility Particle Sizer (SMPS+C, Grimm Aerosol Technik, Ainring, Germany) in front of the inlet of the APCI ion source. A schematic sketch of the setup, used for the UHRMS measurement of the ambient particle phase is illustrated in Figure 7.4 in the Supporting Information to chapter 4. The obtained high-resolution data were analyzed by the MZmine 2.27 software package (<http://mzmine.github.io>) in terms of performing a non-target approach to screen for mass traces above a certain intensity value. Molecular formulas for the identified signals were calculated using a mass tolerance of ± 2 ppm and the following constraints: #C (1 – 45), #H (1 – 60), #O (0 – 20), #N (0 – 4), #S (0 – 2). Additionally, the abundance and intensity of the ^{13}C isotopic peak were checked by XCalibur 2.2 (Thermo Scientific). Neutral formulas with chemically impossible compositions, non-integer or negative double bond equivalents (DBE) and unreasonable O/C and H/C element ratios ($\text{O/C} < 3$; $0.3 < \text{H/C} < 3$) were discarded. Furthermore, the resulting molecular formulas were checked on a volatility parametrization to exclude ~ 40 potential interferences of highly abundant gas phase molecules (Li *et al.*, 2016).

4.3 Results and Discussion

4.3.1 Characterization of the APCI-Orbitrap-MS with Organic Model Aerosol

The APCI-Orbitrap-MS setup was characterized by a lab-generated aerosol of the atmospherically representative tricarboxylic acid (MBTCA). MBTCA is a higher generation oxidation product of α -pinene and formed by OH radical initiated oxidation of cis-pinonic acid (Donahue *et al.*, 2012; Müller *et al.*, 2012; Szmigielski *et al.*, 2007). The aerosol mass concentration was varied in 12 calibration steps by adjusting a valve in front of an in-line High Efficiency Particulate Air (HEPA)-Filter. Particle number concentrations of 40, 70 and 100 nm particles that passed the DMA were measured with a CPC. The aerosol mass concentration was calculated based on a particle density of 1.2 g/cm³. The resulting aerosol mass concentration ranged between 1.3 ng/m³ (40 nm) and 0.8 μ g/m³ (100 nm). As shown in Figure 4.2a, the aerosol mass concentration and the Orbitrap signal intensity are highly correlated and follow each other in time and intensity. A change of the aerosol mass concentration caused an immediate response to the MS Signal. Figure 4.2b shows the mass spectrum of MBTCA in the negative mode at a concentration of 0.8 μ g/m³. MBTCA is expected to be a fragile compound that quickly dissociates upon ionization since it contains three carboxylic acid groups. However, for all calibration studies using MBTCA, the deprotonated ion signal ([M-H]⁻) showed the highest signal intensity, which demonstrates the soft ionization character of the APCI at the selected instrumental conditions.

Measurements of the effective air temperature inside the vaporizer revealed temperatures of ~160 °C (set point of the vaporizer 350 °C) at a flow rate of ~1 SLPM. The loss of water (m/z 18.0105) responsible for m/z 185.0452 is, probably due to dehydration during the vaporization processes and was estimated to be 3 % of the [M-H]⁻ base peak. Interestingly, also an esterification product of MBTCA with methanol was observed to be 10 % of the base peak intensity. Whether the esterification product was formed in the particle phase (e.g., during the drying step in the particle formation procedure) - supporting the hypothesis of an increased reactivity of carboxylic acids for condensation reactions in aerosol particles (Bateman *et al.*, 2008) – or have been formed in the liquid phase within the nebulizer is not clear from our measurements.

However, APCI-Orbitrap-MS is demonstrated to be a soft ionization technique, which shows fragmentation of the deprotonated ion signals of relatively fragile analytes such as multicarboxylic acids in the range of 3 – 10 %. Additionally, we performed laboratory chamber experiments on the oxidation of α -pinene by ozone using the APCI-Orbitrap-MS technique. As in earlier studies, the negative ionization mass spectrum clearly shows a monomer and a dimer-mode of α -pinene oxidation products (see Figure 7.5 in the Supporting Information to chapter 4 for more information). We assume that the observed signals represent the particle phase oxidation products, mainly by the formation of stable deprotonated ions ([M-H]⁻). Further experiments on the molecular characterization of products from atmospheric oxidation reactions will be the focus of future studies.

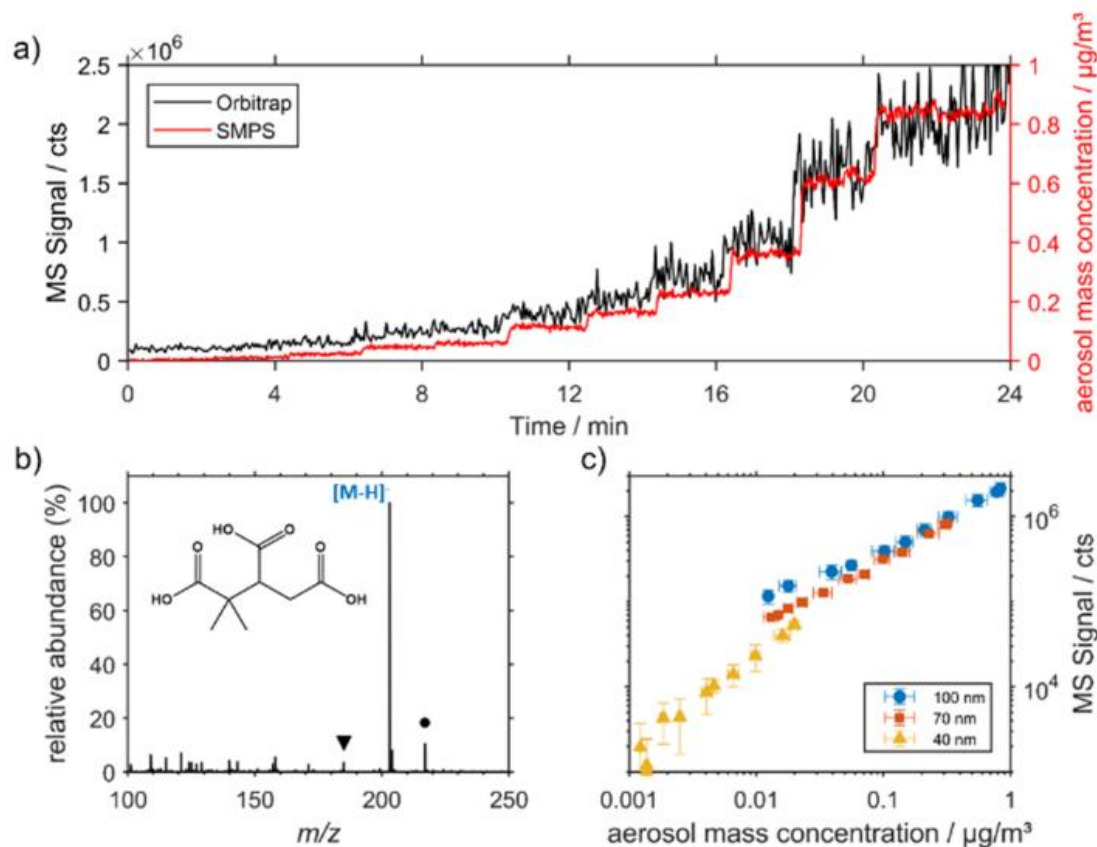


Figure 4.2 (a) MS Signal as a function of time and concentration for the analysis of a 100 nm particle size MBTCA aerosol. (b) Mass spectra of the analysis of MBTCA aerosol in the negative ion mode. The signal for the deprotonated molecule (m/z 203.0561 ([M-H]⁻)) shows the highest intensity. The signal marked with a triangle corresponds to the loss of water ([M-H-H₂O]⁻). The signal marked with a spot is caused by esterification with methanol. (c) Correlation between aerosol mass concentration and MS signal of MBTCA ([M-H]⁻) for 40, 70 and 100 nm particles; error bars show one standard deviation of the average signal of 2 min.

Atmospheric concentrations of MBTCA and other secondary oxidation products in the particle phase are expected to be in the low ng/m³ range (Gómez-González *et al.*, 2012; Warnke *et al.*, 2006; Zhang *et al.*, 2010). Accordingly, the calibration range was adjusted to cover these aerosol mass concentrations. The calibration was performed at three different particle sizes. As can be seen in Figure 4.2c, the calibration for 40, 70 and 100 nm particles showed a linear response over three orders of magnitude.

Based on the assumption that the average intensity during the calibration process using pure MBTCA aerosol equals the same mass concentration during the real-time measurements of the mixed ambient particle phase, a linear interpolation was applied to determine the ambient mass concentration. The calculation of the detection limit (LOD) was based on the linear regression of the calibration plot and determined for MBTCA in the particle phase to be at ~1.3 ng/m³ for the averaged particle size diameters of 40 nm, 70 nm, and 100 nm particles. It is assumed that the detection limits for similar small carboxylic acids, which are main oxidation products of biogenic VOCs are in the low ng/m³ range.

Therefore reported detection limits of the APCI-Orbitrap-MS are comparable to other CIMS techniques (Brüggemann *et al.*, 2015; Canagaratna *et al.*, 2007; Gallimore & Kalberer, 2013; Vogel *et al.*, 2013).

4.3.2 Ultra-High-Resolution Orbitrap Analysis of Atmospheric Aerosol Particles in Real-Time

During two periods in 2017 (09 May – 12 May and 14 Aug – 17 Aug) the APCI-Orbitrap-MS was deployed for real-time measurements of ambient aerosol particles at the chemistry department site of the University of Mainz. High-Resolution data of negative and positive ionization mode was obtained in an alternating cycle of 1 hour each.

As an example, Figure 4.3a shows the MS² spectrum in the negative ionization mode of m/z 203 ($\pm m/z$ 0.4) during ambient measurements. The neutral losses of the ambient C₈H₁₂O₆ compound are identical to the MS² spectra recorded from MBTCA (within an accuracy of 2 ppm, see Figure 7.6 in the Supporting Information to chapter 4). This demonstrates the ability of APCI-Orbitrap MS measurements to unambiguously detect and identify organic compounds in real-time. Obviously, the presence of isobaric compounds with identical/similar fragmentation patterns cannot be excluded with such a technique. However, the exact mass of m/z 203.0561 showed a significant increase starting at 9 AM until 2 PM indicating the formation via photo-induced oxidation of organic aerosol compounds by fast oxidational aging processes (Figure 4.3b) as expected for MBTCA (Donahue *et al.*, 2012). The sudden drop of the signal intensity at 2 PM was caused by a heavy rain event on an otherwise sunny day (see Figure 7.7 in the Supporting Information to chapter 4).

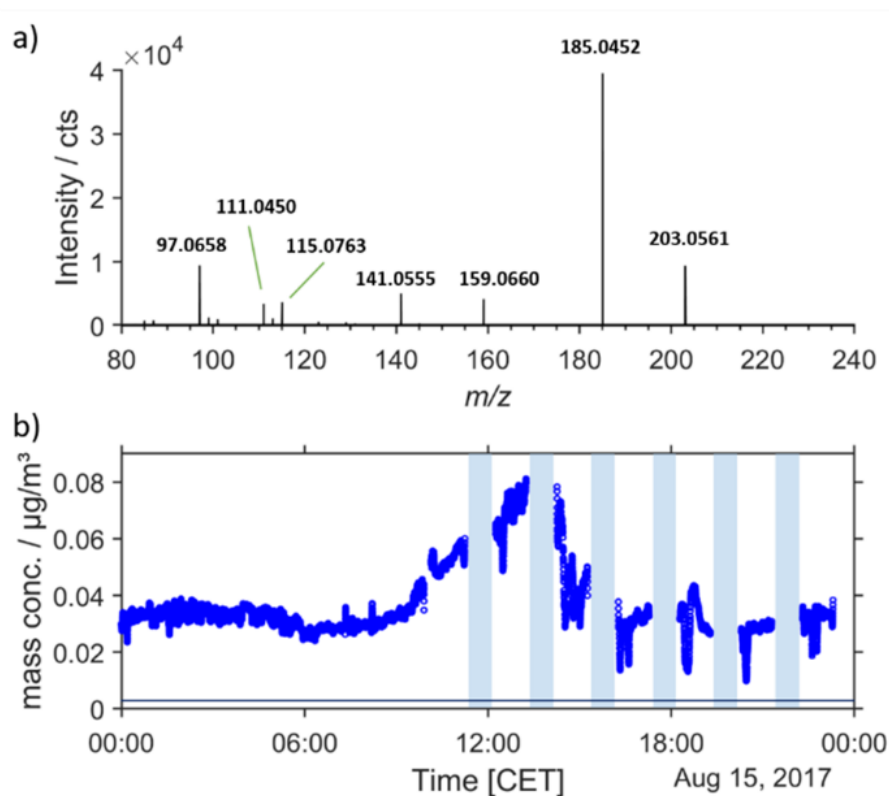


Figure 4.3 (a) Ambient MS² spectrum of m/z 203 (HCD energy 30 %). The fragmentation pattern strongly indicates the presence of MBTCA: m/z 203.0561 = [M-H]⁻, m/z 185.0452 = [M-H₂O]⁻, m/z 159.0660 = [M-CO₂]⁻, m/z 141.0555 = [M-H₂O-CO₂]⁻, m/z 115.0763 = [M-2CO₂]⁻, m/z 97.0658 = [M-H₂O-2CO₂]⁻, (b) Time trace of MBTCA (m/z 203.0561, [M-H]⁻) from 15th of August 2017. The shaded areas depict the positive ionization mode during the experiment. The horizontal line shows the limit of detection. The increasing intensity of the MBTCA signal during daytime agrees with its suggested formation via photo-induced oxidation (Müller *et al.*, 2012).

Based on the performed calibration with MBTCA particles, we assess the ambient MBTCA aerosol mass concentrations to be about 37 ng/m³ on average during the measurements. The highest concentration was 80 ng/m³ and the lowest was measured 10 ng/m³. These mass concentrations are well in accordance with former studies of ambient particle measurements (Zhang *et al.*, 2010).

Background corrected one-hour average mass spectra obtained in both ionization modes are shown in Figure 4.4. Background signals were recorded daily for each ionization mode by inserting a particle filter in front of the denuder system.

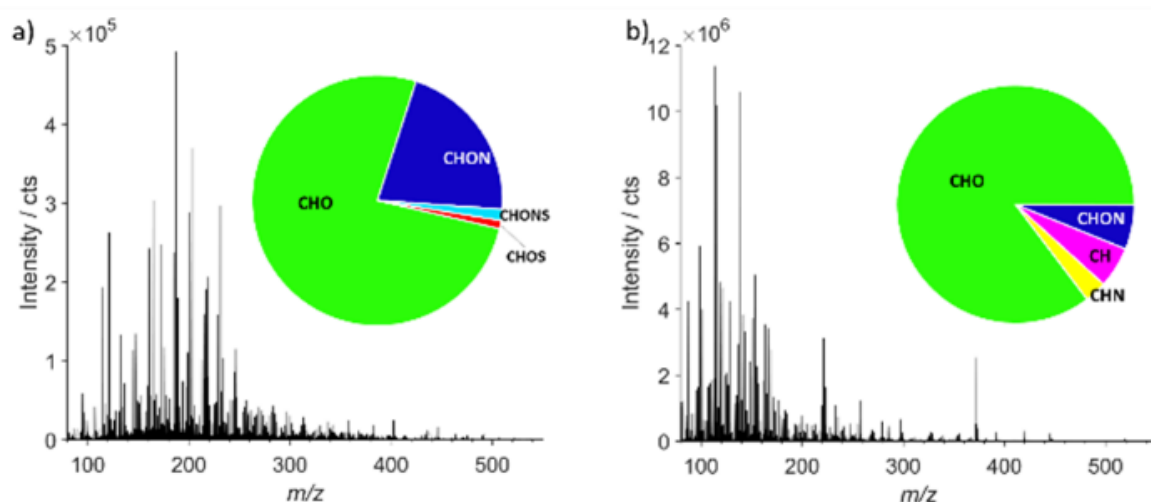


Figure 4.4 Average mass spectra in the negative (a) and positive (b) ionization mode of the APCI-Orbitrap-MS obtained on the 15th of August 2017 (negative mode: 8:32 – 9:32 AM, positive mode: 15:15 – 16:15 PM, Central European Time). Both mass spectra are background corrected.

As can be seen in Figure 4.4, the majority of the measured ions were associated with compounds below 300 Da. Overall, the non-target screening distinguished 931 and 247 monoisotopic formulas above a signal-threshold of 3 000 cts in negative and positive mode respectively. The largest group of identified formulas were associated with molecules containing CHO atoms only (685 (neg), 201 (pos)), followed by CHON compounds (202 (neg), 20 (pos)). CHOS-containing molecular formulas were identified in both ionization modes (11 (neg), 3 (pos)), whereas CHN- (8) and CH-containing (14) compounds were only found in the positive ionization mode. Additionally, 33 (neg) and 1 (pos) CHONS-containing species have been detected.

Based on the elemental composition the presence of particle phase organics during day and night was examined more closely. Nighttime spectra were averaged between 0 and 5 AM. Table 4.1 shows the number of detected compounds during night and day as well as the intensity-weighted elemental ratios, DBE and average carbon oxidation state (\overline{OS}_C) values.

Table 4.1 Intensity-weighted average values of elemental ratios, DBE, and \overline{OS}_C .

mode		#	H:C	O:C	DBE	\overline{OS}_C
negative	Day	867	1.53	0.37	2.93	-0.86
	Night	812	1.33	0.49	3.78	-0.76
positive	Day	237	1.49	0.22	3.61	-1.10
	Night	199	1.48	0.23	3.61	-1.12

number of detected molecular formulas.

Generally, the CHO-containing compounds dominate both time periods. Only minor differences were observed in the distribution of CHO- (night 74 % - day 76 %) and CHON-containing (night 21 % - day 19 %) molecules in the negative ionization mode. Nitrogen-containing molecules measured in this ionization mode are most likely organic nitrates, formed from reactions of biogenic VOCs and nitrate radicals (NO_3) (Lee *et al.*, 2016). More detailed information about the distribution of the detected compounds between night and day is given in Figure 7.10 and Figure 7.11 in the Supporting Information to chapter 4.

Van Krevelen diagrams, which plot the H/C ratio as a function of the O/C ratio, are regularly used to describe the overall composition of organic molecules in complex matrices (Kim *et al.*, 2003; Nozière *et al.*, 2015). So far, van Krevelen diagrams were predominantly used to illustrate individual compounds detected by offline measurement techniques (Nizkorodov *et al.*, 2011). Figure 4.5 shows a van Krevelen diagram based on measurements during 09 May – 12 May 2017 for the ambient particle phase composition of organic aerosols.

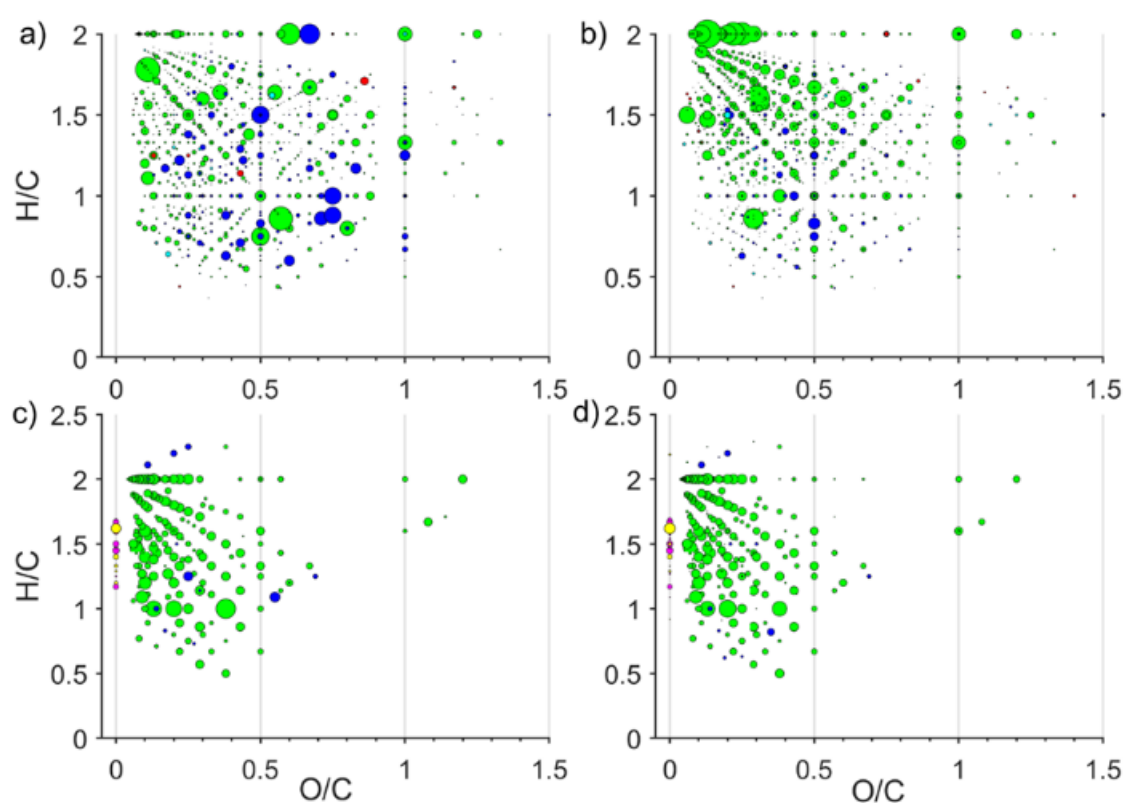


Figure 4.5 Van Krevelen plots for the detected compounds in the negative ionization mode at nighttime (a) and daytime (b) and positive ionization mode at nighttime (c) and daytime (d). The colors correspond to the CHO (green), CHON (blue), CHOS (red), CHONS (cyan), CH (magenta) and CHN (yellow) formulas assignments. The marker areas reflect the relative ion intensity of the signals. The ion intensities in the positive ionization mode are reduced by a factor of 4 for a better comparability.

The measured elemental compositions were further subdivided into negative (a, b) and positive (c, d) ionization modes and into the night- and daytime periods. The figure clearly shows diurnal variations in the elemental composition of the particle phase. For example, there are more and different CHON-containing species in higher concentrations at nighttime than at daytime. Even clearer, Figure 4.5 shows that the CHON-containing compounds are more intense at nighttime which may be due to the enhanced impact of NO_x-initiated nighttime SOA formation.

Many intense signals are observed in the range between $1 < \text{H/C} < 1.8$ and $\text{O/C} < 1$, which is often attributed to compounds from secondary organic origin (Wozniak et al., 2008). CHO-containing molecules are observed in higher concentrations during daytime and due to the relatively low degree of unsaturation (especially for compounds with $\text{H/C} > 1.5$), they are frequently associated with aliphatic compounds. Several of these formulas correspond to fatty acids ($\text{H/C} = 2$ and $\text{O/C} < 0.5$) which could be explained by cooking activities during daytime (a large university canteen lies in the vicinity of the measurement site). The strong appearance of fatty acids also explains the high H/C and low O/C ratio (Table 1) at daytime relative to the nighttime composition. Furthermore, within the group of CHO compounds potential oxidation products of isoprene, monoterpenes and especially sesquiterpenes (Ehn et al., 2014; Fu et al., 2009; Hallquist et al., 2009; Jaoui et al., 2013; Mentel et al., 2015; Tu et al., 2016) were detected in the range between $1 < \text{H/C} < 1.8$ and $0.3 < \text{O/C} < 0.6$ for C₁₅-compounds and $0.5 < \text{O/C} < 0.9$ for C₁₀-compounds. Although the measurement site is located in an urban area, several forested German Uplands lay in the vicinity of the site (Taunus, Hunsrück, Odenwald). More detailed information about the distribution of the oxygen content in CHO compounds during night and day detected in negative ionization mode is given in Figure 7.13 in the Supporting Information to chapter 4. Briefly, the number of compound distribution of the CHO-containing formulas during night and day is very similar. However, the percentage of each CHO subclass to the total signal varied clearly. During daytime, the CHO compounds containing two or three oxygen atoms dominated the total signal. At night, the dominant CHO species contained three and four oxygen atoms contributing to 18 % to the total signal, each.

In the positive ionization mode, most of the detected elemental compositions appear in the range $\text{O/C} < 0.5$ and $0.6 < \text{H/C} < 2$ and their concentrations remain in the same range during night- and daytime.

An alternative possibility to describe the complex composition of organic molecules was introduced by Kroll et al. (2011). The average carbon oxidation state ($\overline{\text{OS}}_C$) is calculated for each molecular formula detected in both ionization modes for night- and daytime using the following equation:

$$\overline{\text{OS}}_C = - \sum_i \text{OS}_i \frac{n_i}{n_C} \quad (4.1)$$

In this equation, OS_{*i*} is the oxidation state associated with element *i* and n_i/n_C is the molar ratio of element *i* to carbon within the molecule.

Figure 4.6 shows the Kroll plot of the detected molecular formulas. Again the negative ionization mode at nighttime (a) and daytime (b) and the positive ionization mode at nighttime (c) and daytime (d) are compared. The majority of particle phase organic molecules have \overline{OS}_C values between -2 and +1 and contain up to 20 carbon atoms. The intensity-weighted mean average carbon oxidation states of the compounds measured in the negative ionization mode is -0.76 at night and -0.86 at daytime. More obvious differences between day and night are observed for a series of nitrogen-containing compounds between \overline{OS}_C values of -4 and -2 (Figure 4.6a). Containing two nitrogen, these compounds can be attributed to classes of oxidized pyrimidines and a variety of nitrogen heterocycles (Laskin *et al.*, 2009). We assume that the compounds in the range $-1.8 < \overline{OS}_C < 0$, most of which contain less than 15 carbon atoms are organic nitrates.

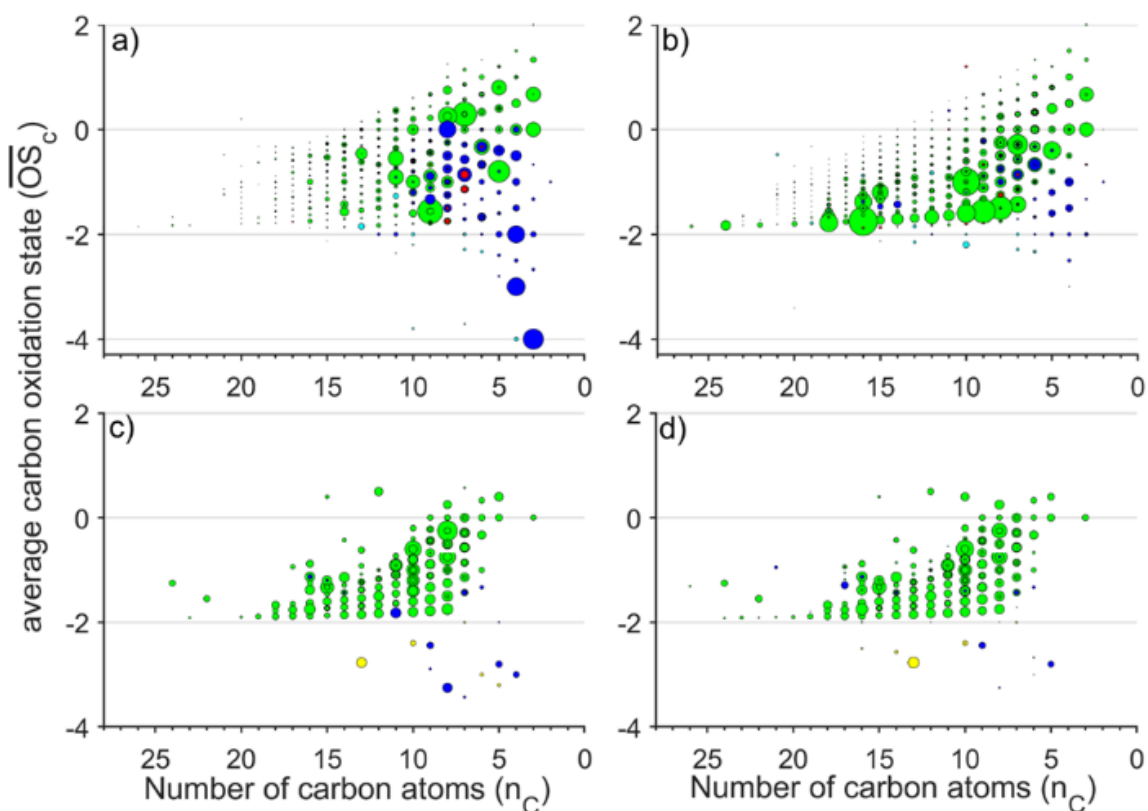


Figure 4.6 Carbon oxidation state plots for the detected compounds in the negative ionization mode at nighttime (a) and daytime (b) and positive ionization mode at nighttime (c) and daytime (d). The colors correspond to the CHO (green), CHON (blue), CHOS (red), CHONS (cyan), CH (magenta) and CHN (yellow) formulas assignments. The marker areas reflect the relative ion intensity of the signals. The ion intensities in the positive ionization mode are reduced by a factor of 4 for a better comparability.

In the positive ionization mode, the \overline{OS}_C values are -1.12 at night and -1.10 at day. However, only minor differences were detected in the molecular formulas distribution between night and day in the positive mode. Also in the positive mode, several nitrogen-containing compounds are detected in the range between \overline{OS}_C -4 and -2. Besides carbon and hydrogen, these compounds are mainly composed of

one nitrogen and one oxygen atom. Biomass burning emissions as well as secondary brown carbon products have been speculated to produce such elemental compositions (Kampf et al., 2016; Laskin et al., 2009). One noteworthy compound with an intensive signal possesses the molecular formula $C_8H_{10}N_4O_2$, the elemental composition of caffeine.

About 90 out of the 150 detected CHON-containing molecules in the negative ionization mode consist of one nitrogen and 3 – 5 oxygen atoms (see Figure 7.12 for more information about the distribution of the oxygen content in CHON compounds). This observation can be explained by the presence of organic nitrates and multi-functionalized nitrates expected to partition into the particle phase. Other CHON-containing molecules with two nitrogen atoms might belong to particulate di-nitrates (Lee *et al.*, 2016). Accordingly, we assume organic mono-nitrates consist of one nitrogen, an odd number of hydrogen and three or more oxygen, and organic di-nitrates consist of two nitrogen, an even number of hydrogen and minimum six oxygen. We assess 122 molecular compositions as organic nitrates during night and 126 during daytime. Altogether 108 molecular compositions were detected during both periods whereas 14 compounds were most prominent at nighttime and 18 at daytime. The contribution of the organic nitrates to the total particulate organic aerosol signal measured by APCI-Orbitrap-MS varies between 14 % at night and 5 % at day. This contribution is in accordance with former findings (Ayres *et al.*, 2015; Lee *et al.*, 2016; Xu *et al.*, 2015).

An interesting observation is the number of detected C_5 , C_{10} and C_{15} organic nitrates, which are potentially related to their formation from biogenic VOCs precursors. Table 4.2 shows the exact m/z ratios, the elemental composition and the calculated values of H/C, O/C, and DBE. The predominant detection period was during nighttime and in the early morning hours. To support the hypothesis of biogenically derived organic nitrates, MS^2 spectra were recorded from certain of these compounds. Often a clear and characteristic NO_3^- -signal was observed (see Figure 7.8 in the Supporting Information to chapter 4 for a ultra-high-resolution MS^2 spectra of an ambient organic nitrate), strongly supporting the proposed organic nitrate. The unambiguous identification of organic nitrates or di-nitrates, due to the C_5 -, C_{10} - or C_{15} -backbone most likely biogenically-derived, is definitely an advantage of the APCI-Orbitrap-MS and a direct consequence of the high mass resolution. For example, the base-lined differentiation between organic di-nitrates (e.g., $C_{15}H_{24}N_2O_{11}$) and non-nitrogen-containing organics at odd m/z ratios would not be possible using mass spectrometers with resolutions lower than about $R \sim 30\,000$ (see Figure 7.9 in the Supporting Information to chapter 4 for a simulated mass spectra). APCI-Orbitrap-MS experiments now can unambiguously assign the molecular composition of nighttime CHON-containing compounds.

Table 4.2 Identified C₅, C₁₀, and C₁₅ organic nitrates in ambient aerosol particles.

measured m/z ($[M-H]^-$)	elemental composition	H/C	O/C	DBE
142.0145	C ₅ H ₅ N ₁ O ₄	1.00	0.80	4
144.0302	C ₅ H ₇ N ₁ O ₄	1.40	0.80	3
146.0458	C ₅ H ₉ N ₁ O ₄	1.80	0.80	2
158.0094	C ₅ H ₅ N ₁ O ₅	1.00	1.00	4
160.0251	C ₅ H ₇ N ₁ O ₅	1.40	1.00	3
226.0720	C ₁₀ H ₁₃ N ₁ O ₅	1.30	0.50	5
242.0670	C ₁₀ H ₁₃ N ₁ O ₆	1.30	0.60	5
258.0618	C ₁₀ H ₁₃ N ₁ O ₇	1.30	0.70	5
274.0568	C ₁₀ H ₁₃ N ₁ O ₈	1.30	0.80	5
212.0928	C ₁₀ H ₁₅ N ₁ O ₄	1.50	0.40	4
228.0877	C ₁₀ H ₁₅ N ₁ O ₅	1.50	0.50	4
244.0825	C ₁₀ H ₁₅ N ₁ O ₆	1.50	0.60	4
260.0775	C ₁₀ H ₁₅ N ₁ O ₇	1.50	0.70	4
276.0723	C ₁₀ H ₁₅ N ₁ O ₈	1.50	0.80	4
292.0673	C ₁₀ H ₁₅ N ₁ O ₉	1.50	0.90	4
262.0931	C ₁₀ H ₁₇ N ₁ O ₇	1.70	0.70	3
278.0879	C ₁₀ H ₁₇ N ₁ O ₈	1.70	0.80	3
328.1400	C ₁₅ H ₂₃ N ₁ O ₇	1.53	0.47	5
344.1349	C ₁₅ H ₂₃ N ₁ O ₈	1.53	0.53	5
360.1298	C ₁₅ H ₂₃ N ₁ O ₉	1.53	0.60	5
376.1247	C ₁₅ H ₂₃ N ₁ O ₁₀	1.53	0.67	5
407.1304	C ₁₅ H ₂₄ N ₂ O ₁₁	1.60	0.73	5
330.1556	C ₁₅ H ₂₅ N ₁ O ₇	1.67	0.47	4
346.1505	C ₁₅ H ₂₅ N ₁ O ₈	1.67	0.53	4
362.1455	C ₁₅ H ₂₅ N ₁ O ₉	1.67	0.60	4

Figure 4.7 shows the temporal behavior of the measured aerosol size distribution, the aerosol mass concentration and selected mass traces during one of the measurement periods. The organic aerosol mass concentration showed a maximum of about 7 $\mu\text{g}/\text{m}^3$ with an average value of 3.4 $\mu\text{g}/\text{m}^3$.

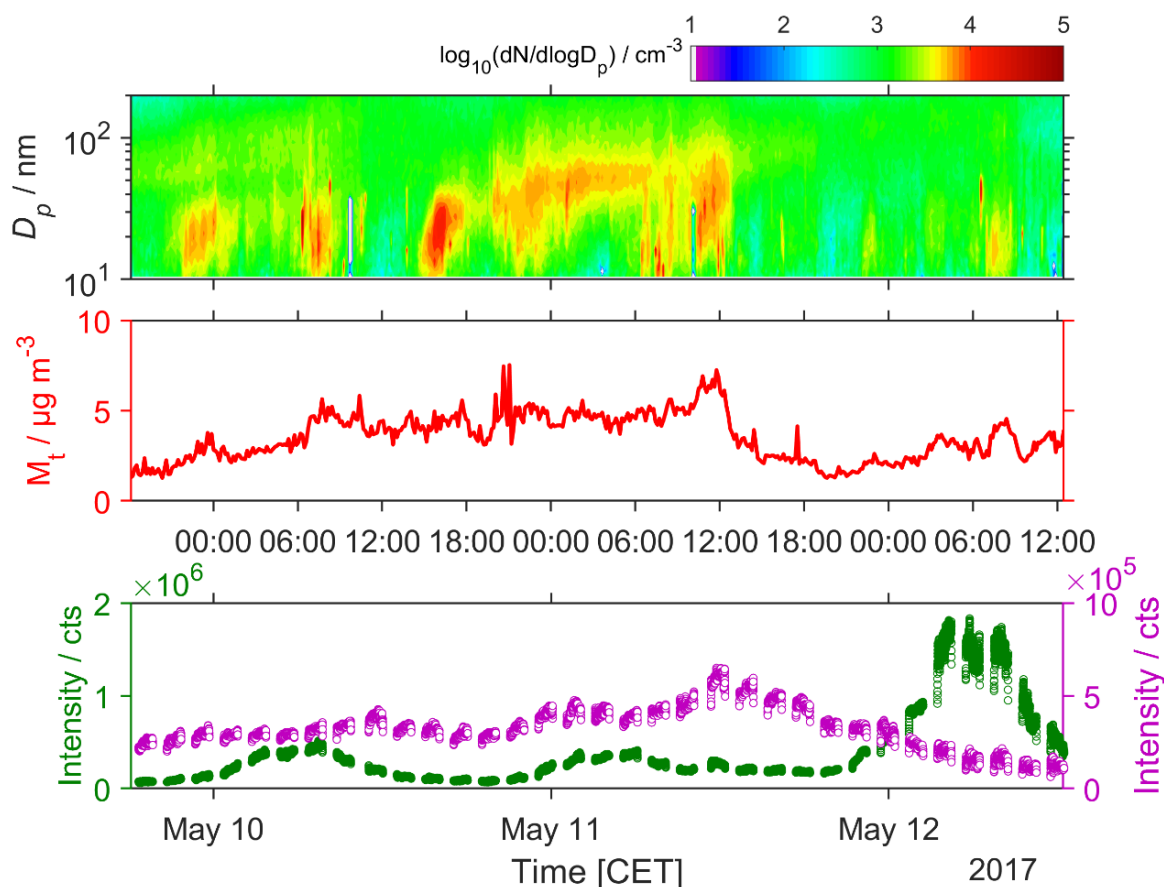


Figure 4.7 (upper panel) $\text{PM}_{2.5}$ particle size distribution during one of the measurement periods. The color key relate to the number size distribution ($\log_{10}(\text{dN}/\text{dlogD}_p)/\text{cm}^{-3}$). (central panel) Particle mass concentration. (lower panel) Temporal behavior of the protonated signals of $\text{C}_5\text{H}_{10}\text{O}_6$ (m/z 167.0550, $([\text{M}+\text{H}]^+)$, green) and $\text{C}_9\text{H}_{10}\text{O}_3$ (m/z 167.0701, $([\text{M}+\text{H}]^+)$, purple) in 1 h alternating ionization mode.

As an example of the performance of the APCI-Orbitrap-MS, Figure 4.7 also shows the temporal evolution of m/z ratios with very similar masses ($\text{C}_5\text{H}_{10}\text{O}_6$ (m/z 167.0550, $([\text{M}+\text{H}]^+)$) and $\text{C}_9\text{H}_{10}\text{O}_3$ (m/z 167.0701, $([\text{M}+\text{H}]^+)$). The protonated ions of the two compounds differ only by 0.0151 Da and both show clearly a different temporal behavior. Obviously, $\text{C}_5\text{H}_{10}\text{O}_6$ is not related to the general trend of the particle mass concentration and peaks regularly at 6 AM whereas $\text{C}_9\text{H}_{10}\text{O}_3$ is more or less following the particle mass concentration. Although the detailed origin of both compounds needs further investigations, the comparison exemplifies the potential of real-time APCI-Orbitrap-MS measurements to characterize individual compounds in organic aerosols. By means of the exact determination of the m/z ratios and if appropriate additional MS^2 experiments, the likelihood of misinterpretations due to overlapping peaks is crucially reduced with the applied technique.

4.4 Conclusions and Outlook

For the first time, the use of an online-APCI-Orbitrap-MS technique is presented and its ability to perform real-time single organic compound detection in ambient particles in the negative and positive ionization mode is demonstrated. Due to the soft ionization procedure, molecular ions are preserved and the deprotonated or protonated ions represent the main signal. The mass spectrometric system can also be used to perform MS² experiments for structure validation and identification due to the combination of high mass resolution ($R=140\,000$) and accuracy (<2 ppm). Since many organic compounds consist not only of carbon, hydrogen, and oxygen but also heteroatoms, high mass resolution is necessary. However, even for compounds without heteroatoms, molecular formulas can unambiguously be specified also at higher masses when chemical ionization is used in combination with Orbitrap mass resolution. The APCI-Orbitrap-MS was characterized by laboratory-generated MBTCA aerosol and showed a high time resolution and a linear response over three orders of magnitude for 40 nm, 70 nm and 100 nm particles. Detection limits were determined for MBTCA in the range of 1.3 ng/m³.

As a proof of principle, the ambient aerosol composition was measured in real time by sampling PM_{2.5} particles. A non-target screening showed the molecular composition of ambient organic aerosol during night- and daytime both in negative and positive ionization mode. With the presented mass spectrometric system it was possible to detect highly oxidized organic nitrates, organic di-nitrates and nitrooxy organosulfates with a very high time resolution in the ambient particle phase.

With the presented technique non-target screening, as well as single organic compound detection and quantification in aerosols can be performed either in laboratory experiments or under ambient atmospheric conditions without preconcentration or filter sampling steps. Consequently, APCI-Orbitrap-MS offers a number of advantages for the analysis of organic aerosols. The technique presented can easily be applied in laboratory-based mass spectrometric studies (e.g., at atmospheric simulation chambers), however, as demonstrated here, it is even more useful to be applied in field studies with an increasing complexity of the ambient organic aerosol. The expected future development of Orbitrap technology to be more instrumentally robust and more routine in operation will even facilitate a reliable and versatile application of such systems and will help to shed light on the atmospheric aerosol composition and formation mechanisms.

5 Conclusions and Outlook

The application of ultra-high-resolution mass spectrometry (UHRMS) to the field of aerosol research on a trace-analytical level for the analysis of organic aerosols was demonstrated for three complex matrices within this thesis. Ancient ice cores, filter samples of laboratory chamber experiments and ambient organic aerosols were analyzed in a qualitative and quantitative manner. The used ionization techniques (i.e., ESI and APCI) coupled to the Orbitrap mass spectrometer ensured a soft ionization in negative as well as positive mode. For the simultaneous detection and quantification of organic molecules in ancient ice cores, a method using UHPLC coupled to ESI-MS was developed. The analyzed molecules covered a broad range of atmospheric tracers, comprising levoglucosan, lignin-derived biomass burning markers, atmospheric SOA markers originating from isoprene, terpenes, and sesquiterpenes as well as fatty acids. For purification and enrichment of the analytes, an SPE method using anion exchange functionalities was developed and validated. Ice core sections from the Belukha glacier in the Altai mountain range covering the years 1826 – 1828 and 1866 – 1869 were analyzed, demonstrating the performance of the developed method. Several organic trace components were determined the first time in an ice core from the Belukha glacier in the Altai mountain range and quantified within a single analytical method. A PCA revealed six principal components accounting for ~90 % of the data variance in total. The main principal components were attributed to biomass burning and biogenic SOA, plant waxes, and sesquiterpene and short chain fatty acid emissions. For most of the analytes, the concentration maxima were found in summertime, which coincides with the time of the main precipitation in the Altai mountain range.

Concerning future ice cores studies, it should be considered to extend the method to other adequate compound classes such as pesticides to evaluate enhanced anthropogenic influence. Possibly, the method can also be adapted to other water-based matrices like the detection of drug residues in fresh water. Furthermore, a non-target screening could yield information on major chemical compound classes in historic ice core records. Especially, an anthropogenic influence in the years after the industrial revolution might be observable due to a higher amount of sulfur-, nitrogen- or halogen-containing compounds. Besides such studies, a non-target screening of an Antarctic ice core could give important data on the molecular composition of atmospheric chemical systems hundreds of thousands of years in the past.

A second matrix type investigated in this study were organic aerosol particles. In order to confirm the formulas of organic molecules and characterizing the molecular composition in sub-100 nm particles, a filter sampling method was established. The particles were sampled during the CLOUD campaign at CERN, Geneva and investigated using UHPLC coupled to ESI-UHRMS. The advantages of the ultra-high mass resolution in combination with a high mass accuracy allowed the determination of molecular compositions of single organic compounds occurring in nucleating particles. Unique and comprehensive lists of the molecular composition at biogenic nucleation experiments of α -pinene and

Δ -3-carene VOC precursors in a perfectly clean laboratory chamber were obtained. The compounds were categorized according to their elemental composition in subclasses containing carbon, hydrogen, and oxygen (CHO), nitrogen-containing compounds (CHON), sulfur-containing compounds (CHOS), and sulfur and nitrogen-containing compounds (CHONS). Besides the comprehensive characterization, detailed identification by MS² studies verified the existence of dimeric organic nitrates and nitrooxy organosulfates. Especially, due to reduced matrix and clustering effects during ionization and because of additional information of isomers and corresponding retention times, future investigations on filter sampling should include UHPLC and desist from direct injection MS.

Inspired by the CLOUD 10 campaign at CERN, Geneva, the need for real-time high-resolution mass spectrometric techniques was noticed. By reason of relatively low mass resolutions of existing online mass spectrometric techniques in the field of aerosol research, we established the use of an online-APCI-Orbitrap-MS technique. The APCI-Orbitrap-MS was optimized and characterized by model aerosols to evaluate detection limits and fragmentation patterns. The signals of protonated and deprotonated molecular ions dominated the mass spectra, while signals of fragmentation were detected to a minimum extent (<10 %). The application of the APCI-Orbitrap-MS technique in a proof-of-principle study for the real-time measurement of ambient aerosol particles demonstrated a powerful tool for molecular characterization using a non-target approach in negative and positive ionization mode. Moreover, single organic compound detection, structure elucidation using MS², and quantification in aerosols were proven to be possible without preconcentration or filter sampling steps.

The technique presented can easily be applied in laboratory-based mass spectrometric studies (e.g., at atmospheric simulation chambers), however, as demonstrated here, it is likely even more useful when applied in field studies with an increasing complexity of the composition of the organic aerosol particles. Future developments in Orbitrap technology will probably lead to more robust instruments and will allow more routine operations, which will facilitate a reliable and versatile application of such systems, aiding in investigations on atmospheric aerosol composition and formation mechanisms.

Further validation of the APCI-Orbitrap-MS technique in combination with complementary MS techniques, such as the Aerosol Mass Spectrometer (AMS) and the Chemical Ionization Atmospheric Pressure interface Time of Flight Mass Spectrometer (CI-APiToF-MS) will help to assess the potential of the technique. Besides technical optimizations, especially the data handling and analysis of large UHRMS datasets should be focused in upcoming projects. Software solutions facilitating data processing steps and directly visualizing appropriate graphs are needed and will contribute to establishing the technique in aerosol research.

6 References

- Abdi, H., and Williams, L.J. (2010). Principal component analysis. *Wiley Interdisciplinary Reviews: Computational Statistics*, 2, pp. 433–459.
- Acosta Navarro, J.C., Smolander, S., Struthers, H., Zorita, E., Ekman, A.M.L., Kaplan, J.O., Guenther, A., Arneth, A., and Riipinen, I. (2014). Global emissions of terpenoid VOCs from terrestrial vegetation in the last millennium. *Journal of Geophysical Research: Atmospheres*, 119, pp. 6867–6885.
- Almeida, J., Schobesberger, S., Kürten, A., Ortega, I.K., Kupiainen-Määttä, O., Praplan, A.P., Adamov, A., Amorim, A., Bianchi, F., Breitenlechner, M., David, A., Dommen, J., Donahue, N.M., Downard, A., Dunne, E., Duplissy, J., Ehrhart, S., Flagan, R.C., Franchin, A., Guida, R., Hakala, J., Hansel, A., Heinritzi, M., Henschel, H., Jokinen, T., Junninen, H., Kajos, M., Kangasluoma, J., Keskinen, H., Kupc, A., Kurtén, T., Kvashin, A.N., Laaksonen, A., Lehtipalo, K., Leiminger, M., Leppä, J., Loukonen, V., Makhmutov, V., Mathot, S., McGrath, M.J., Nieminen, T., Olenius, T., Onnela, A., Petäjä, T., Riccobono, F., Riipinen, I., Rissanen, M., Rondo, L., Ruuskanen, T., Santos, F.D., Sarnela, N., Schallhart, S., Schnitzhofer, R., Seinfeld, J.H., Simon, M., Sipilä, M., Stozhkov, Y., Stratmann, F., Tomé, A., Tröstl, J., Tsagkogeorgas, G., Vaattovaara, P., Viisanen, Y., Virtanen, A., Vrtala, A., Wagner, P.E., Weingartner, E., Wex, H., Williamson, C., Wimmer, D., Ye, P., Yli-Juuti, T., Carslaw, K.S., Kulmala, M., Curtius, J., Baltensperger, U., Worsnop, D.R., Vehkamäki, H., and Kirkby, J. (2013). Molecular understanding of sulphuric acid-amine particle nucleation in the atmosphere. *Nature*, 502, pp. 359–363.
- Altieri, K.E., Turpin, B.J., and Seitzinger, S.P. (2009). Oligomers, organosulfates, and nitrooxy organosulfates in rainwater identified by ultra-high resolution electrospray ionization FT-ICR mass spectrometry. *Atmospheric Chemistry and Physics*, 9, pp. 2533–2542.
- Angelis, M.D., Traversi, R., and Udusti, R. (2012). Long-term trends of mono-carboxylic acids in Antarctica. Comparison of changes in sources and transport processes at the two EPICA deep drilling sites. *Tellus B: Chemical and Physical Meteorology*, 64, p. 17331.
- Atkinson, R., and Arey, J. (2003). Atmospheric degradation of volatile organic compounds. *Chemical reviews*, 103, pp. 4605–4638.
- Ayres, B.R., Allen, H.M., Draper, D.C., Brown, S.S., Wild, R.J., Jimenez, J.L., Day, D.A., Campuzano-Jost, P., Hu, W., Gouw, J. de, Koss, A., Cohen, R.C., Duffey, K.C., Romer, P., Baumann, K., Edgerton, E., Takahama, S., Thornton, J.A., Lee, B.H., Lopez-Hilfiker, F.D., Mohr, C., Wennberg, P.O., Nguyen, T.B., Teng, A., Goldstein, A.H., Olson, K., and Fry, J.L. (2015). Organic nitrate aerosol formation via NO₃ + biogenic volatile organic compounds in the southeastern United States. *Atmospheric Chemistry and Physics*, 15, pp. 13377–13392.
- Barbante, C., Schwikowski, M., Döring, T., Gäggeler, H.W., Schotterer, U., Tobler, L., van de Velde, K., Ferrari, C., Cozzi, G., Turetta, A., Rosman, K., Bolshov, M., Capodaglio, G., Cescon, P., and Boutron, C. (2004). Historical Record of European Emissions of Heavy Metals to the Atmosphere Since the 1650s from Alpine Snow/Ice Cores Drilled near Monte Rosa. *Environmental Science & Technology*, 38, pp. 4085–4090.
- Barsanti, K.C., and Pankow, J.F. (2004). Thermodynamics of the formation of atmospheric organic particulate matter by accretion reactions—Part 1. Aldehydes and ketones. *Atmospheric Environment*, 38, pp. 4371–4382.
- Bateman, A.P., Nizkorodov, S.A., Laskin, J., and Laskin, A. (2010). High-resolution electrospray ionization mass spectrometry analysis of water-soluble organic aerosols collected with a particle into liquid sampler. *Analytical chemistry*, 82, pp. 8010–8016.
- Bateman, A.P., Walser, M.L., Desyaterik, Y., Laskin, J., Laskin, A., and Nizkorodov, S.A. (2008). The Effect of Solvent on the Analysis of Secondary Organic Aerosol Using Electrospray Ionization Mass Spectrometry. *Environmental Science & Technology*, 42, pp. 7341–7346.

- Bianchi, F., Tröstl, J., Junninen, H., Frege, C., Henne, S., Hoyle, C.R., Molteni, U., Herrmann, E., Adamov, A., Bukowiecki, N., Chen, X., Duplissy, J., Gysel, M., Hutterli, M., Kangasluoma, J., Kontkanen, J., Kürten, A., Manninen, H.E., Münch, S., Peräkylä, O., Petäjä, T., Rondo, L., Williamson, C., Weingartner, E., Curtius, J., Worsnop, D.R., Kulmala, M., Dommen, J., and Baltensperger, U. (2016). New particle formation in the free troposphere. A question of chemistry and timing. *Science (New York, N.Y.)*, 352, pp. 1109–1112.
- Borrás, E., and Tortajada-Genaro, L.A. (2012). Secondary organic aerosol formation from the photo-oxidation of benzene. *Atmospheric Environment*, 47, pp. 154–163.
- Boucher, O., and LOHMANN, U. (1995). The sulfate-CCN-cloud albedo effect. *Tellus B*, 47, pp. 281–300.
- Bourgeois, J.C. (1986). A pollen record from the Agassiz Ice Cap, northern Ellesmere Island, Canada. *Boreas*, 15, pp. 345–354.
- Brüggemann, M., Karu, E., Stelzer, T., and Hoffmann, T. (2015). Real-Time Analysis of Ambient Organic Aerosols Using Aerosol Flowing Atmospheric-Pressure Afterglow Mass Spectrometry (AeroFAPA-MS). *Environmental science & technology*, 49, pp. 5571–5578.
- Brüggemann, M., Poulain, L., Held, A., Stelzer, T., Zuth, C., Richters, S., Mutzel, A., van Pinxteren, D., Iinuma, Y., Katkevica, S., Rabe, R., Herrmann, H., and Hoffmann, T. (2017). Real-time detection of highly oxidized organosulfates and BSOA marker compounds during the F-BEACH 2014 field study. *Atmospheric Chemistry and Physics*, 17, pp. 1453–1469.
- Canagaratna, M.R., Jayne, J.T., Jimenez, J.L., Allan, J.D., Alfarra, M.R., Zhang, Q., Onasch, T.B., Drewnick, F., Coe, H., Middlebrook, A., Delia, A., Williams, L.R., Trimborn, A.M., Northway, M.J., DeCarlo, P.F., Kolb, C.E., Davidovits, P., and Worsnop, D.R. (2007). Chemical and microphysical characterization of ambient aerosols with the aerodyne aerosol mass spectrometer. *Mass spectrometry reviews*, 26, pp. 185–222.
- Carroll, D.I., Dzidic, I., Stillwell, R.N., Haegele, K.D., and Horning, E.C. (2002). Atmospheric pressure ionization mass spectrometry. Corona discharge ion source for use in a liquid chromatograph-mass spectrometer-computer analytical system. *Analytical Chemistry*, 47, pp. 2369–2373.
- Cheng, Y., Brook, J.R., Li, S.-M., and Leithead, A. (2011). Seasonal variation in the biogenic secondary organic aerosol tracer cis-pinonic acid. Enhancement due to emissions from regional and local biomass burning. *Atmospheric Environment*, 45, pp. 7105–7112.
- Claeys, M., Vermeylen, R., Yasmeen, F., Gómez-González, Y., Chi, X., Maenhaut, W., Mészáros, T., and Salma, I. (2012). Chemical characterisation of humic-like substances from urban, rural and tropical biomass burning environments using liquid chromatography with UV/vis photodiode array detection and electrospray ionisation mass spectrometry. *Environmental Chemistry*, 9, p. 273.
- Cochran, R.E., Smoliakova, I.P., and Kubátová, A. (2016). Detection of nitrated and oxygenated polycyclic aromatic hydrocarbons using atmospheric pressure chemical ionization high resolution mass spectrometry. *International Journal of Mass Spectrometry*, 397-398, pp. 6–17.
- DeCarlo, P.F., Kimmel, J.R., Trimborn, A., Northway, M.J., Jayne, J.T., Aiken, A.C., Gonin, M., Fuhrer, K., Horvath, T., Docherty, K.S., Worsnop, D.R., and Jimenez, J.L. (2006). Field-deployable, high-resolution, time-of-flight aerosol mass spectrometer. *Analytical chemistry*, 78, pp. 8281–8289.
- Detle, H.P., Qi, M., Schröder, D.C., Godt, A., and Koop, T. (2014). Glass-forming properties of 3-methylbutane-1,2,3-tricarboxylic acid and its mixtures with water and pinonic acid. *The journal of physical chemistry. A*, 118, pp. 7024–7033.
- Dias, A., Ehrhart, S., Vogel, A., Williamson, C., Almeida, J., Kirkby, J., Mathot, S., Mumford, S., and Onnela, A. (2017). Temperature uniformity in the CERN CLOUD chamber. *Atmospheric Measurement Techniques*, 10, pp. 5075–5088.
- Ding, X., Wang, X.-M., and Zheng, M. (2011). The influence of temperature and aerosol acidity on biogenic secondary organic aerosol tracers. Observations at a rural site in the central Pearl River Delta region, South China. *Atmospheric Environment*, 45, pp. 1303–1311.

- Donahue, N.M., Henry, K.M., Mentel, T.F., Kiendler-Scharr, A., Spindler, C., Bohn, B., Brauers, T., Dorn, H.P., Fuchs, H., Tillmann, R., Wahner, A., Saathoff, H., Naumann, K.-H., Möhler, O., Leisner, T., Müller, L., Reinnig, M.-C., Hoffmann, T., Salo, K., Hallquist, M., Frosch, M., Bilde, M., Tritscher, T., Barmet, P., Praplan, A.P., DeCarlo, P.F., Dommen, J., Prévôt, A.S.H., and Baltensperger, U. (2012). Aging of biogenic secondary organic aerosol via gas-phase OH radical reactions. *Proceedings of the National Academy of Sciences of the United States of America*, 109, pp. 13503–13508.
- Donahue, N.M., Ortega, I.K., Chuang, W., Riipinen, I., Riccobono, F., Schobesberger, S., Dommen, J., Baltensperger, U., Kulmala, M., Worsnop, D.R., and Vehkamäki, H. (2013). How do organic vapors contribute to new-particle formation? *Faraday Discussions*, 165, p. 91.
- Donahue, N.M., Robinson, A.L., Stanier, C.O., and Pandis, S.N. (2006). Coupled Partitioning, Dilution, and Chemical Aging of Semivolatile Organics. *Environmental Science & Technology*, 40, pp. 2635–2643.
- Donahue, N.M., Robinson, A.L., Trump, E.R., Riipinen, I., and Kroll, J.H. (2014). Volatility and aging of atmospheric organic aerosol. *Topics in current chemistry*, 339, pp. 97–143.
- Donahue, N.M., Trump, E.R., Pierce, J.R., and Riipinen, I. (2011). Theoretical constraints on pure vapor-pressure driven condensation of organics to ultrafine particles. *Geophysical Research Letters*, 38, n/a-n/a.
- Duplissy, J., Merikanto, J., Franchin, A., Tsagkogeorgas, G., Kangasluoma, J., Wimmer, D., Vuollekoski, H., Schobesberger, S., Lehtipalo, K., Flagan, R.C., Brus, D., Donahue, N.M., Vehkamäki, H., Almeida, J., Amorim, A., Barmet, P., Bianchi, F., Breitenlechner, M., Dunne, E.M., Guida, R., Henschel, H., Junninen, H., Kirkby, J., Kürten, A., Kupc, A., Määttänen, A., Makhmutov, V., Mathot, S., Nieminen, T., Onnela, A., Praplan, A.P., Riccobono, F., Rondo, L., Steiner, G., Tome, A., Walther, H., Baltensperger, U., Carslaw, K.S., Dommen, J., Hansel, A., Petäjä, T., Sipilä, M., Stratmann, F., Vrtala, A., Wagner, P.E., Worsnop, D.R., Curtius, J., and Kulmala, M. (2016). Effect of ions on sulfuric acid-water binary particle formation. 2. Experimental data and comparison with QC-normalized classical nucleation theory. *Journal of Geophysical Research: Atmospheres*, 121, pp. 1752–1775.
- Duporté, G., Flaud, P.-M., Geneste, E., Augagneur, S., Pangui, E., Lamkaddam, H., Gratien, A., Doussin, J.-F., Budzinski, H., Villenave, E., and Perraudin, E. (2016). Experimental Study of the Formation of Organosulfates from α -Pinene Oxidation. Part I. Product Identification, Formation Mechanisms and Effect of Relative Humidity. *The journal of physical chemistry. A*, 120, pp. 7909–7923.
- Ehn, M., Kleist, E., Junninen, H., Petäjä, T., Lönn, G., Schobesberger, S., Dal Maso, M., Trimborn, A., Kulmala, M., Worsnop, D.R., Wahner, A., Wildt, J., and Mentel, T.F. (2012). Gas phase formation of extremely oxidized pinene reaction products in chamber and ambient air. *Atmospheric Chemistry and Physics*, 12, pp. 5113–5127.
- Ehn, M., Thornton, J.A., Kleist, E., Sipilä, M., Junninen, H., Pullinen, I., Springer, M., Rubach, F., Tillmann, R., Lee, B., Lopez-Hilfiker, F., Andres, S., Acir, I.-H., Rissanen, M., Jokinen, T., Schobesberger, S., Kangasluoma, J., Kontkanen, J., Nieminen, T., Kurtén, T., Nielsen, L.B., Jørgensen, S., Kjaergaard, H.G., Canagaratna, M., Maso, M.D., Berndt, T., Petäjä, T., Wahner, A., Kerminen, V.-M., Kulmala, M., Worsnop, D.R., Wildt, J., and Mentel, T.F. (2014). A large source of low-volatility secondary organic aerosol. *Nature*, 506, pp. 476–479.
- Eichler, A., Brüttsch, S., Olivier, S., Papina, T., and Schwikowski, M. (2009). A 750 year ice core record of past biogenic emissions from Siberian boreal forests. *Geophysical Research Letters*, 36, p. 1.
- Eichler, A., Tinner, W., Brüttsch, S., Olivier, S., Papina, T., and Schwikowski, M. (2011). An ice-core based history of Siberian forest fires since AD 1250. *Quaternary Science Reviews*, 30, pp. 1027–1034.
- Eichler, P., Müller, M., D'Anna, B., and Wisthaler, A. (2015). A novel inlet system for online chemical analysis of semi-volatile submicron particulate matter. *Atmospheric Measurement Techniques*, 8, pp. 1353–1360.

- Fang, J., Kawamura, K., Ishimura, Y., and Matsumoto, K. (2002). Carbon Isotopic Composition of Fatty Acids in the Marine Aerosols from the Western North Pacific. Implication for the Source and Atmospheric Transport. *Environmental Science & Technology*, 36, pp. 2598–2604.
- Farmer, D.K., and Jimenez, J.L. (2010). Real-time atmospheric chemistry field instrumentation. *Analytical chemistry*, 82, pp. 7879–7884.
- Fine, P.M., Cass, G.R., and Simoneit, B.R.T. (2004). Chemical Characterization of Fine Particle Emissions from the Wood Stove Combustion of Prevalent United States Tree Species. *Environmental Engineering Science*, 21, pp. 705–721.
- Finlayson-Pitts, B.J., and Pitts, J.N. (2000). Chemistry of the upper and lower atmosphere. Theory, experiments, and applications. Academic Press: San Diego, Calif.
- Fu, P., Kawamura, K., Chen, J., and Barrie, L.A. (2009). Isoprene, Monoterpene, and Sesquiterpene Oxidation Products in the High Arctic Aerosols during Late Winter to Early Summer. *Environmental Science & Technology*, 43, pp. 4022–4028.
- Fu, P., Kawamura, K., Seki, O., Izawa, Y., Shiraiwa, T., and Ashworth, K. (2016). Historical Trends of Biogenic SOA Tracers in an Ice Core from Kamchatka Peninsula. *Environmental Science & Technology Letters*, 3, pp. 351–358.
- Fu, P.Q., Kawamura, K., Chen, J., Charrière, B., and Sempéré, R. (2013). Organic molecular composition of marine aerosols over the Arctic Ocean in summer. Contributions of primary emission and secondary aerosol formation. *Biogeosciences*, 10, pp. 653–667.
- Gabrieli, J., Vallelonga, P., Cozzi, G., Gabrielli, P., Gambaro, A., Sigl, M., Decet, F., Schwikowski, M., Gäggeler, H., Boutron, C., Cescon, P., and Barbante, C. (2010). Post 17th-century changes of European PAH emissions recorded in high-altitude Alpine snow and ice. *Environmental science & technology*, 44, pp. 3260–3266.
- Gabrielli, P., Barbante, C., Boutron, C., Cozzi, G., Gaspari, V., Planchon, F., Ferrari, C., Turetta, C., Hong, S., and Cescon, P. (2005). Variations in atmospheric trace elements in Dome C (East Antarctica) ice over the last two climatic cycles. *Atmospheric Environment*, 39, pp. 6420–6429.
- Gallimore, P.J., Giorio, C., Mahon, B.M., and Kalberer, M. (2017). Online molecular characterisation of organic aerosols in an atmospheric chamber using extractive electrospray ionisation mass spectrometry. *Atmospheric Chemistry and Physics*, 17, pp. 14485–14500.
- Gallimore, P.J., and Kalberer, M. (2013). Characterizing an extractive electrospray ionization (EESI) source for the online mass spectrometry analysis of organic aerosols. *Environmental science & technology*, 47, pp. 7324–7331.
- Gambaro, A., Zangrando, R., Gabrielli, P., Barbante, C., and Cescon, P. (2008). Direct determination of levoglucosan at the picogram per milliliter level in Antarctic ice by high-performance liquid chromatography/electrospray ionization triple quadrupole mass spectrometry. *Analytical chemistry*, 80, pp. 1649–1655.
- George, C., Ammann, M., D'Anna, B., Donaldson, D.J., and Nizkorodov, S.A. (2015). Heterogeneous photochemistry in the atmosphere. *Chemical reviews*, 115, pp. 4218–4258.
- Giorio, C., Kehrwald, N., Barbante, C., Kalberer, M., King, A.C.F., Thomas, E.R., Wolff, E.W., and Zennaro, P. (2018). Prospects for reconstructing paleoenvironmental conditions from organic compounds in polar snow and ice. *Quaternary Science Reviews*, 183, pp. 1–22.
- Gómez-González, Y., Wang, W., Vermeylen, R., Chi, X., Neiryneck, J., Janssens, I.A., Maenhaut, W., and Claeys, M. (2012). Chemical characterisation of atmospheric aerosols during a 2007 summer field campaign at Brasschaat, Belgium. Sources and source processes of biogenic secondary organic aerosol. *Atmospheric Chemistry and Physics*, 12, pp. 125–138.
- Gordon, H., Sengupta, K., Rap, A., Duplissy, J., Frege, C., Williamson, C., Heinritzi, M., Simon, M., Yan, C., Almeida, J., Tröstl, J., Nieminen, T., Ortega, I.K., Wagner, R., Dunne, E.M., Adamov, A., Amorim, A., Bernhammer, A.-K., Bianchi, F., Breitenlechner, M., Brilke, S., Chen, X., Craven, J.S., Dias, A., Ehrhart, S., Fischer, L., Flagan, R.C., Franchin, A., Fuchs, C., Guida, R., Hakala, J., Hoyle, C.R., Jokinen, T., Junninen, H., Kangasluoma, J., Kim, J., Kirkby, J., Krapf, M., Kürten, A., Laaksonen, A., Lehtipalo, K., Makhmutov, V., Mathot, S., Molteni, U., Monks, S.A., Onnela, A., Peräkylä, O., Piel, F., Petäjä, T., Praplan, A.P., Pringle, K.J., Richards, N.A.D., Rissanen,

- M.P., Rondo, L., Sarnela, N., Schobesberger, S., Scott, C.E., Seinfeld, J.H., Sharma, S., Sipilä, M., Steiner, G., Stozhkov, Y., Stratmann, F., Tomé, A., Virtanen, A., Vogel, A.L., Wagner, A.C., Wagner, P.E., Weingartner, E., Wimmer, D., Winkler, P.M., Ye, P., Zhang, X., Hansel, A., Dommen, J., Donahue, N.M., Worsnop, D.R., Baltensperger, U., Kulmala, M., Curtius, J., and Carslaw, K.S. (2016). Reduced anthropogenic aerosol radiative forcing caused by biogenic new particle formation. *Proceedings of the National Academy of Sciences of the United States of America*, 113, pp. 12053–12058.
- Grieman, M.M., Aydin, M., Fritzsche, D., McConnell, J.R., Opel, T., Sigl, M., and Saltzman, E.S. (2017a). Aromatic acids in a Eurasian Arctic ice core. A 2600-year proxy record of biomass burning. *Climate of the Past*, 13, pp. 395–410.
- Grieman, M.M., Aydin, M., Isaksson, E., Schwikowski, M., and Saltzman, E.S. (2017b). Methoxy aromatic acids in an Arctic ice core from Svalbard. A proxy record of biomass burning. *Climate of the Past Discussions*, pp. 1–24.
- Grieman, M.M., Greaves, J., and Saltzman, E.S. (2015). A method for analysis of vanillic acid in polar ice cores. *Climate of the Past*, 11, pp. 227–232.
- Gross, J.H. (2004). *Mass spectrometry. A textbook*. Springer: Berlin.
- Gross, J.H. (2013). *Massenspektrometrie*. Springer Berlin Heidelberg: Berlin, Heidelberg.
- Guenther, A., Hewitt, C.N., Erickson, D., Fall, R., Geron, C., Graedel, T., Harley, P., Klinger, L., Lerdau, M., McKay, W.A., Pierce, T., Scholes, B., Steinbrecher, R., Tallamraju, R., Taylor, J., and Zimmerman, P. (1995). A global model of natural volatile organic compound emissions. *Journal of Geophysical Research*, 100, p. 8873.
- Guenther, A.B., Jiang, X., Heald, C.L., Sakulyanontvittaya, T., Duhl, T., Emmons, L.K., and Wang, X. (2012). The Model of Emissions of Gases and Aerosols from Nature version 2.1 (MEGAN2.1). An extended and updated framework for modeling biogenic emissions. *Geoscientific Model Development*, 5, pp. 1471–1492.
- Hallquist, M., Wenger, J.C., Baltensperger, U., Rudich, Y., Simpson, D., Claeys, M., Dommen, J., Donahue, N.M., George, C., Goldstein, A.H., Hamilton, J.F., Herrmann, H., Hoffmann, T., Iinuma, Y., Jang, M., Jenkin, M.E., Jimenez, J.L., Kiendler-Scharr, A., Maenhaut, W., McFiggans, G., Mentel, T.F., Monod, A., Prévôt, A.S.H., Seinfeld, J.H., Surratt, J.D., Szmigielski, R., and Wildt, J. (2009). The formation, properties and impact of secondary organic aerosol. Current and emerging issues. *Atmospheric Chemistry and Physics*, 9, pp. 5155–5236.
- Hari, P. & Kulmala, M. (2005). Station for measuring ecosystem-atmosphere relations (SMEAR II). *Boreal Environ Res*, pp. 315–322.
- Helmig, D., Ortega, J., Duhl, T., Tanner, D., Guenther, A., Harley, P., Wiedinmyer, C., Milford, J., and Sakulyanontvittaya, T. (2007). Sesquiterpene Emissions from Pine Trees – Identifications, Emission Rates and Flux Estimates for the Contiguous United States. *Environmental Science & Technology*, 41, pp. 1545–1553.
- Henderson, K., Laube, A., Gäggeler, H.W., Olivier, S., Papina, T., and Schwikowski, M. (2006). Temporal variations of accumulation and temperature during the past two centuries from Belukha ice core, Siberian Altai. *Journal of Geophysical Research*, 111, p. 9185.
- Hennion, M.-C. (1999). Solid-phase extraction. Method development, sorbents, and coupling with liquid chromatography. *Journal of Chromatography A*, 856, pp. 3–54.
- Hoffmann, D., Tilgner, A., Iinuma, Y., and Herrmann, H. (2010). Atmospheric stability of levoglucosan. A detailed laboratory and modeling study. *Environmental science & technology*, 44, pp. 694–699.
- Hoffmann, T., Bandur, R., Hoffmann, S., and Warscheid, B. (2002). On-line characterization of gaseous and particulate organic analytes using atmospheric pressure chemical ionization mass spectrometry. *Spectrochimica Acta Part B: Atomic Spectroscopy*, 57, pp. 1635–1647.
- Hoffmann, T., Bandur, R., Marggraf, U., and Linscheid, M. (1998). Molecular composition of organic aerosols formed in the α -pinene/O₃ reaction. Implications for new particle formation processes. *Journal of Geophysical Research*, 103, pp. 25569–25578.

- Hoffmann, T., Huang, R.-J., and Kalberer, M. (2011). Atmospheric analytical chemistry. *Analytical chemistry*, 83, pp. 4649–4664.
- Hoffmann, T., ODUM, J.R.A.Y., BOWMAN, F., COLLINS, D., Klockow, D., Flagan, R.C., and Seinfeld, J.H. (1997). Formation of Organic Aerosols from the Oxidation of Biogenic Hydrocarbons. *Journal of Atmospheric Chemistry*, 26, pp. 189–222.
- Hoffmann, T., Zetzsch, C., and Rossi, M.J. (2007). Chemie von Aerosolen. *Chemie in unserer Zeit*, 41, pp. 232–246.
- Horan, A.J., Apsokardu, M.J., and Johnston, M.V. (2017). Droplet Assisted Inlet Ionization for Online Analysis of Airborne Nanoparticles. *Analytical chemistry*, 89, pp. 1059–1062.
- Hu, Q., Noll, R.J., Li, H., Makarov, A., Hardman, M., and Graham Cooks, R. (2005). The Orbitrap. A new mass spectrometer. *Journal of mass spectrometry : JMS*, 40, pp. 430–443.
- Hughey, C.A., Hendrickson, C.L., Rodgers, R.P., Marshall, A.G., and Qian, K. (2001). Kendrick Mass Defect Spectrum. A Compact Visual Analysis for Ultrahigh-Resolution Broadband Mass Spectra. *Analytical Chemistry*, 73, pp. 4676–4681.
- Hutterli, M.A. (2003). Sensitivity of hydrogen peroxide (H₂O₂) and formaldehyde (HCHO) preservation in snow to changing environmental conditions. Implications for ice core records. *Journal of Geophysical Research*, 108, p. 2789.
- Iinuma, Y., Böge, O., Gräfe, R., and Herrmann, H. (2010). Methyl-nitrocatechols. Atmospheric tracer compounds for biomass burning secondary organic aerosols. *Environmental science & technology*, 44, pp. 8453–8459.
- Iinuma, Y., Brüggemann, E., Gnauk, T., Müller, K., Andreae, M.O., Helas, G., Parmar, R., and Herrmann, H. (2007a). Source characterization of biomass burning particles. The combustion of selected European conifers, African hardwood, savanna grass, and German and Indonesian peat. *Journal of Geophysical Research*, 112, p. 1148.
- Iinuma, Y., Müller, C., Berndt, T., Böge, O., Claeys, M., and Herrmann, H. (2007b). Evidence for the Existence of Organosulfates from β -Pinene Ozonolysis in Ambient Secondary Organic Aerosol. *Environmental Science & Technology*, 41, pp. 6678–6683.
- Iinuma, Y., Müller, C., Böge, O., Gnauk, T., and Herrmann, H. (2007c). The formation of organic sulfate esters in the limonene ozonolysis secondary organic aerosol (SOA) under acidic conditions. *Atmospheric Environment*, 41, pp. 5571–5583.
- IPCC (2013). IPCC: Climate Change 2013: The Physical Science Basis. Contribution of Working Group I to the Fifth Assessment Report of the Intergovernmental Panel on Climate Change. Cambridge University Press, Cambridge, UK, and New York, NY, USA.
- Jaoui, M., Kleindienst, T.E., Docherty, K.S., Lewandowski, M., and Offenberg, J.H. (2013). Secondary organic aerosol formation from the oxidation of a series of sesquiterpenes. α -cedrene, β -caryophyllene, α -humulene and α -farnesene with O₃, OH and NO₃ radicals. *Environmental Chemistry*, 10, p. 178.
- Jimenez, J.L., Canagaratna, M.R., Donahue, N.M., Prevot, A.S.H., Zhang, Q., Kroll, J.H., DeCarlo, P.F., Allan, J.D., Coe, H., Ng, N.L., Aiken, A.C., Docherty, K.S., Ulbrich, I.M., Grieshop, A.P., Robinson, A.L., Duplissy, J., Smith, J.D., Wilson, K.R., Lanz, V.A., Hueglin, C., Sun, Y.L., Tian, J., Laaksonen, A., Raatikainen, T., Rautiainen, J., Vaattovaara, P., Ehn, M., Kulmala, M., Tomlinson, J.M., Collins, D.R., Cubison, M.J., Dunlea, E.J., Huffman, J.A., Onasch, T.B., Alfarra, M.R., Williams, P.I., Bower, K., Kondo, Y., Schneider, J., Drewnick, F., Borrmann, S., Weimer, S., Demerjian, K., Salcedo, D., Cottrell, L., Griffin, R., Takami, A., Miyoshi, T., Hatakeyama, S., Shimojo, A., Sun, J.Y., Zhang, Y.M., Dzepina, K., Kimmel, J.R., Sueper, D., Jayne, J.T., Herndon, S.C., Trimborn, A.M., Williams, L.R., Wood, E.C., Middlebrook, A.M., Kolb, C.E., Baltensperger, U., and Worsnop, D.R. (2009). Evolution of organic aerosols in the atmosphere. *Science (New York, N.Y.)*, 326, pp. 1525–1529.
- Jokinen, T., Berndt, T., Makkonen, R., Kerminen, V.-M., Junninen, H., Paasonen, P., Stratmann, F., Herrmann, H., Guenther, A.B., Worsnop, D.R., Kulmala, M., Ehn, M., and Sipilä, M. (2015). Production of extremely low volatile organic compounds from biogenic emissions. Measured

- yields and atmospheric implications. *Proceedings of the National Academy of Sciences of the United States of America*, 112, pp. 7123–7128.
- Jokinen, T., Sipilä, M., Richters, S., Kerminen, V.-M., Paasonen, P., Stratmann, F., Worsnop, D., Kulmala, M., Ehn, M., Herrmann, H., and Berndt, T. (2014). Rapid autoxidation forms highly oxidized RO₂ radicals in the atmosphere. *Angewandte Chemie (International ed. in English)*, 53, pp. 14596–14600.
- Jouzel, J. (2013). A brief history of ice core science over the last 50 yr. *Climate of the Past*, 9, pp. 2525–2547.
- Kahnt, A., Behrouzi, S., Vermeulen, R., Safi Shalamzari, M., Vercauteren, J., Roekens, E., Claeys, M., and Maenhaut, W. (2013). One-year study of nitro-organic compounds and their relation to wood burning in PM₁₀ aerosol from a rural site in Belgium. *Atmospheric Environment*, 81, pp. 561–568.
- Kampf, C.J., Filippi, A., Zuth, C., Hoffmann, T., and Opatz, T. (2016). Secondary brown carbon formation via the dicarbonyl imine pathway. Nitrogen heterocycle formation and synergistic effects. *Physical chemistry chemical physics : PCCP*, 18, pp. 18353–18364.
- Kanakidou, M., Seinfeld, J.H., Pandis, S.N., Barnes, I., Dentener, F.J., Facchini, M.C., van Dingenen, R., Ervens, B., Nenes, A., Nielsen, C.J., Swietlicki, E., Putaud, J.P., Balkanski, Y., Fuzzi, S., Horth, J., Moortgat, G.K., Winterhalter, R., Myhre, C.E.L., Tsigaridis, K., Vignati, E., Stephanou, E.G., and Wilson, J. (2005). Organic aerosol and global climate modelling. A review. *Atmospheric Chemistry and Physics*, 5, pp. 1053–1123.
- Kawamura, K., Izawa, Y., Mochida, M., and Shiraiwa, T. (2012). Ice core records of biomass burning tracers (levoglucosan and dehydroabietic, vanillic and p-hydroxybenzoic acids) and total organic carbon for past 300years in the Kamchatka Peninsula, Northeast Asia. *Geochimica et Cosmochimica Acta*, 99, pp. 317–329.
- Kawamura, K., Suzuki, I., Fujii, Y., and Watanabe, O. (1996). Ice core record of fatty acids over the past 450 years in Greenland. *Geophysical Research Letters*, 23, pp. 2665–2668.
- Kawamura, K., Yokoyama, K., Fujii, Y., and Watanabe, O. (2001). A Greenland ice core record of low molecular weight dicarboxylic acids, ketocarboxylic acids, and α -dicarbonyls. A trend from Little Ice Age to the present (1540 to 1989 A.D.). *Journal of Geophysical Research*, 106, pp. 1331–1345.
- Kehrwald, N., Zangrando, R., Gabrielli, P., Jaffrezo, J.-L., Boutron, C., Barbante, C., and Gambaro, A. (2012). Levoglucosan as a specific marker of fire events in Greenland snow. *Tellus B: Chemical and Physical Meteorology*, 64, p. 18196.
- Kehrwald, N., Zangrando, R., Gambaro, A., Cescon, P., and Barbante, C. (2010). Specific molecular markers in ice cores provide large-scale patterns in biomass burning. *PAGES news*, 18, pp. 59–61.
- Keil, R., Saleme, K., Forrest, B., Neibauer, J., and Logsdon, M. (2011). Differential presence of anthropogenic compounds dissolved in the marine waters of Puget Sound, WA and Barkley Sound, BC. *Marine Pollution Bulletin*, 62, pp. 2404–2411.
- Kim, S., Kramer, R.W., and Hatcher, P.G. (2003). Graphical Method for Analysis of Ultrahigh-Resolution Broadband Mass Spectra of Natural Organic Matter, the Van Krevelen Diagram. *Analytical Chemistry*, 75, pp. 5336–5344.
- Kirkby, J., Curtius, J., Almeida, J., Dunne, E., Duplissy, J., Ehrhart, S., Franchin, A., Gagné, S., Ickes, L., Kürten, A., Kupc, A., Metzger, A., Riccobono, F., Rondo, L., Schobesberger, S., Tsagkogeorgas, G., Wimmer, D., Amorim, A., Bianchi, F., Breitenlechner, M., David, A., Dommen, J., Downard, A., Ehn, M., Flagan, R.C., Haider, S., Hansel, A., Hauser, D., Jud, W., Junninen, H., Kreissl, F., Kvashin, A., Laaksonen, A., Lehtipalo, K., Lima, J., Lovejoy, E.R., Makhmutov, V., Mathot, S., Mikkilä, J., Minginette, P., Mogo, S., Nieminen, T., Onnela, A., Pereira, P., Petäjä, T., Schnitzhofer, R., Seinfeld, J.H., Sipilä, M., Stozhkov, Y., Stratmann, F., Tomé, A., Vanhanen, J., Viisanen, Y., Virtala, A., Wagner, P.E., Walther, H., Weingartner, E., Wex, H., Winkler, P.M., Carslaw, K.S., Worsnop, D.R., Baltensperger, U., and Kulmala, M. (2011). Role of sulphuric acid, ammonia and galactic cosmic rays in atmospheric aerosol nucleation. *Nature*, 476, pp. 429–433.

- Kirkby, J., Duplissy, J., Sengupta, K., Frege, C., Gordon, H., Williamson, C., Heinritzi, M., Simon, M., Yan, C., Almeida, J., Tröstl, J., Nieminen, T., Ortega, I.K., Wagner, R., Adamov, A., Amorim, A., Bernhammer, A.-K., Bianchi, F., Breitenlechner, M., Brilke, S., Chen, X., Craven, J., Dias, A., Ehrhart, S., Flagan, R.C., Franchin, A., Fuchs, C., Guida, R., Hakala, J., Hoyle, C.R., Jokinen, T., Junninen, H., Kangasluoma, J., Kim, J., Krapf, M., Kürten, A., Laaksonen, A., Lehtipalo, K., Makhmutov, V., Mathot, S., Molteni, U., Onnela, A., Peräkylä, O., Piel, F., Petäjä, T., Praplan, A.P., Pringle, K., Rap, A., Richards, N.A.D., Riipinen, I., Rissanen, M.P., Rondo, L., Sarnela, N., Schobesberger, S., Scott, C.E., Seinfeld, J.H., Sipilä, M., Steiner, G., Stozhkov, Y., Stratmann, F., Tomé, A., Virtanen, A., Vogel, A.L., Wagner, A.C., Wagner, P.E., Weingartner, E., Wimmer, D., Winkler, P.M., Ye, P., Zhang, X., Hansel, A., Dommen, J., Donahue, N.M., Worsnop, D.R., Baltensperger, U., Kulmala, M., Carslaw, K.S., and Curtius, J. (2016). Ion-induced nucleation of pure biogenic particles. *Nature*, 533, pp. 521–526.
- Kitanovski, Z., Grgić, I., Yasmeen, F., Claeys, M., and Cusak, A. (2012). Development of a liquid chromatographic method based on ultraviolet-visible and electrospray ionization mass spectrometric detection for the identification of nitrocatechols and related tracers in biomass burning atmospheric organic aerosol. *Rapid communications in mass spectrometry : RCM*, 26, pp. 793–804.
- Kostiainen, R., and Kauppila, T.J. (2009). Effect of eluent on the ionization process in liquid chromatography-mass spectrometry. *Journal of chromatography. A*, 1216, pp. 685–699.
- Kourtchev, I., Doussin, J.-F., Giorio, C., Mahon, B., Wilson, E.M., Maurin, N., Pangui, E., Venables, D.S., Wenger, J.C., and Kalberer, M. (2015). Molecular composition of fresh and aged secondary organic aerosol from a mixture of biogenic volatile compounds. A high-resolution mass spectrometry study. *Atmospheric Chemistry and Physics*, 15, pp. 5683–5695.
- Krechmer, J.E., Groessl, M., Zhang, X., Junninen, H., Massoli, P., Lambe, A.T., Kimmel, J.R., Cubison, M.J., Graf, S., Lin, Y.-H., Budisulistiorini, S.H., Zhang, H., Surratt, J.D., Knochenmuss, R., Jayne, J.T., Worsnop, D.R., Jimenez, J.-L., and Canagaratna, M.R. (2016). Ion mobility spectrometry–mass spectrometry (IMS–MS) for on- and offline analysis of atmospheric gas and aerosol species. *Atmospheric Measurement Techniques*, 9, pp. 3245–3262.
- Kristensen, K., Cui, T., Zhang, H., Gold, A., Glasius, M., and Surratt, J.D. (2014). Dimers in α -pinene secondary organic aerosol. Effect of hydroxyl radical, ozone, relative humidity and aerosol acidity. *Atmospheric Chemistry and Physics*, 14, pp. 4201–4218.
- Kroll, J.H., Donahue, N.M., Jimenez, J.L., Kessler, S.H., Canagaratna, M.R., Wilson, K.R., Altieri, K.E., Mazzoleni, L.R., Wozniak, A.S., Bluhm, H., Mysak, E.R., Smith, J.D., Kolb, C.E., and Worsnop, D.R. (2011). Carbon oxidation state as a metric for describing the chemistry of atmospheric organic aerosol. *Nature chemistry*, 3, pp. 133–139.
- Kroll, J.H., and Seinfeld, J.H. (2008). Chemistry of secondary organic aerosol. Formation and evolution of low-volatility organics in the atmosphere. *Atmospheric Environment*, 42, pp. 3593–3624.
- Kückelmann, U., Warscheid, B., and Hoffmann, T. (2000). On-Line Characterization of Organic Aerosols Formed from Biogenic Precursors Using Atmospheric Pressure Chemical Ionization Mass Spectrometry. *Analytical Chemistry*, 72, pp. 1905–1912.
- Kulkarni, P., Baron, P.A., and Willeke, K. (2011). *Aerosol Measurement*. John Wiley & Sons, Inc: Hoboken, NJ, USA.
- Kulmala, M., Kontkanen, J., Junninen, H., Lehtipalo, K., Manninen, H.E., Nieminen, T., Petäjä, T., Sipilä, M., Schobesberger, S., Rantala, P., Franchin, A., Jokinen, T., Järvinen, E., Äijälä, M., Kangasluoma, J., Hakala, J., Aalto, P.P., Paasonen, P., Mikkilä, J., Vanhanen, J., Aalto, J., Hakola, H., Makkonen, U., Ruuskanen, T., Mauldin, R.L., Duplissy, J., Vehkamäki, H., Bäck, J., Kortelainen, A., Riipinen, I., Kurtén, T., Johnston, M.V., Smith, J.N., Ehn, M., Mentel, T.F., Lehtinen, K.E.J., Laaksonen, A., Kerminen, V.-M., and Worsnop, D.R. (2013). Direct observations of atmospheric aerosol nucleation. *Science (New York, N.Y.)*, 339, pp. 943–946.
- Largiuni, O. (2003). Formaldehyde record from Lys glacier firn core, Monte Rosa massif (Italy). *Atmospheric Environment*, 37, pp. 3849–3860.

- Laskin, A., Smith, J.S., and Laskin, J. (2009). Molecular Characterization of Nitrogen-Containing Organic Compounds in Biomass Burning Aerosols Using High-Resolution Mass Spectrometry. *Environmental Science & Technology*, 43, pp. 3764–3771.
- Laskin, J., Laskin, A., and Nizkorodov, S.A. (2018). Mass Spectrometry Analysis in Atmospheric Chemistry. *Analytical chemistry*, 90, pp. 166–189.
- Lee, B.H., Mohr, C., Lopez-Hilfiker, F.D., Lutz, A., Hallquist, M., Lee, L., Romer, P., Cohen, R.C., Iyer, S., Kurtén, T., Hu, W., Day, D.A., Campuzano-Jost, P., Jimenez, J.L., Xu, L., Ng, N.L., Guo, H., Weber, R.J., Wild, R.J., Brown, S.S., Koss, A., Gouw, J. de, Olson, K., Goldstein, A.H., Seco, R., Kim, S., McAvey, K., Shepson, P.B., Starn, T., Baumann, K., Edgerton, E.S., Liu, J., Shilling, J.E., Miller, D.O., Brune, W., Schobesberger, S., D'Ambro, E.L., and Thornton, J.A. (2016). Highly functionalized organic nitrates in the southeast United States. Contribution to secondary organic aerosol and reactive nitrogen budgets. *Proceedings of the National Academy of Sciences of the United States of America*, 113, pp. 1516–1521.
- Legrand, M., and Angelis, M. de (1996). Light carboxylic acids in Greenland ice. A record of past forest fires and vegetation emissions from the boreal zone. *Journal of Geophysical Research*, 101, pp. 4129–4145.
- Legrand, M., Angelis, M. de, Staffelbach, T., Neftel, A., and Stauffer, B. (1992). Large perturbations of ammonium and organic acids content in the summit-Greenland Ice Core. Fingerprint from forest fires? *Geophysical Research Letters*, 19, pp. 473–475.
- Legrand, M., Preunkert, S., Jourdain, B., Guilhermet, J., Faïñ, X., Alekhina, I., and Petit, J.R. (2013). Water-soluble organic carbon in snow and ice deposited at Alpine, Greenland, and Antarctic sites. A critical review of available data and their atmospheric relevance. *Climate of the Past*, 9, pp. 2195–2211.
- Legrand, M., Preunkert, S., Wagenbach, D., Cachier, H., and Puxbaum, H. (2003). A historical record of formate and acetate from a high-elevation Alpine glacier. Implications for their natural versus anthropogenic budgets at the European scale. *Journal of Geophysical Research: Atmospheres*, 108, n/a-n/a.
- Lelieveld, J., Evans, J.S., Fnais, M., Giannadaki, D., and Pozzer, A. (2015). The contribution of outdoor air pollution sources to premature mortality on a global scale. *Nature*, 525, pp. 367–371.
- Li, Y., Pöschl, U., and Shiraiwa, M. (2016). Molecular corridors and parameterizations of volatility in the chemical evolution of organic aerosols. *Atmospheric Chemistry and Physics*, 16, pp. 3327–3344.
- Lintelmann, J., Fischer, K., and Matuschek, G. (2006). Determination of oxygenated polycyclic aromatic hydrocarbons in particulate matter using high-performance liquid chromatography-tandem mass spectrometry. *Journal of Chromatography A*, 1133, pp. 241–247.
- Lopez-Hilfiker, F.D., Mohr, C., Ehn, M., Rubach, F., Kleist, E., Wildt, J., Mentel, T.F., Lutz, A., Hallquist, M., Worsnop, D., and Thornton, J.A. (2014). A novel method for online analysis of gas and particle composition. Description and evaluation of a Filter Inlet for Gases and AEROSols (FIGAERO). *Atmospheric Measurement Techniques*, 7, pp. 983–1001.
- Maggi, V., Orombelli, G., Stenni, B., Flora, O., Udisti, R., Becagli, S., Traversi, R., Vermigli, S., and Petit, J.-R. (1998). 70 years of northern Victoria Land (Antarctica) accumulation rate. *Annals of Glaciology*, 27, pp. 215–219.
- Maggi, V., Villa, S., Finizio, A., Delmonte, B., Casati, P., and Marino, F. (2006). Variability of Anthropogenic and Natural Compounds in High Altitude–high Accumulation Alpine Glaciers. *Hydrobiologia*, 562, pp. 43–56.
- Makarov, A. (2000). Electrostatic Axially Harmonic Orbital Trapping. A High-Performance Technique of Mass Analysis. *Analytical Chemistry*, 72, pp. 1156–1162.
- Marshall, A.G., and Chen, T. (2015). 40 years of Fourier transform ion cyclotron resonance mass spectrometry. *International Journal of Mass Spectrometry*, 377, pp. 410–420.
- Mayewski, P.A., Lyons, W.B., Spencer, M.J., Twickler, M., Dansgaard, W., Koci, B., Davidson, C.I., and Honrath, R.E. (1986). Sulfate and nitrate concentrations from a South Greenland ice core. *Science (New York, N.Y.)*, 232, pp. 975–977.

- Mazzoleni, L.R., Zielinska, B., and Moosmüller, H. (2007). Emissions of Levoglucosan, Methoxy Phenols, and Organic Acids from Prescribed Burns, Laboratory Combustion of Wildland Fuels, and Residential Wood Combustion. *Environmental Science & Technology*, 41, pp. 2115–2122.
- McConnell, J.R., Edwards, R., Kok, G.L., Flanner, M.G., Zender, C.S., Saltzman, E.S., Banta, J.R., Pasteris, D.R., Carter, M.M., and Kahl, J.D.W. (2007). 20th-century industrial black carbon emissions altered Arctic climate forcing. *Science (New York, N.Y.)*, 317, pp. 1381–1384.
- Mentel, T.F., Springer, M., Ehn, M., Kleist, E., Pullinen, I., Kurtén, T., Rissanen, M., Wahner, A., and Wildt, J. (2015). Formation of highly oxidized multifunctional compounds. Autoxidation of peroxy radicals formed in the ozonolysis of alkenes – deduced from structure–product relationships. *Atmospheric Chemistry and Physics*, 15, pp. 6745–6765.
- Mogliani, A.G., García-Expósito, E., Aguado, G.P., Parella, T., Branchadell, V., Moltrasio, G.Y., and Ortuño, R.M. (2000). Divergent Routes to Chiral Cyclobutane Synthons from (–)- α -Pinene and Their Use in the Stereoselective Synthesis of Dehydro Amino Acids. *The Journal of Organic Chemistry*, 65, pp. 3934–3940.
- Müller, L., Reinnig, M.-C., Naumann, K.H., Saathoff, H., Mentel, T.F., Donahue, N.M., and Hoffmann, T. (2012). Formation of 3-methyl-1,2,3-butanetricarboxylic acid via gas phase oxidation of pinonic acid – a mass spectrometric study of SOA aging. *Atmospheric Chemistry and Physics*, 12, pp. 1483–1496.
- Müller-Tautges, C. (2014). Development and application of mass-spectrometric methods for the quantification and characterization of organic compounds in ice core. Dissertation: Mainz.
- Müller-Tautges, C., Eichler, A., Schwikowski, M., Pezzatti, G.B., Conedera, M., and Hoffmann, T. (2016). Historic records of organic compounds from a high Alpine glacier. Influences of biomass burning, anthropogenic emissions, and dust transport. *Atmospheric Chemistry and Physics*, 16, pp. 1029–1043.
- Mutzel, A., Poulain, L., Berndt, T., Iinuma, Y., Rodigast, M., Böge, O., Richters, S., Spindler, G., Sipilä, M., Jokinen, T., Kulmala, M., and Herrmann, H. (2015). Highly Oxidized Multifunctional Organic Compounds Observed in Tropospheric Particles. A Field and Laboratory Study. *Environmental science & technology*, 49, pp. 7754–7761.
- NEEM community members (2013). Eemian interglacial reconstructed from a Greenland folded ice core. *Nature*, 493, pp. 489–494.
- Nguyen, Q.T., Christensen, M.K., Cozzi, F., Zare, A., Hansen, A.M.K., Kristensen, K., Tulinius, T.E., Madsen, H.H., Christensen, J.H., Brandt, J., Massling, A., Nøjgaard, J.K., and Glasius, M. (2014). Understanding the anthropogenic influence on formation of biogenic secondary organic aerosols in Denmark via analysis of organosulfates and related oxidation products. *Atmospheric Chemistry and Physics*, 14, pp. 8961–8981.
- Nizkorodov, S.A., Laskin, J., and Laskin, A. (2011). Molecular chemistry of organic aerosols through the application of high resolution mass spectrometry. *Physical chemistry chemical physics : PCCP*, 13, pp. 3612–3629.
- Nolte, C.G., Schauer, J.J., Cass, G.R., and Simoneit, B.R.T. (2001). Highly Polar Organic Compounds Present in Wood Smoke and in the Ambient Atmosphere. *Environmental Science & Technology*, 35, pp. 1912–1919.
- Nozière, B., Kalberer, M., Claeys, M., Allan, J., D'Anna, B., Decesari, S., Finessi, E., Glasius, M., Grgić, I., Hamilton, J.F., Hoffmann, T., Iinuma, Y., Jaoui, M., Kahnt, A., Kampf, C.J., Kourtchev, I., Maenhaut, W., Marsden, N., Saarikoski, S., Schnelle-Kreis, J., Surratt, J.D., Szidat, S., Szmigielski, R., and Wisthaler, A. (2015). The molecular identification of organic compounds in the atmosphere. State of the art and challenges. *Chemical reviews*, 115, pp. 3919–3983.
- Olivier, S. (2003). Glaciochemical investigation of an ice core from Belukha glacier, Siberian Altai. *Geophysical Research Letters*, 30, p. 47.
- Oros, D.R., and Simoneit, B.R.T. (2001a). Identification and emission factors of molecular tracers in organic aerosols from biomass burning Part 1. Temperate climate conifers. *Applied Geochemistry*, 16, pp. 1513–1544.

- Oros, D.R., and Simoneit, B.R.T. (2001b). Identification and emission factors of molecular tracers in organic aerosols from biomass burning Part 2. Deciduous trees. *Applied Geochemistry*, 16, pp. 1545–1565.
- Pankow, J.F. (1994a). An absorption model of gas/particle partitioning of organic compounds in the atmosphere. *Atmospheric Environment*, 28, pp. 185–188.
- Pankow, J.F. (1994b). An absorption model of the gas/aerosol partitioning involved in the formation of secondary organic aerosol. *Atmospheric Environment*, 28, pp. 189–193.
- Petit, J.R., Jouzel, J., Raynaud, D., Barkov, N.I., Barnola, J.-M., Basile, I., Bender, M., Chappellaz, J., Davis, M., Delaygue, G., Delmotte, M., Kotlyakov, V.M., Legrand, M., Lipenkov, V.Y., Lorius, C., Pépin, L., Ritz, C., Saltzman, E., and Stievenard, M. (1999). Climate and atmospheric history of the past 420,000 years from the Vostok ice core, Antarctica. *Nature*, 399, pp. 429–436.
- Pfeffer, W.T., Arendt, A.A., Bliss, A., Bolch, T., Cogley, J.G., Gardner, A.S., Hagen, J.-O., Hock, R., Kaser, G., Kienholz, C., Miles, E.S., Moholdt, G., Mölg, N., Paul, F., Radić, V., Rastner, P., Raup, B.H., Rich, J., and Sharp, M.J. (2014). The Randolph Glacier Inventory. A globally complete inventory of glaciers. *Journal of Glaciology*, 60, pp. 537–552.
- Pokhrel, A., Kawamura, K., Ono, K., Seki, O., Fu, P., Matoba, S., and Shiraiwa, T. (2016). Ice core records of monoterpene- and isoprene-SOA tracers from Aurora Peak in Alaska since 1660s. Implication for climate change variability in the North Pacific Rim. *Atmospheric Environment*, 130, pp. 105–112.
- Pokhrel, A., Kawamura, K., Seki, O., Matoba, S., and Shiraiwa, T. (2015). Ice core profiles of saturated fatty acids (C 12:0 –C 30:0) and oleic acid (C 18:1) from southern Alaska since 1734 AD: A link to climate change in the Northern Hemisphere. *Atmospheric Environment*, 100, pp. 202–209.
- Poole, C.F. (2003). New trends in solid-phase extraction. *TrAC Trends in Analytical Chemistry*, 22, pp. 362–373.
- Pope, C.A., and Dockery, D.W. (2006). Health Effects of Fine Particulate Air Pollution. Lines that Connect. *Journal of the Air & Waste Management Association*, 56, pp. 709–742.
- Pöschl, U. (2005). Atmospheric aerosols. Composition, transformation, climate and health effects. *Angewandte Chemie (International ed. in English)*, 44, pp. 7520–7540.
- Pöschl, U., and Shiraiwa, M. (2015). Multiphase chemistry at the atmosphere-biosphere interface influencing climate and public health in the anthropocene. *Chemical reviews*, 115, pp. 4440–4475.
- Pratt, K.A., and Prather, K.A. (2012a). Mass spectrometry of atmospheric aerosols--recent developments and applications. Part I. Off-line mass spectrometry techniques. *Mass spectrometry reviews*, 31, pp. 1–16.
- Pratt, K.A., and Prather, K.A. (2012b). Mass spectrometry of atmospheric aerosols--recent developments and applications. Part II. On-line mass spectrometry techniques. *Mass spectrometry reviews*, 31, pp. 17–48.
- Preunkert, S., Legrand, M., and Wagenbach, D. (2001). Sulfate trends in a Col du Dôme (French Alps) ice core. A record of anthropogenic sulfate levels in the European midtroposphere over the twentieth century. *Journal of Geophysical Research: Atmospheres*, 106, pp. 31991–32004.
- Preunkert, S., Wagenbach, D., and Legrand, M. (2003). A seasonally resolved alpine ice core record of nitrate. Comparison with anthropogenic inventories and estimation of preindustrial emissions of NO in Europe. *Journal of Geophysical Research: Atmospheres*, 108, 19,707.
- Ramanathan, V., Crutzen, P.J., Kiehl, J.T., and Rosenfeld, D. (2001). Aerosols, climate, and the hydrological cycle. *Science (New York, N.Y.)*, 294, pp. 2119–2124.
- Ravishankara, A.R. (1997). Heterogeneous and Multiphase Chemistry in the Troposphere. *Science (New York, N.Y.)*, 276, pp. 1058–1065.
- Riccobono, F., Schobesberger, S., Scott, C.E., Dommen, J., Ortega, I.K., Rondo, L., Almeida, J., Amorim, A., Bianchi, F., Breitenlechner, M., David, A., Downard, A., Dunne, E.M., Duplissy, J., Ehrhart, S., Flagan, R.C., Franchin, A., Hansel, A., Junninen, H., Kajos, M., Keskinen, H., Kupc, A., Kürten, A., Kvashin, A.N., Laaksonen, A., Lehtipalo, K., Makhmutov, V., Mathot, S., Nieminen, T., Onnela, A., Petäjä, T., Praplan, A.P., Santos, F.D., Schallhart, S., Seinfeld, J.H.,

- Sipilä, M., Spracklen, D.V., Stozhkov, Y., Stratmann, F., Tomé, A., Tsagkogeorgas, G., Vaattovaara, P., Viisanen, Y., Vrtala, A., Wagner, P.E., Weingartner, E., Wex, H., Wimmer, D., Carslaw, K.S., Curtius, J., Donahue, N.M., Kirkby, J., Kulmala, M., Worsnop, D.R., and Baltensperger, U. (2014). Oxidation products of biogenic emissions contribute to nucleation of atmospheric particles. *Science (New York, N.Y.)*, 344, pp. 717–721.
- Riipinen, I., Pierce, J.R., Yli-Juuti, T., Nieminen, T., Häkkinen, S., Ehn, M., Junninen, H., Lehtipalo, K., Petäjä, T., Slowik, J., Chang, R., Shantz, N.C., Abbatt, J., Leaitch, W.R., Kerminen, V.-M., Worsnop, D.R., Pandis, S.N., Donahue, N.M., and Kulmala, M. (2011). Organic condensation. A vital link connecting aerosol formation to cloud condensation nuclei (CCN) concentrations. *Atmospheric Chemistry and Physics*, 11, pp. 3865–3878.
- Riipinen, I., Yli-Juuti, T., Pierce, J.R., Petäjä, T., Worsnop, D.R., Kulmala, M., and Donahue, N.M. (2012). The contribution of organics to atmospheric nanoparticle growth. *Nature Geoscience*, 5, pp. 453–458.
- Rogge, W.F., Hildemann, L.M., Mazurek, M.A., Cass, G.R., and Simoneit, B.R.T. (1993). Sources of fine organic aerosol. 4. Particulate abrasion products from leaf surfaces of urban plants. *Environmental Science & Technology*, 27, pp. 2700–2711.
- Romonosky, D.E., Li, Y., Shiraiwa, M., Laskin, A., Laskin, J., and Nizkorodov, S.A. (2017). Aqueous Photochemistry of Secondary Organic Aerosol of α -Pinene and α -Humulene Oxidized with Ozone, Hydroxyl Radical, and Nitrate Radical. *The journal of physical chemistry. A*, 121, pp. 1298–1309.
- Rudich, Y., Donahue, N.M., and Mentel, T.F. (2007). Aging of organic aerosol. Bridging the gap between laboratory and field studies. *Annual review of physical chemistry*, 58, pp. 321–352.
- Schauer, J.J., Kleeman, M.J., Cass, G.R., and Simoneit, B.R.T. (2001). Measurement of Emissions from Air Pollution Sources. 3. C 1 –C 29 Organic Compounds from Fireplace Combustion of Wood. *Environmental Science & Technology*, 35, pp. 1716–1728.
- Schmitt-Kopplin, P., Gelencsér, A., Dabek-Zlotorzynska, E., Kiss, G., Hertkorn, N., Harir, M., Hong, Y., and Gebefügi, I. (2010). Analysis of the unresolved organic fraction in atmospheric aerosols with ultrahigh-resolution mass spectrometry and nuclear magnetic resonance spectroscopy. *Organosulfates as photochemical smog constituents. Analytical chemistry*, 82, pp. 8017–8026.
- Schneidmesser, E. von, Monks, P.S., Allan, J.D., Bruhwiler, L., Forster, P., Fowler, D., Lauer, A., Morgan, W.T., Paasonen, P., Righi, M., Sindelarova, K., and Sutton, M.A. (2015). Chemistry and the Linkages between Air Quality and Climate Change. *Chemical reviews*, 115, pp. 3856–3897.
- Schobesberger, S., Junninen, H., Bianchi, F., Lönn, G., Ehn, M., Lehtipalo, K., Dommen, J., Ehrhart, S., Ortega, I.K., Franchin, A., Nieminen, T., Riccobono, F., Hutterli, M., Duplissy, J., Almeida, J., Amorim, A., Breitenlechner, M., Downard, A.J., Dunne, E.M., Flagan, R.C., Kajos, M., Keskinen, H., Kirkby, J., Kupc, A., Kürten, A., Kurtén, T., Laaksonen, A., Mathot, S., Onnela, A., Praplan, A.P., Rondo, L., Santos, F.D., Schallhart, S., Schnitzhofer, R., Sipilä, M., Tomé, A., Tsagkogeorgas, G., Vehkamäki, H., Wimmer, D., Baltensperger, U., Carslaw, K.S., Curtius, J., Hansel, A., Petäjä, T., Kulmala, M., Donahue, N.M., and Worsnop, D.R. (2013). Molecular understanding of atmospheric particle formation from sulfuric acid and large oxidized organic molecules. *Proceedings of the National Academy of Sciences of the United States of America*, 110, pp. 17223–17228.
- Schulz, H., Harder, V., Ibalid-Mulli, A., Khandoga, A., Koenig, W., Krombach, F., Radykewicz, R., Stampfl, A., Thorand, B., and Peters, A. (2005). Cardiovascular effects of fine and ultrafine particles. *Journal of aerosol medicine : the official journal of the International Society for Aerosols in Medicine*, 18, pp. 1–22.
- Schwartz, S.E. (1996). The whitehouse effect—Shortwave radiative forcing of climate by anthropogenic aerosols. An overview. *Journal of Aerosol Science*, 27, pp. 359–382.
- Schwikowski, M., DOSCHER, A., Gäggeler, H.W., and SCHOTTERER, U. (1999). Anthropogenic versus natural sources of atmospheric sulphate from an Alpine ice core. *Tellus B*, 51, pp. 938–951.
- Scigelova, M., and Makarov, A. (2006). Orbitrap mass analyzer—overview and applications in proteomics. *Proteomics*, 6 Suppl 2, pp. 16–21.

- Seinfeld, J.H., and Pandis, S.N. (NJ : Wiley, 2006). Atmospheric chemistry and physics. From air pollution to climate change (2nd ed.). Wiley: Hoboken, NJ.
- Shen, R.-Q., Ding, X., He, Q.-F., Cong, Z.-Y., Yu, Q.-Q., and Wang, X.-M. (2015). Seasonal variation of secondary organic aerosol tracers in Central Tibetan Plateau. *Atmospheric Chemistry and Physics*, 15, pp. 8781–8793.
- Short, S.K., and Holdsworth, G. (1985). Pollen, Oxygen Isotope Content and Seasonality in an Ice Core from the Penny Ice Cap, Baffin Island. *ARCTIC*, 38.
- Simoneit, B.R.T. (2002). Biomass burning — a review of organic tracers for smoke from incomplete combustion. *Applied Geochemistry*, 17, pp. 129–162.
- Simoneit, B.R.T., Schauer, J.J., Nolte, C.G., Oros, D.R., Elias, V.O., Fraser, M.P., Rogge, W.F., and Cass, G.R. (1999). Levoglucosan, a tracer for cellulose in biomass burning and atmospheric particles. *Atmospheric Environment*, 33, pp. 173–182.
- Slade, J.H., and Knopf, D.A. (2013). Heterogeneous OH oxidation of biomass burning organic aerosol surrogate compounds. Assessment of volatilisation products and the role of OH concentration on the reactive uptake kinetics. *Physical chemistry chemical physics : PCCP*, 15, pp. 5898–5915.
- Spurny, K.R. (Ed.) (1998). *Advances in aerosol filtration*.
- Staffelbach, T., Neftel, A., Stauffer, B., and Jacob, D. (1991). A record of the atmospheric methane sink from formaldehyde in polar ice cores. *Nature*, 349, pp. 603–605.
- Stohl, A., and Sodemann, H. (2010). Characteristics of atmospheric transport into the Antarctic troposphere. *Journal of Geophysical Research*, 115, p. 2864.
- Surratt, J.D., Gómez-González, Y., Chan, A.W.H., Vermeylen, R., Shahgholi, M., Kleindienst, T.E., Edney, E.O., Offenberg, J.H., Lewandowski, M., Jaoui, M., Maenhaut, W., Claeys, M., Flagan, R.C., and Seinfeld, J.H. (2008). Organosulfate formation in biogenic secondary organic aerosol. *The journal of physical chemistry. A*, 112, pp. 8345–8378.
- Surratt, J.D., Kroll, J.H., Kleindienst, T.E., Edney, E.O., Claeys, M., Sorooshian, A., Ng, N.L., Offenberg, J.H., Lewandowski, M., Jaoui, M., Flagan, R.C., and Seinfeld, J.H. (2007). Evidence for Organosulfates in Secondary Organic Aerosol. *Environmental Science & Technology*, 41, pp. 517–527.
- Szmigielski, R., Surratt, J.D., Gómez-González, Y., van der Veken, P., Kourtshev, I., Vermeylen, R., Blockhuys, F., Jaoui, M., Kleindienst, T.E., Lewandowski, M., Offenberg, J.H., Edney, E.O., Seinfeld, J.H., Maenhaut, W., and Claeys, M. (2007). 3-methyl-1,2,3-butanetricarboxylic acid. An atmospheric tracer for terpene secondary organic aerosol. *Geophysical Research Letters*, 34, D16312.
- Thurman, E.M., and Mills, M.S. (1998). *Solid phase extraction. Principles and practice*.
- Tröstl, J., Chuang, W.K., Gordon, H., Heinritzi, M., Yan, C., Molteni, U., Ahlm, L., Frege, C., Bianchi, F., Wagner, R., Simon, M., Lehtipalo, K., Williamson, C., Craven, J.S., Duplissy, J., Adamov, A., Almeida, J., Bernhammer, A.-K., Breitenlechner, M., Brilke, S., Dias, A., Ehrhart, S., Flagan, R.C., Franchin, A., Fuchs, C., Guida, R., Gysel, M., Hansel, A., Hoyle, C.R., Jokinen, T., Junninen, H., Kangasluoma, J., Keskinen, H., Kim, J., Krapf, M., Kürten, A., Laaksonen, A., Lawler, M., Leiminger, M., Mathot, S., Möhler, O., Nieminen, T., Onnela, A., Petäjä, T., Piel, F.M., Miettinen, P., Rissanen, M.P., Rondo, L., Sarnela, N., Schobesberger, S., Sengupta, K., Sipilä, M., Smith, J.N., Steiner, G., Tomè, A., Virtanen, A., Wagner, A.C., Weingartner, E., Wimmer, D., Winkler, P.M., Ye, P., Carslaw, K.S., Curtius, J., Dommen, J., Kirkby, J., Kulmala, M., Riipinen, I., Worsnop, D.R., Donahue, N.M., and Baltensperger, U. (2016). The role of low-volatility organic compounds in initial particle growth in the atmosphere. *Nature*, 533, pp. 527–531.
- Tu, P., Hall, W.A., and Johnston, M.V. (2016). Characterization of Highly Oxidized Molecules in Fresh and Aged Biogenic Secondary Organic Aerosol. *Analytical chemistry*, 88, pp. 4495–4501.
- Uglietti, C., ZAPF, A., Jenk, T.M., Sigl, M., Szidat, S., Salazar, G., and Schwikowski, M. (2016). Radiocarbon dating of glacier ice. Overview, optimisation, validation and potential. *The Cryosphere*, 10, pp. 3091–3105.

- Urban, R.C., Alves, C.A., Allen, A.G., Cardoso, A.A., and Campos, M.L.A.M. (2016). Organic aerosols in a Brazilian agro-industrial area. Speciation and impact of biomass burning. *Atmospheric Research*, 169, pp. 271–279.
- van Eijck, A., Opatz, T., Taraborrelli, D., Sander, R., and Hoffmann, T. (2013). New tracer compounds for secondary organic aerosol formation from β -caryophyllene oxidation. *Atmospheric Environment*, 80, pp. 122–130.
- Vogel, A.L., Äijälä, M., Brüggemann, M., Ehn, M., Junninen, H., Petäjä, T., Worsnop, D.R., Kulmala, M., Williams, J., and Hoffmann, T. (2013). Online atmospheric pressure chemical ionization ion trap mass spectrometry (APCI-IT-MSⁿ) for measuring organic acids in concentrated bulk aerosol – a laboratory and field study. *Atmospheric Measurement Techniques*, 6, pp. 431–443.
- Vogel, A.L., Schneider, J., Müller-Tautges, C., Klimach, T., and Hoffmann, T. (2016a). Aerosol Chemistry Resolved by Mass Spectrometry. Insights into Particle Growth after Ambient New Particle Formation. *Environmental science & technology*.
- Vogel, A.L., Schneider, J., Müller-Tautges, C., Phillips, G.J., Pöhlker, M.L., Rose, D., Zuth, C., Makkonen, U., Hakola, H., Crowley, J.N., Andreae, M.O., Pöschl, U., and Hoffmann, T. (2016b). Aerosol Chemistry Resolved by Mass Spectrometry. Linking Field Measurements of Cloud Condensation Nuclei Activity to Organic Aerosol Composition. *Environmental science & technology*.
- Wang, X., Hayeck, N., Brüggemann, M., Yao, L., Chen, H., Zhang, C., Emmelin, C., Chen, J., George, C., and Wang, L. (2017). Chemical Characteristics of Organic Aerosols in Shanghai. A Study by Ultrahigh-Performance Liquid Chromatography Coupled With Orbitrap Mass Spectrometry. *Journal of Geophysical Research: Atmospheres*, 122, 11,703–11,722.
- Warnke, J., Bandur, R., and Hoffmann, T. (2006). Capillary-HPLC-ESI-MS/MS method for the determination of acidic products from the oxidation of monoterpenes in atmospheric aerosol samples. *Analytical and bioanalytical chemistry*, 385, pp. 34–45.
- Weber, R.J., Orsini, D., Daun, Y., Lee, Y.-N., Klotz, P.J., and Brechtel, F. (2001). A Particle-into-Liquid Collector for Rapid Measurement of Aerosol Bulk Chemical Composition. *Aerosol Science and Technology*, 35, pp. 718–727.
- WENT, F.W. (1960). Blue Hazes in the Atmosphere. *Nature*, 187, pp. 641–643.
- Wilson, W.E., and Suh, H.H. (1997). Fine Particles and Coarse Particles. Concentration Relationships Relevant to Epidemiologic Studies. *Journal of the Air & Waste Management Association*, 47, pp. 1238–1249.
- Wozniak, A.S., Bauer, J.E., Sleighter, R.L., Dickhut, R.M., and Hatcher, P.G. (2008). Technical Note. Molecular characterization of aerosol-derived water soluble organic carbon using ultrahigh resolution electrospray ionization Fourier transform ion cyclotron resonance mass spectrometry. *Atmospheric Chemistry and Physics*, 8, pp. 5099–5111.
- Xu, L., Guo, H., Boyd, C.M., Klein, M., Bougiatioti, A., Cerully, K.M., Hite, J.R., Isaacman-VanWertz, G., Kreisberg, N.M., Knote, C., Olson, K., Koss, A., Goldstein, A.H., Hering, S.V., Gouw, J. de, Baumann, K., Lee, S.-H., Nenes, A., Weber, R.J., and Ng, N.L. (2015). Effects of anthropogenic emissions on aerosol formation from isoprene and monoterpenes in the southeastern United States. *Proceedings of the National Academy of Sciences of the United States of America*, 112, pp. 37–42.
- Yao, P., Schwab, V.F., Roth, V.-N., Xu, B., Yao, T., and Gleixner, G. (2013). Levoglucosan concentrations in ice-core samples from the Tibetan Plateau determined by reverse-phase high-performance liquid chromatography–mass spectrometry. *Journal of Glaciology*, 59, pp. 599–612.
- Yasmeen, F., Vermeylen, R., Szmigielski, R., Iinuma, Y., Böge, O., Herrmann, H., Maenhaut, W., and Claeys, M. (2010). Terpenylic acid and related compounds. Precursors for dimers in secondary organic aerosol from the ozonolysis of α - and β -pinene. *Atmospheric Chemistry and Physics*, 10, pp. 9383–9392.
- Ye, J., Abbatt, J.P.D., and Chan, A.W.H. (2018). Novel pathway of SO₂ oxidation in the atmosphere. Reactions with monoterpene ozonolysis intermediates and secondary organic aerosol. *Atmospheric Chemistry and Physics*, 18, pp. 5549–5565.

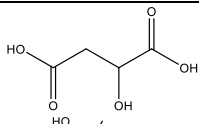
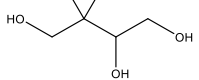
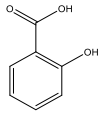
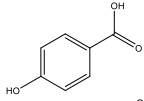
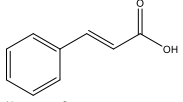
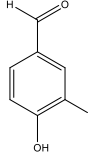
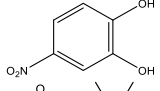
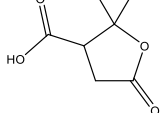
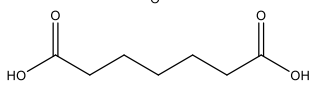
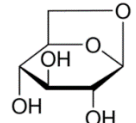
- You, C., Song, L., Xu, B., and Gao, S. (2016). Method for determination of levoglucosan in snow and ice at trace concentration levels using ultra-performance liquid chromatography coupled with triple quadrupole mass spectrometry. *Talanta*, 148, pp. 534–538.
- You, C., Yao, T., Gao, S., Gong, P., and Zhao, H. (2014). Simultaneous Determination of Levoglucosan, Mannosan and Galactosan at Trace Levels in Snow Samples by GC/MS. *Chromatographia*, 77, pp. 969–974.
- Zennaro, P., Kehrwald, N., McConnell, J.R., Schüpbach, S., Maselli, O.J., Marlon, J., Vallelonga, P., Leuenberger, D., Zangrando, R., Spolaor, A., Borrotti, M., Barbaro, E., Gambaro, A., and Barbante, C. (2014). Fire in ice. Two millennia of boreal forest fire history from the Greenland NEEM ice core. *Climate of the Past*, 10, pp. 1905–1924.
- Zhang, X., McVay, R.C., Huang, D.D., Dalleska, N.F., Aumont, B., Flagan, R.C., and Seinfeld, J.H. (2015). Formation and evolution of molecular products in α -pinene secondary organic aerosol. *Proceedings of the National Academy of Sciences of the United States of America*, 112, pp. 14168–14173.
- Zhang, Y.Y., Müller, L., Winterhalter, R., Moortgat, G.K., Hoffmann, T., and Pöschl, U. (2010). Seasonal cycle and temperature dependence of pinene oxidation products, dicarboxylic acids and nitrophenols in fine and coarse air particulate matter. *Atmospheric Chemistry and Physics*, 10, pp. 7859–7873.
- Zhou, S., and Cook, K.D. (2000). Protonation in electrospray mass spectrometry. Wrong-way-round or right-way-round? *Journal of the American Society for Mass Spectrometry*, 11, pp. 961–966.

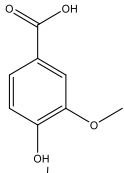
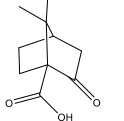
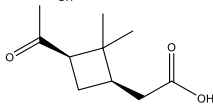
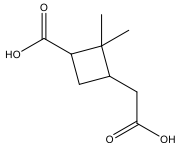
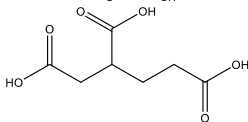
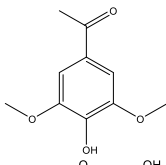
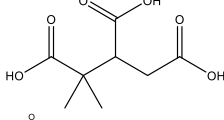
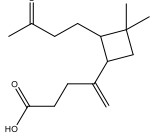
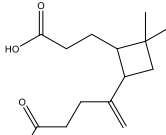
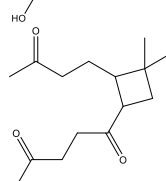
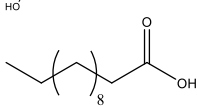
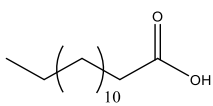
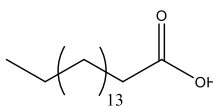
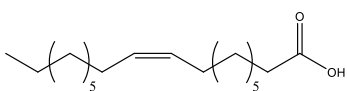
7 Appendix

7.1 Supporting Information to Chapter 2

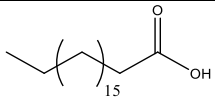
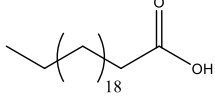
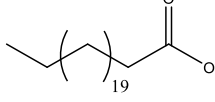
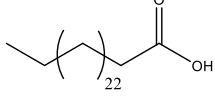
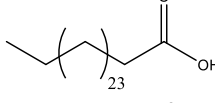
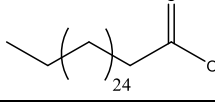
The following section presents supplementary information about the analytes used for method development. The elemental composition, the molecular structure and the m/z of the deprotonated ion of each analyte is presented in Table 7.1. The Pearson correlation coefficients of the compounds detected in the ice core sections are shown in Table 7.2. Furthermore Figure 7.1 shows the chromatogram of a 4-nitrocatechol standard and detected in an ice core section, respectively. The ultra-high resolution mass spectra shows the exact mass of 4-nitrocatechol detected in an ice core section.

Table 7.1 Analytes, elemental composition, molecular structure and m/z of the deprotonated signal used for quantification and method development.

Analyte	elemental composition	structure	m/z ([M-H] ⁻)
D-malic acid	C ₄ H ₆ O ₅		133.0142
2-methyl-tetrols	C ₅ H ₁₂ O ₄		135.0663
salicylic acid	C ₇ H ₆ O ₃		137.0244
4-hydroxybenzoic acid	C ₇ H ₆ O ₃		137.0244
cinnamic acid	C ₉ H ₈ O ₂		147.0451
vanillin	C ₈ H ₈ O ₃		151.0400
4-nitrocatechol	C ₆ H ₅ N ₁ O ₄		154.0145
terebic acid	C ₇ H ₁₀ O ₄		157.0506
pimelic acid	C ₇ H ₁₂ O ₄		159.0663
levoglucosan	C ₆ H ₁₀ O ₅		161.0455

vanillic acid	$C_8H_8O_4$		167.0349
keto-pinonic acid	$C_{10}H_{14}O_3$		181.0870
cis-pinonic acid	$C_{10}H_{16}O_3$		183.1027
pinic acid	$C_9H_{14}O_4$		185.0819
BTCA	$C_7H_{10}O_6$		189.0405
acetosyringone	$C_{10}H_{12}O_4$		195.0662
MBTCA	$C_8H_{12}O_6$		203.0561
β -caryophyllonic acid	$C_{15}H_{24}O_3$		251.1653
β -caryophyllinic acid	$C_{14}H_{22}O_4$		253.1445
β -nocaryophyllonic acid	$C_{14}H_{22}O_4$		253.1445
lauric acid	$C_{12}H_{24}O_2$		199.1704
myristic acid	$C_{14}H_{28}O_2$		227.2017
heptadecanoic acid	$C_{17}H_{34}O_2$		269.2486
oleic acid	$C_{18}H_{34}O_2$		281.2486

7. Appendix

nonadecanoic acid	$C_{19}H_{38}O_2$		297.2799
behenic acid	$C_{22}H_{44}O_2$		339.3269
tricosanoic acid	$C_{23}H_{46}O_2$		353.3425
hexacosanoic acid	$C_{26}H_{52}O_2$		395.3895
heptacosanoic acid	$C_{27}H_{54}O_2$		409.4051
octacosanoic acid	$C_{28}H_{56}O_2$		423.4208

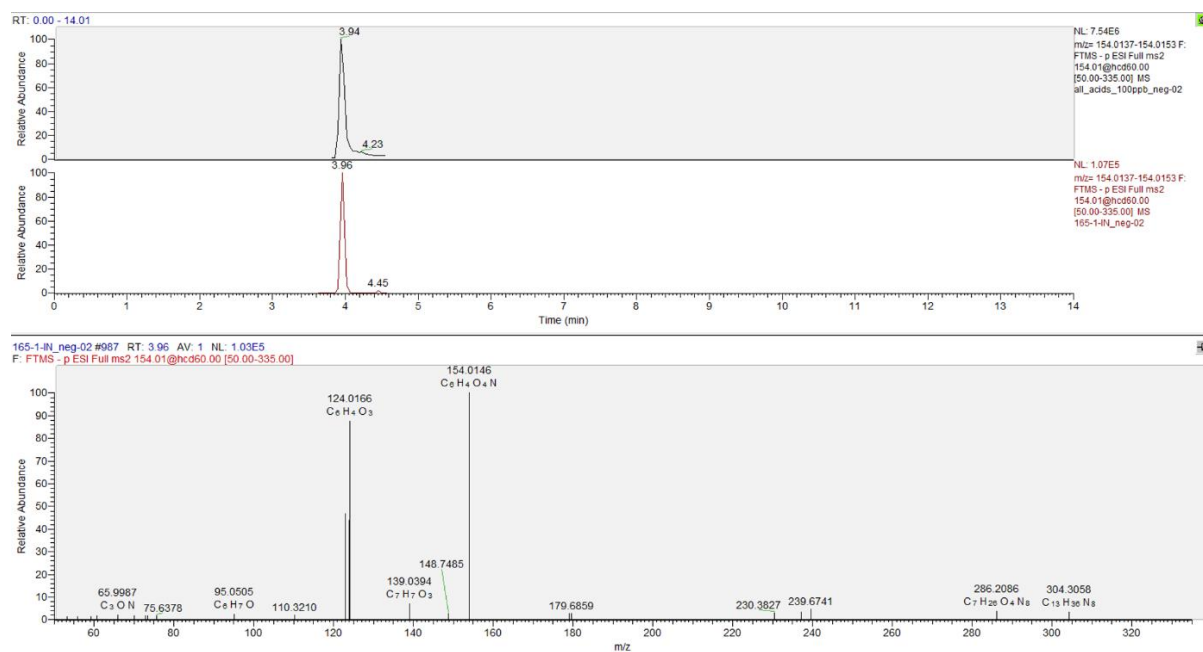


Figure 7.1 Chromatogram of m/z 154.0145 ($[M-H]^-$, $R_t = 3.96$ min) measured in a 100 ppb standard solution of 4-nitrocatechol (upper panel) and detected in a Belukha ice core section (middle panel). The MS^2 spectrum of the parent ion m/z 154.0145 ($C_6H_4O_4N^-$, ($[M-H]^-$)) shows the signal of the deprotonated ion m/z 154.0146 ($[M-H]^-$) and the fragment ion m/z 124.0166 ($[M-H-NO]^-$) used for quantification (lower panel).

Table 7.2 Pearson Correlation coefficients (r) of the analytes in the Belukha ice core sections. Correlation lower than |0.4| were removed due to clarity. Correlation higher than 0.6 is shown in bold.

	levoglucosan	D malic acid	2-methyl tetrols	BTCA	terebic acid	MBTCA	4-hydroxybenzoic acid
levoglucosan	1.00						
D malic acid	0.76	1.00					
2-methyl tetrols	0.69	0.66	1.00				
BTCA	0.91	0.76	0.61	1.00			
terebic acid	0.65	0.44	0.43	0.75	1.00		
MBTCA	0.81	0.69	0.71	0.88	0.79	1.00	
4-hydroxybenzoic acid	0.98	0.73	0.69	0.88	0.61	0.78	1.00
vanillic acid	0.71	0.56		0.55	0.45	0.56	0.75
pimelic acid	0.79	0.59	0.65	0.76	0.71	0.82	0.79
4-nitrocatechol	0.83	0.62	0.74	0.72	0.48	0.72	0.82
vanillin							
pinic acid	0.82	0.66	0.81	0.78	0.74	0.81	0.82
acetosyringone							
cis-pinonic acid					0.53	0.57	
salicylic acid				0.50			
keto-pinic acid							
cinnamic acid	0.50			0.70	0.58	0.50	0.43
β -nocaryophyllonic acid	0.62	0.65	0.59	0.68	0.63	0.81	0.61
β -caryophyllinic acid					0.47	0.53	
β -caryophyllonic acid				0.44		0.52	
lauric acid							
myristic acid							
oleic acid							
heptadecanoic acid							
nonadecanoic acid							
behenic acid							
tricosanoic acid							
hexacosanoic acid							
heptacosanoic acid							
octacosanoic acid							

Table 7.3 (continued).

	vanillic acid	pimelic acid	4-nitrocatechol	vanillin	pinic acid	acetosyringone	cis-pinonic acid
vanillic acid	1.00						
pimelic acid	0.54	1.00					
4-nitrocatechol	0.49	0.82	1.00				
vanillin				1.00			
pinic acid	0.61	0.81	0.75		1.00		
acetosyringone						1.00	

7. Appendix

<i>cis</i> -pinonic acid		0.46				1.00
salicylic acid						0.44
keto-pinonic acid						
cinnamic acid						
β -nocaryophyllonic acid	0.50	0.77	0.65		0.69	0.85
β -caryophyllinic acid	0.43	0.45	0.40	0.42		0.85
β -caryophyllonic acid		0.52	0.51			0.63
lauric acid				0.44		0.68
myristic acid				0.41		
oleic acid	-0.49					
heptadecanoic acid						
nonadecanoic acid						
behenic acid						
tricosanoic acid						
hexacosanoic acid						
heptacosanoic acid						
octacosanoic acid						

Table 7.4 (continued).

	salicylic acid	keto-pinonic acid	cinnamic acid	β -nocaryophyllonic acid	β -caryophyllinic acid	β -caryophyllonic acid
salicylic acid	1.00					
keto-pinonic acid		1.00				
cinnamic acid	0.66		1.00			
β -nocaryophyllonic acid	0.41			1.00		
β -caryophyllinic acid	0.54			0.77	1.00	
β -caryophyllonic acid	0.66		0.49	0.61	0.51	1.00
lauric acid	0.56			0.45	0.81	0.54
myristic acid	0.50				0.53	
oleic acid	0.46					
heptadecanoic acid	0.48					
nonadecanoic acid	0.49					
behenic acid	0.64		0.42			
tricosanoic acid	0.55					
hexacosanoic acid	0.51		0.42			
heptacosanoic acid						
octacosanoic acid	0.50		0.42			

Table 7.5 (continued).

	lauric acid	myristic acid	oleic acid	heptadecanoic acid	nonadecanoic acid	behenic acid	tricosanoic acid
lauric acid	1.00						
myristic acid	0.84	1.00					
oleic acid		0.55	1.00				
heptadecanoic acid	0.58	0.71	0.79	1.00			

nonadecanoic acid	0.56	0.65	0.76	0.98	1.00		
behenic acid	0.47	0.59	0.78	0.83	0.85	1.00	
tricosanoic acid	0.42	0.54	0.80	0.88	0.91	0.96	1.00
hexacosanoic acid	0.40	0.49	0.79	0.86	0.88	0.92	0.98
heptacosanoic acid			0.69	0.79	0.81	0.85	0.94
octacosanoic acid		0.49	0.79	0.81	0.82	0.90	0.95

Table 7.6 (continued).

	hexacosanoic acid	heptacosanoic acid	octacosanoic acid
hexacosanoic acid	1.00		
heptacosanoic acid	0.96	1.00	
octacosanoic acid	0.98	0.93	1.00

7.2 Supporting Information to Chapter 3

The following section presents chromatograms confirming the presence of pinic acid in CLOUD filter extracts via detection of adequate retention times. A MS² spectra of the proposed C₂₀, CHONS containing compound confirms the formula due to characteristic neutral losses. The detected compounds in the filter extracts of the CLOUD experiments are listed in Table 7.7 to Table 7.10 according to their molecular composition.

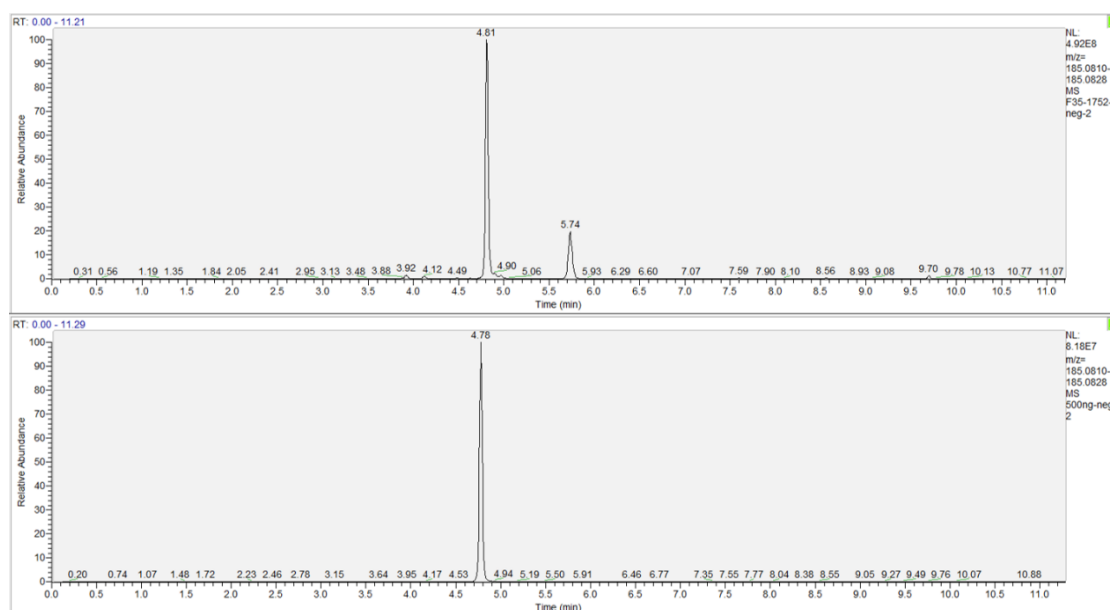


Figure 7.2 Chromatogram of m/z 185.0819 ($[M-H]^-$) measured in the filter extract of experiment 1752 (upper panel) and in a 500 ng/mL standard solution of self-synthesized pinic acid (lower panel). The retention time confirmed pinic acid formed in the CLOUD experiments. Additionally, three pinic acid isomers with lower relative abundance were present in the CLOUD filter extracts.

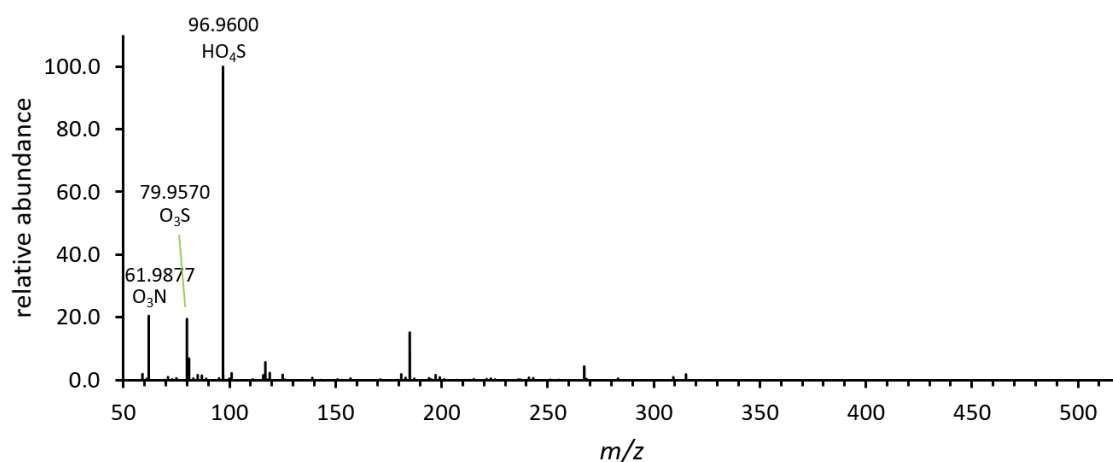


Figure 7.3 Negative mode MS² spectrum of the parent ion C₂₀H₃₂O₁₂NS ([M-H]⁻) at *m/z* 510.1646. The fragmentation pattern indicates the presence of a nitrooxy organosulfate: *m/z* 96.9600 (HSO₄⁻), *m/z* 79.9570 (SO₃⁻), *m/z* 61.9877 (NO₃⁻).

Table 7.7 CHO-containing organic compounds detected on filter samples during CLOUD 10 by UHPLC(-)ESI-UHRMS.

measured <i>m/z</i> [M-H] ⁻	elemental composition	DBE	\overline{OS}_c	1749	1750	1751	1752
				Rt (min)	Rt (min)	Rt (min)	Rt (min)
99.0451	C ₅ H ₈ O ₂	2	-0.80			4.41	
101.0244	C ₄ H ₆ O ₃	2	0.00		2.74	2.73	2.74
103.0036	C ₃ H ₄ O ₄	2	1.33				0.91
111.0451	C ₆ H ₈ O ₂	3	-0.67	4.16	4.15	4.15	4.16
111.0815	C ₇ H ₁₂ O ₁	2	-1.43	7.49	7.48	4.00; 5.08; 7.48	4.01; 4.94; 7.49
113.0608	C ₆ H ₁₀ O ₂	2	-1.00	3.86	3.85	3.85	3.45; 3.86
115.0400	C ₅ H ₈ O ₃	2	-0.40	3.60	3.59	3.60	3.60
121.0294	C ₇ H ₆ O ₂	5	-0.29	1.00	1.00		
127.0401	C ₆ H ₈ O ₃	3	-0.33	3.07	3.06	3.07	
127.0764	C ₇ H ₁₂ O ₂	2	-1.14			4.29; 4.80; 5.14	4.30; 4.45; 4.80; 5.15
127.1128	C ₈ H ₁₆ O ₁	1	-1.75	9.41	9.41	9.41	9.41
129.1285	C ₈ H ₁₈ O ₁	0	-2.00	9.41	9.41	9.41	9.41
131.0349	C ₅ H ₈ O ₄	2	0.00	4.06	4.04	4.05	4.06
131.0713	C ₆ H ₁₂ O ₃	1	-1.00				3.82
137.0971	C ₉ H ₁₄ O ₁	3	-1.33		5.12	5.12	
139.1128	C ₉ H ₁₆ O ₁	2	-1.56	7.49	7.47	7.48	7.48
141.0557	C ₇ H ₁₀ O ₃	3	-0.57	4.35	4.33	4.33	4.35; 4.44
141.0921	C ₈ H ₁₄ O ₂	2	-1.25	4.81; 5.73	4.8; 5.72	5.72	4.80
143.0349	C ₆ H ₈ O ₄	3	0.00	3.70	3.69	3.69	3.70
145.0506	C ₆ H ₁₀ O ₄	2	-0.33		10.34		4.28
155.0349	C ₇ H ₈ O ₄	4	0.00	3.44; 3.68	3.43; 3.67	3.67	3.44; 3.68
155.0714	C ₈ H ₁₂ O ₃	3	-0.75	4.81	4.81	4.81	4.81; 4.94
155.1077	C ₉ H ₁₆ O ₂	2	-1.33	5.13	5.12	5.12	5.13
157.0506	C ₇ H ₁₀ O ₄	3	-0.29	3.44; 3.86	3.43; 3.85	3.00; 3.43; 3.85	3.44; 3.86

7.2. Supporting Information to Chapter 3

157.0869	C ₈ H ₁₄ O ₃	2	-1.00		6.25	6.25	6.27
158.9934	C ₅ H ₄ O ₆	4	1.60		0.91	0.90	
159.0662	C ₇ H ₁₂ O ₄	2	-0.57				4.79
165.0192	C ₈ H ₆ O ₄	6	0.25	1.00	1.00		
167.0712	C ₉ H ₁₂ O ₃	4	-0.67			4.80	4.80
167.1077	C ₁₀ H ₁₆ O ₂	3	-1.20			5.50; 9.12	5.52
169.0507	C ₈ H ₁₀ O ₄	4	-0.25				5.91
169.0869	C ₉ H ₁₄ O ₃	3	-0.89	3.74; 5.25; 6.23	3.72; 5.09; 5.24; 6.22	3.72; 5.09; 5.24; 6.22	3.74; 4.77; 5.10; 5.25; 5.89; 6.23
171.0662	C ₈ H ₁₂ O ₄	3	-0.50	4.3; 4.45; 4.80; 5.15	4.29; 4.44; 4.79; 5.14	4.29; 4.44; 4.79; 5.14	4.30; 4.45; 4.80; 5.15
173.0454	C ₇ H ₁₀ O ₅	3	0.00	2.47; 2.72	2.39; 2.47; 2.71	2.31; 2.46	1.32; 2.27; 2.46; 2.72
173.0818	C ₈ H ₁₄ O ₄	2	-0.75	3.56	3.55	3.55	3.56; 3.69
173.1182	C ₉ H ₁₈ O ₃	1	-1.33				6.76; 6.99; 7.52
175.0610	C ₇ H ₁₂ O ₅	2	-0.29	2.46; 2.58	2.47; 2.57	2.49; 2.54	2.42; 2.58
181.0870	C ₁₀ H ₁₄ O ₃	4	-0.80		4.38	4.37; 5.12; 7.45	4.39; 5.13
183.0661	C ₉ H ₁₂ O ₄	4	-0.44	4.36	4.35; 4.71	4.35; 4.71	4.72; 4.88
183.1024	C ₁₀ H ₁₆ O ₃	3	-1.00	6.40; 7.49	6.4; 7.48	6.39; 7.48	6.40; 7.48; 8.50
185.0818	C ₉ H ₁₄ O ₄	3	-0.67	3.91; 4.12; 4.81; 5.73	3.9; 4.10; 4.80; 5.72	3.90; 4.10; 4.80; 5.72	3.91; 4.12; 4.81; 5.73
187.0611	C ₈ H ₁₂ O ₅	3	-0.25	4.17; 4.60	4.15	3.08; 4.04; 4.15	3.07; 3.45; 4.03; 4.08; 4.17
187.0975	C ₉ H ₁₆ O ₄	2	-0.89	9.58			
189.0768	C ₈ H ₁₄ O ₅	2	-0.50		3.42	3.42	3.43
189.1131	C ₉ H ₁₈ O ₄	1	-1.11				4.11; 4.23; 4.68
197.0819	C ₁₀ H ₁₄ O ₄	4	-0.60	3.89; 4.08	3.87; 4.06	3.87; 4.06	3.89; 4.65; 5.09
199.0612	C ₉ H ₁₂ O ₅	4	-0.22				4.02
199.0975	C ₁₀ H ₁₆ O ₄	3	-0.80	3.97; 4.39; 4.59; 4.91; 4.39	3.96; 4.37; 4.55; 4.90; 5.12	3.95; 4.37; 4.52; 4.90; 5.12	3.97; 4.38; 4.58; 4.91; 5.13
201.0767	C ₉ H ₁₄ O ₅	3	-0.44	3.70	3.58; 3.69	3.69; 4.56	3.70; 3.95; 4.57
201.1132	C ₁₀ H ₁₈ O ₄	2	-1.00	9.41	6.01; 9.41	6.02; 9.41	6.02; 9.41
203.0561	C ₈ H ₁₂ O ₆	3	0.00	3.62	3.60; 4.22	3.60; 4.21	1.00
205.0716	C ₈ H ₁₄ O ₆	2	-0.25		3.94	3.94	3.95
211.0974	C ₁₁ H ₁₆ O ₄	4	-0.73	5.51; 5.72; 9.44; 9.67	5.51; 5.71; 9.44; 9.67	5.51; 5.71; 9.12; 9.44	5.52; 5.72; 9.44; 9.67
213.0767	C ₁₀ H ₁₄ O ₅	4	-0.40	3.77	3.76	3.76; 4.30	3.77; 4.32
213.1496	C ₁₂ H ₂₂ O ₃	2	-1.33				8.97
215.0560	C ₉ H ₁₂ O ₆	4	0.00	3.60	3.59; 3.95	1.00; 3.59; 3.96	3.60; 3.97
215.0922	C ₁₀ H ₁₆ O ₅	3	-0.60	4.45; 4.72; 6.14	4.29; 4.44; 4.71; 6.13	4.44; 4.71; 6.13	4.45; 4.72; 6.14
217.0715	C ₉ H ₁₄ O ₆	3	-0.22	4.02		4.26; 4.83; 5.02	3.37; 5.02
219.0872	C ₉ H ₁₆ O ₆	2	-0.44		3.79; 4.00; 4.83		
223.1339	C ₁₃ H ₂₀ O ₃	4	-1.08			9.28	
225.1131	C ₁₂ H ₁₈ O ₄	4	-0.83			7.22	
227.0923	C ₁₁ H ₁₆ O ₅	4	-0.55				7.36
227.1288	C ₁₂ H ₂₀ O ₄	3	-1.00		8.25	8.25	9.16
229.0715	C ₁₀ H ₁₄ O ₆	4	-0.20		3.48	3.48; 4.63	3.49; 3.95; 4.20; 4.28; 4.42; 4.63; 5.03
229.1443	C ₁₂ H ₂₂ O ₄	2	-1.17	10.00	10.01	10.00	

7. Appendix

231.0872	C ₁₀ H ₁₆ O ₆	3	-0.40	4.28; 4.42; 5.03	3.93; 4.16; 4.27; 4.41; 5.02	3.93; 4.19; 4.27; 4.41; 5.02	
233.0665	C ₉ H ₁₄ O ₇	3	0.00	3.78	3.77	3.77	1.00; 3.79
235.1703	C ₁₅ H ₂₄ O ₂	4	-1.33	9.83	9.83	9.83	9.83
239.0924	C ₁₂ H ₁₆ O ₅	5	-0.50	5.52; 9.12	5.51; 9.12	5.51; 9.12	5.51
241.1081	C ₁₂ H ₁₈ O ₅	4	-0.67	7.8; 9.33	7.8; 9.33	7.80; 9.33	9.33
241.1444	C ₁₃ H ₂₂ O ₄	3	-1.08	9.28	9.28	9.28	9.28
243.0871	C ₁₁ H ₁₆ O ₆	4	-0.36	5.72	5.71	5.71	5.72
245.1029	C ₁₁ H ₁₈ O ₆	3	-0.55		7.93	7.93; 8.24	
247.0821	C ₁₀ H ₁₆ O ₇	3	-0.20	3.95	3.94	3.94	
255.1236	C ₁₃ H ₂₀ O ₅	4	-0.77	8.87; 9.04	8.87; 9.04	8.87; 9.04	8.73; 8.87
257.1030	C ₁₂ H ₁₈ O ₆	4	-0.50	7.31			
257.1392	C ₁₃ H ₂₂ O ₅	3	-0.92	8.97	8.97	8.97	8.65; 8.97
259.1184	C ₁₂ H ₂₀ O ₆	3	-0.67		8.99	8.99	
259.1548	C ₁₃ H ₂₄ O ₅	2	-1.08			7.75; 9.08	7.60; 7.75; 8.38; 8.82
259.1912	C ₁₄ H ₂₈ O ₄	1	-1.43			10.15	10.15
261.0977	C ₁₁ H ₁₈ O ₇	3	-0.36				5.00
261.1341	C ₁₂ H ₂₂ O ₆	2	-0.83			4.70	4.71
263.1134	C ₁₁ H ₂₀ O ₇	2	-0.55		4.39	4.39	4.40
271.1186	C ₁₃ H ₂₀ O ₆	4	-0.62				7.29
271.1550	C ₁₄ H ₂₄ O ₅	3	-1.00				8.68
271.2277	C ₁₆ H ₃₂ O ₃	1	-1.63				10.05
273.1342	C ₁₃ H ₂₂ O ₆	3	-0.77	7.83	7.82	4.86; 7.83	4.87; 7.84
279.1083	C ₁₁ H ₂₀ O ₈	2	-0.36				3.84
279.1599	C ₁₆ H ₂₄ O ₄	5	-1.00	9.83		9.82	9.83
283.1550	C ₁₅ H ₂₄ O ₅	4	-0.93	8.35; 8.46; 9.00; 9.07	8.34; 8.46; 9.00; 9.07	9.07	
285.2434	C ₁₇ H ₃₄ O ₃	1	-1.65		10.13	10.13	10.13
287.2227	C ₁₆ H ₃₂ O ₄	1	-1.50				9.57
297.1706	C ₁₆ H ₂₆ O ₅	4	-1.00				9.57
299.1498	C ₁₅ H ₂₄ O ₆	4	-0.80	7.64; 8.46; 9.10	7.63; 8.46; 9.10	7.63; 8.46; 9.10	7.63; 8.46; 9.10
303.2175	C ₁₆ H ₃₂ O ₅	1	-1.38	10.17	10.16	10.17	10.17
305.1604	C ₁₄ H ₂₆ O ₇	2	-0.86			4.95	
309.2070	C ₁₈ H ₃₀ O ₄	4	-1.22	9.84	9.84	9.84	9.83
313.1656	C ₁₆ H ₂₆ O ₆	4	-0.88	9.21			
317.0674	C ₁₆ H ₁₄ O ₇	10	0.00	5.36; 5.48	4.77; 4.96; 5.35; 5.47		
335.0417	C ₁₅ H ₁₂ O ₉	10	0.40	4.33			
337.1656	C ₁₈ H ₂₆ O ₆	6	-0.78			9.47	
337.2019	C ₁₉ H ₃₀ O ₅	5	-1.05	9.25; 9.33	9.25; 9.33; 9.38	9.25; 9.32; 9.51	9.25; 9.33
341.1603	C ₁₇ H ₂₆ O ₇	5	-0.71			8.90; 9.67	8.90
343.1395	C ₁₆ H ₂₄ O ₈	5	-0.50	4.31	4.29	4.29	
347.1085	C ₂₅ H ₁₆ O ₂	18	-0.48				8.97
347.1134	C ₁₈ H ₂₀ O ₇	9	-0.33	9.32			
349.0572	C ₁₆ H ₁₄ O ₉	10	0.25	4.34			
349.0927	C ₁₇ H ₁₈ O ₈	9	-0.12	8.60			
351.1811	C ₁₉ H ₂₈ O ₆	6	-0.84			9.60	

353.1967	C ₁₉ H ₃₀ O ₆	5	-0.95		9.17; 9.30	9.17; 9.30	9.17
355.1761	C ₁₈ H ₂₈ O ₇	5	-0.78		9.64	9.64	
357.1553	C ₁₇ H ₂₆ O ₈	5	-0.59	8.47	8.47; 8.88	8.47; 8.87	8.47; 8.88
365.0520	C ₁₆ H ₁₄ O ₁₀	10	0.38	3.64			
365.0728	C ₁₃ H ₁₈ O ₁₂	5	0.46	10.45	10.48; 10.61	10.46; 10.57	10.47
365.1238	C ₁₈ H ₂₂ O ₈	8	-0.33				4.39
367.1763	C ₁₉ H ₂₈ O ₇	6	-0.74	9.32	9.32	9.21; 9.32	9.32
373.2230	C ₁₉ H ₃₄ O ₇	3	-1.05	9.53	9.53	9.53	
375.0210	C ₁₃ H ₁₂ O ₁₃	8	1.08			9.80	
381.1189	C ₁₈ H ₂₂ O ₉	8	-0.22	4.44	4.43	4.43	4.44
383.2075	C ₂₀ H ₃₂ O ₇	5	-0.90			9.39	9.39
387.1659	C ₁₈ H ₂₈ O ₉	5	-0.56				4.30
393.1044	C ₁₅ H ₂₂ O ₁₂	5	0.13			10.87; 10.92	
395.0721	C ₂₈ H ₁₂ O ₃	23	-0.21				4.82
397.0779	C ₁₇ H ₁₈ O ₁₁	9	0.24	10.52; 10.62; 10.69	10.58	10.60	10.61
399.0930	C ₁₇ H ₂₀ O ₁₁	8	0.12	4.06	4.04	4.05	4.06
399.1657	C ₁₉ H ₂₈ O ₉	6	-0.53	8.99; 9.13	8.99; 9.12	8.99; 9.13; 9.29	8.99; 9.13
407.0835	C ₁₅ H ₂₀ O ₁₃	6	0.40			10.60	
409.0992	C ₁₅ H ₂₂ O ₁₃	5	0.27		10.62	10.59	10.58
411.0936	C ₁₈ H ₂₀ O ₁₁	9	0.11	10.85; 10.98		10.65; 10.72; 10.87; 10.93	10.48; 10.57; 10.72; 10.91; 11.02
415.1971	C ₂₀ H ₃₂ O ₉	5	-0.70			4.37	4.38
415.2336	C ₂₁ H ₃₆ O ₈	4	-0.95		9.65	9.65	
447.2027	C ₂₄ H ₃₂ O ₈	9	-0.67		9.37		
453.1254	C ₁₇ H ₂₆ O ₁₄	5	0.12			10.68	
457.1511	C ₂₄ H ₂₆ O ₉	12	-0.33			4.79	
469.2088	C ₂₃ H ₃₄ O ₁₀	7	-0.61			9.67	
507.0049	C ₂₀ H ₁₂ O ₁₆	15	1.00	1.00	1.00		
577.3745	C ₃₃ H ₅₄ O ₈	7	-1.15				9.84
615.2813	C ₃₃ H ₄₄ O ₁₁	12	-0.67		9.10		
633.3645	C ₃₅ H ₅₄ O ₁₀	9	-0.97				9.83

Table 7.8 CHON-containing organic compounds detected on filter samples during CLOUD 10 by UHPLC(-)ESI-UHRMS.

measured <i>m/z</i> [M-H] ⁻	elemental composition	DBE	\overline{OS}_c	1749	1750	1751	1752
				Rt (min)	Rt (min)	Rt (min)	Rt (min)
168.0302	C ₇ H ₇ O ₄ N ₁	5	-0.57	9.38	9.38		
182.0095	C ₇ H ₅ O ₅ N ₁	6	0.00	3.53			
196.0614	C ₉ H ₁₁ O ₄ N ₁	5	-0.89			4.44	
210.0771	C ₁₀ H ₁₃ O ₄ N ₁	5	-1.00	9.05	9.05	9.05	9.05
226.1084	C ₁₁ H ₁₇ O ₄ N ₁	4	-1.27	4.27			
229.0247	C ₁₁ H ₆ O ₄ N ₂	10	-0.73				4.30
229.1191	C ₁₀ H ₁₈ O ₄ N ₂	3	-2.00	3.74	3.72	3.73	3.73

7. Appendix

239.0536	C ₆ H ₁₂ O ₈ N ₂	2	-1.00	4.30	4.31; 4.45; 5.15	4.29; 4.44	
240.1240	C ₁₂ H ₁₉ O ₄ N ₁	4	-1.33	4.73	4.72	4.72	
242.1033	C ₁₁ H ₁₇ O ₅ N ₁	4	-1.09	4.08			
243.0404	C ₁₂ H ₈ O ₄ N ₂	10	-0.83			4.79; 5.72	
255.0622	C ₁₀ H ₁₂ O ₆ N ₂	6	-1.00	9.41	9.41	9.41	9.42
256.1190	C ₁₂ H ₁₉ O ₅ N ₁	4	-1.17	4.02			
270.1345	C ₁₃ H ₂₁ O ₅ N ₁	4	-1.23	4.48	4.47	4.47	
272.1138	C ₁₂ H ₁₉ O ₆ N ₁	4	-1.00	3.84			
273.1454	C ₁₂ H ₂₂ O ₅ N ₂	3	-1.83	4.54; 4.91	4.53; 4.90	4.53; 4.90	4.54; 4.91
275.0511	C ₉ H ₁₂ O ₈ N ₂	5	-0.67	4.8; 5.73	4.79; 5.72	4.78; 5.72	4.79; 5.74
278.0878	C ₁₀ H ₁₇ O ₈ N ₁	3	-0.60	5.01	5.00	4.55; 5.01	5.01
289.1404	C ₁₂ H ₂₂ O ₆ N ₂	3	-1.67	3.38	3.38	3.38	
299.0746	C ₈ H ₁₆ O ₁₀ N ₂	2	-0.75			4.40	4.41
302.1972	C ₁₅ H ₂₉ O ₅ N ₁	2	-1.60				9.29
305.0617	C ₁₀ H ₁₄ O ₉ N ₂	5	-0.60			5.23	
307.0410	C ₉ H ₁₂ O ₁₀ N ₂	5	-0.22	4.30	4.29	4.29	
308.0987	C ₁₁ H ₁₉ O ₉ N ₁	3	-0.55	7.05	7.05	7.05	7.06
323.1108	C ₁₁ H ₂₀ O ₉ N ₂	3	-1.09	8.87			
325.0902	C ₁₀ H ₁₈ O ₁₀ N ₂	3	-0.80			5.51	
353.1580	C ₁₃ H ₂₆ O ₉ N ₂	2	-1.38				4.38
355.0992	C ₁₁ H ₂₀ O ₁₁ N ₂	3	-0.73	8.73	8.73	8.73	8.73
359.0746	C ₁₃ H ₁₆ O ₁₀ N ₂	7	-0.46	4.45	4.43	4.43	4.44
365.1213	C ₁₃ H ₂₂ O ₁₀ N ₂	4	-0.92		4.29	4.29	
369.1528	C ₁₃ H ₂₆ O ₁₀ N ₂	2	-1.23				5.26
373.0901	C ₁₄ H ₁₈ O ₁₀ N ₂	7	-0.57	4.82	4.81	4.81	4.82
382.1870	C ₁₉ H ₂₉ O ₇ N ₁	6	-1.05	10.03	10.03	10.03	
387.1060	C ₁₅ H ₂₀ O ₁₀ N ₂	7	-0.67	4.39	4.37	4.37	4.38
395.0721	C ₁₆ H ₁₆ O ₁₀ N ₂	10	-0.38	4.82	4.81	4.81	
397.1840	C ₁₅ H ₃₀ O ₁₀ N ₂	2	-1.33				7.22
419.0957	C ₁₅ H ₂₀ O ₁₂ N ₂	7	-0.40				4.43
437.1166	C ₁₄ H ₂₂ O ₁₂ N ₄	6	-1.29	4.80		4.79	4.80

Table 7.9 CHOS-containing organic compounds detected on filter samples during CLOUD 10 by UHPLC-(-)ESI-UHRMS.

measured <i>m/z</i> [M-H] ⁻	elemental composition	DBE	\overline{OS}_C	1749	1750	1751	1752
				Rt (min)	Rt (min)	Rt (min)	Rt (min)
151.0070	C ₄ H ₈ O ₄ S ₁	1	-1.50	0.93	0.93	0.93	
152.9863	C ₃ H ₆ O ₅ S ₁	1	-0.67	0.96	0.96	0.95	
154.9655	C ₂ H ₄ O ₆ S ₁	1	1.00	0.83	0.83	0.83	
168.9811	C ₃ H ₆ O ₆ S ₁	1	0.00		0.91	0.91	
169.0175	C ₄ H ₁₀ O ₅ S ₁	0	-1.50	0.99			
179.0383	C ₆ H ₁₂ O ₄ S ₁	1	-1.67	9.90			
180.9813	C ₄ H ₆ O ₆ S ₁	2	0.00		0.84		

181.0176	C ₅ H ₁₀ O ₅ S ₁	1	-1.20	3.91			
182.9968	C ₄ H ₈ O ₆ S ₁	1	-0.50	1.00	1.00	1.00	
185.0123	C ₄ H ₁₀ O ₆ S ₁	0	-1.00	0.97	0.97	0.95	
193.0175	C ₆ H ₁₀ O ₅ S ₁	2	-1.00	3.56	3.55	3.55	
193.0902	C ₈ H ₁₈ O ₃ S ₁	0	-2.25	5.55	5.54	5.54	
197.0125	C ₅ H ₁₀ O ₆ S ₁	1	-0.80	3.95	3.94	3.94	
205.0539	C ₈ H ₁₄ O ₄ S ₁	2	-1.50	4.23	4.21	4.22	
209.0851	C ₈ H ₁₈ O ₄ S ₁	0	-2.00	9.31	9.31	9.31	
210.9918	C ₅ H ₈ O ₇ S ₁	2	0.00			1.00	
211.0281	C ₆ H ₁₂ O ₆ S ₁	1	-1.00	3.69; 4.29	3.10; 3.22; 3.68; 4.27	3.11; 3.23; 3.68; 4.28	3.69
219.0332	C ₈ H ₁₂ O ₅ S ₁	3	-1.00	3.88	3.85	3.85	
219.0694	C ₉ H ₁₆ O ₄ S ₁	2	-1.56	3.82; 4.08	3.80; 4.06	3.80; 4.06	
221.0852	C ₉ H ₁₈ O ₄ S ₁	1	-1.78	10.14			
223.1007	C ₉ H ₂₀ O ₄ S ₁	0	-2.00	9.59	9.59	9.59	
225.0436	C ₇ H ₁₄ O ₆ S ₁	1	-1.14	3.82; 3.97; 7.59	3.80; 3.95; 7.58	3.81; 3.95; 7.58	
231.0695	C ₁₀ H ₁₆ O ₄ S ₁	3	-1.40	4.49; 9.27	4.48; 4.63; 9.27	9.27	
235.0643	C ₉ H ₁₆ O ₅ S ₁	2	-1.33	4.33; 4.66	3.90; 4.32; 4.65	3.90; 4.32; 4.65	3.91; 4.34
237.0436	C ₈ H ₁₄ O ₆ S ₁	2	-1.00	3.63	3.62	3.62	
239.0233	C ₇ H ₁₂ O ₇ S ₁	2	-0.57		1.00	1.00	
239.0593	C ₈ H ₁₆ O ₆ S ₁	1	-1.25	4.39; 4.57; 4.87	4.38; 4.56; 4.87	4.38; 4.56; 4.87	
241.0750	C ₈ H ₁₈ O ₆ S ₁	0	-1.50	5.15	5.14	5.14	
244.9759	C ₈ H ₆ O ₇ S ₁	6	0.25	4.15	4.13	4.13	
245.0487	C ₁₀ H ₁₄ O ₅ S ₁	4	-1.00	4.82	4.81	4.81	
247.0644	C ₁₀ H ₁₆ O ₅ S ₁	3	-1.20		4.57; 4.84; 5.39; 5.89	0.00	
249.0800	C ₁₀ H ₁₈ O ₅ S ₁	2	-1.40	3.80; 3.92; 4.36; 4.58; 4.78; 4.85; 4.98; 5.14; 5.36; 5.48; 5.64; 5.90; 6.31; 6.57	3.78; 3.91; 4.35; 4.45; 4.77; 4.97; 5.13; 5.35; 5.47; 5.61; 6.29; 6.57	3.78; 4.35; 4.78; 4.84; 4.97; 5.13; 5.35; 5.48; 5.89; 6.30; 6.57	
251.0593	C ₉ H ₁₆ O ₆ S ₁	2	-1.11	3.16	3.15	3.16; 4.83; 4.89; 4.99; 5.08; 5.40; 5.49; 6.54; 8.12; 8.99; 9.49	
253.0750	C ₉ H ₁₈ O ₆ S ₁	1	-1.33	4.92; 4.99; 5.09; 5.40; 6.54; 8.13; 8.99; 9.50	4.91; 4.99; 5.07; 5.39; 5.50; 6.53; 8.12; 8.99; 9.49		4.99
257.0699	C ₈ H ₁₈ O ₇ S ₁	0	-1.25	3.30; 3.53	3.29; 3.52	3.29; 3.52	
263.0592	C ₁₀ H ₁₆ O ₆ S ₁	3	-1.00	4.65; 4.97; 5.54	3.67; 4.04; 4.64; 4.96; 5.53	4.04; 4.64; 4.96; 5.53	
265.0384	C ₉ H ₁₄ O ₇ S ₁	3	-0.67	4.16	4.14	4.14	
267.0542	C ₉ H ₁₆ O ₇ S ₁	2	-0.89	3.63; 3.91; 4.33	3.62; 4.31	3.62; 4.31	
267.0906	C ₁₀ H ₂₀ O ₆ S ₁	1	-1.40	8.57; 9.72	8.57; 9.73	8.57; 9.72	
269.0335	C ₈ H ₁₄ O ₈ S ₁	2	-0.50	3.94	3.92	3.92; 5.72	5.73
274.9867	C ₉ H ₈ O ₈ S ₁	6	0.22	4.45; 4.61	4.60	4.60	
277.0385	C ₁₀ H ₁₄ O ₇ S ₁	4	-0.60	4.50	4.49	4.49	
279.0542	C ₁₀ H ₁₆ O ₇ S ₁	3	-0.80	3.79; 4.02; 4.33; 4.56; 4.65; 4.72	3.77; 4.00; 4.32; 4.55; 4.64; 4.71	3.77; 4.00; 4.32; 4.55; 4.64; 4.82	
279.0904	C ₁₁ H ₂₀ O ₆ S ₁	2	-1.27			6.39	6.40
279.1270	C ₁₂ H ₂₄ O ₅ S ₁	1	-1.67	9.11	9.11	9.11	
281.0698	C ₁₀ H ₁₈ O ₇ S ₁	2	-1.00	4.06; 4.61	4.04; 4.60	4.05; 4.60	

7. Appendix

281.1063	C ₁₁ H ₂₂ O ₆ S ₁	1	-1.45	9.20; 9.77	9.20	9.20; 10.02	
283.0493	C ₉ H ₁₆ O ₈ S ₁	2	-0.67			3.94	
287.0443	C ₈ H ₁₆ O ₉ S ₁	1	-0.50	8.84			
291.1272	C ₁₃ H ₂₄ O ₅ S ₁	2	-1.54		9.68; 9.93		
293.0700	C ₁₁ H ₁₈ O ₇ S ₁	3	-0.91	5.45	5.45		
295.0493	C ₁₀ H ₁₆ O ₈ S ₁	3	-0.60	4.41; 4.52	4.38; 4.51	4.38	
295.0852	C ₁₁ H ₂₀ O ₇ S ₁	2	-1.09	4.38	4.37	0.00	4.38
295.1219	C ₁₂ H ₂₄ O ₆ S ₁	1	-1.50	8.83; 8.90; 9.47; 9.89; 10.00	8.82; 8.90; 9.47; 9.89; 10.05	8.83; 8.90; 9.47; 9.89	
297.0647	C ₁₀ H ₁₈ O ₈ S ₁	2	-0.80	3.64; 3.75; 3.92; 4.10	3.63; 3.73; 3.91; 4.08	3.63; 3.78; 3.91; 4.08	
299.0447	C ₉ H ₁₆ O ₉ S ₁	2	-0.44			5.23	
299.0955	C ₁₄ H ₂₀ O ₅ S ₁	5	-1.14	10.34			10.33
309.1376	C ₁₃ H ₂₆ O ₆ S ₁	1	-1.54	10.14	10.14	10.13	
309.1741	C ₁₄ H ₃₀ O ₅ S ₁	0	-1.86		9.44		
311.0442	C ₁₀ H ₁₆ O ₉ S ₁	3	-0.40	4.06	4.04	4.04	
311.1781	C ₁₇ H ₂₈ O ₃ S ₁	4	-1.65			10.60	
321.0647	C ₁₂ H ₁₈ O ₈ S ₁	4	-0.67	4.48; 4.69	4.46; 4.68		
321.1010	C ₁₃ H ₂₂ O ₇ S ₁	3	-1.08	8.55	8.55	8.55	
323.1169	C ₁₃ H ₂₄ O ₇ S ₁	2	-1.23	9.69	9.70	8.21	
323.1535	C ₁₄ H ₂₈ O ₆ S ₁	1	-1.57	9.43; 10.25	9.43; 9.53; 9.65; 9.70; 9.91	9.43; 9.55; 9.60; 9.70; 9.91	
323.1897	C ₁₅ H ₃₂ O ₅ S ₁	0	-1.87	9.59			
327.1267	C ₁₆ H ₂₄ O ₅ S ₁	5	-1.25	10.71		10.71	
332.9558	C ₁₀ H ₆ O ₁₁ S ₁	8	1.00	1.01			
335.0417	C ₁₆ H ₁₆ O ₄ S ₂	9	-1.25		4.31		
337.1689	C ₁₅ H ₃₀ O ₆ S ₁	1	-1.60	9.54; 10.40	9.54; 10.42	9.54	
337.2053	C ₁₆ H ₃₄ O ₅ S ₁	0	-1.88	9.77; 9.91	9.77; 9.91	9.77; 9.91	
349.0572	C ₁₇ H ₁₈ O ₄ S ₂	9	-1.29		4.33	4.33	
351.1846	C ₁₆ H ₃₂ O ₆ S ₁	1	-1.63	9.68; 9.76	9.67; 9.76; 9.96; 10.06; 10.19; 10.47; 10.54	9.67; 9.74; 9.95; 10.05; 10.19; 10.32; 10.46	
355.1584	C ₁₈ H ₂₈ O ₅ S ₁	5	-1.33			11.17	11.19
361.1689	C ₁₇ H ₃₀ O ₆ S ₁	3	-1.41	8.67		8.67	
365.0520	C ₁₇ H ₁₈ O ₅ S ₂	9	-1.18		3.63	3.63	
365.2001	C ₁₇ H ₃₄ O ₆ S ₁	1	-1.65	10.21	9.86; 10.21	10.20	
365.2362	C ₁₈ H ₃₈ O ₅ S ₁	0	-1.89	10.22; 10.47	10.22; 10.52	10.51	
367.1792	C ₁₆ H ₃₂ O ₇ S ₁	1	-1.50			9.07; 9.25	
369.1174	C ₂₁ H ₂₂ O ₄ S ₁	11	-0.95			3.70	
371.1528	C ₁₈ H ₂₈ O ₆ S ₁	5	-1.22	10.38	10.38	10.38	10.05; 10.29; 10.38
371.1895	C ₁₉ H ₃₂ O ₅ S ₁	4	-1.47	9.70	9.55; 9.71	9.54; 9.70	
373.0959	C ₁₆ H ₂₂ O ₈ S ₁	6	-0.75	9.45; 9.74	9.45	9.45	9.45
373.1687	C ₁₈ H ₃₀ O ₆ S ₁	4	-1.33	9.91; 10.04	9.92; 10.05	10.05	
377.0695	C ₁₈ H ₁₈ O ₇ S ₁	10	-0.56				10.00
377.1285	C ₁₆ H ₂₆ O ₈ S ₁	4	-1.00	9.26			
379.2157	C ₁₈ H ₃₆ O ₆ S ₁	1	-1.67	10.05	10.05; 10.19	10.05	
381.1587	C ₁₆ H ₃₀ O ₈ S ₁	2	-1.25		9.93		
385.0594	C ₁₆ H ₁₈ O ₉ S ₁	8	-0.38			9.87	

389.0490	C ₂₂ H ₁₄ O ₅ S ₁	16	-0.45			3.84	3.85
389.2001	C ₁₉ H ₃₄ O ₆ S ₁	3	-1.47	8.97; 9.08	8.97; 9.08	8.97; 9.08	
393.1590	C ₁₇ H ₃₀ O ₈ S ₁	3	-1.18	9.51			
393.2315	C ₁₉ H ₃₈ O ₆ S ₁	1	-1.68	10.48	10.50	10.52; 10.70	
395.1530	C ₂₀ H ₂₈ O ₆ S ₁	7	-1.10	9.59	9.59	9.59	
403.1793	C ₁₉ H ₃₂ O ₇ S ₁	4	-1.26	10.31	10.31	10.31	
407.2470	C ₂₀ H ₄₀ O ₆ S ₁	1	-1.70	10.64; 10.79	10.67; 10.76; 11.06	10.66; 10.72; 11.06	
409.1322	C ₂₀ H ₂₆ O ₇ S ₁	8	-0.90	9.84	9.84	9.84	
419.0957	C ₂₄ H ₂₀ O ₅ S ₁	15	-0.67	4.43	4.42	4.42	
421.1900	C ₁₉ H ₃₄ O ₈ S ₁	3	-1.26	9.88	9.88	9.87	
423.0752	C ₁₉ H ₂₀ O ₉ S ₁	10	-0.42			9.82	9.83
425.2213	C ₁₉ H ₃₈ O ₈ S ₁	1	-1.47		9.53		
429.1946	C ₂₁ H ₃₄ O ₇ S ₁	5	-1.24		10.96		
433.1534	C ₁₉ H ₃₀ O ₉ S ₁	5	-0.95	9.57			
449.2211	C ₂₁ H ₃₈ O ₈ S ₁	3	-1.33	10.21	10.20		
463.2369	C ₂₂ H ₄₀ O ₈ S ₁	3	-1.36	10.33	10.34		
465.2524	C ₂₂ H ₄₂ O ₈ S ₁	2	-1.45			10.49; 10.57	
485.2211	C ₂₄ H ₃₈ O ₈ S ₁	6	-1.17			10.47	

Table 7.10 CHONS-containing organic compounds detected on filter samples during CLOUD 10 by UHPLC(-ESI-UHRMS).

measured <i>m/z</i> [M-H] ⁻	elemental composition	DBE	\overline{OS}_C	1749	1750	1751	1752
				Rt (min)	Rt (min)	Rt (min)	Rt (min)
294.0651	C ₁₀ H ₁₇ O ₇ N ₁ S ₁	3	-1.40	8.52; 8.86; 9.11; 9.18; 9.27	8.52; 8.86; 9.10; 9.18; 9.27	8.51; 8.86; 9.11; 9.18; 9.27	8.52; 9.27
310.0602	C ₁₀ H ₁₇ O ₈ N ₁ S ₁	3	-1.20	7.39	7.37	7.39	
312.0394	C ₉ H ₁₅ O ₉ N ₁ S ₁	3	-0.89	4.76	4.73		
342.0497	C ₁₀ H ₁₇ O ₁₀ N ₁ S ₁	3	-0.80	4.40; 5.92	5.91	5.92	
510.1646	C ₂₀ H ₃₃ O ₁₂ N ₁ S ₁	5	-1.00	9.96			

7.3 Supporting Information to Chapter 4

The following section presents background information, additional graphs, and the lists of compounds detected by the ultra-high-resolution mass spectrometry of atmospheric aerosol particles in real-time. A scheme of the instrumental setup for the measurement of aerosol particles is presented in Figure 7.4.

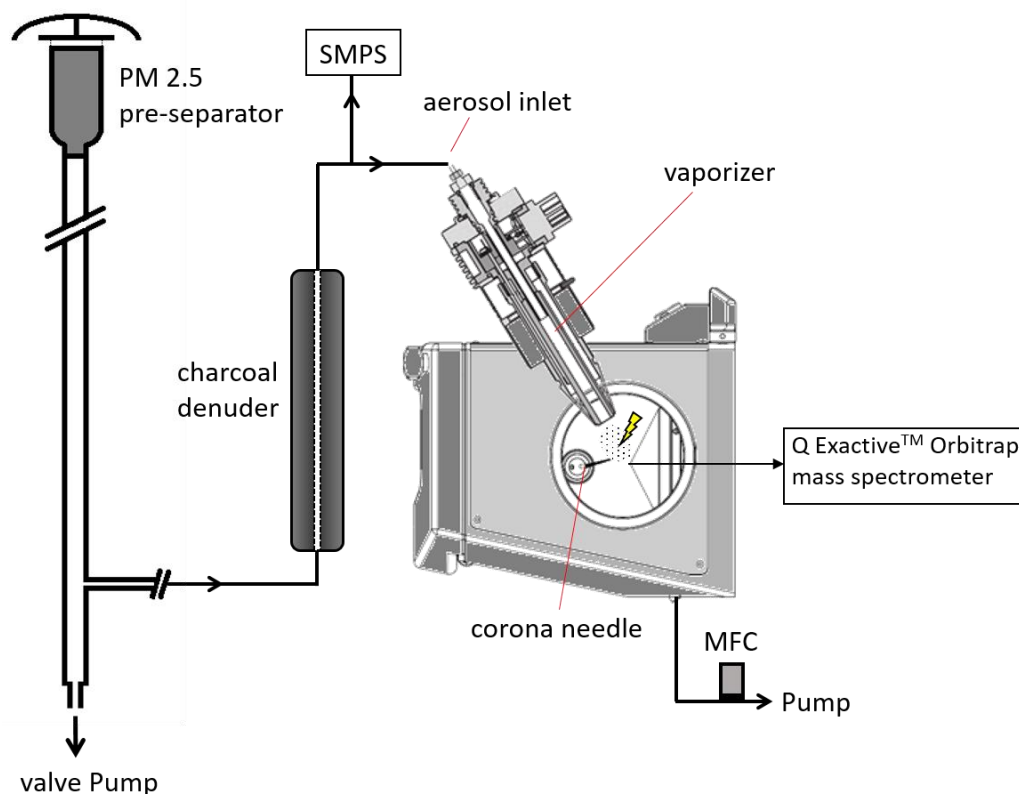


Figure 7.4 Scheme of the instrumental setup for the measurement of ambient aerosol particles. Ambient particles were sampled using a PM_{2.5} pre-separator. By use of a charcoal denuder, the particle phase was separated from the gas phase and the number and mass concentration was analyzed by a SMPS system. Subsequently, the particles were vaporized, ionized and analyzed by APCI-Orbitrap MS.

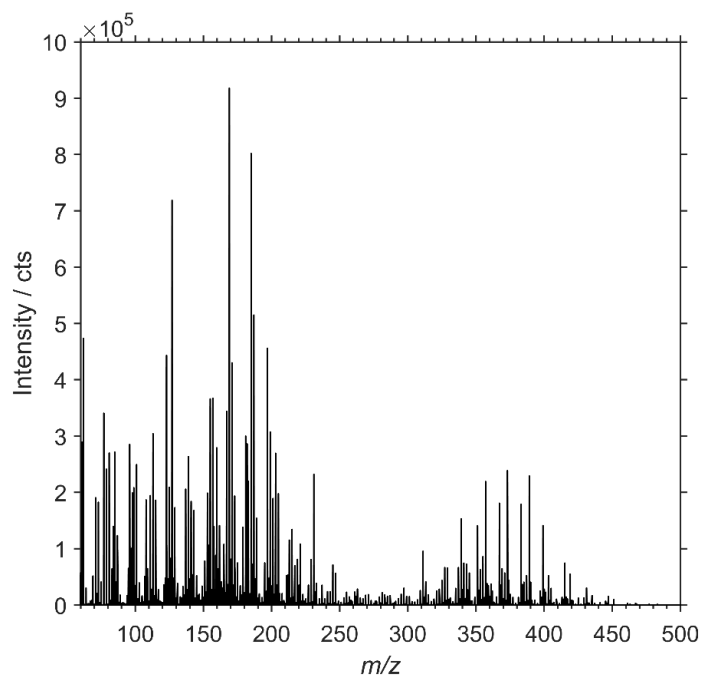


Figure 7.5 APCI-Orbitrap mass spectrum of oxidation products formed in the reaction of α -pinene with ozone in the negative ionization mode. The spectra shows a monomer and a dimer-mode of main oxidation products. The detected particle phase was separated from the gas-phase prior to the ionization by use of a charcoal denuder system. α -pinene was purchased from Sigma-Aldrich (purity > 99%). The experiment was performed in a cylindrical reaction chamber made of glass with a volume of 85 L at a temperature of 296 ± 2 K. The α -pinene mixing ratio was 140 ppb. Ozone was produced by UV irradiation of a synthetic air supply and measured with a Dasibi Environmental Corp. O_3 analyzer (model 1008-RS, Glendale, CA, USA). The O_3 concentration was adjusted to a range of 1 ppm.

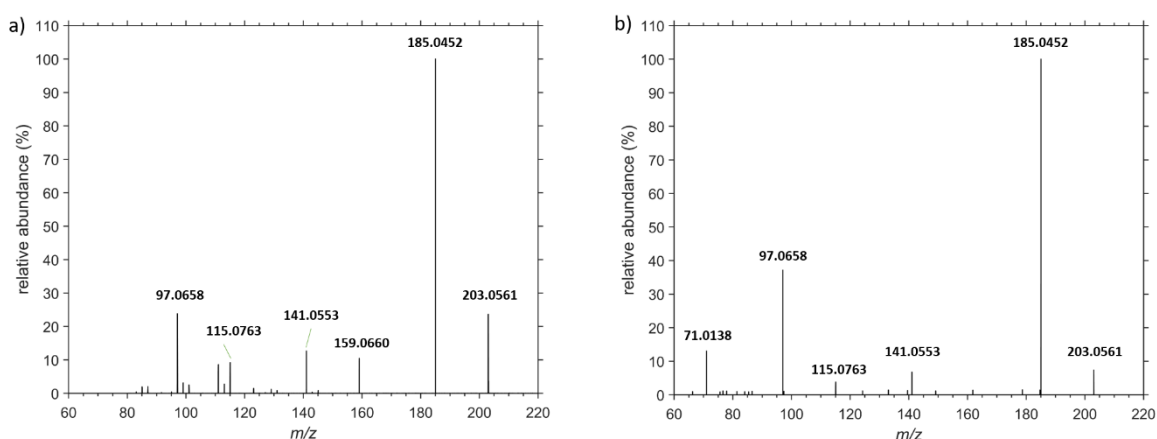


Figure 7.6 a) Ambient MS^2 spectrum of m/z 203 (± 0.4 Th) recorded with APCI-Orbitrap-MS. b) MS^2 spectrum of synthesized laboratory standard MBTCA recorded with UHPLC-Orbitrap-MS at a retention time of 3.05 min. The fragmentation pattern strongly indicates the presence of MBTCA in the ambient particle phase: m/z 203.0561 = $[M-H]^-$, m/z 185.0452 = $[M-H_2O]^-$, m/z 159.0660 = $[M-CO_2]^-$, m/z 141.0553 = $[M-H_2O-CO_2]^-$, m/z 115.0763 = $[M-2CO_2]^-$, m/z 97.0658 = $[M-H_2O-2CO_2]^-$. Additional signals may originate from isobaric interferences.

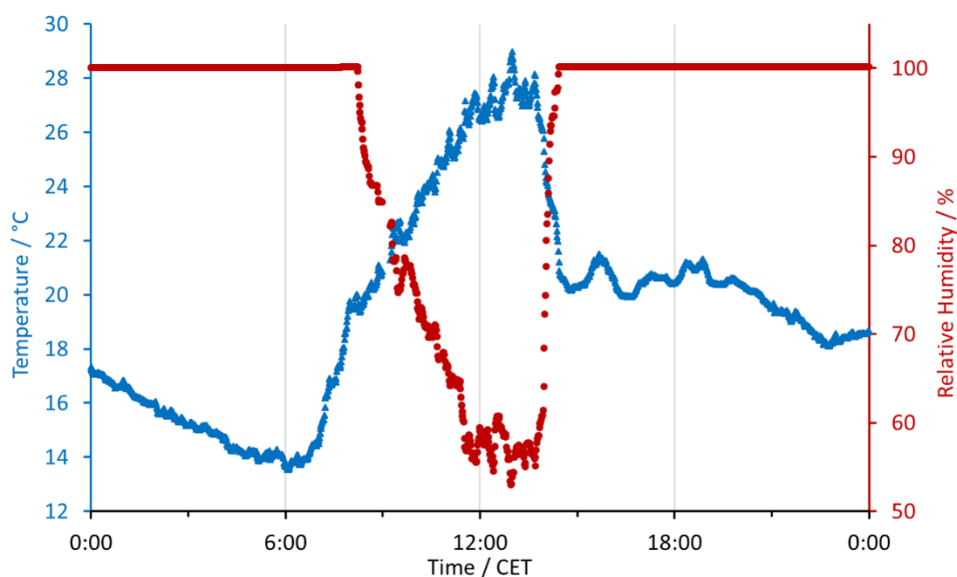


Figure 7.7 Temperature and Relative Humidity (RH) profiles on August 15th, 2017. The sudden drop in the temperature and the increase of the RH at 14:00 was caused by a heavy rain event in Mainz, Germany. (Reference: Institute for Atmospheric Physics, Johannes Gutenberg University Mainz, 55128 Mainz).

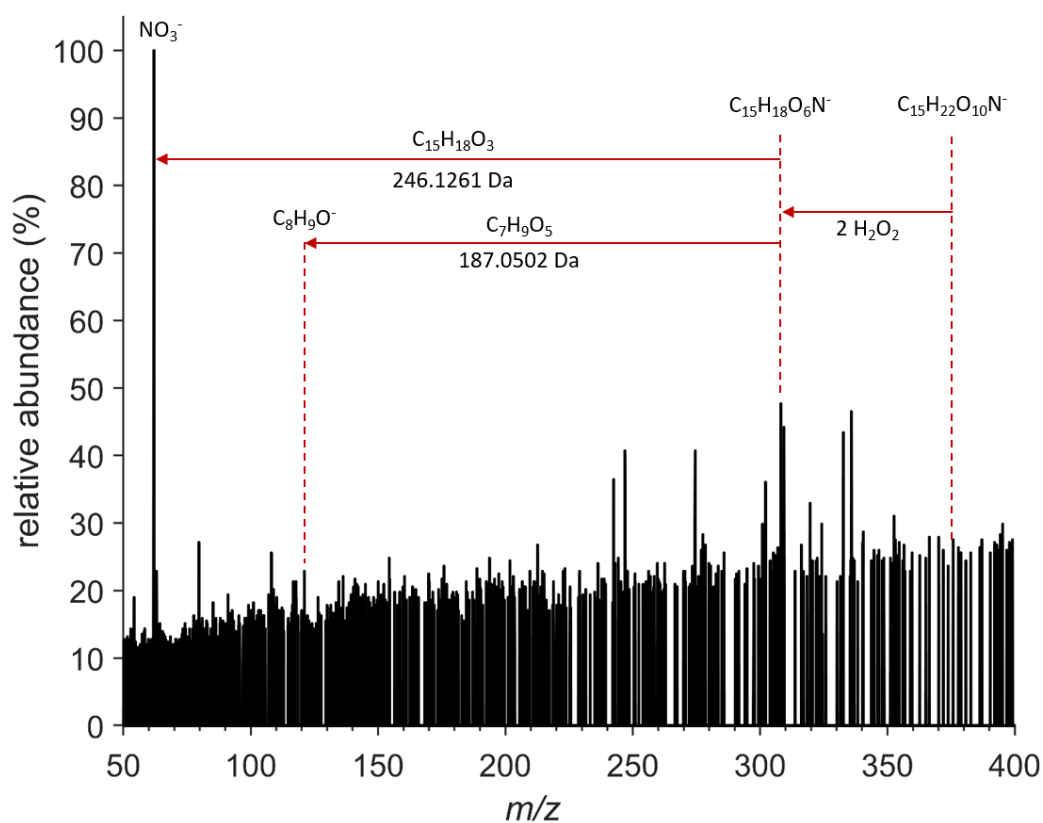


Figure 7.8 Ambient MS²-spectrum of m/z 376.12 (\pm 0.4) (HCD energy 10 %). The fragmentation pattern indicates the presence of an organic peroxy nitrate ($C_{15}H_{23}O_{10}N$): m/z 376.1247 = $[M-H]^-$, m/z 308.1127 = $[M-2H_2O_2]^-$, m/z 121.0625 = $[C_{15}H_{18}O_6N-C_7H_9O_5N]^-$, m/z 61.9885 = $[M-C_{15}H_{18}O_3]^-$.

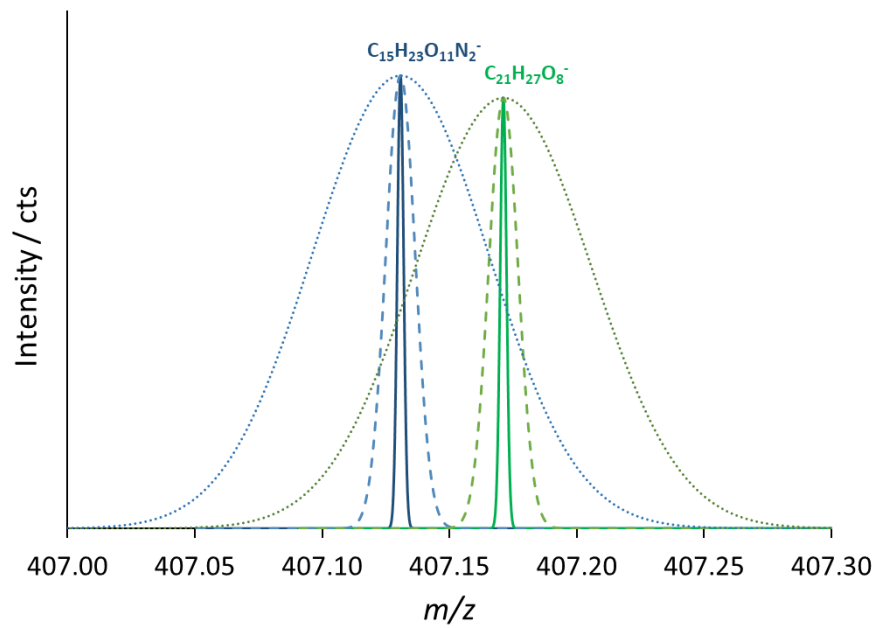


Figure 7.9 Simulated mass spectra of $C_{15}H_{23}O_{11}N_2^-$ (blue) and $C_{21}H_{27}O_8^-$ (green) at the Orbitrap resolving power of $R = 140\,000$ (bold lines), $R = 30\,000$ (dashed lines) and $R = 5\,000$ (dotted lines) illustrate the mass spectra of both compounds at a mass resolving power of $R = 5\,000$.

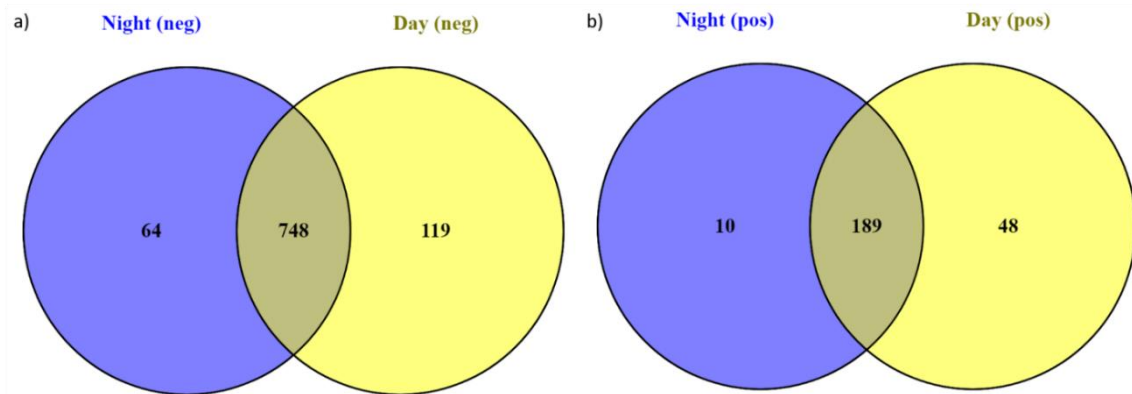


Figure 7.10 Venn Diagrams of the detected molecular formulas in negative ionization mode (a) and positive ionization mode (b) for night- and daytime (Oliveros, J.C. (2007 – 2015) *Venny. An interactive tool for comparing lists with Venn's diagrams*. <http://bioinfogp.cnb.csic.es/tools/venny/index.html>).

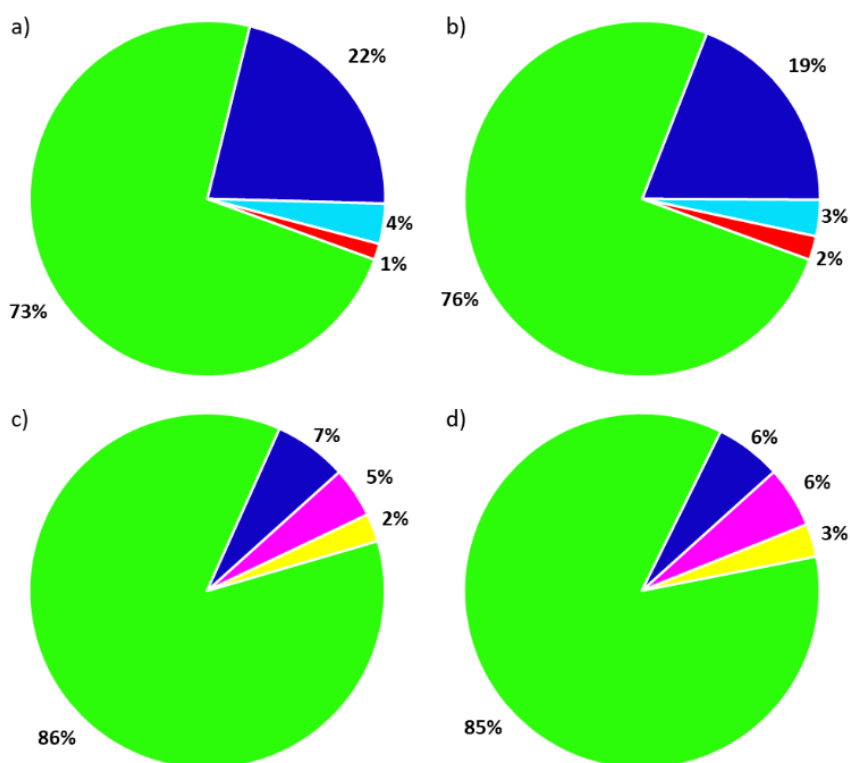


Figure 7.11 Pie Charts of the detected molecular formulas classes in negative ionization mode at night (a) and day (b) and positive ionization mode at night (c) and day (d). The colors correspond to the CHO (green), CHON (blue), CHOS (red), CHONS (cyan), CH (magenta) and CHN (yellow) formulas assignments.

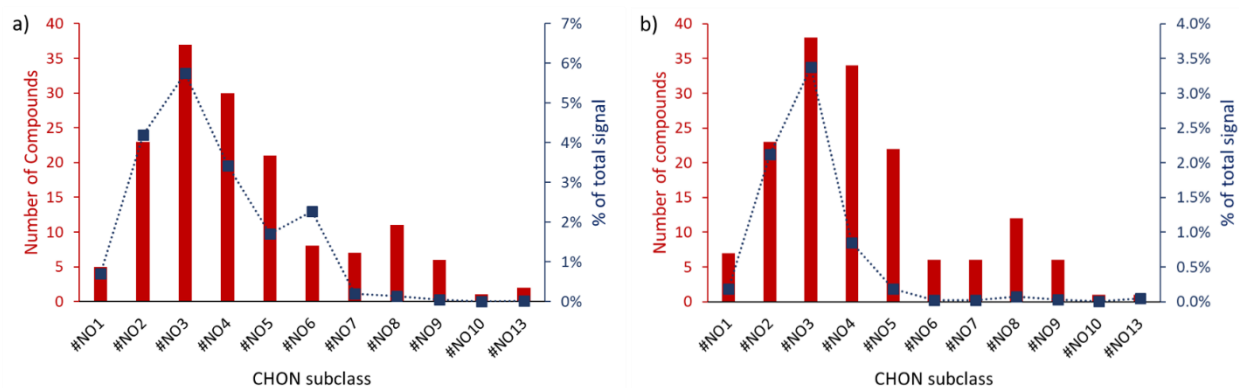


Figure 7.12 Number of compound distribution of the CHON-containing formulas (left axis) and intensity-weighted contribution of the corresponding O-containing subclass to the measured particulate organic aerosol (right axis) in the negative ionization mode at nighttime (a) and daytime (b). The contribution of organic nitrates is calculated to 14 % at night and 5 % at day.

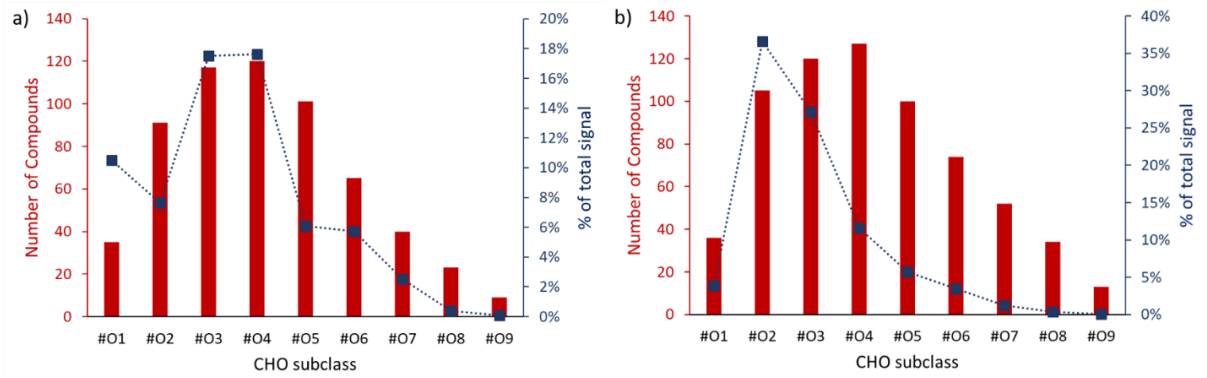


Figure 7.13 Number of compound distribution of the CHO-containing formulas (left axis) and intensity-weighted contribution of the corresponding O-containing subclass to the measured particulate organic aerosol (right axis) in the negative ionization mode at nighttime (a) and daytime (b).

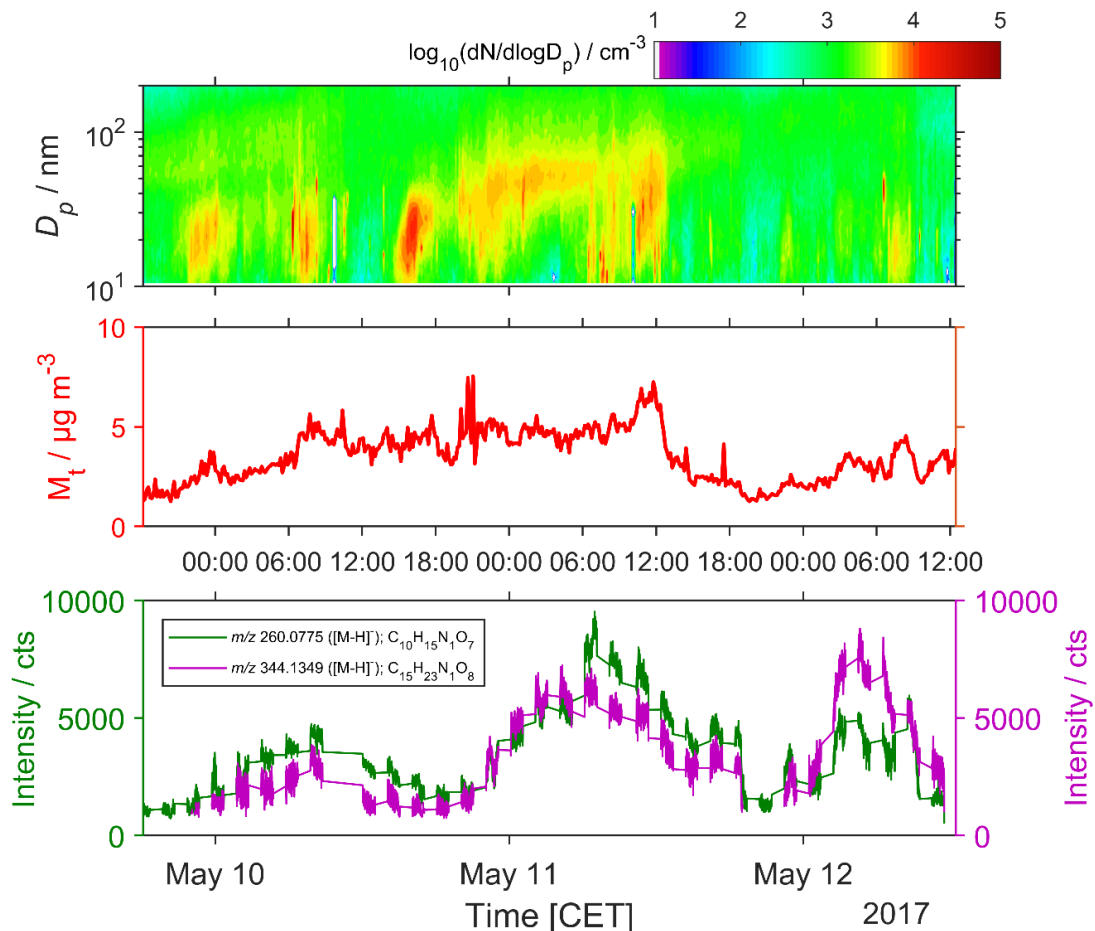


Figure 7.14 Temporal variation during the measurement period. (upper panel) $PM_{2.5}$ Particle Size distribution measured with an SMPS. The color keys relate to the number size distribution ($\log_{10}(dN/d\log D_p)/cm^{-3}$). (central panel) Aerosol mass concentration. (lower panel) Time traces of the deprotonated signals of $C_{10}H_{15}NO_7$ (m/z 260.0775, [M-H] $^-$) and $C_{15}H_{23}NO_8$ (m/z 344.1349, [M-H] $^-$).

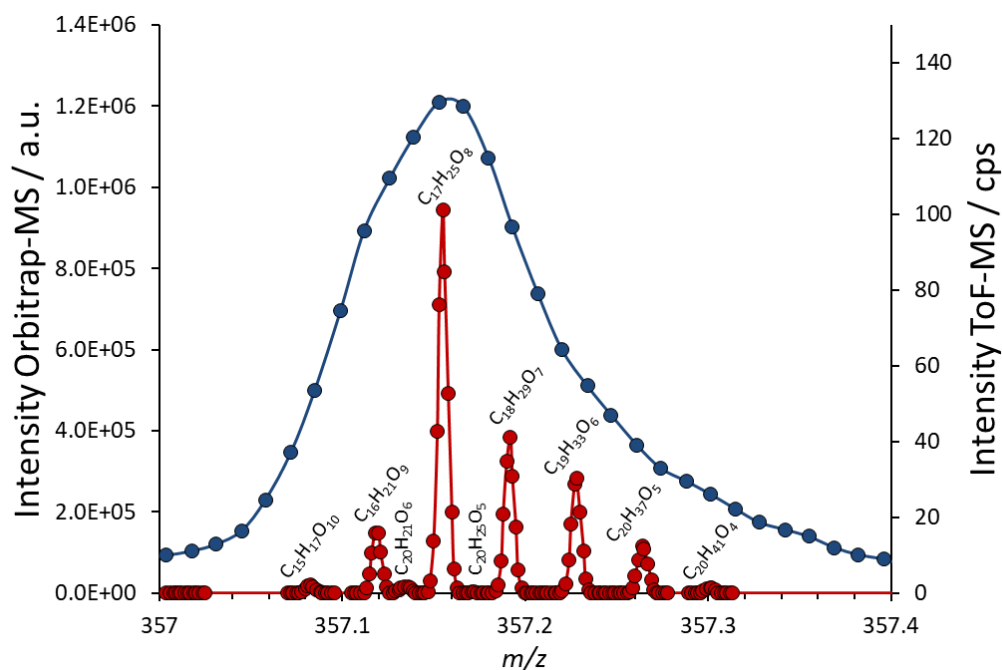


Figure 7.15 Mass spectra of the reaction of α -pinene with ozone obtained in the negative ionization mode by an Orbitrap-MS (red, $R \sim 70\,000$ @ m/z 400) and a ToF-CIMS (blue, $R \sim 4\,000$ @ m/z 400). The spectra shows an insight of the dimer-mode at the nominal mass of m/z 357. The Orbitrap-MS spectra clearly shows the signals hidden under a ToF-MS spectra.

Table 7.11 CHO-containing molecular formulas determined by APCI-Orbitrap-MS in negative ionization mode from 09 May – 12 May 2017.

measured m/z [M-H] ⁻	elemental composition	H/C	O/C	DBE	measured m/z [M-H] ⁻	elemental composition	H/C	O/C	DBE
87.0087	C ₃ H ₄ O ₃	1.33	1.00	2	237.0404	C ₁₁ H ₁₀ O ₆	0.91	0.55	7
89.0244	C ₃ H ₆ O ₃	2.00	1.00	1	237.0768	C ₁₂ H ₁₄ O ₅	1.17	0.42	6
99.0088	C ₄ H ₄ O ₃	1.00	0.75	3	237.1132	C ₁₃ H ₁₈ O ₄	1.38	0.31	5
100.9880	C ₃ H ₂ O ₄	0.67	1.33	3	237.1343	C ₁₀ H ₂₂ O ₆	2.20	0.60	0
101.0244	C ₄ H ₆ O ₃	1.50	0.75	2	237.1495	C ₁₄ H ₂₂ O ₃	1.57	0.21	4
103.0037	C ₃ H ₄ O ₄	1.33	1.33	2	237.1859	C ₁₅ H ₂₆ O ₂	1.73	0.13	3
103.0401	C ₄ H ₈ O ₃	2.00	0.75	1	239.0349	C ₁₄ H ₈ O ₄	0.57	0.29	11
105.0193	C ₃ H ₆ O ₄	2.00	1.33	1	239.0713	C ₁₅ H ₁₂ O ₃	0.80	0.20	10
111.0088	C ₅ H ₄ O ₃	0.80	0.60	4	239.0924	C ₁₂ H ₁₆ O ₅	1.33	0.42	5
112.9879	C ₄ H ₂ O ₄	0.50	1.00	4	239.1288	C ₁₃ H ₂₀ O ₄	1.54	0.31	4
113.0244	C ₅ H ₆ O ₃	1.20	0.60	3	239.1652	C ₁₄ H ₂₄ O ₃	1.71	0.21	3
115.0037	C ₄ H ₄ O ₄	1.00	1.00	3	239.2016	C ₁₅ H ₂₈ O ₂	1.87	0.13	2
115.0401	C ₅ H ₈ O ₃	1.60	0.60	2	241.0353	C ₁₀ H ₁₀ O ₇	1.00	0.70	6
117.0193	C ₄ H ₆ O ₄	1.50	1.00	2	241.0506	C ₁₄ H ₁₀ O ₄	0.71	0.29	10
117.0557	C ₅ H ₁₀ O ₃	2.00	0.60	1	241.0564	C ₇ H ₁₄ O ₉	2.00	1.29	1
119.0349	C ₄ H ₈ O ₄	2.00	1.00	1	241.0717	C ₁₁ H ₁₄ O ₆	1.27	0.55	5

119.0502	C ₈ H ₈ O ₁	1.00	0.13	5	241.0870	C ₁₅ H ₁₄ O ₃	0.93	0.20	9
121.0295	C ₇ H ₆ O ₂	0.86	0.29	5	241.1081	C ₁₂ H ₁₈ O ₅	1.50	0.42	4
121.0659	C ₈ H ₁₀ O ₁	1.25	0.13	4	241.1445	C ₁₃ H ₂₂ O ₄	1.69	0.31	3
123.0088	C ₆ H ₄ O ₃	0.67	0.50	5	241.1809	C ₁₄ H ₂₆ O ₃	1.86	0.21	2
123.0452	C ₇ H ₈ O ₂	1.14	0.29	4	241.2173	C ₁₅ H ₃₀ O ₂	2.00	0.13	1
123.0815	C ₈ H ₁₂ O ₁	1.50	0.13	3	243.0509	C ₁₀ H ₁₂ O ₇	1.20	0.70	5
125.0244	C ₆ H ₆ O ₃	1.00	0.50	4	243.0661	C ₁₄ H ₁₂ O ₄	0.86	0.29	9
125.0608	C ₇ H ₁₀ O ₂	1.43	0.29	3	243.0873	C ₁₁ H ₁₆ O ₆	1.45	0.55	4
125.0971	C ₈ H ₁₄ O ₁	1.75	0.13	2	243.1025	C ₁₅ H ₁₆ O ₃	1.07	0.20	8
127.0037	C ₅ H ₄ O ₄	0.80	0.80	4	243.1237	C ₁₂ H ₂₀ O ₅	1.67	0.42	3
127.0400	C ₆ H ₈ O ₃	1.33	0.50	3	243.1600	C ₁₃ H ₂₄ O ₄	1.85	0.31	2
127.0764	C ₇ H ₁₂ O ₂	1.71	0.29	2	243.1964	C ₁₄ H ₂₈ O ₃	2.00	0.21	1
127.1128	C ₈ H ₁₆ O ₁	2.00	0.13	1	245.0302	C ₉ H ₁₀ O ₈	1.11	0.89	5
129.0194	C ₅ H ₆ O ₄	1.20	0.80	3	245.0454	C ₁₃ H ₁₀ O ₅	0.77	0.38	9
129.0557	C ₆ H ₁₀ O ₃	1.67	0.50	2	245.0666	C ₁₀ H ₁₄ O ₇	1.40	0.70	4
129.0921	C ₇ H ₁₄ O ₂	2.00	0.29	1	245.0818	C ₁₄ H ₁₄ O ₄	1.00	0.29	8
130.9985	C ₄ H ₄ O ₅	1.00	1.25	3	245.1030	C ₁₁ H ₁₈ O ₆	1.64	0.55	3
131.0349	C ₅ H ₈ O ₄	1.60	0.80	2	245.1182	C ₁₅ H ₁₈ O ₃	1.20	0.20	7
131.0502	C ₉ H ₈ O ₁	0.89	0.11	6	245.1393	C ₁₂ H ₂₂ O ₅	1.83	0.42	2
131.0713	C ₆ H ₁₂ O ₃	2.00	0.50	1	245.1546	C ₁₆ H ₂₂ O ₂	1.38	0.13	6
133.0142	C ₄ H ₆ O ₅	1.50	1.25	2	247.0459	C ₉ H ₁₂ O ₈	1.33	0.89	4
133.0295	C ₈ H ₆ O ₂	0.75	0.25	6	247.0611	C ₁₃ H ₁₂ O ₅	0.92	0.38	8
133.0506	C ₅ H ₁₀ O ₄	2.00	0.80	1	247.0823	C ₁₀ H ₁₆ O ₇	1.60	0.70	3
133.0659	C ₉ H ₁₀ O ₁	1.11	0.11	5	247.0975	C ₁₄ H ₁₆ O ₄	1.14	0.29	7
135.0088	C ₇ H ₄ O ₃	0.57	0.43	6	247.1186	C ₁₁ H ₂₀ O ₆	1.82	0.55	2
135.0299	C ₄ H ₈ O ₅	2.00	1.25	1	247.1339	C ₁₅ H ₂₀ O ₃	1.33	0.20	6
135.0452	C ₈ H ₈ O ₂	1.00	0.25	5	247.1702	C ₁₆ H ₂₄ O ₂	1.50	0.13	5
135.0815	C ₉ H ₁₂ O ₁	1.33	0.11	4	249.0404	C ₁₂ H ₁₀ O ₆	0.83	0.50	8
137.0244	C ₇ H ₆ O ₃	0.86	0.43	5	249.0615	C ₉ H ₁₄ O ₈	1.56	0.89	3
137.0607	C ₈ H ₁₀ O ₂	1.25	0.25	4	249.0768	C ₁₃ H ₁₄ O ₅	1.08	0.38	7
137.0971	C ₉ H ₁₄ O ₁	1.56	0.11	3	249.1131	C ₁₄ H ₁₈ O ₄	1.29	0.29	6
139.0037	C ₆ H ₄ O ₄	0.67	0.67	5	249.1495	C ₁₅ H ₂₂ O ₃	1.47	0.20	5
139.0400	C ₇ H ₈ O ₃	1.14	0.43	4	249.1859	C ₁₆ H ₂₆ O ₂	1.63	0.13	4
139.0764	C ₈ H ₁₂ O ₂	1.50	0.25	3	251.0560	C ₁₂ H ₁₂ O ₆	1.00	0.50	7
139.1128	C ₉ H ₁₆ O ₁	1.78	0.11	2	251.0925	C ₁₃ H ₁₆ O ₅	1.23	0.38	6
141.0193	C ₆ H ₆ O ₄	1.00	0.67	4	251.1288	C ₁₄ H ₂₀ O ₄	1.43	0.29	5
141.0557	C ₇ H ₁₀ O ₃	1.43	0.43	3	251.1652	C ₁₅ H ₂₄ O ₃	1.60	0.20	4
141.0921	C ₈ H ₁₄ O ₂	1.75	0.25	2	251.2016	C ₁₆ H ₂₈ O ₂	1.75	0.13	3
141.1285	C ₉ H ₁₈ O ₁	2.00	0.11	1	253.0717	C ₁₂ H ₁₄ O ₆	1.17	0.50	6
142.9985	C ₅ H ₄ O ₅	0.80	1.00	4	253.0869	C ₁₆ H ₁₄ O ₃	0.88	0.19	10
143.0349	C ₆ H ₈ O ₄	1.33	0.67	3	253.1081	C ₁₃ H ₁₈ O ₅	1.38	0.38	5
143.0502	C ₁₀ H ₈ O ₁	0.80	0.10	7	253.1445	C ₁₄ H ₂₂ O ₄	1.57	0.29	4
143.0713	C ₇ H ₁₂ O ₃	1.71	0.43	2	253.1808	C ₁₅ H ₂₆ O ₃	1.73	0.20	3
143.1077	C ₈ H ₁₆ O ₂	2.00	0.25	1	253.2172	C ₁₆ H ₃₀ O ₂	1.88	0.13	2
145.0142	C ₅ H ₆ O ₅	1.20	1.00	3	255.0510	C ₁₁ H ₁₂ O ₇	1.09	0.64	6
145.0294	C ₉ H ₆ O ₂	0.67	0.22	7	255.0663	C ₁₅ H ₁₂ O ₄	0.80	0.27	10
145.0506	C ₆ H ₁₀ O ₄	1.67	0.67	2	255.0874	C ₁₂ H ₁₆ O ₆	1.33	0.50	5

7. Appendix

145.0658	C ₁₀ H ₁₀ O ₁	1.00	0.10	6	255.1026	C ₁₆ H ₁₆ O ₃	1.00	0.19	9
145.0870	C ₇ H ₁₄ O ₃	2.00	0.43	1	255.1238	C ₁₃ H ₂₀ O ₅	1.54	0.38	4
147.0087	C ₈ H ₄ O ₃	0.50	0.38	7	255.1602	C ₁₄ H ₂₄ O ₄	1.71	0.29	3
147.0299	C ₅ H ₈ O ₅	1.60	1.00	2	255.1966	C ₁₅ H ₂₈ O ₃	1.87	0.20	2
147.0451	C ₉ H ₈ O ₂	0.89	0.22	6	255.2329	C ₁₆ H ₃₂ O ₂	2.00	0.13	1
147.0662	C ₆ H ₁₂ O ₄	2.00	0.67	1	257.0302	C ₁₀ H ₁₀ O ₈	1.00	0.80	6
147.0815	C ₁₀ H ₁₂ O ₁	1.20	0.10	5	257.0666	C ₁₁ H ₁₄ O ₇	1.27	0.64	5
149.0093	C ₄ H ₆ O ₆	1.50	1.50	2	257.0819	C ₁₅ H ₁₄ O ₄	0.93	0.27	9
149.0243	C ₈ H ₆ O ₃	0.75	0.38	6	257.1030	C ₁₂ H ₁₈ O ₆	1.50	0.50	4
149.0455	C ₅ H ₁₀ O ₅	2.00	1.00	1	257.1183	C ₁₆ H ₁₈ O ₃	1.13	0.19	8
149.0607	C ₉ H ₁₀ O ₂	1.11	0.22	5	257.1394	C ₁₃ H ₂₂ O ₅	1.69	0.38	3
149.0971	C ₁₀ H ₁₄ O ₁	1.40	0.10	4	257.1758	C ₁₄ H ₂₆ O ₄	1.86	0.29	2
151.0037	C ₇ H ₄ O ₄	0.57	0.57	6	257.2121	C ₁₅ H ₃₀ O ₃	2.00	0.20	1
151.0400	C ₈ H ₈ O ₃	1.00	0.38	5	259.0459	C ₁₀ H ₁₂ O ₈	1.20	0.80	5
151.0764	C ₉ H ₁₂ O ₂	1.33	0.22	4	259.0610	C ₁₄ H ₁₂ O ₅	0.86	0.36	9
151.1128	C ₁₀ H ₁₆ O ₁	1.60	0.10	3	259.0822	C ₁₁ H ₁₆ O ₇	1.45	0.64	4
153.0193	C ₇ H ₆ O ₄	0.86	0.57	5	259.0975	C ₁₅ H ₁₆ O ₄	1.07	0.27	8
153.0557	C ₈ H ₁₀ O ₃	1.25	0.38	4	259.1186	C ₁₂ H ₂₀ O ₆	1.67	0.50	3
153.0921	C ₉ H ₁₄ O ₂	1.56	0.22	3	259.1338	C ₁₆ H ₂₀ O ₃	1.25	0.19	7
153.1284	C ₁₀ H ₁₈ O ₁	1.80	0.10	2	259.1550	C ₁₃ H ₂₄ O ₅	1.85	0.38	2
154.9986	C ₆ H ₄ O ₅	0.67	0.83	5	259.1702	C ₁₇ H ₂₄ O ₂	1.41	0.12	6
155.0350	C ₇ H ₈ O ₄	1.14	0.57	4	261.0614	C ₁₀ H ₁₄ O ₈	1.40	0.80	4
155.0714	C ₈ H ₁₂ O ₃	1.50	0.38	3	261.0768	C ₁₄ H ₁₄ O ₅	1.00	0.36	8
155.1077	C ₉ H ₁₆ O ₂	1.78	0.22	2	261.0978	C ₁₁ H ₁₈ O ₇	1.64	0.64	3
155.1441	C ₁₀ H ₂₀ O ₁	2.00	0.10	1	261.1132	C ₁₅ H ₁₈ O ₄	1.20	0.27	7
157.0142	C ₆ H ₆ O ₅	1.00	0.83	4	261.1343	C ₁₂ H ₂₂ O ₆	1.83	0.50	2
157.0506	C ₇ H ₁₀ O ₄	1.43	0.57	3	261.1495	C ₁₆ H ₂₂ O ₃	1.38	0.19	6
157.0658	C ₁₁ H ₁₀ O ₁	0.91	0.09	7	261.1857	C ₁₇ H ₂₆ O ₂	1.53	0.12	5
157.0870	C ₈ H ₁₄ O ₃	1.75	0.38	2	263.0560	C ₁₃ H ₁₂ O ₆	0.92	0.46	8
157.1233	C ₉ H ₁₈ O ₂	2.00	0.22	1	263.0772	C ₁₀ H ₁₆ O ₈	1.60	0.80	3
159.0298	C ₆ H ₈ O ₅	1.33	0.83	3	263.0924	C ₁₄ H ₁₆ O ₅	1.14	0.36	7
159.0451	C ₁₀ H ₈ O ₂	0.80	0.20	7	263.1287	C ₁₅ H ₂₀ O ₄	1.33	0.27	6
159.0662	C ₇ H ₁₂ O ₄	1.71	0.57	2	263.1652	C ₁₆ H ₂₄ O ₃	1.50	0.19	5
159.1026	C ₈ H ₁₆ O ₃	2.00	0.38	1	263.2015	C ₁₇ H ₂₈ O ₂	1.65	0.12	4
161.0091	C ₅ H ₆ O ₆	1.20	1.20	3	265.0717	C ₁₃ H ₁₄ O ₆	1.08	0.46	7
161.0244	C ₉ H ₆ O ₃	0.67	0.33	7	265.1081	C ₁₄ H ₁₈ O ₅	1.29	0.36	6
161.0455	C ₆ H ₁₀ O ₅	1.67	0.83	2	265.1444	C ₁₅ H ₂₂ O ₄	1.47	0.27	5
161.0607	C ₁₀ H ₁₀ O ₂	1.00	0.20	6	265.1808	C ₁₆ H ₂₆ O ₃	1.63	0.19	4
161.0819	C ₇ H ₁₄ O ₄	2.00	0.57	1	265.2172	C ₁₇ H ₃₀ O ₂	1.76	0.12	3
161.0971	C ₁₁ H ₁₄ O ₁	1.27	0.09	5	267.0509	C ₁₂ H ₁₂ O ₇	1.00	0.58	7
163.0037	C ₈ H ₄ O ₄	0.50	0.50	7	267.0662	C ₁₆ H ₁₂ O ₄	0.75	0.25	11
163.0248	C ₅ H ₈ O ₆	1.60	1.20	2	267.0873	C ₁₃ H ₁₆ O ₆	1.23	0.46	6
163.0401	C ₉ H ₈ O ₃	0.89	0.33	6	267.1026	C ₁₇ H ₁₆ O ₃	0.94	0.18	10
163.0613	C ₆ H ₁₂ O ₅	2.00	0.83	1	267.1237	C ₁₄ H ₂₀ O ₅	1.43	0.36	5
163.0764	C ₁₀ H ₁₂ O ₂	1.20	0.20	5	267.1601	C ₁₅ H ₂₄ O ₄	1.60	0.27	4
163.1128	C ₁₁ H ₁₆ O ₁	1.45	0.09	4	267.1965	C ₁₆ H ₂₈ O ₃	1.75	0.19	3
165.0193	C ₈ H ₆ O ₄	0.75	0.50	6	267.2329	C ₁₇ H ₃₂ O ₂	1.88	0.12	2

165.0408	C ₅ H ₁₀ O ₆	2.00	1.20	1	269.0667	C ₁₂ H ₁₄ O ₇	1.17	0.58	6
165.0556	C ₉ H ₁₀ O ₃	1.11	0.33	5	269.0819	C ₁₆ H ₁₄ O ₄	0.88	0.25	10
165.0920	C ₁₀ H ₁₄ O ₂	1.40	0.20	4	269.1030	C ₁₃ H ₁₈ O ₆	1.38	0.46	5
165.1284	C ₁₁ H ₁₈ O ₁	1.64	0.09	3	269.1394	C ₁₄ H ₂₂ O ₅	1.57	0.36	4
166.9983	C ₇ H ₄ O ₅	0.57	0.71	6	269.1758	C ₁₅ H ₂₆ O ₄	1.73	0.27	3
167.0200	C ₄ H ₈ O ₇	2.00	1.75	1	269.2122	C ₁₆ H ₃₀ O ₃	1.88	0.19	2
167.0349	C ₈ H ₈ O ₄	1.00	0.50	5	269.2486	C ₁₇ H ₃₄ O ₂	2.00	0.12	1
167.0713	C ₉ H ₁₂ O ₃	1.33	0.33	4	271.0459	C ₁₁ H ₁₂ O ₈	1.09	0.73	6
167.1077	C ₁₀ H ₁₆ O ₂	1.60	0.20	3	271.0822	C ₁₂ H ₁₆ O ₇	1.33	0.58	5
167.1440	C ₁₁ H ₂₀ O ₁	1.82	0.09	2	271.0975	C ₁₆ H ₁₆ O ₄	1.00	0.25	9
169.0142	C ₇ H ₆ O ₅	0.86	0.71	5	271.1187	C ₁₃ H ₂₀ O ₆	1.54	0.46	4
169.0506	C ₈ H ₁₀ O ₄	1.25	0.50	4	271.1551	C ₁₄ H ₂₄ O ₅	1.71	0.36	3
169.0658	C ₁₂ H ₁₀ O ₁	0.83	0.08	8	271.1915	C ₁₅ H ₂₈ O ₄	1.87	0.27	2
169.0870	C ₉ H ₁₄ O ₃	1.56	0.33	3	271.2278	C ₁₆ H ₃₂ O ₃	2.00	0.19	1
169.1233	C ₁₀ H ₁₈ O ₂	1.80	0.20	2	273.0615	C ₁₁ H ₁₄ O ₈	1.27	0.73	5
169.1597	C ₁₁ H ₂₂ O ₁	2.00	0.09	1	273.0768	C ₁₅ H ₁₄ O ₅	0.93	0.33	9
171.0299	C ₇ H ₈ O ₅	1.14	0.71	4	273.0979	C ₁₂ H ₁₈ O ₇	1.50	0.58	4
171.0452	C ₁₁ H ₈ O ₂	0.73	0.18	8	273.1132	C ₁₆ H ₁₈ O ₄	1.13	0.25	8
171.0663	C ₈ H ₁₂ O ₄	1.50	0.50	3	273.1343	C ₁₃ H ₂₂ O ₆	1.69	0.46	3
171.1026	C ₉ H ₁₆ O ₃	1.78	0.33	2	273.1707	C ₁₄ H ₂₆ O ₅	1.86	0.36	2
171.1390	C ₁₀ H ₂₀ O ₂	2.00	0.20	1	273.1859	C ₁₈ H ₂₆ O ₂	1.44	0.11	6
173.0090	C ₆ H ₆ O ₆	1.00	1.00	4	275.0409	C ₁₀ H ₁₂ O ₉	1.20	0.90	5
173.0243	C ₁₀ H ₆ O ₃	0.60	0.30	8	275.0773	C ₁₁ H ₁₆ O ₈	1.45	0.73	4
173.0454	C ₇ H ₁₀ O ₅	1.43	0.71	3	275.0925	C ₁₅ H ₁₆ O ₅	1.07	0.33	8
173.0606	C ₁₁ H ₁₀ O ₂	0.91	0.18	7	275.1137	C ₁₂ H ₂₀ O ₇	1.67	0.58	3
173.0818	C ₈ H ₁₄ O ₄	1.75	0.50	2	275.1289	C ₁₆ H ₂₀ O ₄	1.25	0.25	7
173.1182	C ₉ H ₁₈ O ₃	2.00	0.33	1	275.1653	C ₁₇ H ₂₄ O ₃	1.41	0.18	6
175.0247	C ₆ H ₈ O ₆	1.33	1.00	3	275.2016	C ₁₈ H ₂₈ O ₂	1.56	0.11	5
175.0400	C ₁₀ H ₈ O ₃	0.80	0.30	7	277.0716	C ₁₄ H ₁₄ O ₆	1.00	0.43	8
175.0611	C ₇ H ₁₂ O ₅	1.71	0.71	2	277.1079	C ₁₅ H ₁₈ O ₅	1.20	0.33	7
175.0764	C ₁₁ H ₁₂ O ₂	1.09	0.18	6	277.1443	C ₁₆ H ₂₂ O ₄	1.38	0.25	6
175.0975	C ₈ H ₁₆ O ₄	2.00	0.50	1	277.1808	C ₁₇ H ₂₆ O ₃	1.53	0.18	5
175.1128	C ₁₂ H ₁₆ O ₁	1.33	0.08	5	277.2170	C ₁₈ H ₃₀ O ₂	1.67	0.11	4
177.0193	C ₉ H ₆ O ₄	0.67	0.44	7	279.0872	C ₁₄ H ₁₆ O ₆	1.14	0.43	7
177.0404	C ₆ H ₁₀ O ₆	1.67	1.00	2	279.1237	C ₁₅ H ₂₀ O ₅	1.33	0.33	6
177.0556	C ₁₀ H ₁₀ O ₃	1.00	0.30	6	279.1600	C ₁₆ H ₂₄ O ₄	1.50	0.25	5
177.0920	C ₁₁ H ₁₄ O ₂	1.27	0.18	5	279.1964	C ₁₇ H ₂₈ O ₃	1.65	0.18	4
177.1284	C ₁₂ H ₁₈ O ₁	1.50	0.08	4	279.2328	C ₁₈ H ₃₂ O ₂	1.78	0.11	3
178.9986	C ₈ H ₄ O ₅	0.50	0.63	7	281.0666	C ₁₃ H ₁₄ O ₇	1.08	0.54	7
179.0350	C ₉ H ₈ O ₄	0.89	0.44	6	281.1029	C ₁₄ H ₁₈ O ₆	1.29	0.43	6
179.0561	C ₆ H ₁₂ O ₆	2.00	1.00	1	281.1393	C ₁₅ H ₂₂ O ₅	1.47	0.33	5
179.0713	C ₁₀ H ₁₂ O ₃	1.20	0.30	5	281.1605	C ₁₂ H ₂₆ O ₇	2.17	0.58	0
179.1077	C ₁₁ H ₁₆ O ₂	1.45	0.18	4	281.1756	C ₁₆ H ₂₆ O ₄	1.63	0.25	4
179.1441	C ₁₂ H ₂₀ O ₁	1.67	0.08	3	281.2121	C ₁₇ H ₃₀ O ₃	1.76	0.18	3
181.0142	C ₈ H ₆ O ₅	0.75	0.63	6	281.2484	C ₁₈ H ₃₄ O ₂	1.89	0.11	2
181.0506	C ₉ H ₁₀ O ₄	1.11	0.44	5	283.0610	C ₁₆ H ₁₂ O ₅	0.75	0.31	11
181.0870	C ₁₀ H ₁₄ O ₃	1.40	0.30	4	283.0822	C ₁₃ H ₁₆ O ₇	1.23	0.54	6

7. Appendix

181.1234	C ₁₁ H ₁₈ O ₂	1.64	0.18	3	283.0974	C ₁₇ H ₁₆ O ₄	0.94	0.24	10
181.1598	C ₁₂ H ₂₂ O ₁	1.83	0.08	2	283.1186	C ₁₄ H ₂₀ O ₆	1.43	0.43	5
183.0298	C ₈ H ₈ O ₅	1.00	0.63	5	283.1550	C ₁₅ H ₂₄ O ₅	1.60	0.33	4
183.0662	C ₉ H ₁₂ O ₄	1.33	0.44	4	283.1913	C ₁₆ H ₂₈ O ₄	1.75	0.25	3
183.1025	C ₁₀ H ₁₆ O ₃	1.60	0.30	3	283.2277	C ₁₇ H ₃₂ O ₃	1.88	0.18	2
183.1389	C ₁₁ H ₂₀ O ₂	1.82	0.18	2	283.2642	C ₁₈ H ₃₆ O ₂	2.00	0.11	1
183.1753	C ₁₂ H ₂₄ O ₁	2.00	0.08	1	285.0614	C ₁₂ H ₁₄ O ₈	1.17	0.67	6
185.0091	C ₇ H ₆ O ₆	0.86	0.86	5	285.0767	C ₁₆ H ₁₄ O ₅	0.88	0.31	10
185.0455	C ₈ H ₁₀ O ₅	1.25	0.63	4	285.0978	C ₁₃ H ₁₈ O ₇	1.38	0.54	5
185.0607	C ₁₂ H ₁₀ O ₂	0.83	0.17	8	285.1131	C ₁₇ H ₁₈ O ₄	1.06	0.24	9
185.0819	C ₉ H ₁₄ O ₄	1.56	0.44	3	285.1342	C ₁₄ H ₂₂ O ₆	1.57	0.43	4
185.1182	C ₁₀ H ₁₈ O ₃	1.80	0.30	2	285.1706	C ₁₅ H ₂₆ O ₅	1.73	0.33	3
185.1546	C ₁₁ H ₂₂ O ₂	2.00	0.18	1	285.2070	C ₁₆ H ₃₀ O ₄	1.88	0.25	2
187.0247	C ₇ H ₈ O ₆	1.14	0.86	4	287.0408	C ₁₁ H ₁₂ O ₉	1.09	0.82	6
187.0400	C ₁₁ H ₈ O ₃	0.73	0.27	8	287.0771	C ₁₂ H ₁₆ O ₈	1.33	0.67	5
187.0611	C ₈ H ₁₂ O ₅	1.50	0.63	3	287.0923	C ₁₆ H ₁₆ O ₅	1.00	0.31	9
187.0764	C ₁₂ H ₁₂ O ₂	1.00	0.17	7	287.1135	C ₁₃ H ₂₀ O ₇	1.54	0.54	4
187.0975	C ₉ H ₁₆ O ₄	1.78	0.44	2	287.1287	C ₁₇ H ₂₀ O ₄	1.18	0.24	8
187.1339	C ₁₀ H ₂₀ O ₃	2.00	0.30	1	287.1498	C ₁₄ H ₂₄ O ₆	1.71	0.43	3
189.0040	C ₆ H ₆ O ₇	1.00	1.17	4	287.1863	C ₁₅ H ₂₈ O ₅	1.87	0.33	2
189.0193	C ₁₀ H ₆ O ₄	0.60	0.40	8	287.2227	C ₁₆ H ₃₂ O ₄	2.00	0.25	1
189.0404	C ₇ H ₁₀ O ₆	1.43	0.86	3	289.0564	C ₁₁ H ₁₄ O ₉	1.27	0.82	5
189.0557	C ₁₁ H ₁₀ O ₃	0.91	0.27	7	289.0928	C ₁₂ H ₁₈ O ₈	1.50	0.67	4
189.0768	C ₈ H ₁₄ O ₅	1.75	0.63	2	289.1080	C ₁₆ H ₁₈ O ₅	1.13	0.31	8
189.0920	C ₁₂ H ₁₄ O ₂	1.17	0.17	6	289.1292	C ₁₃ H ₂₂ O ₇	1.69	0.54	3
189.1131	C ₉ H ₁₈ O ₄	2.00	0.44	1	289.1808	C ₁₈ H ₂₆ O ₃	1.44	0.17	6
190.9986	C ₉ H ₄ O ₅	0.44	0.56	8	291.1237	C ₁₆ H ₂₀ O ₅	1.25	0.31	7
191.0197	C ₆ H ₈ O ₇	1.33	1.17	3	291.1601	C ₁₇ H ₂₄ O ₄	1.41	0.24	6
191.0349	C ₁₀ H ₈ O ₄	0.80	0.40	7	291.1965	C ₁₈ H ₂₈ O ₃	1.56	0.17	5
191.0561	C ₇ H ₁₂ O ₆	1.71	0.86	2	293.1030	C ₁₅ H ₁₈ O ₆	1.20	0.40	7
191.0713	C ₁₁ H ₁₂ O ₃	1.09	0.27	6	293.1394	C ₁₆ H ₂₂ O ₅	1.38	0.31	6
191.1077	C ₁₂ H ₁₆ O ₂	1.33	0.17	5	293.1758	C ₁₇ H ₂₆ O ₄	1.53	0.24	5
193.0141	C ₉ H ₆ O ₅	0.67	0.56	7	293.2121	C ₁₈ H ₃₀ O ₃	1.67	0.17	4
193.0353	C ₆ H ₁₀ O ₇	1.67	1.17	2	293.2484	C ₁₉ H ₃₄ O ₂	1.79	0.11	3
193.0505	C ₁₀ H ₁₀ O ₄	1.00	0.40	6	295.0821	C ₁₄ H ₁₆ O ₇	1.14	0.50	7
193.0869	C ₁₁ H ₁₄ O ₃	1.27	0.27	5	295.0973	C ₁₈ H ₁₆ O ₄	0.89	0.22	11
193.1233	C ₁₂ H ₁₈ O ₂	1.50	0.17	4	295.1184	C ₁₅ H ₂₀ O ₆	1.33	0.40	6
195.0298	C ₉ H ₈ O ₅	0.89	0.56	6	295.1548	C ₁₆ H ₂₄ O ₅	1.50	0.31	5
195.0662	C ₁₀ H ₁₂ O ₄	1.20	0.40	5	295.1911	C ₁₇ H ₂₈ O ₄	1.65	0.24	4
195.1026	C ₁₁ H ₁₆ O ₃	1.45	0.27	4	295.2275	C ₁₈ H ₃₂ O ₃	1.78	0.17	3
195.1389	C ₁₂ H ₂₀ O ₂	1.67	0.17	3	295.2639	C ₁₉ H ₃₆ O ₂	1.89	0.11	2
197.0091	C ₈ H ₆ O ₆	0.75	0.75	6	297.0977	C ₁₄ H ₁₈ O ₇	1.29	0.50	6
197.0455	C ₉ H ₁₀ O ₅	1.11	0.56	5	297.1129	C ₁₈ H ₁₈ O ₄	1.00	0.22	10
197.0607	C ₁₃ H ₁₀ O ₂	0.77	0.15	9	297.1341	C ₁₅ H ₂₂ O ₆	1.47	0.40	5
197.0819	C ₁₀ H ₁₄ O ₄	1.40	0.40	4	297.1705	C ₁₆ H ₂₆ O ₅	1.63	0.31	4
197.1182	C ₁₁ H ₁₈ O ₃	1.64	0.27	3	297.1857	C ₂₀ H ₂₆ O ₂	1.30	0.10	8
197.1546	C ₁₂ H ₂₂ O ₂	1.83	0.17	2	297.2069	C ₁₇ H ₃₀ O ₄	1.76	0.24	3

197.1910	C ₁₃ H ₂₆ O ₁	2.00	0.08	1	297.2432	C ₁₈ H ₃₄ O ₃	1.89	0.17	2
199.0247	C ₈ H ₈ O ₆	1.00	0.75	5	297.2796	C ₁₉ H ₃₈ O ₂	2.00	0.11	1
199.0400	C ₁₂ H ₈ O ₃	0.67	0.25	9	299.0770	C ₁₃ H ₁₆ O ₈	1.23	0.62	6
199.0612	C ₉ H ₁₂ O ₅	1.33	0.56	4	299.0922	C ₁₇ H ₁₆ O ₅	0.94	0.29	10
199.0976	C ₁₀ H ₁₆ O ₄	1.60	0.40	3	299.1133	C ₁₄ H ₂₀ O ₇	1.43	0.50	5
199.1339	C ₁₁ H ₂₀ O ₃	1.82	0.27	2	299.1497	C ₁₅ H ₂₄ O ₆	1.60	0.40	4
199.1703	C ₁₂ H ₂₄ O ₂	2.00	0.17	1	299.1861	C ₁₆ H ₂₈ O ₅	1.75	0.31	3
201.0193	C ₁₁ H ₆ O ₄	0.55	0.36	9	299.2013	C ₂₀ H ₂₈ O ₂	1.40	0.10	7
201.0404	C ₈ H ₁₀ O ₆	1.25	0.75	4	299.2225	C ₁₇ H ₃₂ O ₄	1.88	0.24	2
201.0556	C ₁₂ H ₁₀ O ₃	0.83	0.25	8	299.2589	C ₁₈ H ₃₆ O ₃	2.00	0.17	1
201.0768	C ₉ H ₁₄ O ₅	1.56	0.56	3	301.0563	C ₁₂ H ₁₄ O ₉	1.17	0.75	6
201.0920	C ₁₃ H ₁₄ O ₂	1.08	0.15	7	301.0926	C ₁₃ H ₁₈ O ₈	1.38	0.62	5
201.1132	C ₁₀ H ₁₈ O ₄	1.80	0.40	2	301.1079	C ₁₇ H ₁₈ O ₅	1.06	0.29	9
201.1495	C ₁₁ H ₂₂ O ₃	2.00	0.27	1	301.1290	C ₁₄ H ₂₂ O ₇	1.57	0.50	4
201.1860	C ₁₂ H ₂₆ O ₂	2.17	0.17	0	301.1654	C ₁₅ H ₂₆ O ₆	1.73	0.40	3
203.0197	C ₇ H ₈ O ₇	1.14	1.00	4	301.2018	C ₁₆ H ₃₀ O ₅	1.88	0.31	2
203.0349	C ₁₁ H ₈ O ₄	0.73	0.36	8	301.2170	C ₂₀ H ₃₀ O ₂	1.50	0.10	6
203.0561	C ₈ H ₁₂ O ₆	1.50	0.75	3	301.2382	C ₁₇ H ₃₄ O ₄	2.00	0.24	1
203.0713	C ₁₂ H ₁₂ O ₃	1.00	0.25	7	303.0719	C ₁₂ H ₁₆ O ₉	1.33	0.75	5
203.0924	C ₉ H ₁₆ O ₅	1.78	0.56	2	303.1083	C ₁₃ H ₂₀ O ₈	1.54	0.62	4
203.1077	C ₁₃ H ₁₆ O ₂	1.23	0.15	6	303.1236	C ₁₇ H ₂₀ O ₅	1.18	0.29	8
203.1288	C ₁₀ H ₂₀ O ₄	2.00	0.40	1	303.1447	C ₁₄ H ₂₄ O ₇	1.71	0.50	3
205.0141	C ₁₀ H ₆ O ₅	0.60	0.50	8	303.2326	C ₂₀ H ₃₂ O ₂	1.60	0.10	5
205.0353	C ₇ H ₁₀ O ₇	1.43	1.00	3	305.1756	C ₁₈ H ₂₆ O ₄	1.44	0.22	6
205.0505	C ₁₁ H ₁₀ O ₄	0.91	0.36	7	305.2482	C ₂₀ H ₃₄ O ₂	1.70	0.10	4
205.0716	C ₈ H ₁₄ O ₆	1.75	0.75	2	307.1185	C ₁₆ H ₂₀ O ₆	1.25	0.38	7
205.0869	C ₁₂ H ₁₄ O ₃	1.17	0.25	6	307.1549	C ₁₇ H ₂₄ O ₅	1.41	0.29	6
205.1080	C ₉ H ₁₈ O ₅	2.00	0.56	1	307.1912	C ₁₈ H ₂₈ O ₄	1.56	0.22	5
205.1233	C ₁₃ H ₁₈ O ₂	1.38	0.15	5	307.2276	C ₁₉ H ₃₂ O ₃	1.68	0.16	4
205.1596	C ₁₄ H ₂₂ O ₁	1.57	0.07	4	307.2639	C ₂₀ H ₃₆ O ₂	1.80	0.10	3
207.0298	C ₁₀ H ₈ O ₅	0.80	0.50	7	309.0978	C ₁₅ H ₁₈ O ₇	1.20	0.47	7
207.0509	C ₇ H ₁₂ O ₇	1.71	1.00	2	309.1341	C ₁₆ H ₂₂ O ₆	1.38	0.38	6
207.0662	C ₁₁ H ₁₂ O ₄	1.09	0.36	6	309.1705	C ₁₇ H ₂₆ O ₅	1.53	0.29	5
207.1026	C ₁₂ H ₁₆ O ₃	1.33	0.25	5	309.1858	C ₂₁ H ₂₆ O ₂	1.24	0.10	9
207.1389	C ₁₃ H ₂₀ O ₂	1.54	0.15	4	309.2069	C ₁₈ H ₃₀ O ₄	1.67	0.22	4
209.0091	C ₉ H ₆ O ₆	0.67	0.67	7	309.2432	C ₁₉ H ₃₄ O ₃	1.79	0.16	3
209.0455	C ₁₀ H ₁₀ O ₅	1.00	0.50	6	309.2797	C ₂₀ H ₃₈ O ₂	1.90	0.10	2
209.0819	C ₁₁ H ₁₄ O ₄	1.27	0.36	5	311.0770	C ₁₄ H ₁₆ O ₈	1.14	0.57	7
209.1182	C ₁₂ H ₁₈ O ₃	1.50	0.25	4	311.0923	C ₁₈ H ₁₆ O ₅	0.89	0.28	11
209.1546	C ₁₃ H ₂₂ O ₂	1.69	0.15	3	311.1134	C ₁₅ H ₂₀ O ₇	1.33	0.47	6
211.0247	C ₉ H ₈ O ₆	0.89	0.67	6	311.1286	C ₁₉ H ₂₀ O ₄	1.05	0.21	10
211.0400	C ₁₃ H ₈ O ₃	0.62	0.23	10	311.1498	C ₁₆ H ₂₄ O ₆	1.50	0.38	5
211.0611	C ₁₀ H ₁₂ O ₅	1.20	0.50	5	311.1862	C ₁₇ H ₂₈ O ₅	1.65	0.29	4
211.0764	C ₁₄ H ₁₂ O ₂	0.86	0.14	9	311.2014	C ₂₁ H ₂₈ O ₂	1.33	0.10	8
211.0975	C ₁₁ H ₁₆ O ₄	1.45	0.36	4	311.2225	C ₁₈ H ₃₂ O ₄	1.78	0.22	3
211.1339	C ₁₂ H ₂₀ O ₃	1.67	0.25	3	311.2590	C ₁₉ H ₃₆ O ₃	1.89	0.16	2
211.1703	C ₁₃ H ₂₄ O ₂	1.85	0.15	2	311.2953	C ₂₀ H ₄₀ O ₂	2.00	0.10	1

7. Appendix

211.2066	C ₁₄ H ₂₈ O ₁	2.00	0.07	1	313.0927	C ₁₄ H ₁₈ O ₈	1.29	0.57	6
213.0193	C ₁₂ H ₆ O ₄	0.50	0.33	10	313.1079	C ₁₈ H ₁₈ O ₅	1.00	0.28	10
213.0405	C ₉ H ₁₀ O ₆	1.11	0.67	5	313.1291	C ₁₅ H ₂₂ O ₇	1.47	0.47	5
213.0557	C ₁₃ H ₁₀ O ₃	0.77	0.23	9	313.1655	C ₁₆ H ₂₆ O ₆	1.63	0.38	4
213.0767	C ₁₀ H ₁₄ O ₅	1.40	0.50	4	313.1807	C ₂₀ H ₂₆ O ₃	1.30	0.15	8
213.1132	C ₁₁ H ₁₈ O ₄	1.64	0.36	3	313.2019	C ₁₇ H ₃₀ O ₅	1.76	0.29	3
213.1496	C ₁₂ H ₂₂ O ₃	1.83	0.25	2	313.2171	C ₂₁ H ₃₀ O ₂	1.43	0.10	7
213.1860	C ₁₃ H ₂₆ O ₂	2.00	0.15	1	313.2382	C ₁₈ H ₃₄ O ₄	1.89	0.22	2
215.0196	C ₈ H ₈ O ₇	1.00	0.88	5	315.0720	C ₁₃ H ₁₆ O ₉	1.23	0.69	6
215.0349	C ₁₂ H ₈ O ₄	0.67	0.33	9	315.1084	C ₁₄ H ₂₀ O ₈	1.43	0.57	5
215.0561	C ₉ H ₁₂ O ₆	1.33	0.67	4	315.1447	C ₁₅ H ₂₄ O ₇	1.60	0.47	4
215.0713	C ₁₃ H ₁₂ O ₃	0.92	0.23	8	315.1811	C ₁₆ H ₂₈ O ₆	1.75	0.38	3
215.0925	C ₁₀ H ₁₆ O ₅	1.60	0.50	3	315.1963	C ₂₀ H ₂₈ O ₃	1.40	0.15	7
215.1287	C ₁₁ H ₂₀ O ₄	1.82	0.36	2	315.2537	C ₁₈ H ₃₆ O ₄	2.00	0.22	1
215.1651	C ₁₂ H ₂₄ O ₃	2.00	0.25	1	317.0876	C ₁₃ H ₁₈ O ₉	1.38	0.69	5
217.0140	C ₁₁ H ₆ O ₅	0.55	0.45	9	317.1240	C ₁₄ H ₂₂ O ₈	1.57	0.57	4
217.0352	C ₈ H ₁₀ O ₇	1.25	0.88	4	317.2120	C ₂₀ H ₃₀ O ₃	1.50	0.15	6
217.0505	C ₁₂ H ₁₀ O ₄	0.83	0.33	8	321.1705	C ₁₈ H ₂₆ O ₅	1.44	0.28	6
217.0716	C ₉ H ₁₄ O ₆	1.56	0.67	3	321.2069	C ₁₉ H ₃₀ O ₄	1.58	0.21	5
217.0869	C ₁₃ H ₁₄ O ₃	1.08	0.23	7	321.2433	C ₂₀ H ₃₄ O ₃	1.70	0.15	4
217.1080	C ₁₀ H ₁₈ O ₅	1.80	0.50	2	321.2796	C ₂₁ H ₃₈ O ₂	1.81	0.10	3
217.1232	C ₁₄ H ₁₈ O ₂	1.29	0.14	6	323.1134	C ₁₆ H ₂₀ O ₇	1.25	0.44	7
217.1444	C ₁₁ H ₂₂ O ₄	2.00	0.36	1	323.1498	C ₁₇ H ₂₄ O ₆	1.41	0.35	6
219.0145	C ₇ H ₈ O ₈	1.14	1.14	4	323.1861	C ₁₈ H ₂₈ O ₅	1.56	0.28	5
219.0298	C ₁₁ H ₈ O ₅	0.73	0.45	8	323.2225	C ₁₉ H ₃₂ O ₄	1.68	0.21	4
219.0509	C ₈ H ₁₂ O ₇	1.50	0.88	3	323.2589	C ₂₀ H ₃₆ O ₃	1.80	0.15	3
219.0662	C ₁₂ H ₁₂ O ₄	1.00	0.33	7	325.0927	C ₁₅ H ₁₈ O ₈	1.20	0.53	7
219.0873	C ₉ H ₁₆ O ₆	1.78	0.67	2	325.1290	C ₁₆ H ₂₂ O ₇	1.38	0.44	6
219.1026	C ₁₃ H ₁₆ O ₃	1.23	0.23	6	325.1654	C ₁₇ H ₂₆ O ₆	1.53	0.35	5
219.1237	C ₁₀ H ₂₀ O ₅	2.00	0.50	1	325.1866	C ₁₄ H ₃₀ O ₈	2.14	0.57	0
219.1389	C ₁₄ H ₂₀ O ₂	1.43	0.14	5	325.2018	C ₁₈ H ₃₀ O ₅	1.67	0.28	4
219.1753	C ₁₅ H ₂₄ O ₁	1.60	0.07	4	325.2382	C ₁₉ H ₃₄ O ₄	1.79	0.21	3
221.0454	C ₁₁ H ₁₀ O ₅	0.91	0.45	7	325.2746	C ₂₀ H ₃₈ O ₃	1.90	0.15	2
221.0666	C ₈ H ₁₄ O ₇	1.75	0.88	2	325.3110	C ₂₁ H ₄₂ O ₂	2.00	0.10	1
221.0818	C ₁₂ H ₁₄ O ₄	1.17	0.33	6	327.1084	C ₁₅ H ₂₀ O ₈	1.33	0.53	6
221.1182	C ₁₃ H ₁₈ O ₃	1.38	0.23	5	327.1447	C ₁₆ H ₂₄ O ₇	1.50	0.44	5
221.1543	C ₁₄ H ₂₂ O ₂	1.57	0.14	4	327.1811	C ₁₇ H ₂₈ O ₆	1.65	0.35	4
223.0399	C ₁₄ H ₈ O ₃	0.57	0.21	11	327.2175	C ₁₈ H ₃₂ O ₅	1.78	0.28	3
223.0611	C ₁₁ H ₁₂ O ₅	1.09	0.45	6	327.2538	C ₁₉ H ₃₆ O ₄	1.89	0.21	2
223.0763	C ₁₅ H ₁₂ O ₂	0.80	0.13	10	329.0876	C ₁₄ H ₁₈ O ₉	1.29	0.64	6
223.0975	C ₁₂ H ₁₆ O ₄	1.33	0.33	5	329.1240	C ₁₅ H ₂₂ O ₈	1.47	0.53	5
223.1339	C ₁₃ H ₂₀ O ₃	1.54	0.23	4	329.1604	C ₁₆ H ₂₆ O ₇	1.63	0.44	4
223.1703	C ₁₄ H ₂₄ O ₂	1.71	0.14	3	329.2331	C ₁₈ H ₃₄ O ₅	1.89	0.28	2
225.0404	C ₁₀ H ₁₀ O ₆	1.00	0.60	6	331.1033	C ₁₄ H ₂₀ O ₉	1.43	0.64	5
225.0557	C ₁₄ H ₁₀ O ₃	0.71	0.21	10	331.1397	C ₁₅ H ₂₄ O ₈	1.60	0.53	4
225.0768	C ₁₁ H ₁₄ O ₅	1.27	0.45	5	331.1913	C ₂₀ H ₂₈ O ₄	1.40	0.20	7
225.0920	C ₁₅ H ₁₄ O ₂	0.93	0.13	9	333.2069	C ₂₀ H ₃₀ O ₄	1.50	0.20	6

225.1132	C ₁₂ H ₁₈ O ₄	1.50	0.33	4	333.2433	C ₂₁ H ₃₄ O ₃	1.62	0.14	5
225.1495	C ₁₃ H ₂₂ O ₃	1.69	0.23	3	335.1862	C ₁₉ H ₂₈ O ₅	1.47	0.26	6
225.1859	C ₁₄ H ₂₆ O ₂	1.86	0.14	2	335.2226	C ₂₀ H ₃₂ O ₄	1.60	0.20	5
225.2223	C ₁₅ H ₃₀ O ₁	2.00	0.07	1	335.2589	C ₂₁ H ₃₆ O ₃	1.71	0.14	4
227.0196	C ₉ H ₈ O ₇	0.89	0.78	6	337.1655	C ₁₈ H ₂₆ O ₆	1.44	0.33	6
227.0349	C ₁₃ H ₈ O ₄	0.62	0.31	10	337.2019	C ₁₉ H ₃₀ O ₅	1.58	0.26	5
227.0561	C ₁₀ H ₁₂ O ₆	1.20	0.60	5	337.2382	C ₂₀ H ₃₄ O ₄	1.70	0.20	4
227.0713	C ₁₄ H ₁₂ O ₃	0.86	0.21	9	337.2746	C ₂₁ H ₃₈ O ₃	1.81	0.14	3
227.0924	C ₁₁ H ₁₆ O ₅	1.45	0.45	4	337.3110	C ₂₂ H ₄₂ O ₂	1.91	0.09	2
227.1288	C ₁₂ H ₂₀ O ₄	1.67	0.33	3	339.1447	C ₁₇ H ₂₄ O ₇	1.41	0.41	6
227.1652	C ₁₃ H ₂₄ O ₃	1.85	0.23	2	339.1811	C ₁₈ H ₂₈ O ₆	1.56	0.33	5
227.2016	C ₁₄ H ₂₈ O ₂	2.00	0.14	1	339.2174	C ₁₉ H ₃₂ O ₅	1.68	0.26	4
229.0352	C ₉ H ₁₀ O ₇	1.11	0.78	5	339.2538	C ₂₀ H ₃₆ O ₄	1.80	0.20	3
229.0505	C ₁₃ H ₁₀ O ₄	0.77	0.31	9	339.3266	C ₂₂ H ₄₄ O ₂	2.00	0.09	1
229.0716	C ₁₀ H ₁₄ O ₆	1.40	0.60	4	341.1239	C ₁₆ H ₂₂ O ₈	1.38	0.50	6
229.0869	C ₁₄ H ₁₄ O ₃	1.00	0.21	8	341.1603	C ₁₇ H ₂₆ O ₇	1.53	0.41	5
229.1080	C ₁₁ H ₁₈ O ₅	1.64	0.45	3	341.1967	C ₁₈ H ₃₀ O ₆	1.67	0.33	4
229.1444	C ₁₂ H ₂₂ O ₄	1.83	0.33	2	343.1032	C ₁₅ H ₂₀ O ₉	1.33	0.60	6
229.1596	C ₁₆ H ₂₂ O ₁	1.38	0.06	6	343.1396	C ₁₆ H ₂₄ O ₈	1.50	0.50	5
229.1808	C ₁₃ H ₂₆ O ₃	2.00	0.23	1	343.1548	C ₂₀ H ₂₄ O ₅	1.20	0.25	9
231.0145	C ₈ H ₈ O ₈	1.00	1.00	5	343.2123	C ₁₈ H ₃₂ O ₆	1.78	0.33	3
231.0298	C ₁₂ H ₈ O ₅	0.67	0.42	9	345.1189	C ₁₅ H ₂₂ O ₉	1.47	0.60	5
231.0509	C ₉ H ₁₂ O ₇	1.33	0.78	4	349.2018	C ₂₀ H ₃₀ O ₅	1.50	0.25	6
231.0662	C ₁₃ H ₁₂ O ₄	0.92	0.31	8	349.2382	C ₂₁ H ₃₄ O ₄	1.62	0.19	5
231.0873	C ₁₀ H ₁₆ O ₆	1.60	0.60	3	351.1811	C ₁₉ H ₂₈ O ₆	1.47	0.32	6
231.1026	C ₁₄ H ₁₆ O ₃	1.14	0.21	7	351.2538	C ₂₁ H ₃₆ O ₄	1.71	0.19	4
231.1237	C ₁₁ H ₂₀ O ₅	1.82	0.45	2	351.3266	C ₂₃ H ₄₄ O ₂	1.91	0.09	2
231.1389	C ₁₅ H ₂₀ O ₂	1.33	0.13	6	353.1604	C ₁₈ H ₂₆ O ₇	1.44	0.39	6
231.1602	C ₁₂ H ₂₄ O ₄	2.00	0.33	1	353.1968	C ₁₉ H ₃₀ O ₆	1.58	0.32	5
231.1753	C ₁₆ H ₂₄ O ₁	1.50	0.06	5	353.2695	C ₂₁ H ₃₈ O ₄	1.81	0.19	3
233.0302	C ₈ H ₁₀ O ₈	1.25	1.00	4	353.3423	C ₂₃ H ₄₆ O ₂	2.00	0.09	1
233.0454	C ₁₂ H ₁₀ O ₅	0.83	0.42	8	355.1396	C ₁₇ H ₂₄ O ₈	1.41	0.47	6
233.0666	C ₉ H ₁₄ O ₇	1.56	0.78	3	355.1760	C ₁₈ H ₂₈ O ₇	1.56	0.39	5
233.0819	C ₁₃ H ₁₄ O ₄	1.08	0.31	7	357.1189	C ₁₆ H ₂₂ O ₉	1.38	0.56	6
233.1029	C ₁₀ H ₁₈ O ₆	1.80	0.60	2	357.1553	C ₁₇ H ₂₆ O ₈	1.53	0.47	5
233.1182	C ₁₄ H ₁₈ O ₃	1.29	0.21	6	365.2331	C ₂₁ H ₃₄ O ₅	1.62	0.24	5
233.1546	C ₁₅ H ₂₂ O ₂	1.47	0.13	5	365.3422	C ₂₄ H ₄₆ O ₂	1.92	0.08	2
235.0247	C ₁₁ H ₈ O ₆	0.73	0.55	8	367.1760	C ₁₉ H ₂₈ O ₇	1.47	0.37	6
235.0458	C ₈ H ₁₂ O ₈	1.50	1.00	3	367.2487	C ₂₁ H ₃₆ O ₅	1.71	0.24	4
235.0611	C ₁₂ H ₁₂ O ₅	1.00	0.42	7	367.3579	C ₂₄ H ₄₈ O ₂	2.00	0.08	1
235.0975	C ₁₃ H ₁₆ O ₄	1.23	0.31	6	369.1552	C ₁₈ H ₂₆ O ₈	1.44	0.44	6
235.1339	C ₁₄ H ₂₀ O ₃	1.43	0.21	5	381.2280	C ₂₁ H ₃₄ O ₆	1.62	0.29	5
235.1703	C ₁₅ H ₂₄ O ₂	1.60	0.13	4	381.3372	C ₂₄ H ₄₆ O ₃	1.92	0.13	2
					383.2437	C ₂₁ H ₃₆ O ₆	1.71	0.29	4
					395.3892	C ₂₆ H ₅₂ O ₂	2.00	0.08	1
					423.4205	C ₂₈ H ₅₆ O ₂	2.00	0.07	1

Table 7.12 CHON-containing molecular formulas determined by APCI-Orbitrap-MS in negative ionization mode from 09 May – 12 May 2017.

measured <i>m/z</i> [M-H] ⁻	elemental composition	H/C	O/C	DBE	measured <i>m/z</i> [M-H] ⁻	elemental composition	H/C	O/C	DBE
82.0298	C ₄ H ₅ N ₁ O ₁	1.25	0.25	3	180.0666	C ₉ H ₁₁ N ₁ O ₃	1.22	0.33	5
84.0455	C ₄ H ₇ N ₁ O ₁	1.75	0.25	2	182.0095	C ₇ H ₅ N ₁ O ₅	0.71	0.71	6
86.0248	C ₃ H ₅ N ₁ O ₂	1.67	0.67	2	182.0459	C ₈ H ₉ N ₁ O ₄	1.13	0.50	5
86.0611	C ₄ H ₉ N ₁ O ₁	2.25	0.25	1	182.0822	C ₉ H ₁₃ N ₁ O ₃	1.44	0.33	4
87.0200	C ₂ H ₄ N ₂ O ₂	2.00	1.00	2	183.0046	C ₆ H ₄ N ₂ O ₅	0.67	0.83	6
88.0040	C ₂ H ₃ N ₁ O ₃	1.50	1.50	2	184.0250	C ₇ H ₇ N ₁ O ₅	1.00	0.71	5
94.0298	C ₅ H ₅ N ₁ O ₁	1.00	0.20	4	184.0614	C ₈ H ₁₁ N ₁ O ₄	1.38	0.50	4
96.0091	C ₄ H ₃ N ₁ O ₂	0.75	0.50	4	186.0407	C ₇ H ₉ N ₁ O ₅	1.29	0.71	4
98.0247	C ₄ H ₅ N ₁ O ₂	1.25	0.50	3	186.0771	C ₈ H ₁₃ N ₁ O ₄	1.63	0.50	3
100.0040	C ₃ H ₃ N ₁ O ₃	1.00	1.00	3	186.1135	C ₉ H ₁₇ N ₁ O ₃	1.89	0.33	2
100.0404	C ₄ H ₇ N ₁ O ₂	1.75	0.50	2	188.0353	C ₁₀ H ₇ N ₁ O ₃	0.70	0.30	8
101.0356	C ₃ H ₆ N ₂ O ₂	2.00	0.67	2	188.0564	C ₇ H ₁₁ N ₁ O ₅	1.57	0.71	3
102.0196	C ₃ H ₅ N ₁ O ₃	1.67	1.00	2	190.0145	C ₉ H ₅ N ₁ O ₄	0.56	0.44	8
102.0560	C ₄ H ₉ N ₁ O ₂	2.25	0.50	1	190.0509	C ₁₀ H ₉ N ₁ O ₃	0.90	0.30	7
108.0455	C ₆ H ₇ N ₁ O ₁	1.17	0.17	4	192.0302	C ₉ H ₇ N ₁ O ₄	0.78	0.44	7
110.0247	C ₅ H ₅ N ₁ O ₂	1.00	0.40	4	192.0666	C ₁₀ H ₁₁ N ₁ O ₃	1.10	0.30	6
111.0200	C ₄ H ₄ N ₂ O ₂	1.00	0.50	4	194.0821	C ₁₀ H ₁₃ N ₁ O ₃	1.30	0.30	5
112.0040	C ₄ H ₃ N ₁ O ₃	0.75	0.75	4	196.0250	C ₈ H ₇ N ₁ O ₅	0.88	0.63	6
112.0404	C ₅ H ₇ N ₁ O ₂	1.40	0.40	3	196.0615	C ₉ H ₁₁ N ₁ O ₄	1.22	0.44	5
112.9993	C ₃ H ₂ N ₂ O ₃	0.67	1.00	4	197.0203	C ₇ H ₆ N ₂ O ₅	0.86	0.71	6
113.0357	C ₄ H ₆ N ₂ O ₂	1.50	0.50	3	198.0407	C ₈ H ₉ N ₁ O ₅	1.13	0.63	5
114.0196	C ₄ H ₅ N ₁ O ₃	1.25	0.75	3	198.0771	C ₉ H ₁₃ N ₁ O ₄	1.44	0.44	4
114.0560	C ₅ H ₉ N ₁ O ₂	1.80	0.40	2	200.0564	C ₈ H ₁₁ N ₁ O ₅	1.38	0.63	4
115.0149	C ₃ H ₄ N ₂ O ₃	1.33	1.00	3	202.0509	C ₁₁ H ₉ N ₁ O ₃	0.82	0.27	8
116.0353	C ₄ H ₇ N ₁ O ₃	1.75	0.75	2	202.0721	C ₈ H ₁₃ N ₁ O ₅	1.63	0.63	3
118.0298	C ₇ H ₅ N ₁ O ₁	0.71	0.14	6	204.0301	C ₁₀ H ₇ N ₁ O ₄	0.70	0.40	8
120.0455	C ₇ H ₇ N ₁ O ₁	1.00	0.14	5	205.0618	C ₁₀ H ₁₀ N ₂ O ₃	1.00	0.30	7
122.0248	C ₆ H ₅ N ₁ O ₂	0.83	0.33	5	206.0094	C ₉ H ₅ N ₁ O ₅	0.56	0.56	8
124.0040	C ₅ H ₃ N ₁ O ₃	0.60	0.60	5	206.0457	C ₁₀ H ₉ N ₁ O ₄	0.90	0.40	7
125.0356	C ₅ H ₆ N ₂ O ₂	1.20	0.40	4	208.0251	C ₉ H ₇ N ₁ O ₅	0.78	0.56	7
126.0560	C ₆ H ₉ N ₁ O ₂	1.50	0.33	3	208.0462	C ₆ H ₁₁ N ₁ O ₇	1.83	1.17	2
127.0149	C ₄ H ₄ N ₂ O ₃	1.00	0.75	4	208.0614	C ₁₀ H ₁₁ N ₁ O ₄	1.10	0.40	6
127.0513	C ₅ H ₈ N ₂ O ₂	1.60	0.40	3	208.0978	C ₁₁ H ₁₅ N ₁ O ₃	1.36	0.27	5
127.9989	C ₄ H ₃ N ₁ O ₄	0.75	1.00	4	210.0407	C ₉ H ₉ N ₁ O ₅	1.00	0.56	6
128.0353	C ₅ H ₇ N ₁ O ₃	1.40	0.60	3	210.0771	C ₁₀ H ₁₃ N ₁ O ₄	1.30	0.40	5
128.0717	C ₆ H ₁₁ N ₁ O ₂	1.83	0.33	2	212.0200	C ₈ H ₇ N ₁ O ₆	0.88	0.75	6
130.0145	C ₄ H ₅ N ₁ O ₄	1.25	1.00	3	212.0564	C ₉ H ₁₁ N ₁ O ₅	1.22	0.56	5
130.0509	C ₅ H ₉ N ₁ O ₃	1.80	0.60	2	212.0928	C ₁₀ H ₁₅ N ₁ O ₄	1.50	0.40	4
134.0247	C ₇ H ₅ N ₁ O ₂	0.71	0.29	6	212.1292	C ₁₁ H ₁₉ N ₁ O ₃	1.73	0.27	3
134.0611	C ₈ H ₉ N ₁ O ₁	1.13	0.13	5	213.0669	C ₁₂ H ₁₀ N ₂ O ₂	0.83	0.17	9
136.0403	C ₇ H ₇ N ₁ O ₂	1.00	0.29	5	216.0512	C ₈ H ₁₁ N ₁ O ₆	1.38	0.75	4

137.0356	C ₆ H ₆ N ₂ O ₂	1.00	0.33	5	220.0250	C ₁₀ H ₇ N ₁ O ₅	0.70	0.50	8
138.0196	C ₆ H ₅ N ₁ O ₃	0.83	0.50	5	220.0462	C ₇ H ₁₁ N ₁ O ₇	1.57	1.00	3
138.0560	C ₇ H ₉ N ₁ O ₂	1.29	0.29	4	222.0407	C ₁₀ H ₉ N ₁ O ₅	0.90	0.50	7
139.0149	C ₅ H ₄ N ₂ O ₃	0.80	0.60	5	222.0771	C ₁₁ H ₁₃ N ₁ O ₄	1.18	0.36	6
139.9989	C ₅ H ₃ N ₁ O ₄	0.60	0.80	5	224.0564	C ₁₀ H ₁₁ N ₁ O ₅	1.10	0.50	6
140.0353	C ₆ H ₇ N ₁ O ₃	1.17	0.50	4	225.1244	C ₁₁ H ₁₈ N ₂ O ₃	1.64	0.27	4
140.0716	C ₇ H ₁₁ N ₁ O ₂	1.57	0.29	3	226.0357	C ₉ H ₉ N ₁ O ₆	1.00	0.67	6
141.0305	C ₅ H ₆ N ₂ O ₃	1.20	0.60	4	226.0720	C ₁₀ H ₁₃ N ₁ O ₅	1.30	0.50	5
142.0145	C ₅ H ₅ N ₁ O ₄	1.00	0.80	4	226.1084	C ₁₁ H ₁₇ N ₁ O ₄	1.55	0.36	4
142.0509	C ₆ H ₉ N ₁ O ₃	1.50	0.50	3	228.0513	C ₉ H ₁₁ N ₁ O ₆	1.22	0.67	5
142.0873	C ₇ H ₁₃ N ₁ O ₂	1.86	0.29	2	228.0876	C ₁₀ H ₁₅ N ₁ O ₅	1.50	0.50	4
144.0302	C ₅ H ₇ N ₁ O ₄	1.40	0.80	3	230.0669	C ₉ H ₁₃ N ₁ O ₆	1.44	0.67	4
144.0665	C ₆ H ₁₁ N ₁ O ₃	1.83	0.50	2	236.0411	C ₇ H ₁₁ N ₁ O ₈	1.57	1.14	3
146.0247	C ₈ H ₅ N ₁ O ₂	0.63	0.25	7	238.0356	C ₁₀ H ₉ N ₁ O ₆	0.90	0.60	7
146.0458	C ₅ H ₉ N ₁ O ₄	1.80	0.80	2	238.0720	C ₁₁ H ₁₃ N ₁ O ₅	1.18	0.45	6
147.0200	C ₇ H ₄ N ₂ O ₂	0.57	0.29	7	239.1400	C ₁₂ H ₂₀ N ₂ O ₃	1.67	0.25	4
148.0404	C ₈ H ₇ N ₁ O ₂	0.88	0.25	6	240.0513	C ₁₀ H ₁₁ N ₁ O ₆	1.10	0.60	6
150.0196	C ₇ H ₅ N ₁ O ₃	0.71	0.43	6	242.0670	C ₁₀ H ₁₃ N ₁ O ₆	1.30	0.60	5
150.0560	C ₈ H ₉ N ₁ O ₂	1.13	0.25	5	244.0825	C ₁₀ H ₁₅ N ₁ O ₆	1.50	0.60	4
151.0512	C ₇ H ₈ N ₂ O ₂	1.14	0.29	5	248.0411	C ₈ H ₁₁ N ₁ O ₈	1.38	1.00	4
152.0353	C ₇ H ₇ N ₁ O ₃	1.00	0.43	5	250.0568	C ₈ H ₁₃ N ₁ O ₈	1.63	1.00	3
152.0716	C ₈ H ₁₁ N ₁ O ₂	1.38	0.25	4	250.1448	C ₁₄ H ₂₁ N ₁ O ₃	1.50	0.21	5
153.0305	C ₆ H ₆ N ₂ O ₃	1.00	0.50	5	258.0618	C ₁₀ H ₁₃ N ₁ O ₇	1.30	0.70	5
154.0146	C ₆ H ₅ N ₁ O ₄	0.83	0.67	5	260.0775	C ₁₀ H ₁₅ N ₁ O ₇	1.50	0.70	4
154.0510	C ₇ H ₉ N ₁ O ₃	1.29	0.43	4	262.0567	C ₉ H ₁₃ N ₁ O ₈	1.44	0.89	4
154.0873	C ₈ H ₁₃ N ₁ O ₂	1.63	0.25	3	262.0931	C ₁₀ H ₁₇ N ₁ O ₇	1.70	0.70	3
155.0098	C ₅ H ₄ N ₂ O ₄	0.80	0.80	5	264.0724	C ₉ H ₁₅ N ₁ O ₈	1.67	0.89	3
155.9938	C ₅ H ₃ N ₁ O ₅	0.60	1.00	5	264.1604	C ₁₅ H ₂₃ N ₁ O ₃	1.53	0.20	5
156.0302	C ₆ H ₇ N ₁ O ₄	1.17	0.67	4	266.1397	C ₁₄ H ₂₁ N ₁ O ₄	1.50	0.29	5
156.0666	C ₇ H ₁₁ N ₁ O ₃	1.57	0.43	3	274.0568	C ₁₀ H ₁₃ N ₁ O ₈	1.30	0.80	5
158.0094	C ₅ H ₅ N ₁ O ₅	1.00	1.00	4	275.1608	C ₁₂ H ₂₄ N ₂ O ₅	2.00	0.42	2
158.0458	C ₆ H ₉ N ₁ O ₄	1.50	0.67	3	276.0723	C ₁₀ H ₁₅ N ₁ O ₈	1.50	0.80	4
160.0251	C ₅ H ₇ N ₁ O ₅	1.40	1.00	3	276.1603	C ₁₆ H ₂₃ N ₁ O ₃	1.44	0.19	6
160.0403	C ₉ H ₇ N ₁ O ₂	0.78	0.22	7	278.0516	C ₉ H ₁₃ N ₁ O ₉	1.44	1.00	4
161.0356	C ₈ H ₆ N ₂ O ₂	0.75	0.25	7	278.0879	C ₁₀ H ₁₇ N ₁ O ₈	1.70	0.80	3
162.0196	C ₈ H ₅ N ₁ O ₃	0.63	0.38	7	278.1760	C ₁₆ H ₂₅ N ₁ O ₃	1.56	0.19	5
162.0560	C ₉ H ₉ N ₁ O ₂	1.00	0.22	6	292.0673	C ₁₀ H ₁₅ N ₁ O ₉	1.50	0.90	4
163.9989	C ₇ H ₃ N ₁ O ₄	0.43	0.57	7	302.0879	C ₁₂ H ₁₇ N ₁ O ₈	1.42	0.67	5
164.0353	C ₈ H ₇ N ₁ O ₃	0.88	0.38	6	302.2334	C ₁₆ H ₃₃ N ₁ O ₄	2.06	0.25	1
164.0717	C ₉ H ₁₁ N ₁ O ₂	1.22	0.22	5	304.1036	C ₁₂ H ₁₉ N ₁ O ₈	1.58	0.67	4
165.0305	C ₇ H ₆ N ₂ O ₃	0.86	0.43	6	306.2073	C ₁₈ H ₂₉ N ₁ O ₃	1.61	0.17	5
166.0144	C ₇ H ₅ N ₁ O ₄	0.71	0.57	6	318.0828	C ₁₂ H ₁₇ N ₁ O ₉	1.42	0.75	5
166.0509	C ₈ H ₉ N ₁ O ₃	1.13	0.38	5	318.1192	C ₁₃ H ₂₁ N ₁ O ₈	1.62	0.62	4
167.0461	C ₇ H ₈ N ₂ O ₃	1.14	0.43	5	320.0985	C ₁₂ H ₁₉ N ₁ O ₉	1.58	0.75	4
168.0302	C ₇ H ₇ N ₁ O ₄	1.00	0.57	5	326.2334	C ₁₈ H ₃₃ N ₁ O ₄	1.83	0.22	3
168.0665	C ₈ H ₁₁ N ₁ O ₃	1.38	0.38	4	328.0162	C ₈ H ₁₁ N ₁ O ₁₃	1.38	1.63	4
170.0094	C ₆ H ₅ N ₁ O ₅	0.83	0.83	5	328.1400	C ₁₅ H ₂₃ N ₁ O ₇	1.53	0.47	5

7. Appendix

170.0458	C ₇ H ₉ N ₁ O ₄	1.29	0.57	4	330.1556	C ₁₅ H ₂₅ N ₁ O ₇	1.67	0.47	4
170.0822	C ₈ H ₁₃ N ₁ O ₃	1.63	0.38	3	330.2648	C ₁₈ H ₃₇ N ₁ O ₄	2.06	0.22	1
171.0200	C ₉ H ₄ N ₂ O ₂	0.44	0.22	9	344.1349	C ₁₅ H ₂₃ N ₁ O ₈	1.53	0.53	5
171.0412	C ₆ H ₈ N ₂ O ₄	1.33	0.67	4	346.1505	C ₁₅ H ₂₅ N ₁ O ₈	1.67	0.53	4
172.0251	C ₆ H ₇ N ₁ O ₅	1.17	0.83	4	348.1207	C ₁₆ H ₁₉ N ₃ O ₆	1.19	0.38	9
172.0615	C ₇ H ₁₁ N ₁ O ₄	1.57	0.57	3	360.1298	C ₁₅ H ₂₃ N ₁ O ₉	1.53	0.60	5
174.0407	C ₆ H ₉ N ₁ O ₅	1.50	0.83	3	360.2390	C ₁₈ H ₃₅ N ₁ O ₆	1.94	0.33	2
176.0352	C ₉ H ₇ N ₁ O ₃	0.78	0.33	7	362.1455	C ₁₅ H ₂₅ N ₁ O ₉	1.67	0.60	4
177.0669	C ₉ H ₁₀ N ₂ O ₂	1.11	0.22	6	370.0631	C ₁₁ H ₁₇ N ₁ O ₁₃	1.55	1.18	4
178.0145	C ₈ H ₅ N ₁ O ₄	0.63	0.50	7	376.1247	C ₁₅ H ₂₃ N ₁ O ₁₀	1.53	0.67	5
178.0509	C ₉ H ₉ N ₁ O ₃	1.00	0.33	6	382.1869	C ₁₉ H ₂₉ N ₁ O ₇	1.53	0.37	6
179.9938	C ₇ H ₃ N ₁ O ₅	0.43	0.71	7	406.0212	C ₂₀ H ₉ N ₁ O ₉	0.45	0.45	17
180.0302	C ₈ H ₇ N ₁ O ₄	0.88	0.50	6	407.1304	C ₁₅ H ₂₄ N ₂ O ₁₁	1.60	0.73	5

Table 7.13 CHONS-containing formulas determined by APCI-Orbitrap-MS in negative ionization mode from 09 May – 12 May 2017.

measured <i>m/z</i> [M-H] ⁻	elemental composition	H/C	O/C	DBE
150.0018	C ₇ H ₅ N ₁ O ₁ S ₁	0.71	0.14	6
156.0125	C ₆ H ₇ N ₁ O ₂ S ₁	1.17	0.33	4
170.0281	C ₇ H ₉ N ₁ O ₂ S ₁	1.29	0.29	4
210.0594	C ₁₀ H ₁₃ N ₁ O ₂ S ₁	1.30	0.20	5
212.0750	C ₁₀ H ₁₅ N ₁ O ₂ S ₁	1.50	0.20	4
224.0425	C ₇ H ₁₅ N ₁ O ₃ S ₂	2.14	0.43	1
228.1174	C ₁₀ H ₁₉ N ₃ O ₁ S ₁	1.90	0.10	3
294.0653	C ₁₀ H ₁₇ N ₁ O ₇ S ₁	1.70	0.70	3
310.0064	C ₉ H ₁₃ N ₁ O ₇ S ₂	1.44	0.78	4
312.0035	C ₈ H ₁₁ N ₁ O ₁₀ S ₁	1.38	1.25	4
314.1579	C ₁₉ H ₂₅ N ₁ O ₁ S ₁	1.32	0.05	8
324.0221	C ₁₀ H ₁₅ N ₁ O ₇ S ₂	1.50	0.70	4
326.0191	C ₉ H ₁₃ N ₁ O ₁₀ S ₁	1.44	1.11	4
330.0446	C ₁₆ H ₁₃ N ₁ O ₅ S ₁	0.81	0.31	11
336.1021	C ₁₅ H ₁₉ N ₃ O ₄ S ₁	1.27	0.27	8
338.0378	C ₁₁ H ₁₇ N ₁ O ₇ S ₂	1.55	0.64	4
340.0347	C ₁₀ H ₁₅ N ₁ O ₁₀ S ₁	1.50	1.00	4
342.0498	C ₁₀ H ₁₇ N ₁ O ₁₀ S ₁	1.70	1.00	3
352.0533	C ₁₂ H ₁₉ N ₁ O ₇ S ₂	1.58	0.58	4
354.0504	C ₁₁ H ₁₇ N ₁ O ₁₀ S ₁	1.55	0.91	4
357.9910	C ₉ H ₁₃ N ₁ O ₁₀ S ₂	1.44	1.11	4
359.9880	C ₈ H ₁₁ N ₁ O ₁₃ S ₁	1.38	1.63	4
366.0690	C ₁₃ H ₂₁ N ₁ O ₇ S ₂	1.62	0.54	4
368.0660	C ₁₂ H ₁₉ N ₁ O ₁₀ S ₁	1.58	0.83	4
372.0600	C ₁₁ H ₁₉ N ₁ O ₁₁ S ₁	1.73	1.00	3

372.0653	C ₁₇ H ₁₅ N ₃ O ₅ S ₁	0.88	0.29	12
375.9928	C ₁₉ H ₇ N ₁ O ₆ S ₁	0.37	0.32	17
380.0846	C ₁₄ H ₂₃ N ₁ O ₇ S ₂	1.64	0.50	4
382.0817	C ₁₃ H ₂₁ N ₁ O ₁₀ S ₁	1.62	0.77	4
400.0300	C ₁₀ H ₁₅ N ₃ O ₁₂ S ₁	1.50	1.20	5
402.2104	C ₂₃ H ₃₃ N ₁ O ₃ S ₁	1.43	0.13	8
404.0241	C ₂₁ H ₁₁ N ₁ O ₆ S ₁	0.52	0.29	17
404.2778	C ₂₀ H ₄₃ N ₃ O ₁ S ₂	2.15	0.05	1

Table 7.14 CHOS-containing molecular formulas determined by APCI-Orbitrap-MS in negative ionization mode from 09 May – 12 May 2017.

measured m/z [M-H] ⁻	elemental composition	H/C	O/C	DBE
120.9599	C ₂ H ₂ O ₄ S ₁	1.0	2.0	2
152.9863	C ₃ H ₆ O ₅ S ₁	2.0	1.7	1
174.9859	C ₉ H ₄ O ₂ S ₁	0.4	0.2	8
223.0282	C ₇ H ₁₂ O ₆ S ₁	1.7	0.9	2
225.0075	C ₆ H ₁₀ O ₇ S ₁	1.7	1.2	2
239.0596	C ₈ H ₁₆ O ₆ S ₁	2.0	0.8	1
265.1638	C ₁₆ H ₂₆ O ₁ S ₁	1.6	0.1	4
277.1637	C ₁₇ H ₂₆ O ₁ S ₁	1.5	0.1	5
373.0450	C ₁₁ H ₁₈ O ₁₂ S ₁	1.6	1.1	3
375.0243	C ₁₀ H ₁₆ O ₁₃ S ₁	1.6	1.3	3
384.9713	C ₁₀ H ₁₀ O ₁₄ S ₁	1.0	1.4	6

Table 7.15 CHO-containing molecular formulas determined by APCI-Orbitrap-MS in positive ionization mode from 09 May – 12 May 2017.

measured m/z [M+H] ⁺	elemental composition	H/C	O/C	DBE	measured m/z [M+H] ⁺	elemental composition	H/C	O/C	DBE
91.0388	C ₃ H ₆ O ₃	2.00	1.00	1	183.1376	C ₁₁ H ₁₈ O ₂	1.64	0.18	3
115.0388	C ₅ H ₆ O ₃	1.20	0.60	3	183.1740	C ₁₂ H ₂₂ O ₁	1.83	0.08	2
121.0282	C ₇ H ₄ O ₂	0.57	0.29	6	185.0804	C ₉ H ₁₂ O ₄	1.33	0.44	4
121.0646	C ₈ H ₈ O ₁	1.00	0.13	5	185.1169	C ₁₀ H ₁₆ O ₃	1.60	0.30	3
123.0438	C ₇ H ₆ O ₂	0.86	0.29	5	185.1533	C ₁₁ H ₂₀ O ₂	1.82	0.18	2
123.0802	C ₈ H ₁₀ O ₁	1.25	0.13	4	185.1896	C ₁₂ H ₂₄ O ₁	2.00	0.08	1
125.0231	C ₆ H ₄ O ₃	0.67	0.50	5	187.0958	C ₉ H ₁₄ O ₄	1.56	0.44	3
125.0595	C ₇ H ₈ O ₂	1.14	0.29	4	187.1324	C ₁₀ H ₁₈ O ₃	1.80	0.30	2
127.0387	C ₆ H ₆ O ₃	1.00	0.50	4	187.1689	C ₁₁ H ₂₂ O ₂	2.00	0.18	1
127.0751	C ₇ H ₁₀ O ₂	1.43	0.29	3	191.1060	C ₁₂ H ₁₄ O ₂	1.17	0.17	6
129.0543	C ₆ H ₈ O ₃	1.33	0.50	3	191.1422	C ₁₃ H ₁₈ O ₁	1.38	0.08	5
129.0907	C ₇ H ₁₂ O ₂	1.71	0.29	2	193.1215	C ₁₂ H ₁₆ O ₂	1.33	0.17	5

7. Appendix

129.1271	C ₈ H ₁₆ O ₁	2.00	0.13	1	193.1583	C ₁₃ H ₂₀ O ₁	1.54	0.08	4
131.1064	C ₇ H ₁₄ O ₂	2.00	0.29	1	195.1012	C ₁₁ H ₁₄ O ₃	1.27	0.27	5
131.1428	C ₈ H ₁₈ O ₁	2.25	0.13	0	195.1376	C ₁₂ H ₁₈ O ₂	1.50	0.17	4
133.0645	C ₉ H ₈ O ₁	0.89	0.11	6	197.0805	C ₁₀ H ₁₂ O ₄	1.20	0.40	5
133.0857	C ₆ H ₁₂ O ₃	2.00	0.50	1	197.1165	C ₁₁ H ₁₆ O ₃	1.45	0.27	4
133.1221	C ₇ H ₁₆ O ₂	2.29	0.29	0	197.1532	C ₁₂ H ₂₀ O ₂	1.67	0.17	3
135.0438	C ₈ H ₆ O ₂	0.75	0.25	6	197.1896	C ₁₃ H ₂₄ O ₁	1.85	0.08	2
135.0802	C ₉ H ₁₀ O ₁	1.11	0.11	5	199.0959	C ₁₀ H ₁₄ O ₄	1.40	0.40	4
137.0595	C ₈ H ₈ O ₂	1.00	0.25	5	199.1323	C ₁₁ H ₁₈ O ₃	1.64	0.27	3
137.0958	C ₉ H ₁₂ O ₁	1.33	0.11	4	199.1688	C ₁₂ H ₂₂ O ₂	1.83	0.17	2
139.0387	C ₇ H ₆ O ₃	0.86	0.43	5	199.2052	C ₁₃ H ₂₆ O ₁	2.00	0.08	1
139.0751	C ₈ H ₁₀ O ₂	1.25	0.25	4	201.1112	C ₁₀ H ₁₆ O ₄	1.60	0.40	3
139.1115	C ₉ H ₁₄ O ₁	1.56	0.11	3	201.1845	C ₁₂ H ₂₄ O ₂	2.00	0.17	1
141.0543	C ₇ H ₈ O ₃	1.14	0.43	4	203.1427	C ₁₄ H ₁₈ O ₁	1.29	0.07	6
141.0907	C ₈ H ₁₂ O ₂	1.50	0.25	3	205.1580	C ₁₄ H ₂₀ O ₁	1.43	0.07	5
141.1271	C ₉ H ₁₆ O ₁	1.78	0.11	2	207.1739	C ₁₄ H ₂₂ O ₁	1.57	0.07	4
143.0700	C ₇ H ₁₀ O ₃	1.43	0.43	3	209.1167	C ₁₂ H ₁₆ O ₃	1.33	0.25	5
143.1064	C ₈ H ₁₄ O ₂	1.75	0.25	2	209.1532	C ₁₃ H ₂₀ O ₂	1.54	0.15	4
143.1428	C ₉ H ₁₈ O ₁	2.00	0.11	1	209.1896	C ₁₄ H ₂₄ O ₁	1.71	0.07	3
145.0492	C ₆ H ₈ O ₄	1.33	0.67	3	211.0749	C ₁₄ H ₁₀ O ₂	0.71	0.14	10
145.0856	C ₇ H ₁₂ O ₃	1.71	0.43	2	211.1326	C ₁₂ H ₁₈ O ₃	1.50	0.25	4
145.1220	C ₈ H ₁₆ O ₂	2.00	0.25	1	211.1688	C ₁₃ H ₂₂ O ₂	1.69	0.15	3
147.0438	C ₉ H ₆ O ₂	0.67	0.22	7	211.2052	C ₁₄ H ₂₆ O ₁	1.86	0.07	2
147.0801	C ₁₀ H ₁₀ O ₁	1.00	0.10	6	213.1478	C ₁₂ H ₂₀ O ₃	1.67	0.25	3
147.1014	C ₇ H ₁₄ O ₃	2.00	0.43	1	213.1845	C ₁₃ H ₂₄ O ₂	1.85	0.15	2
149.0231	C ₈ H ₄ O ₃	0.50	0.38	7	213.2208	C ₁₄ H ₂₈ O ₁	2.00	0.07	1
149.0445	C ₅ H ₈ O ₅	1.60	1.00	2	215.2003	C ₁₃ H ₂₆ O ₂	2.00	0.15	1
149.0595	C ₉ H ₈ O ₂	0.89	0.22	6	217.1067	C ₁₀ H ₁₆ O ₅	1.60	0.50	3
149.0807	C ₆ H ₁₂ O ₄	2.00	0.67	1	217.1583	C ₁₅ H ₂₀ O ₁	1.33	0.07	6
149.0958	C ₁₀ H ₁₂ O ₁	1.20	0.10	5	219.1739	C ₁₅ H ₂₂ O ₁	1.47	0.07	5
151.0385	C ₈ H ₆ O ₃	0.75	0.38	6	221.1532	C ₁₄ H ₂₀ O ₂	1.43	0.14	5
151.0751	C ₉ H ₁₀ O ₂	1.11	0.22	5	221.1893	C ₁₅ H ₂₄ O ₁	1.60	0.07	4
151.1115	C ₁₀ H ₁₄ O ₁	1.40	0.10	4	223.1324	C ₁₃ H ₁₈ O ₃	1.38	0.23	5
153.0543	C ₈ H ₈ O ₃	1.00	0.38	5	223.1688	C ₁₄ H ₂₂ O ₂	1.57	0.14	4
153.0907	C ₉ H ₁₂ O ₂	1.33	0.22	4	223.2052	C ₁₅ H ₂₆ O ₁	1.73	0.07	3
153.1271	C ₁₀ H ₁₆ O ₁	1.60	0.10	3	225.0603	C ₇ H ₁₂ O ₈	1.71	1.14	2
155.0699	C ₈ H ₁₀ O ₃	1.25	0.38	4	225.1478	C ₁₃ H ₂₀ O ₃	1.54	0.23	4
155.1063	C ₉ H ₁₄ O ₂	1.56	0.22	3	225.1844	C ₁₄ H ₂₄ O ₂	1.71	0.14	3
155.1427	C ₁₀ H ₁₈ O ₁	1.80	0.10	2	225.2208	C ₁₅ H ₂₈ O ₁	1.87	0.07	2
157.0492	C ₇ H ₈ O ₄	1.14	0.57	4	227.1636	C ₁₃ H ₂₂ O ₃	1.69	0.23	3
157.0857	C ₈ H ₁₂ O ₃	1.50	0.38	3	227.2001	C ₁₄ H ₂₆ O ₂	1.86	0.14	2
157.1220	C ₉ H ₁₆ O ₂	1.78	0.22	2	227.2365	C ₁₅ H ₃₀ O ₁	2.00	0.07	1
157.1584	C ₁₀ H ₂₀ O ₁	2.00	0.10	1	229.2158	C ₁₄ H ₂₈ O ₂	2.00	0.14	1
159.0649	C ₇ H ₁₀ O ₄	1.43	0.57	3	233.1896	C ₁₆ H ₂₄ O ₁	1.50	0.06	5
159.1012	C ₈ H ₁₄ O ₃	1.75	0.38	2	235.1688	C ₁₅ H ₂₂ O ₂	1.47	0.13	5
159.1376	C ₉ H ₁₈ O ₂	2.00	0.22	1	237.1845	C ₁₅ H ₂₄ O ₂	1.60	0.13	4
161.0593	C ₁₀ H ₈ O ₂	0.80	0.20	7	237.2210	C ₁₆ H ₂₈ O ₁	1.75	0.06	3

161.0806	C ₇ H ₁₂ O ₄	1.71	0.57	2	239.1425	C ₁₇ H ₁₈ O ₁	1.06	0.06	9
161.0958	C ₁₁ H ₁₂ O ₁	1.09	0.09	6	239.2002	C ₁₅ H ₂₆ O ₂	1.73	0.13	3
161.1169	C ₈ H ₁₆ O ₃	2.00	0.38	1	239.2365	C ₁₆ H ₃₀ O ₁	1.88	0.06	2
163.0386	C ₉ H ₆ O ₃	0.67	0.33	7	241.2157	C ₁₅ H ₂₈ O ₂	1.87	0.13	2
163.0750	C ₁₀ H ₁₀ O ₂	1.00	0.20	6	241.2521	C ₁₆ H ₃₂ O ₁	2.00	0.06	1
163.0963	C ₇ H ₁₄ O ₄	2.00	0.57	1	243.2317	C ₁₅ H ₃₀ O ₂	2.00	0.13	1
163.1114	C ₁₁ H ₁₄ O ₁	1.27	0.09	5	243.2680	C ₁₆ H ₃₄ O ₁	2.13	0.06	0
163.1322	C ₈ H ₁₈ O ₃	2.25	0.38	0	245.1746	C ₁₃ H ₂₄ O ₄	1.85	0.31	2
165.0541	C ₉ H ₈ O ₃	0.89	0.33	6	247.1689	C ₁₆ H ₂₂ O ₂	1.38	0.13	6
165.0907	C ₁₀ H ₁₂ O ₂	1.20	0.20	5	249.1845	C ₁₆ H ₂₄ O ₂	1.50	0.13	5
165.1271	C ₁₁ H ₁₆ O ₁	1.45	0.09	4	251.1995	C ₁₆ H ₂₆ O ₂	1.63	0.13	4
167.0550	C ₅ H ₁₀ O ₆	2.00	1.20	1	253.1431	C ₁₄ H ₂₀ O ₄	1.43	0.29	5
167.0700	C ₉ H ₁₀ O ₃	1.11	0.33	5	253.1790	C ₁₅ H ₂₄ O ₃	1.60	0.20	4
167.1063	C ₁₀ H ₁₄ O ₂	1.40	0.20	4	253.2159	C ₁₆ H ₂₈ O ₂	1.75	0.13	3
167.1427	C ₁₁ H ₁₈ O ₁	1.64	0.09	3	253.2523	C ₁₇ H ₃₂ O ₁	1.88	0.06	2
169.0492	C ₈ H ₈ O ₄	1.00	0.50	5	255.2314	C ₁₆ H ₃₀ O ₂	1.88	0.13	2
169.0856	C ₉ H ₁₂ O ₃	1.33	0.33	4	255.2678	C ₁₇ H ₃₄ O ₁	2.00	0.06	1
169.1220	C ₁₀ H ₁₆ O ₂	1.60	0.20	3	257.2470	C ₁₆ H ₃₂ O ₂	2.00	0.13	1
169.1583	C ₁₁ H ₂₀ O ₁	1.82	0.09	2	261.1846	C ₁₇ H ₂₄ O ₂	1.41	0.12	6
171.0648	C ₈ H ₁₀ O ₄	1.25	0.50	4	265.1795	C ₁₆ H ₂₄ O ₃	1.50	0.19	5
171.1012	C ₉ H ₁₄ O ₃	1.56	0.33	3	267.2681	C ₁₈ H ₃₄ O ₁	1.89	0.06	2
171.1376	C ₁₀ H ₁₈ O ₂	1.80	0.20	2	269.2472	C ₁₇ H ₃₂ O ₂	1.88	0.12	2
171.1740	C ₁₁ H ₂₂ O ₁	2.00	0.09	1	269.2836	C ₁₈ H ₃₆ O ₁	2.00	0.06	1
173.0805	C ₈ H ₁₂ O ₄	1.50	0.50	3	271.2629	C ₁₇ H ₃₄ O ₂	2.00	0.12	1
173.1168	C ₉ H ₁₆ O ₃	1.78	0.33	2	275.1638	C ₁₇ H ₂₂ O ₃	1.29	0.18	7
173.1533	C ₁₀ H ₂₀ O ₂	2.00	0.20	1	277.1795	C ₁₇ H ₂₄ O ₃	1.41	0.18	6
175.0751	C ₁₁ H ₁₀ O ₂	0.91	0.18	7	279.1588	C ₁₆ H ₂₂ O ₄	1.38	0.25	6
175.1112	C ₁₂ H ₁₄ O ₁	1.17	0.08	6	281.2835	C ₁₉ H ₃₆ O ₁	1.89	0.05	2
177.0543	C ₁₀ H ₈ O ₃	0.80	0.30	7	283.2629	C ₁₈ H ₃₄ O ₂	1.89	0.11	2
177.0907	C ₁₁ H ₁₂ O ₂	1.09	0.18	6	283.2993	C ₁₉ H ₃₈ O ₁	2.00	0.05	1
177.1121	C ₈ H ₁₆ O ₄	2.00	0.50	1	285.2785	C ₁₈ H ₃₆ O ₂	2.00	0.11	1
177.1270	C ₁₂ H ₁₆ O ₁	1.33	0.08	5	297.0821	C ₁₀ H ₁₆ O ₁₀	1.60	1.00	3
179.0700	C ₁₀ H ₁₀ O ₃	1.00	0.30	6	297.3150	C ₂₀ H ₄₀ O ₁	2.00	0.05	1
179.1063	C ₁₁ H ₁₄ O ₂	1.27	0.18	5	311.3306	C ₂₁ H ₄₂ O ₁	2.00	0.05	1
179.1426	C ₁₂ H ₁₈ O ₁	1.50	0.08	4	325.3461	C ₂₂ H ₄₄ O ₁	2.00	0.05	1
181.0855	C ₁₀ H ₁₂ O ₃	1.20	0.30	5	339.3620	C ₂₃ H ₄₆ O ₁	2.00	0.04	1
181.1219	C ₁₁ H ₁₆ O ₂	1.45	0.18	4	353.3775	C ₂₄ H ₄₈ O ₁	2.00	0.04	1
181.1583	C ₁₂ H ₂₀ O ₁	1.67	0.08	3	371.3152	C ₂₂ H ₄₂ O ₄	1.91	0.18	2
183.0649	C ₉ H ₁₀ O ₄	1.11	0.44	5	373.0977	C ₁₂ H ₂₀ O ₁₃	1.67	1.08	3
183.0801	C ₁₃ H ₁₀ O ₁	0.77	0.08	9	391.2839	C ₂₄ H ₃₈ O ₄	1.58	0.17	6
183.1013	C ₁₀ H ₁₄ O ₃	1.40	0.30	4	419.3150	C ₂₆ H ₄₂ O ₄	1.62	0.15	6
					445.1178	C ₁₅ H ₂₄ O ₁₅	1.60	1.00	4

7. Appendix

Table 7.16 CHON-containing molecular formulas determined by APCI-Orbitrap-MS in positive ionization mode from 09 May – 12 May 2017.

measured <i>m/z</i> [M+H] ⁺	elemental composition	H/C	O/C	DBE
198.1118	C ₁₀ H ₁₅ N ₁ O ₃	1.5	0.3	4
172.1693	C ₁₀ H ₂₁ N ₁ O ₁	2.1	0.1	1
297.082	C ₁₁ H ₁₂ N ₄ O ₆	1.1	0.6	8
250.1183	C ₁₂ H ₁₅ N ₃ O ₃	1.3	0.3	7
252.1592	C ₁₄ H ₂₁ N ₁ O ₃	1.5	0.2	5
298.0819	C ₁₅ H ₁₁ N ₃ O ₄	0.7	0.3	12
445.1198	C ₁₆ H ₂₀ N ₄ O ₁₁	1.3	0.7	9
371.0994	C ₁₇ H ₁₄ N ₄ O ₆	0.8	0.4	13
372.0984	C ₂₁ H ₁₃ N ₃ O ₄	0.6	0.2	17
88.0756	C ₄ H ₉ N ₁ O ₁	2.3	0.3	1
102.0911	C ₅ H ₁₁ N ₁ O ₁	2.2	0.2	1
143.0449	C ₅ H ₆ N ₂ O ₃	1.2	0.6	4
116.1069	C ₆ H ₁₃ N ₁ O ₁	2.2	0.2	1
108.0441	C ₆ H ₅ N ₁ O ₁	0.8	0.2	5
122.0598	C ₇ H ₇ N ₁ O ₁	1.0	0.1	5
181.0717	C ₇ H ₈ N ₄ O ₂	1.1	0.3	6
195.0875	C ₈ H ₁₀ N ₄ O ₂	1.3	0.3	6
148.0391	C ₈ H ₅ N ₁ O ₂	0.6	0.3	7
171.1484	C ₉ H ₁₈ N ₂ O ₁	2.0	0.1	2
158.1537	C ₉ H ₁₉ N ₁ O ₁	2.1	0.1	1

Table 7.17 CHN-containing molecular formulas determined by APCI-Orbitrap-MS in positive ionization mode from 09 May – 12 May 2017.

measured <i>m/z</i> [M+H] ⁺	elemental composition	H/C	O/C	DBE
95.0602	C ₅ H ₆ N ₂	1.20	0	4
108.0804	C ₇ H ₉ N ₁	1.29	0	4
109.0755	C ₆ H ₈ N ₂	1.33	0	4
163.1226	C ₁₀ H ₁₄ N ₂	1.40	0	5
170.0961	C ₁₂ H ₁₁ N ₁	0.92	0	8
220.1817	C ₁₃ H ₂₁ N ₃	1.62	0	5
232.1819	C ₁₄ H ₂₁ N ₃	1.50	0	6
242.2837	C ₁₆ H ₃₅ N ₁	2.19	0	0

Table 7.18 CHOS-containing molecular formulas determined by APCI-Orbitrap-MS in positive ionization mode from 09 May – 12 May 2017.

measured <i>m/z</i> [M+H] ⁺	elemental composition	H/C	O/C	DBE
223.0632	C ₈ H ₁₄ O ₅ S ₁	1.75	0.63	2
355.0694	C ₁₂ H ₁₈ O ₁₀ S ₁	1.5	0.83	4
371.1008	C ₁₃ H ₂₂ O ₁₀ S ₁	1.69	0.77	3

Table 7.19 CH-containing molecular formulas determined by APCI-Orbitrap-MS in positive ionization mode during 09 May – 12 May 2017.

measured <i>m/z</i> [M+H] ⁺	elemental composition	H/C	O/C	DBE
145.1010	C ₁₁ H ₁₂	1.09	0	6
147.1165	C ₁₁ H ₁₄	1.27	0	5
149.1322	C ₁₁ H ₁₆	1.45	0	4
151.1478	C ₁₁ H ₁₈	1.64	0	3
159.1164	C ₁₂ H ₁₄	1.17	0	6
161.1322	C ₁₂ H ₁₆	1.33	0	5
163.1478	C ₁₂ H ₁₈	1.50	0	4
165.1635	C ₁₂ H ₂₀	1.67	0	3
177.1634	C ₁₃ H ₂₀	1.54	0	4
179.1792	C ₁₃ H ₂₂	1.69	0	3
191.1791	C ₁₄ H ₂₂	1.57	0	4
203.1786	C ₁₅ H ₂₂	1.47	0	5
205.1946	C ₁₅ H ₂₄	1.60	0	4
213.1634	C ₁₆ H ₂₀	1.25	0	7

7.4 List of Related Publications and Presentations

Peer-reviewed publications:

C. Zuth, A.L. Vogel, S. Ockenfeld, R. Huesmann, T. Hoffmann, (2018), Ultra-High-Resolution Mass Spectrometry in Real-Time: Atmospheric Pressure Chemical Ionization Orbitrap Mass Spectrometry (APCI-Orbitrap-MS) of Atmospheric Organic Aerosol, *Analytical Chemistry*, accepted

M. Brüggemann, N. Hayeck, C. Bonnineau, S. Pesce, P.A. Alpert, S. Perrier, C. Zuth, T. Hoffmann, J. Chen and C. George, (2017), Interfacial Photochemistry of biogenic surfactants: a major source of abiotic volatile organic compounds, *Faraday Discuss.*, **200**, 59-74

M. Brüggemann, L. Poulain, A. Held, T. Stelzer, C. Zuth, S. Richters, A. Mutzel, D. van Pinxteren, Y. Inuma, S. Katkevica, R. Rabe, H. Herrmann and T. Hoffmann, (2017), Real-time detection of highly oxidized organosulfates and BSOA marker compounds during F-BEACH 2014 field study, *Atmos. Chem. Phys.*, **17**, 1453-1469, 2017. Brüggemann, M. et al., *Atmos. Chem. Phys.*, **17**, 1453-1469

A.L. Vogel, J. Schneider, C. Müller-Tautges, G.J. Phillips, M.L. Pöhlker, D. Rose, C. Zuth, U. Makkonen, H. Hakola, J.N. Crowley, M.O. Andreae, U. Pöschl and T. Hoffmann, (2016), Aerosol Chemistry Resolved by Mass Spectrometry: Linking Field Measurements of Cloud Condensation Nuclei Activity to Organic Aerosol Composition, *Environ. Sci. Technol.*, **50**, 10823-10832

C.J. Kampf, A. Filippi, C. Zuth, T. Hoffmann and T. Opatz, (2016), Secondary brown carbon formation via the dicarbonyl imine pathway: nitrogen heterocycle formation and synergistic effects, *Phys. Chem. Chem. Phys.*, **18**, 18353-18364

Oral Presentations:

Zuth, C., Vogel, A.L., Ockenfeld, S., Huesmann, R., Hoffmann, T.: Online Orbitrap mass spectrometry of organic aerosols: Application for the identification of VOCs and SOA particle phase composition, *European Aerosol Conference*, Zurich, Switzerland, September 2017

Zuth, C., Vogel, A.L., Nowak, J., Worsnop, D.R., Kirkby, J., Hoffmann, T., and the CLOUD collaboration: Molecular Analysis of Aerosol Composition in CLOUD-Chamber Experiments using UHPLC-Orbitrap-MS, *Ph.D. student seminar in analytical chemistry*, Hohenroda, Germany, January 2017

Zuth, C., Vogel, A.L., Nowak, J., Worsnop, D.R., Kirkby, J., Hoffmann, T. and the CLOUD collaboration: Molecular Analysis of Aerosol Composition in CLOUD-Chamber Experiments using UHPLC-Orbitrap-MS, *European Aerosol Conference*, Tours, France, September 2016

Poster Presentations:

Zuth, C., Ockenfeld, S., Vogel, A.L., Hoffmann, T.: Online atmospheric pressure chemical ionization high resolution mass spectrometry (APCI-Orbitrap-MS²) for characterization of the SOA molecular composition, *The Third Sino-European School on Atmospheric Chemistry (SESAC)*, Shanghai, China, November 2017

Zuth, C., Ockenfeld, S., Vogel, A.L., Hoffmann, T.: Online atmospheric pressure chemical ionization high resolution mass spectrometry (APCI-Orbitrap-MS²) for characterization of the SOA molecular composition, *European Aerosol Conference*, Tours, France, September 2016, (Best Poster Award)

Zuth, C., Müller-Tautges C., Eichler, A., Schwikowski, M., Hoffmann, T.: Non-Target Analysis of organic compounds in ice cores using UHPLC-ESI-UHRMS, *European Geosciences Union, General Assembly*, Vienna, Austria, April 2015

7.5 Acknowledgments

not included in the electronic version

7.6 Curriculum Vitae

not included in the electronic version